

A STUDY OF THE DESIGN OF FLUIDIZED
BED REACTORS FOR BIOMASS
GASIFICATION

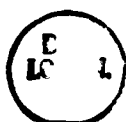


Ajmal Latif MEng.

A Thesis Submitted for the Degree of DOCTOR OF PHILOSOPHY
at the University of London

November 1999

Department of Chemical Engineering
Torrington Place
London WC1E 7JE



ABSTRACT

The present study is in two parts, the first part describes an investigation that was undertaken to determine the feasibility and hydrodynamic behaviour of a cold model circulating fluidized bed system proposed for the continuous combustion-gasification of biomass. The design is based on the principle that the char produced in the gasifier is circulated with the bed material and combusted in a separate reactor to generate the heat required for the gasification process. While high solid circulation rates are required to maintain the heat balance, product and flue gas mixing between the two units must be minimised or eliminated. The design of the circulating bed simply consists of two fluid bed units connected two together via a riser and a downcomer fitted with a non-mechanical valve. Various aspects such as solid circulation rate, gas mixing, solids mixing, and pressure component around the circulating loop were studied.

Results show that the solid circulation and gas mixing are strongly influenced by the riser gas velocity, total solids inventory, and position of the riser from the riser gas jet. Solid circulation fluxes of up to $115\text{kg/m}^2\text{s}$ were attained and easily controlled. The flue gas cross-flow was less than 4% over the range studied. By analysing the experimental data, a series of mathematical correlations were obtained which successfully predict the exponential relationship that exists between the solid circulation rate, gas mixing and the operating parameters. The potential of this system for its purpose is highlighted.

The second part of the study focuses on the design and development of a heated fluidized bed reactor with an on-line gas and solids sampling technique to study the steam gasification of biomass (almond shells). Experiments were conducted at temperatures of up to 800°C to investigate the gasification rates of biomass char under different operating conditions. Understanding the gasification and combustion rates of biomass char is an important step towards the proper designing of biomass gasifiers.

In the heated fluid bed, the extent of the gasification of biomass increased with increasing temperature as indicated by an increase in the quantity of gaseous products. A hydrogen content of up to 43% by volume was obtained. The sampling technique adopted allows the collection of the bed sample at gasification conditions which can be used to predict the composition of the bed. The gasification rate of biomass (almond shell) char was found to be affected by the gasification temperature. In order to evaluate the char gasification rate constants, the shrinking core model with reaction controlling step (SCM) was applied to the char gasification data. The rate constant values obtained from the SCM were $5.14\text{E-}5$, $7.67\text{E-}5$, and $1.26\text{E-}4\text{ s}^{-1}$ for temperatures of 712, 753, and 806°C respectively. The activation energy was evaluated as 89 kJ/mol . These values were in close agreement with those published in the literature. SEM pictures of the surface of the chars shows that at high temperatures, the char formed is very porous and hence very reactive. With regards to practical gasifiers, the results obtained have been used to evaluate an optimum volume for a typical biomass gasifier operating at 850°C . The aim of the present work were satisfactorily achieved.

ACKNOWLEDGEMENTS

I would like to express my most sincere gratitude to the following

Professor John G. Yates for his kind, invaluable and expert supervision and continuous encouragement during the ups and downs of this research and the write up. Although serving as head of department, his guidance and advice was always easy to find.....I shall always be in debt.

Martin Town, Alan Craig, and Barry Bartram from the Mechanical Workshop and Martin Vale, Sarah Bailey and Mark Spurgeon from the Electronics Workshop for constructing the experimental apparatus.

Sam Okagbue, Julian Perfect and Dave Cheesman for their technical support. Anna Harrington, Paty Markey, and Sam Buckley for their administrative work.

My fellow research friends, Paola Lettieri, Ketan Patel, Ralf Kehlenbeck, Xavier Pipen, and Damiano Rossetti, for their interest and friendship.

My mother and to name just a few of my numerous cousins, Marsilla, Zabrina, and Zia, for their love and support.

My uncle, Professor S.S. Hashimi for his moral support.

The Engineering and Physical Sciences Research Council for financing the research.

*To my caring mother and
.....the memories of a wonderful grandmother*

TABLE OF CONTENTS

Abstract	i
Acknowledgements	ii
Dedication	iii
Contents	iv
List of Figures	xi
List of Tables	xv
1 INTRODUCTION	1
1.1 Conclusions	6
1.2 Motivation and Objectives	7
1.3 Layout of Thesis	8
2 ENERGY FROM BIOMASS	9
2.1 What is Biomass?	11
2.2 The Main Processing Routes	12
2.3 Types of carbonaceous material available for gasification	12

2.4 Thermochemical Conversion of Biomass	15
2.5 Gasification	18
2.5.1 Principles of Gasification	19
2.6 Product Gas Contaminants	19
2.7 Tar cracking	20
2.8 Catalytic Cracking	21
2.9 Thermal Cracking	22
2.10 Tar Removal	22
2.11 Char Gasification Kinetics	23
2.12 Sulphur	25
2.13 Biomass Gasification Technology	26
2.13.1 Fluid Bed Gasifier	26
2.13.1.1 Circulating Fluidized Bed	28
2.13.1.2 Pressurised Fluidized Bed	28
2.13.2 Down-Draft Gasifier	29
2.13.3 Entrained Bed Gasifier	30
2.13.4 Fixed Bed Updraft Gasifier	30
2.13.5 Choice of Gasifier	31
2.14 Biomass Feeding	31
2.15 Temperature and Pressure Effects	32
2.16 Biomass to Power Generation	32
2.17 What Are Fuel Cells?	34
2.17.1 Alkaline Fuel Cells	35

2.17.2 Solid oxide fuel Cell	35
2.17.3 Solid Polymer Fuel Cells	35
2.17.4 Molten Carbonate Fuel Cells	35
2.17.5 Phosphoric Acid Fuel Cells	36
2.18 Conclusions	36
3 CIRCULATING FLUIDIZED BEDS	38
3.1 Solids Circulation Rate	42
3.2 Gas Mixing	43
3.3 Solids Residence Time	43
3.4 Conclusions	44
4 DESIGN OF EXPERIMENTAL EQUIPMENT	45
4.1 Description of the Circulating Fluidized Bed and Pilot Plant	45
4.2 Design of the Cold Model Dual Bed Circulating System	50
4.3 Windbox Design	50
4.3.1 Bed 1 And Windbox Design	51
4.3.2 Bed 2 and Windbox Design	55
4.4 Gas Distributor Plate	58
4.4.1 Design Criteria	58
4.4.2 Porous Distributor Plate Design	59
4.4.2.1 Design of bed 1 distributor	60
4.4.2.2 Design of bed 2 distributor	62

4.4.3 Sealing of the distributor	63
4.5 Particulate Filter	64
4.6 Non-Mechanical Valves	65
4.6.1 Aeration Tap Location	66
4.6.2 Design of L-valve Horizontal Length	67
4.7 Design of Solids Sampling Port	68
4.8 Design of the Heated Fluidized Bed Reactor System	69
4.9 Biomass Feeder Design	69
4.10 Sand Feeder	71
4.11 Feeder Probe Design	71
4.12 Fluidized Bed Cover Plate	75
4.13 Heated Windbox Design	76
4.14 Flexible High Temperature Hose	78
4.15 Gas Meter	78
4.16 Thermocouples	78
4.17 Pumps, Piping and Gas Supply	81
4.18 Cold Gas Filter	81
5 EXPERIMENTATION METHODS	82
5.1.1 Bed Inventory	84
5.1.2 Pressure Drop Experiments	84
5.1.3 Solid Circulation Rate Experiments	85
5.1.4 Gas Mixing Experiments	85

5.1.5 Solid Residence Time Experiments	86
5.1.6 Gasifier (bed 2) set-up	86
5.2 Heated Fluidized Bed Gasifier	88
5.2.1 Material (Biomass) Preparation	88
5.2.2 Bed Inventory	89
5.2.3 Gasification Pilot Plant Description	90
5.2.4 Gasification Procedure	93
5.2.4.1 Start-up	93
5.2.4.2 Biomass Gasification	93
5.2.5 Char/Steam Gasification and Sampling	94
5.2.5.1 Char Sampling System	95
5.2.5.2 Char Elimination	96
5.2.5.3 Char Analysis	96
5.3 Gasification Plant Photos	96
6 RESULTS AND DISCUSSION: COLD MODEL CIRCULATING FLUIDIZED	
BED	100
6.1 Preliminary Results	100
6.2 Visual observations	103
6.2.1 Static	105
6.3 Solid circulation	105
6.3.1 Conclusions	115
6.4 Gas Cross-Flow Between Beds	116

6.4.1 Conclusions	122
6.5 Relationship Between Solids Circulation and Gas cross-flow	122
6.6 Correlation of Solid Circulation and Gas Cross-flow	123
6.7 Solid Residence Time In Beds	129
6.8 Pressure Analysis	134
7 RESULTS AND DISCUSSION: HEATED FLUIDIZED BED GASIFIER	141
7.1 Segregation Along the Bed Axis	141
7.2 Bed Sampling Technique	143
7.3 Steady State Run Time	145
7.4 Gaseous Products and Composition	146
7.5 Carbon Conversion	149
7.6 Char Gasification Kinetics	150
7.7 Determination of the Char Gasification Rate Constant, k_c	156
7.8 Effect of Temperature	160
7.9 Determination of Optimum Gasifier Volume	161
7.9.1 Determination of Optimum Combustor Volume	163
7.10 Char Analysis	164
7.11 Conclusions	166
8 GENERAL CONCLUSIONS	168

9 FURTHER WORK	171
9.1 Scaling of Fluidized Beds	171
9.1.1 Preliminary Results	173
9.2 Circulating Fluidized Bed	175
9.3 Heated Fluidized Bed Gasifier	175
NOTATION	176
REFERENCES	180

APPENDICES

Appendix A:	Sand and biomass feeder calibration	194
Appendix B:	Gas chromatograph calibration	198
Appendix C:	Water injection pump calibration	201
Appendix D:	Size distribution and U_{mf} evaluation of experimental materials	203
Appendix E:	Density evaluation of experimental materials	210
Appendix F:	Char density evaluation	213
Appendix G:	Tracer gas (CO ₂) rotameter calibration	214
Appendix H:	Air and nitrogen rotameter calibration	215
Appendix I:	Mechanical drawing of the heated windbox	216

List of Figures

Fig. 1.1 Flow patterns in gas solid fluidized beds (Grace, 1986).	2
Fig. 1.2 Typical circulating fluidized bed system.	3
Fig. 2.1 Typical molecular structures of biomass and coal (Hedley and Bustani, 1989).	11
Fig. 2.2 Alternative Biomass Degradation Routes.	12
Fig. 2.3 Simplified biomass pyrolysis reaction (Diebold, 1994).	18
Fig. 2.4 Main gasifier types (Kurkela et al., 1993).	26
Fig. 2.5 Typical product gas composition for the steam gasification of biomass.	27
Fig. 2.6 Product gas composition as a function of gasifier pressure.	29
Fig. 2.7 Biomass energy conversion using pyrolysis and gasification.	33
Fig. 3.1 Schematic diagram of the circulating fluidized bed system.	39
Fig. 3.2 Pilot plant circulating fluidized bed gasifier-combustor.	41
Fig. 3.3 Side view of the oil shale retort circulating fluidized bed (Chong et al., 1986).	42
Fig. 4.1 Configuration of the circulating fluidized bed system.	46
Fig. 4.2 Principle of biomass combustion-gasification process.	47
Fig. 4.3 Flow sheet of the biomass combustion - gasification plant.	49
Fig. 4.4 Schematics and dimensions of windbox for bed 1 (not to scale).	53
Fig. 4.5 Bed 1 dimensions (not to scale).	54
Fig. 4.6 Schematics and dimensions of windbox for bed 2 (not to scale).	56
Fig. 4.7 Dimensions of bed 2 (not to scale).	57
Fig. 4.8 Dimensions of bed 1 gas distributor plate.	62
Fig. 4.9 Dimensions of bed 2 gas distributor plate.	63
Fig. 4.10 Attachment of gas distributor plate to windbox for bed 1.	64
Fig. 4.11 Schematics of some non-mechanical valves.	65
Fig. 4.12 Schematics and dimensions of the solid sampling port.	68
Fig. 4.13 Schematic diagram of the heated fluidized bed gasifier.	70
Fig. 4.14 Schematic diagram of the biomass feeder.	72

Fig. 4.15 Schematic diagram of the sand feed.	73
Fig. 4.16 Biomass feeder probe.	74
Fig. 4.17 Schematic diagram of the stainless steel bed cover.	75
Fig. 4.18 Schematics of the heated windbox.	79
Fig. 4.19 Schematics of the high temperature flexible tubing.	80
Fig. 5.1 Schematic diagram of the cold bed experimental set up.	83
Fig. 5.2 Schematic diagram of the cold model circulating fluidized bed corresponding to Mark 1.	87
Fig. 5.3 Schematics of the biomass / char gasification pilot plant set-up.	91
Fig. 6.1 Solid circulation rate versus riser superficial gas velocity for Mark 1.	
Fig. 6.2 Gas cross-flow versus riser superficial gas velocity for Mark 1.	102
Fig. 6.3 Solid circulation rate versus riser gas velocity for bed for Mark 2.	102
Fig. 6.4 Gas and solids flow in the L-valve.	103
Fig. 6.5 Tracer particle with metal inclusion.	104
Fig. 6.6 Solids flow through the L-valve.	105
Fig. 6.7 Solid circulation flux versus riser superficial gas velocity.	106
Fig. 6.8 Solid circulation flux versus riser superficial gas velocity.	106
Fig. 6.9 Solid circulation flux versus riser superficial gas velocity.	107
Fig. 6.10 Solid circulation flux versus riser superficial gas velocity.	107
Fig. 6.11 Solid circulation flux versus riser superficial gas velocity.	108
Fig. 6.12 Solid circulation flux versus riser superficial gas velocity.	108
Fig. 6.13 Plot of G_r/U_r versus riser superficial gas velocity, U_r .	109
Fig. 6.14 Solid circulation flux versus riser superficial gas velocity.	110
Fig. 6.15 Solid circulation flux versus riser superficial gas velocity.	111
Fig. 6.16 Solid circulation flux versus riser superficial gas velocity.	111
Fig. 6.17 Solid circulation flux as a function of riser superficial gas velocity.	112
Fig. 6.18 Solid circulation flux as a function of riser superficial gas velocity.	113
Fig. 6.19 Solid circulation flux as a function of riser superficial gas velocity.	113
Fig. 6.20 Solid circulation flux as a function of riser superficial gas velocity	114
Fig. 6.21 Critical riser superficial gas velocity, U_{rc} as a function of X_r .	115

Fig. 6.22 Gas cross-flow versus U_r for bed load 12kg.	117
Fig. 6.23 Gas cross-flow versus U_r for bed load 17kg.	118
Fig. 6.24 Gas cross-flow versus U_r for bed load 22kg.	118
Fig. 6.25 Gas cross-flow versus U_r for $X_r = 1.0\text{cm}$.	119
Fig. 6.26 Gas cross-flow versus U_r for $X_r = 2.5\text{cm}$.	120
Fig. 6.27 Gas cross-flow versus U_r for $X_r = 4.0\text{cm}$.	120
Fig. 6.28 Relationship between the gas cross-flow and X_r .	121
Fig. 6.29 Gas - solid flow at the riser inlet.	122
Fig. 6.30 Relationship between solid circulation and gas cross-flow.	123
Fig. 6.31 Dimensionless gas cross-flow vs. dimensionless riser gas velocity.	124
Fig. 6.32 $K_1 - K_4$ values as a function of β .	126
Fig. 6.33 Re-evaluated K_2 and K_3 values as a function of β .	127
Fig. 6.34 Comparison of experimental and correlation values of the	127
Fig. 6.35 Comparison of experimental and correlation values of the	129
Fig. 6.36 Solids residence time (almond shells) in combustor versus U_r for $X_r = 1.0\text{cm}$.	131
Fig. 6.37 Solids residence time (almond shells) in gasifier versus U_r for $X_r = 1.0\text{cm}$.	131
Fig. 6.38 Solids residence time (almond shells) in combustor versus U_r for $X_r = 2.5\text{cm}$.	132
Fig. 6.39 Solids residence time (almond shell) in gasifier versus U_r for $X_r = 2.5\text{cm}$.	132
Fig. 6.40 Solids residence time (almond shells) in combustor versus U_r for $X_r = 4.0\text{cm}$.	133
Fig. 6.41 Solids residence time (almond shells) in gasifier versus U_r for $X_r = 4.0\text{cm}$.	133
Fig. 6.42 Pressure drop across riser versus riser superficial gas velocity.	134
Fig. 6.43 Pressure drop across downcomer versus riser superficial gas velocity.	135
Fig. 6.44 Pressure drop across combustor versus riser superficial gas velocity.	135
Fig. 6.45 Pressure drop across combustor versus riser superficial gas velocity.	136
Fig. 6.46 Mean riser solids concentration versus solids circulation rate.	137
Fig. 6.47 Mean riser solids concentration versus the ratio G_s/U_r .	138
Fig. 6.48 Typical pressure loop for the circulating fluidized bed.	138
Fig. 6.49 Variation of pressure around the circulating loop as a function of X_r .	139
Fig. 6.50 Variation of pressure around the circulating loop as a function of solids load.	139
Fig. 7.1 Segregation of char in the bed after steady state biomass gasification.	142

Fig. 7.2 Effect of gas velocity on the segregation of char in the bed.	143
Fig. 7.3 Effect of Oxygen leakage on the accuracy of the sampling technique.	144
Fig. 7.4 Reproducibility of the sampling technique; weight percent of char.	145
Fig. 7.5 Steady state dry gas composition.	146
Fig. 7.6 Dry gas composition at steady state.	147
Fig. 7.7 Trace species composition in the dry gas.	147
Fig. 7.8 Total gas yield as a function of temperature.	148
Fig. 7.9 Char and tar (approx.) yield as a function of temperature.	149
Fig. 7.10 Carbon conversion as a function of temperature.	150
Fig. 7.11 Mass of char remaining in the bed as a function of gasification time.	151
Fig. 7.12 Effect of gasification temperature on char conversion.	154
Fig. 7.13 Experimental char gasification rate constant, k_c .	159
Fig. 7.14 Surfaces of chars formed as function of gasification temperature and residence time in the gasifier.	165
Fig. 7.15 Comparison of the mean particle diameter and surface area per unit volume of fresh biomass with the subsequent char formed at 750 °C.	166
Fig. 9.1 Biomass and char mixing patterns function of bed superficial gas velocity.	168

List of Tables

Table 1.1 Applications of fluidized bed reactors.	2
Table 2.1 Typical composition of coals ^a (% by weight, moisture free basis).	13
Table 2.2 Typical composition of biomass ^a (% by weight, moisture free basis).	14
Table 2.3 Manufactured fuels ^a (% by weight, moisture free basis).	14
Table 2.4 Basic reactions in gasification of carbonaceous materials.	17
Table 2.5 Contaminants present in the gasifier product gas.	20
Table 2.6 Investigation of char gasification kinetics using various methods	24
Table 2.7 Typical char gasification kinetic models and references.	24
Table 2.8 Gasification rate constants for various chars.	25
Table 2.9 Product gas composition and yield from pine wood chip gasification.	34
Table 4.1 Stream table for the fluidized bed gasifier.	48
Table 4.2 Gas meter flow rate errors.	78
Table 5.1 Physical and Flow Properties of the Silver Sand.	84
Table 5.2 Composition of the Almond Shells.	89
Table 5.3 Size Distribution of the Almond Shells.	89
Table 5.4 Physical Properties of the Silver Sand.	89
Table 7.1 Char complete conversion times at various temperatures.	154
Table 7.2 k_{cs} values as function of temperature.	156
Table 7.3 Comparison of k_{cs} and k_c values.	158
Table 9.1 Scaling of a hot fluidized bed gasifier to a cold model at ambient conditions.	168

Chapter 1

1 INTRODUCTION

Fluidization is a process where a bed of loosely packed solid particles takes on some of the properties of a fluid when a gas is blown vertically upwards through it. Introducing a gas (gas-solid systems) from the bottom of a column containing solid particles via a gas distributor can cause the particles to vibrate and expand in order to balance the drag force exerted on them by the gas stream. Upon increasing the gas velocity, a point is reached at which the drag force equals the weight of the particles and the bed is said to be fluidized. Depending on the gas velocity through the bed, several flow regimes can be established as shown in Fig. 1.1. These regimes are the fixed bed, bubbling fluidization, slugging fluidization, turbulent fluidization, fast fluidization, and dilute pneumatic conveying. The transition from a fixed to a bubble-free fluidized bed is denoted by the minimum fluidization velocity, U_{mf} , which is the gas velocity at which the solids are just suspended in the gas stream. At very high gas flow rates, much of the solids are thrown into the space above the bed known as the freeboard and a substantial quantity of solids is lost from the bed by elutriation and entrainment, so that gas-solid separators are required to capture a majority of these particles and return them to the bed. Table 1.1 gives a brief list of fluidized bed applications and key references.

Image removed due to third party copyright

Fig. 1.1 Flow patterns in gas solid fluidized beds (Grace, 1986).

Table 1.1 Applications of fluidized bed reactors.

Fluidized bed application	Reference
Combustion and incineration	(Wang and Lin, 1998)
Carbonisation and gasification	(Schrader and Felgener, 1978)
Sohio Process (Acrylonitrile Production)	(Kunii and Levenspiel, 1991)
Synthesis reactions	
Fischer-Tropsch	(Silverman et al., 1986)
Biofluidization	
Cultivation of Micro-organisms	(Schuegerl, 1989)

The ability to maintain a stable and continuous circulation of solids in a gas-solid system has led to the development of the Circulating Fluidized Bed (CFB) for a number of processes, usually large-scale operations, especially in the petroleum industry and power generation. Circulating fluidized beds work in much the same way as bubbling beds but with one major difference. The velocity of the fluid flow is much greater so that there is a more intense mixing of the fluid with the particles in the bed providing excellent gas-solid

contact. Also the high relative velocity between the gas and solid particles results in very high rates of heat and mass transfer. However, the high gas velocities and the recirculation of solids may make the CFB system more expensive in terms of power requirement and investment compared with conventional fluidized bed reactors (Bridgwater, 1995). A typical configuration of a CFB is shown in Fig. 1.2. The high gas velocity in the riser (3-16 m/s) carries the particles (usually 0.05 to 0.5 mm) upwards where they are separated from the gas and returned to the bed via the downcomer. The solid circulation flux (typically 15 to 1000 kg/m²s) is controlled by the gas velocity in the riser and the aeration gas in the downcomer. The driving force for the solids circulation is the bulk density difference in different parts of the circulating system. Solids usually circulate from regions of high bulk density to region of lower bulk density.

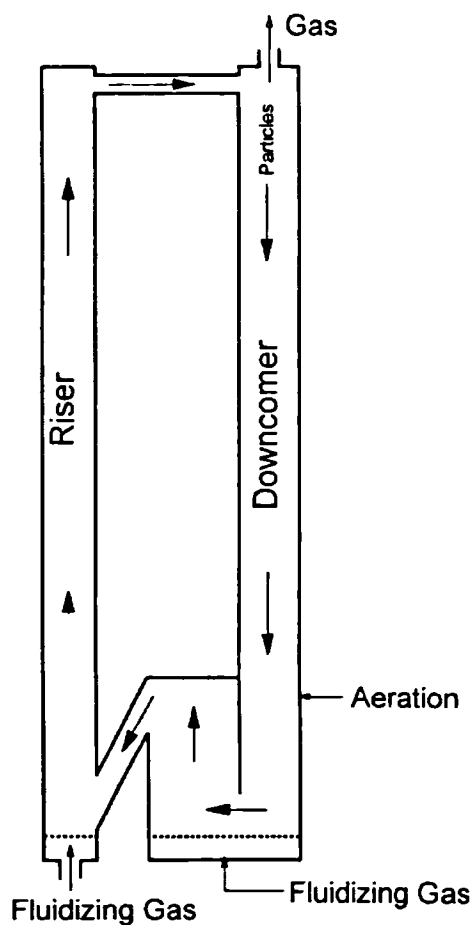


Fig. 1.2 Typical circulating fluidized bed system.

CFBs have been extensively used in the field of solid catalysed gas phase reactions in one of the following two situations. The first is where continuous regeneration of a catalyst that deactivates rapidly is required. In this situation, a steady circulation of solids is maintained where the catalyst is continuously regenerated and returned to the reactor. A second set-up is where heat must be brought into or removed from a reactor. Solids have a relatively large heat capacity as compared to gases and thus a continuous circulation of solids between two vessels can effectively transport heat from one vessel to another and control the temperatures in the units.

In recent years, much attention has been focused on the use of CFBs for the less dense forms of solid fuels such as biomass for the production of energy. The escalation of interest in this field has been partly due to the increasing price of oil and diminishing fossil fuel reserves and tighter control over the emission of greenhouse gases such as carbon dioxide. Biomass is the ecological term for organic material, both above and below the ground and both living and dead, such as trees, crops, grass, tree litter and roots. The types of biomass used in energy production include energy crops like willows and aspen poplar, wood and wood wastes, agricultural and agro-industrial wastes, sewage sludge and municipal wastes. The use of biomass for the production of energy is a carbon dioxide neutral cycle, only releasing the carbon dioxide that it has taken up during growth, since biomass is formed from photosynthesis, a process that converts carbon dioxide and water into oxygen and organic matter. Biomass accounts for nearly 15% of the world energy supplies (Werekobroby and Hagen, 1996). In industrialised countries, biomass fuel supplies about 3% of the total primary energy compared to 35% in developing countries.

The thermochemical conversion of these fuels into heat and power involves one of three processes, direct combustion, pyrolysis, and gasification, for which any sufficient dry combustible material can be used. Combustion involves direct burning to produce heat, which in power generation is applied to boilers to produce steam in order to drive turbines.

Pyrolysis occurs when organic material is decomposed under anaerobic conditions. Pyrolytic processes include slow, conventional and flash heating rates which produce

varying proportions of the solid char, oil and gas. Thermochemical gasification is the conversion by partial oxidation at elevated temperature of a carbonaceous feedstock such as coal or biomass into a gaseous energy carrier. This contains carbon monoxide, carbon dioxide, hydrogen, methane, trace amounts of higher hydrocarbons such as ethene and ethane, water, nitrogen (if air is used as the oxidising agent) and various contaminants such as small char particles, ash, tars, and oils. The tars constitute only a small proportion of the biogas but can cause considerable problems (e.g., equipment fouling) during the gas downstream use. The partial oxidation can be carried out using air, oxygen, steam, or a mixture of these.

Air gasification produces a poor quality gas in terms of heating values (4-7 MJm⁻³ higher heating value) which is suitable for boiler, engine and turbine operation, but not for pipeline transportation due to its low energy density. Oxygen or steam gasification produces a better quality gas (10-18 MJm⁻³ higher heating value) which is suitable for limited pipeline distribution and for use as synthesis gas with the process energy supplied via the combustion of the by-product char in a separate reactor.

Biomass gasification is a highly endothermic process requiring large quantities of heat (see Table 2.4). The heat can be supplied to the gasifier via an independent and external source, so-called 'direct' heating or by circulating an inert bed material between a gasification and a combustion zone, 'indirect' heating. Although the first arrangement has the advantage of physically separating the gasifier from the source of heat and utilising spare energy from processes that might otherwise be wasted, the inevitable drawback is that it is attached to other heat generating processes and requires large surface areas for the heat transfer. Indirect heating produces a gas with consistent heating values regardless of the feedstock's moisture content, however, care must be taken in order to minimise product gas contamination.

The energy content of biomass is measured by its calorific value. There are two measures of the calorific value, gross calorific value and net calorific value. For all practical purposes it is only important to know the net calorific value since the heat is available as

useful energy. For woody biomass resources it is the moisture content of the wood rather than the particular species, that determines the available energy. There are two important determinants of the energy value of non-woody plant biomass, one is the moisture content and the other is the ash content. While the ash content of most wood is constant at about 1%, that of crop residues can vary from about 1% to 20%.

The use of biogas together with fuel cells for the production of electric power in rural areas has the potential for widespread development. Fuel cells are electrochemical devices that convert the energy of a chemical reaction directly into electricity and heat. Unlike primary batteries, fuel cells store the fuel and oxidant externally, allowing continuous operation. While the reaction that drives all fuel cells involves hydrogen, pure hydrogen is currently too expensive to produce and transport in bulk. The current alternative is to process fuels, such as biomass in order to produce hydrogen and to feed this, after suitable gas cleaning, directly to the fuel cell.

Fuel cells can convert up to 60% of the total energy stored in a fuel into electricity. Reusing the heat released during the process allows efficiencies of up to 85% to 90% to be achieved. This makes fuel cells much more attractive than gas turbines and internal combustion engines, which are unable to achieve electrical efficiencies much above 40% and combined electrical and thermal efficiencies much above 60%. However, at present fuel cell units are very expensive and still under development.

1.1 CONCLUSIONS

The future of bioenergy can not be predicted with any certainty, but it is clear that biomass fuels will always exist in large quantities and that their effective use has great potential for bioenergy production. Biomass fuels have yet to compete successfully with fossil fuels on cost grounds and this has a direct effect on bioenergy markets. However, government policies and international agreements such as the Kyoto Protocol as well as the development of new technologies are leading towards a greater use of renewable energy resources such as biomass.

As environmental concerns become increasingly important, it will no longer be just a simple case of power generation, but rather a balance between increased efficiency and reduced environmental impacts with low costs and risks. The diversity and ready availability of biomass along with existing and developing technologies make biomass a strong alternative to fossil fuels for future energy requirements around the world. This allows developing and industrialised countries the ability of producing bioenergy without significant structural changes in the industries.

1.2 MOTIVATION AND OBJECTIVES

The objective of the present work was to study processes for the gasification of biomass in fluidized beds.

The first part investigates the hydrodynamic behaviour of a cold model circulating fluidized bed proposed for the continuous combustion-gasification of biomass. The design is based on the principle that the char produced in the gasifier is circulated with the bed material and combusted in a different reactor to generate the heat required for the gasification process. While high solid circulation rates are required to maintain the balance, product and flue gas mixing between the two units must be minimised or eliminated. Various aspects such as solid circulation rate, gas mixing, solid mixing, and pressure profile around the circulating loop were studied.

The second part focuses on the design and development of a heated fluidized bed reactor for the gasification of biomass (almond shells). Experiments were conducted at temperatures of up to 800°C to investigate the gasification and combustion rates of biomass char under different operating conditions, namely, temperature, static bed height, steam to biomass ratio (kg/kg), biomass feed rate, and biomass type. Understanding the gasification and combustion rates of biomass char is an important step towards the proper designing of biomass gasifiers. Reactivity and gasification of chars have been extensively studied by several investigators, however, most approaches have made the use a thermogravimetric

analyser to obtain char gasification kinetics. It is hoped that the present work extends the knowledge of char gasification kinetics by examining bed samples withdrawn at operating conditions.

1.3 LAYOUT OF THESIS

Chapters 2 and 3 report the literature on the thermochemical conversion of biomass and the use of circulating fluidized beds as well as the available technologies respectively. Chapter 4 deals with the design of the experimental equipment used for the major parts of this work. Chapter 5 is a description of the experimental apparatus and procedure relevant to all the work concerned. Chapter 6 is the results and discussion of the experimental findings of the cold model circulating fluid bed and chapter 7 is the results and discussion for the experimental findings from the heated fluidized reactor. Chapter 8 is a summary of the major conclusions, which can be drawn from this work, and finally chapter 9 contains suggestion for further work.

Chapter 2

2 ENERGY FROM BIOMASS

The deterioration in the supply of conventional fuels, and the problems of climatic changes, have led to a resurgence in research and development studies investigating alternative solid fuel supplies. Thus, increasing attention is given to studies of processes involving the conversion of biomass and related products to gaseous fuels. Gasification of biomass as a source of hydrogen and other valuable gases seems to be the best route for converting it to an energy vector. This can be used in a wide range of applications, for example, in fuel cells for the production of electricity.

The formation of hydrogen from biomass is a recycle process without a net increase of carbon dioxide level or depletion of natural resource, since biomass arises from the photosynthesis of carbon dioxide and water. Further more, most biomass contains less sulphur than fossil fuels, and would be expected to provide an economical advantage in the cleaning of sulphur compounds.

Experimental investigations of biomass gasification (Corella et al., 1991) have shown that the first step in this process is the pyrolysis or devolatilisation of the biomass particles, as a result of which volatile matter and char are produced. This is followed by secondary reactions, involving cracking and reforming of the evolved volatiles and gasification of char. According to this reaction scheme, when the object is the production of organic liquids, the operating temperature should be kept at relatively low values, whereas high operating temperatures and a steam atmosphere maximises the gas yield.

The pyrolysis of lignocellulosic materials has been studied by a great number of researchers using different techniques: furnace reactor (Stamm, 1956, Lewellen et al.,

1976; Hajaligol et al., 1980), vacuum reactor (Bradbury et al., 1979), fluidized bed reactors (Barooah and Long, 1976; Kosstrin, 1980; Liden et al., 1988; Scott et al., 1988; Rapagna et al., 1992), fixed bed reactor (Chatzakis et al., 1995), etc. Also a wide diversity of materials (cellulose, lignin, wood and other types of biomass), with different operating conditions are used. In recent years a considerable number of books and papers have appeared about the gasification and pyrolysis of biomass in fluidized beds. The results obtained by different authors are quite different from one another, due to the numerous factors which influence the product distribution obtained. For this reason the comparison of these results with one another is usually rather difficult. In pyrolysis and gasification in fluidized beds, the product distribution depends on at least the following factors:

1. Gasifying agent (steam, air, steam and oxygen, nitrogen, etc.)
2. Type of biomass used
3. Moisture and size of particle
4. Temperature and pressure in the gasifier
5. Gasifying agent to biomass ratio
6. Presence or not of primary catalysts
7. Amount of char in the bed
8. Superficial gas velocity of the gasifying medium
9. Type, size, and weight of bed particles

There are many more such factors that have a direct or indirect effect on the product distribution.

To further enhance the production of gas, a very efficient gas-solid contacting is needed to ensure high conversion of the gas phase and gas-solid reactions. The fluidized bed reactor, with its high heat and mass transfer characteristics, good particle mixing and ease of handling of solid materials, is the most promising technology for the gasification of biomass.

2.1 WHAT IS BIOMASS?

Biomass is a term given to any kind of carbonaceous material (wood and agricultural) that has the potential to be converted into useful energy via the appropriate technology. It is a renewable resource occurring naturally and repeatedly in the environment. As a result, the proportions of the basic constituents and the overall morphological characteristics of any biomass are specific to its location.

Biomass occurs mainly in a solid form, which is obtainable from sources such as plant tissue, wood, urban refuse, or any other renewable form of organic material which can be produced or made available, after relatively short periods of time. A typical molecular structure of biomass and coal are shown in Fig. 2.1 and by contrast, the molecular structure of biomass is relatively simple, however, the structures of some of the major organic components in biomass are shown on the left of Fig. 2.1 (Klass, 1998). The average chemical formula for biomass has been reported as $\text{CH}_{1.4}\text{O}_{0.6}\text{N}_{0.1}$ (Overend, 1998). Biomass material generally is more oxygenated, has a lower calorific value, and contains a greater amount of moisture than coal.

Image removed due to third party copyright

Fig. 2.1 Typical molecular structures of biomass and coal (Hedley and Bustani, 1989).

2.2 THE MAIN PROCESSING ROUTES

When biomass is processed into a gaseous or liquid product, a degradation of its molecular structure takes place. The ability to totally convert a carbonaceous starting material depends largely on the extent of degradation that can be brought about, and in many cases complete conversion to a product gas or liquid is just impossible, at least in a single step. In general, there are five different routes available for the degradation of a solid carbonaceous material as can be seen from Fig. 2.2.

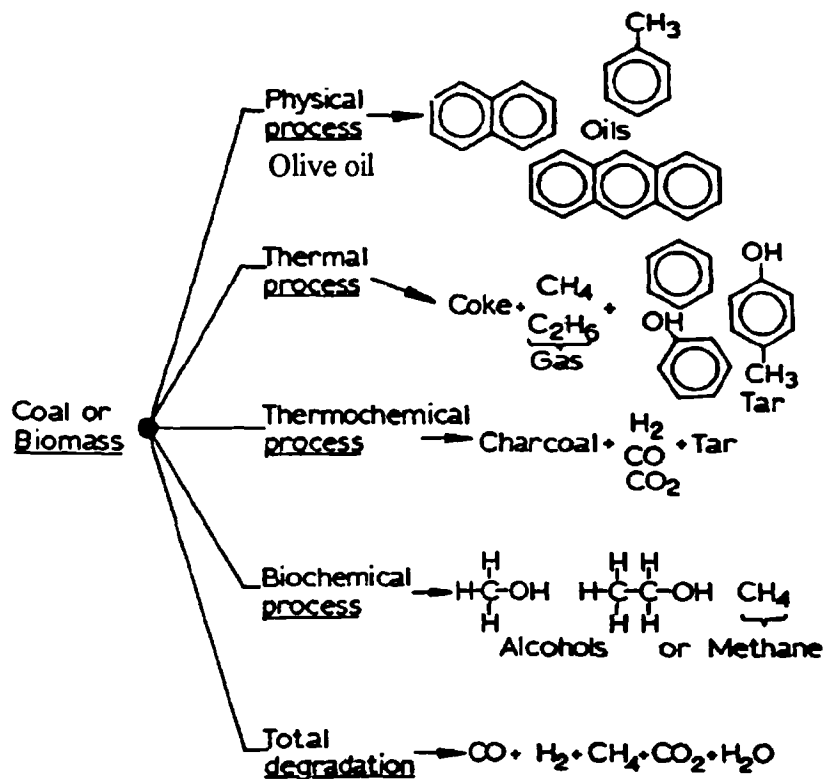


Fig. 2.2 Alternative Biomass Degradation Routes.

2.3 TYPES OF CARBONACEOUS MATERIAL AVAILABLE FOR GASIFICATION

Lists of some of the different more available types of carbonaceous material which can be gasified are presented in Table 2.1 for coals, in Table 2.2 for biomass, and in Table 2.3 for other manufactured fuels.

Many fuels occur with high contents of water for example lignite, and peat in

cost of de-watering and drying operations can be prohibitive and could be the limiting factor for its economic use.

The ash content can vary widely

- from type to type of coal or biomass,
- and from place to place of their origin.

The properties and behaviour of the ash, and its quantity, may be limiting factors in the choice of gasification system.

Table 2.1 Typical composition of coals^a (% by weight, moisture free basis).

	Peat	Lignite	High volatile coking material	Medium volatile coking coke	Anthracite
Carbon	54.6	65.9	76.1	80.4	85.0
Hydrogen	5.20	4.70	4.80	4.50	2.60
Nitrogen + Sulphur	1.90	1.90	3.50	2.70	2.10
Oxygen	33.3	21.6	6.60	3.80	1.60
Ash	5.00	5.90	9.00	8.60	8.70
	100	100	100	100	100
Moisture	20-60	10-50	0-20	0-20	0-15
Volatile matter ^b	68	53	36	25	6
Calorific value ^c (MJ/kg)	12.0	17.7	26.2	27.5	30.4

^asource: (Rose and Cooper, 1977), ^bMoisture and ash free, ^cGross, as received.

Table 2.2 Typical composition of biomass^a (% by weight, moisture free basis).

	Cellulose	Wood	Grass	Municipal refuse	Animal Manure	Sewage sludge
Carbon	44.4	51.8	45.8	41.2	35.1	43.8
Hydrogen	6.20	6.30	5.90	5.50	5.30	6.20
Nitrogen + Sulphur	-	0.10	5.20	0.70	2.90	4.10
Oxygen	49.3	41.3	29.6	38.7	33.2	19.4
Ash	-	0.50	13.5	13.9	23.5	26.5
	100	100	100	100	100	100
Moisture	-	5-50	10-70	18.4	20-70	90-97
Volatile matter ^b	-	80	70	67	63	57
Calorific value ^c (MJ/kg)	17.5	15.4	11.2	10.4	7.40	1.30

^asource: (Kirk-Othmer, 1980; Boyles, 1984), ^bMoisture and ash free, ^cGross, as received.

Table 2.3 Manufactured fuels^a (% by weight, moisture free basis).

	Charcoal	Industrial coke	Low temp. coke
Carbon	92.1	89.2	83.5
Hydrogen	2.40	0.40	2.80
Nitrogen + Sulphur	1.50	1.80	2.80
Oxygen	3.00	1.00	3.80
Ash	1.00	7.60	7.10
	100	100	100
Moisture	2	10	15
Volatile matter ^b	10	1	12
Calorific value ^c (MJ/kg)	33.7	28 0	26.2

^aSource:(Rose and Cooper, 1977 ^bMoisture and ash free, ^cGross, as received.

2.4 THERMOCHEMICAL CONVERSION OF BIOMASS

Biomass is a source of non-fossil renewable fuel that can be used to replace oil and other hydrocarbon fuels. Biomass is widely considered to be a major potential fuel and renewable resource for the future. In terms of size of resource, there is the potential to produce at least 50% of Europe's total energy requirement, from purpose grown biomass using agricultural land no longer required for food, and from wastes and residues from agriculture, commerce and consumers (Grassi and Bridgwater, 1991; Grassi and Bridgwater, 1992). As produced, biomass is a solid and is difficult to use in many applications without substantial modification. Conversion to gaseous and liquid energy carriers has many advantages in handling and application. One of the major problems with biomass is that, as an energy crop, it is labour-intensive to produce, harvest and transport, as it is dispersed over large areas. When it is in the form of wastes, costs are much lower, often negative in the case of domestic solid wastes (Bridgwater and Evans, 1993), but the material usually requires extensive processing to make it compatible with the conversion process.

There are several conversion routes available such as thermal (combustion), thermochemical (gasification, pyrolysis) and biological (anaerobic digestion, fermentation to ethanol). At present thermal and thermochemical processes are more efficient and easier to operate since they result in almost complete conversion. Biomass combustion and char gasification are well understood, however, biomass pyrolysis is still not adequately known although it is the important first step in all thermal and thermochemical conversion processes.

Slow heating rate (less than 10 °C/s) and low temperature (below 500 °C) pyrolysis have been studied extensively and some excellent reviews are available in the literature (Milne, 1979; Shafizadeh, 1982; Shafizadeh, 1985). However, fast and/or flash (heating rate 10 - 10,000 °C/s) and high temperature (greater than 600 °C) pyrolysis has only recently attracted the interest of the research community. Fundamental research has demonstrated that rapid pyrolysis of biomass can be selected for the production of liquid (tar oil, olefins) and other valuable hydrocarbons (Knight et al., 1985). Flash pyrolysis (heating rate 100 - 1000 °C/s) occur at moderate temperatures (500 - 800 °C) and aims at maximising yield of liquid tar and oil

products at the expense of char and gas with vapour residence times of less than 2s. On the other hand, in fast pyrolysis extremely high heating rates (1,000 - 20,000°C/s) are used at temperatures higher than 600°C and very short vapour residence times (less than 0.5s) in order to produce gas at the expense of char and tar/oil (Graham et al., 1984). It has also been shown that the thermal properties, heat flux and pellet length interact in a non-linear way to alter the ultimate yields and instantaneous rate of gas production from a rapidly pyrolysing large pellet of biomass (Chan et al., 1985).

To further enhance the gaseous quality, steam has been used as an active medium. Steam gasification of cellulosic waste or of biomass in fluidised beds was studied in the early 1980's when it was thought this could be an alternative energy source. Nevertheless, the low price of oil and its derivatives, the disposal of cheap natural gas and healthy economies of the countries in the late 1980's meant that this process was not competitive as a source of energy. A lot of new developing technologies were stopped by the absence of continuing funds. Only a few new processes for biomass were commercialised such as the one at Studvik Energy in Sweden, but many pilot plants were dismantled without having solved all the technical problems. This was the case of steam gasification of cellulosic waste in a fluidized bed which can have a good future not only because of oil price increases, but also because it can eliminate solid waste with energy production by the generated gas.

The off-gases from the top of the gasifier at a temperature ranging from 600°C to 900°C and near atmospheric pressure typically contain water vapour, very small amounts of condensable organic oil, and non-condensable gases (Rapagna et al., 1992). The main components of the gaseous phase are hydrogen, carbon monoxide, methane, carbon dioxide, water vapour, and very small amounts of low molecular weight hydrocarbons. The volatiles, primarily produced from the biomass, then undergo reactions in the gaseous phase.

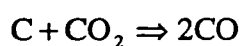
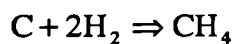
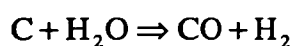
The char remaining after devolatilisation consists primarily of carbon, together with the major part of the ash and some volatile matter. Secondary reactions involve cracking and reforming of the evolved volatiles and gasification of the char. There are basically eight different chemical reactions that can take place during the high

temperature gasification of carbonaceous materials and these are presented in below in Table 2.4.

Table 2.4 Basic reactions in gasification of carbonaceous materials.

		ΔH (kJ/mol)
Combustion		
(1) $C + 0.5O_2 \Rightarrow CO$	Partial combustion	-123.1
(2) $C + O_2 \Rightarrow CO_2$	Total combustion	-405.9
Gasification		
(3) $C + CO_2 \Rightarrow 2CO$	Boudouard reaction	+159.7
(4) $C + H_2O \Rightarrow H_2 + CO$	Steam-carbon reaction	+118.7
(5) $C + 2H_2 \Rightarrow CH_4$	Hydrogasification	-87.4
Pyrolysis		
(6) $4C_nH_m \Rightarrow mCH_4 + (4n-m)C$	Pyrolysis	Exothermic
Gas phase reactions		
(7) $CO + H_2O \Rightarrow H_2 + CO_2$	Water-gas-shift	-40.9
(8) $CO + 3H_2 \Rightarrow CH_4 + H_2O$	Methanation	-206.3

The principal heterogeneous reactions of char with steam and volatiles are (Bungay, 1981):



The endothermic and exothermic reactions involved in the pyrolysis of biomass are complex. Most biomass materials are chemically and physically heterogeneous and their components have different reactivities and yield different product spectra. A

simplification of this complex reaction scheme is shown in Fig. 2.3 (Diebold, 1994). The overall process can be broadly classified into primary and secondary stages. The primary reactions are dependent only on the local solid temperature. When pyrolysis is carried out at high temperatures (above 700°C), the secondary reactions (especially tar cracking reactions) are progressively more important, involving gas-solid interactions and thus depend on the contact time distribution.

Image removed due to third party copyright

Fig. 2.3 Simplified biomass pyrolysis reaction (Diebold, 1994).

2.5 GASIFICATION

Thermochemical gasification involves the conversion of a carbonaceous feedstock such as biomass or coal at elevated temperature into a gaseous energy carrier. The gaseous product generally contains carbon monoxide, carbon dioxide, hydrogen, methane, trace amounts of higher hydrocarbons such as ethane and ethene, water, nitrogen (if air is used as the oxidising agent) and various contaminants such as small char particles, ash, tars and oils. The partial oxidation can be carried out in the presence of air, oxygen, steam or a mixture of these.

If air is used as the gasification medium, a poor-quality gas is produced in terms of heating value (4-7 MJm⁻³ higher heating value). This type of gas is suitable for boiler, engine and turbine operation, but not for pipeline transportation due to its low energy density. A better-quality gas is produced with oxygen (10-18 MJ m⁻³ higher heating value) which is suitable for limited pipeline distribution and for use as synthesis gas for conversion, for example, to methanol and gasoline. Gas of this quality can also be

produced by steam gasification, with the process energy being supplied by combustion of by-product char in a second reactor.

2.5.1 PRINCIPLES OF GASIFICATION

Gasification occurs in different steps as listed below:

- evaporation of moisture by drying,
- pyrolysis resulting in the production of gas, vaporised tars or oils and a solid char residue,
- gasification or partial oxidation of the solid char, tars and gases.

Subjecting a solid fuel to heated (350-500°C) in the absence of an oxidising agent, results in pyrolyses of the fuel to solid char, tar (condensable hydrocarbons), and gases. As mentioned before, the relative yields of gas, liquid and char depend on the rate of heating and the final temperature. Generally the pyrolysis or devolatilisation step is much more rapid than gasification, and consequently the latter is the rate-controlling step. The interaction and reaction of the gas, liquid and solid products of pyrolysis with the oxidising agent give permanent gases (CO, CO₂, H₂,) and lesser quantities of hydrocarbon gases. Char gasification is the interactive combination of several gas-solid and gas-gas reactions in which solid carbon is oxidised to carbon monoxide and carbon dioxide, and hydrogen is generated through the water-gas shift reaction. The gas-solid reactions of char oxidation are the slowest and limit the overall rate of the gasification process. Many factors such as feed composition, water content, and reaction temperature influence the gas composition.

Due to the physical and geometrical limitations of the reactors and also the limitations imposed by the chemical reactions that take place, it is not possible to convert all of the liquid products generated in the pyrolysis stage. As a result, the product gas always contains contaminants in the form of tar.

2.6 PRODUCT GAS CONTAMINANTS

Gas contamination is present in all gasification processes and the extent depending

of course on the type of gasifier and the feedstock fuel. An important step after the gasification process is the gas cleaning which is absolutely necessary in order to prevent erosion, corrosion of the downstream equipment and to minimise environmental impact. Table 2.5 gives a list of the some of the contaminants present in the product gas along with the problems associated with them and typical cleaning method.

Table 2.5 Contaminants present in the gasifier product gas (Bridgwater, 1995).

Contaminant	Example	Problems	Cleaning method
Nitrogen	NH ₃ , HCN	NO _x formation	Scrubbing
Particulates	Bed material, ash, char	Erosion	Filtration, scrubbing
Tars	Aromatics, heavy hydrocarbons,	deposits internally Blocks filters	See below
Alkali metals	Sodium, Potassium	Hot corrosion	Cooling, adsorption
Sulphur	H ₂ S	Emissions	Dolomite scrubbing
Chlorine	HCl	Corrosion	Wet scrubbing

2.7 TAR CRACKING

Katheklakis et al. (1990) have investigated the effect of freeboard residence time (0.8 and 4.5 s) on the molecular mass distribution and yield of fluidized bed pyrolysis tars over the temperature range of 400 - 750 °C. The atmospheric pressure fluidized bed has a movable gas distributor plate which allows the variation of volatiles residence time without varying the fluidized bed conditions. The tars evolved were collected using a wire mesh screen. Significant tar losses were reported for a longer residence time at lower temperatures (500 °C) through covalent bond scission. This decrease has been accompanied with an increase in volatile production. Also the molecular mass fractions of the evolved tars were seen to decrease with increasing temperature, indicating that tar cracking to lower molecular masses becomes dominant.

Tar concentration is mainly a function of gasification temperature, the tar yield increases slightly with an increase in temperature, goes through a maximum (about 650 °C) and then decreases due to the initiation of secondary reactions beyond this

temperature. Stiles and Kandiyoti (1989) have reported this maximum at much lower temperatures during the pyrolysis of lignite and several other biomass materials. The relation between temperature and tar level is a function of reactor type and processing conditions and feedstock.

Megaritis et al., (1998) have reported that fluidized bed tar yields are lower than those obtained in a wire mesh cell over the same temperature range. They have attributed this to the longer residence time of solids (order of minutes) within the fluidized bed which allows for the completion of pyrolysis reactions. Tests have shown that tar production in wood gasification is much greater than in coal or peat gasification and that the tars tend to be heavier, more stable aromatics (Diebold et al., 1992). This may give rise to the formation of soot which can block filters, a problem common to biomass gasification. Therefore coal gasification tar cleaning technology may not be easily applied to biomass feeds. There are two basic ways of destroying tars:

- by catalytic cracking using, for example, dolomite or nickel (Narvaez et al., 1997; Olivares et al., 1997),
- by thermal cracking, for example by partial oxidation or direct thermal contact (Corella et al., 1998).

2.8 CATALYTIC CRACKING

Catalytic cracking of tars is highly effective and tar conversions in the range of 99% can be attained by using dolomite or nickel-based catalysts at temperatures of around 800-900 °C. These tests have been performed using both fossil and renewable feeds. Most investigations have made the use of a second reactor, however some work has been carried out on incorporation of the catalyst in the primary reactor (Rapagna and Foscolo, 1999), which has often been less successful than use of a second reactor (Corella et al., 1988). Elevated freeboard temperatures thermally crack tars and can reduce the load on the catalytic cracker.

Catalyst deactivation is generally not a problem with dolomite. Carbon deposition on the catalysts leads to an initial loss of activity, however, as the bed temperature rises, the compounds gasify and the catalyst is regenerated. Metal catalysts tend to be more

susceptible to contamination. Low hydrogen concentrations in the product gas reduce the catalytic activity of metal-based systems. The low sulphur content of biomass gases can reduce the activity of metal sulphide catalysts through stripping-out of the sulphur. The use of a circulating fluid bed technology offers some advantage in the regeneration of the catalyst in the combustion zone. Attempts to impregnate the catalyst on the surface of the inert bed material in a circulating bed has been promising but has failed in long run tests due to attrition problems (Rapagna and Foscolo, 1999).

2.9 THERMAL CRACKING

Tar levels can be reduced by thermal cracking at temperatures around 800-1000 °C (Diebold, 1994). However, the nature of the tars produced from biomass makes them harder to crack by thermal treatment alone as temperature increases. Although elevated freeboard temperatures in fluid bed gasifiers result in some thermal tar cracking, there are also other options available such as:

- increasing tar residence time in the fluid bed reactor freeboard.
- bringing the tars to direct contact with an independently heated hot surface, this method requires a significant energy supply and thus leads to a decrease in the overall efficiency.
- the addition of air or oxygen to partially oxidise the tars. Although this technique is very effective specially at gasification temperatures as high as 1300 °C, however, the consequences are that it increases CO₂ levels, reduces efficiency and increases costs for oxygen use.

2.10 TAR REMOVAL

A most common technique for the physical removal of particulates, tars, and other contaminants such as hydrogen chloride and ammonia is water scrubbing. Unfortunately, most experience is not so promising particularly in the poor efficiencies of tar removal, (Mackie, 1993). Tars require physical capture and agglomeration or coalesce more than simple cooling; biomass-derived tars are known to be very difficult to coalesce, requiring a complex treatment system to attain 90% tar removal.

Oil scrubbing has also been looked at, but the disadvantages are far greater than the benefits. Electrostatic precipitation is an effective but costly way of removing tars, but there is little experience on biomass-derived gasification products.

2.11 CHAR GASIFICATION KINETICS

In the case of continuous combustion-gasification of biomass in a circulating fluidized bed, the design of the gasifier should not be such as to have complete gasification of the feed material but, also to maintain efficient combustion by circulating some of carbonised material to the combustion section. To further improve the overall process efficiency and economics, gas production in the gasifier should be maximised. As a result, proper understanding of the gasification rate of char is of crucial importance in the successful design of biomass gasifiers.

As said earlier, biomass is decomposed to produce gaseous products and a residual char in the first step. The second step is the secondary reactions of the volatiles and the last step is the gasification of the residual char. The kinetics of the first step has been investigated by Koufopoulos et al. (1991), however, the gasification rate of char (being the slow step) is sensed to be the most critical information required for optimum reactor design. The physical characteristics and hence the reactivity of the char have been found to vary with the history of its genesis, i.e., temperature, partial pressure of gasifying agent, rate of heating, gaseous environment, and particle size all play a part during its formation. Most kinetic measurements of char gasification has been investigated in thermo-gravimetric analysers (TGA) which are operated under conditions far from realistic and commercial equipment. The heat treatments under which the char is formed also affects the subsequent reactivity during the char gasification (Riley and Judd, 1987).

The experimental determination of the gasification and combustion rate of biomass char in a fluidized bed has not been investigated thoroughly and thus the literature on the subject is sparse. Thermo-gravimetric analysis can provide precise data in a well defined gas atmosphere, however, a much slower heating rate of the sample might

result in a significant difference in reaction rate. Burnham (1979) studied the gasification rate of oil-shale using steam and carbon dioxide and found a higher reaction rate from a fluidized bed compared to that from a TGA. However, Bjerle et al. (1980) reported the TGA to give a higher rate than the fluidized bed. Thus it might be a practical concern whether the kinetic data obtained from a TGA can be successfully used for fluidized bed gasifier design. Table 2.6 gives a list of the different methods used to study char gasification and also compares the corresponding kinetics parameters obtained by the authors.

Table 2.6 Investigation of char gasification kinetics using various methods and key references.

Char origin	Gasifying agent	Method	Activation energy E_a (kJ/mol)	Reference
Lignite	H ₂ O	Thermobalance	120-160	(Liliedahl & Sjoström, 1997)
Black liquor	H ₂ O	TGA	210	(Li and Van Heiningen, 1991)
Coal	CO ₂	Thermobalance	79-155	(Kwon et al., 1988)
Coal-derived	H ₂ O	TGA	129	(Matsui et al., 1988)
Coal	CO ₂	TGA	59	(Dutta and Wen, 1977)

The literature is brimful with numerous equations describing the gasification rate of char (mainly coal derived chars) in the kinetic region. The most common ones are listed below in Table 2.7.

Table 2.7 Typical char gasification kinetic models and references.

Kinetic equation	Application	Reference
$dX/d\tau = k(1-X)^n$	General	Traditional
$dX/d\tau = k \exp(bX^2)(1-X)^{2/3}$	Bituminous coals	(Johnson, 1979)
$dX/d\tau = \sqrt{1-\psi \ln(1-X)}(1-X)$	Theoretical pore model	(Bhatia and Perlmutter, 1980)

In the above expressions, k is a rate constant; b , n , and ψ are dimensionless rate constants specific to a particular char, char history, temperature, gasifying mixture, etc. Kojima et al. (1993) have studied the gasification of saw dust char in a experimental Westinghouse type jetting fluidized bed reactor (5 m static bed height). The

gasification rate was determined by evaluation of the difference in the production rate of gaseous carbon between the conditions with and without steam divided by the weight of carbon in the bed for various reactor temperatures. The feed rate of the biomass was somewhat in the range of 9-30mg/s. The results of the gasification rate constant for various materials obtained by the above authors is listed in Table 2.8.

Table 2.8 Gasification rate constants for various chars

Material	Temperature (K)	k_c (s^{-1})
Saw dust char	1260	6×10^{-3}
	1130	1.2×10^{-3}
Coconut shell char	1060	3×10^{-5}
	985	6×10^{-6}
Straw	1205	8×10^{-3}
	1100	2.2×10^{-3}
Graphite	1230	7.5×10^{-6}
	1150	3.5×10^{-6}

2.12 SULPHUR

Generally, biomass feeds have very low sulphur contents and thus sulphur is not on the problems agenda. The specification for turbines is typically 1 PPM and about the same or often much less for fuel cells, For turbines this may be lower in the presence of co-contaminants, such as alkali metals. Some gas compositions have been reported with 0.01 vol.% sulphur (100 PPM). Sulphur removal may therefore be necessary for turbine and fuel cell applications. Sulphur concentrations are lower than those produced in the combustion of fossil fuels, and hence expensive sulphur removal technology is not required. Significant proportions of sulphur can be absorbed by the use of dolomite (CaO:MgO) tar cracker. However, it may not be possible to reach the low levels required. Normally a hot fixed bed of zinc oxide is used as a sulphur guard which is adequate for the concentrations required. This would be relatively inexpensive to install but would create a waste disposal problem from the zinc sulphide produced.

2.13 BIOMASS GASIFICATION TECHNOLOGY

Biomass gasification is a diverse collection of technologies, and it is becoming more diverse every year (Sarkanen and Tillman, 1979). The main gasifier types are shown in

Fig. 2.4.

Image removed due to third party copyright

Fig. 2.4 Main gasifier types (Kurkela et al., 1993).

2.13.1 FLUID BED GASIFIER

The simplicity of single fluidised beds makes them attractive for gasification of biomass. Gases produced by a fluid bed gasifier vary widely depending on several parameters. Fuel moisture, bed temperature, bed depth, gasification rate, bed particle size, char re-injection, air temperature and location of fuel inlet all affect the gas composition.

If oxygen is present, some of the solid carbon and most of the hydrocarbon vapours are oxidised. However solid particles can be satisfactorily removed and unburned carbon particles can be returned to the bed and oxidised or gasified. The gas temperature can be reduced to a manageable level. Fluid bed gasifiers can be designed to have bed temperatures lower than 500 °C or higher than 900 °C. The pyrolysis of biomass is rapid and occurs at whatever temperature the bed is maintained. Selecting the optimum bed temperature depends on what the optimum desirable product is.

The fluid bed process is unique among the biomass gasifiers in one important capability, biomass fuel in any particle size range, any moisture content, and any ash or grit content can be gasified. A typical product gas composition obtained from the steam gasification of biomass (almond shells) in a fluidized bed reactor is shown in Fig. 2.5 (Rapagna and Latif, 1997). The authors have investigated the gasification of biomass in a fluidized bed reactor over the temperature range of 600 - 850 °C. They have shown that for small particle sizes, the differences in the product yield and distribution becomes negligible at high temperatures (around 850 °C). However for larger particles ($d_p > 1\text{mm}$), although the total yield continues to increase over the temperature range studied, but quantitatively it does not reach that obtained with the smaller particles. This suggests the significance of heat transfer limitations as the particle increases in size.

The authors have also reported that char production is negligible for very small biomass particle feed size (300 μm) and high temperatures. For larger biomass feed particles ($d_p = 1\text{mm}$), the char yield decreases over the temperature range but still maintains a significant quantity.

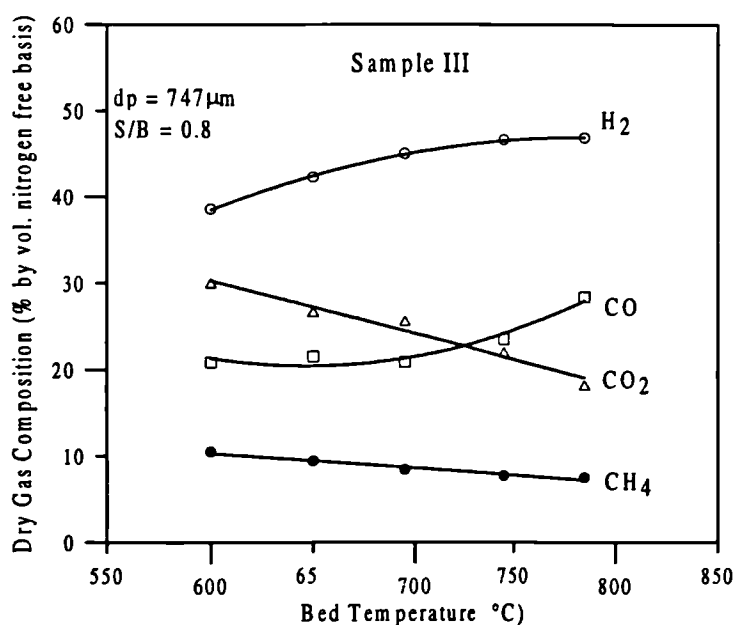


Fig. 2.5 Typical product gas composition for the steam gasification of biomass in a fluidized bed at 800 °C

2.13.1.1 CIRCULATING FLUIDIZED BED

The circulating fluidized bed systems were developed so that the solids entrained with the high fluidizing gas velocity are recycled back to the bed to improve carbon conversion efficiencies as compared with just a bubbling bed. The hot product gas produced in most applications has been used for as process heat or sensible heat recovery in boilers. The use of circulating fluidized bed technology for wood waste conversion has been extensively used in the pulp and paper industry for firing lime and cement kilns and also steam raising for electricity.

2.13.1.2 PRESSURISED FLUIDIZED BED

Megaritis et al. (1998) have recently commissioned a bench scale pressurised fluidized bed reactor designed to study pyrolysis, gasification and combustion of coal or biomass at temperatures and pressures of up to 1000 °C and 40 bar respectively. Batchwise samples of up to 2 g can be injected into the reactor using air valves and a water cooled feeding probe. The feed sample is allowed to react over a fixed period before switching to a helium atmosphere and allowing the reactor to cool. The tar is collected using a wire mesh cooled with liquid nitrogen.

The results show that the total pyrolysis volatile yield from the pyrolysis of coal decreases slightly with increasing pressure. The same trend is reported by results obtained from a high pressure wire mesh reactor under the same experimental conditions. The decrease in the tar yield has been suggested to be due to the physical suppression of tar evolution (Guell and Kandiyoti, 1993). Total pyrolysis tar yield also decreased with increasing temperature, however, the absolute quantity of tars from the two reactors were different. Fluidized bed tar yields were much lower than that from the wire mesh reactor due to a higher degree of tar cracking within the fluidized bed as well as the freeboard. From gasification experiments in CO₂ atmosphere, it is reported that the increasing reactor pressure increases the total volatiles yield.

The effect of operating pressure on the composition of the gaseous products from a gasifier at 800 °C is shown below in Fig. 2.6 (Bettalgi et al. 5

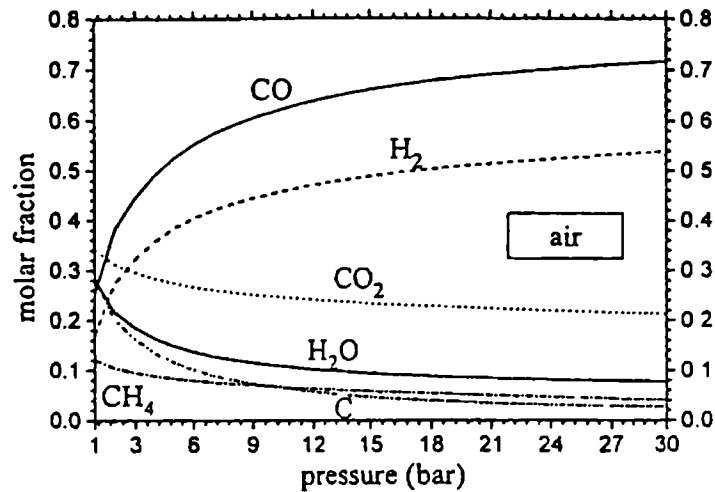


Fig. 2.6 Product gas composition as a function of gasifier operating pressure ($T = 800\text{ }^{\circ}\text{C}$).

The increasing composition of the hydrogen with pressure may be due to the longer residence times and hence longer reaction times of the higher hydrocarbons leading to an increase in the extent of thermal cracking. Operating above pressures of 5 bar does not seem to justify the costs that may be incurred since there is not much difference in the gas composition.

2.13.2 DOWN-DRAFT GASIFIER

The concurrent flow fixed-bed gasifier is suitable for small scale engine applications with dense high quality feedstock such as briquettes, hog fuel, or high quality wood chips. This gasifier permits the pyrolysis products and the gasification air to mix and react. Both pyrolysis products and oxygen are free to react with the charcoal. Thus, the pyrolysis products pass through a hot-char containing combustion zone, in which the tars are cracked thermally and oxidised (Shafizadeh, 1982). The product gas can, after particulate removal, be used as an engine fuel. Based on this gasifier, Syngas Incorporation developed commercial scale units, with low energy gases for boiler applications as a short term goal and for fuelling internal combustion engines for power generation as a long term goal (Graboski and Brogan, 1988). The feedstock for these gasifiers should meet the following requirements:

- very low moisture contents to achieve high enough temperatures in the combustion zone to crack the tars effectively.
- very low fines contents, since the fines have a tendency to increase the pressure drop of the bed, to disturb the feedstock flow, and to cause channelling in the bed.
- low ash content or high ash sintering temperatures to make it possible to use high gasification temperatures.

These requirements are seldom fulfilled by the peat and wood residues, which are available at a reasonable price.

2.13.3 ENTRAINED BED GASIFIER

The entrained flow reactor is a leading gasification alternative in large scale plants. The applicability of this reactor to air gasification of biofuels is limited by the following factors:

- biomass pretreatment to a dry pulverised feed stock is often too expensive,
- feeding of low density pulver in to a pressurised reactor is difficult,
- gasification temperatures in the order of 1100-1400 °C are realistic only in complete combustion of biomass.

The use of combustion to heat externally a tubular, entrained flow reactor was researched at the Naval Weapons Centre to pyrolyse finely ground biomass to produce gases rich in olefins. The pyrolysis gases were compressed and the olefins concentrated. The olefins were then converted to polymer gasoline in a non-catalytic process (Diebold and Smith, 1980).

2.13.4 FIXED BED UPDRAFT GASIFIER

In these gasifiers the solid particles are not free to move and mix. As fuel is consumed by drying, pyrolysis, and gasification, fresh fuel is added to the top of the bed while air enters through the bottom. This approach was developed at Georgia Institute

of Technology and commercialised by Techiar (Tatom et al., 1976). The pyrolysis gases were removed from the top of the unit and contained about 25% water insoluble tars with a 30% yield of char. If the air flow is reversed, the system converts to the downdraft process.

2.13.5 CHOICE OF GASIFIER

Each of the processes above has advantages and disadvantages. The comparative advantages are as follows:

- Fluid bed process: Fuel flexibility in terms of moisture, size and ash content. Stable operation.
- Fixed bed process: Gas composition in terms of high carbon monoxide, low carbon dioxide and nitrogen, lack of ash and grit, low temperature, valuable liquids, and consistent quality.
- Downdraft process: Products of pyrolysis pass through hot charcoal which results in most of the tars/oils being cracked or oxidised to gases.

Since the pyrolysis step contributes significantly to the quality and yield of gas than the char gasification step (Tyler, 1979), the high heating rates achieved in a fluidised bed (greater than 1000 °C/s for fine particles) makes this technology ideal for the maximisation of gas yield.

2.14 BIOMASS FEEDING

The morphological and grain structure of the biomass impose problems that must be considered in designing feeding systems. A screw feeder has been employed in many cases which has reassuring results but very important is to ensure that the particles fall away or are swept away in order to prevent blockage which can lead to serious physical deformation. On a laboratory scale, a small flow of inert gas can be used for purging which ensures that the biomass particles are freely flowing out of the feeding system. However, on a large scale commercial application, purging with an inert gas is not only uneconomical but also reduces gas efficiency. One option is to use carbon dioxide

recycled from the combustor as opposed to purchasing inert gas in bulk. Feeding systems are often a challenge for pressurised gasifiers and one disadvantage of pressurised gasification is that the cost of the feeding system can sometimes exceed that of the gasifier.

2.15 TEMPERATURE AND PRESSURE EFFECTS

ϵ_{mf} increases with temperature for fine particles and is unaffected for coarse particles and U_{mf} usually decreases with an increase in temperature (Rapagnà, 1985). A potentially serious problem at high temperature is that of sintering of particles, because when this occurs the behaviour of the fluidized bed can change drastically. Therefore it is important to ensure that the melting point of the bed particles is well above the operation temperature in the bed.

For many industrial processes that use fluidized beds, operation at atmospheric pressure is adequate. But there are a small number of applications where high pressure operation gives considerable advantage. For example coal combustion. Perhaps the major advantage is the potential reduction in plant size and hence cost that can be achieved for a given heat output.

2.16 BIOMASS TO POWER GENERATION

The gas produced from the gasification of biomass can either be used as feedstock, for example, synthesis gas, or as an energy source for industrial processes such as power generation as shown in Fig. 2.7. Proven technologies are available for the conversion of biomass to synthesis gas, however it has not been possible to achieve economic feasibility except in special cases and therefore further details of this concept shall not be discussed (Hirschfelder and Vierrath, 1999).

The concept of power generation from a gas turbine is well established. The compressed fuel gas is burnt with compressed air and the hot exhaust is fed to the gas turbine where part of the heat energy is used as work with the rest released as waste heat. The work is used to generate electricity with part of it being used to compress the

air. The addition of a heat recovery system after the turbine can increase the overall efficiency.

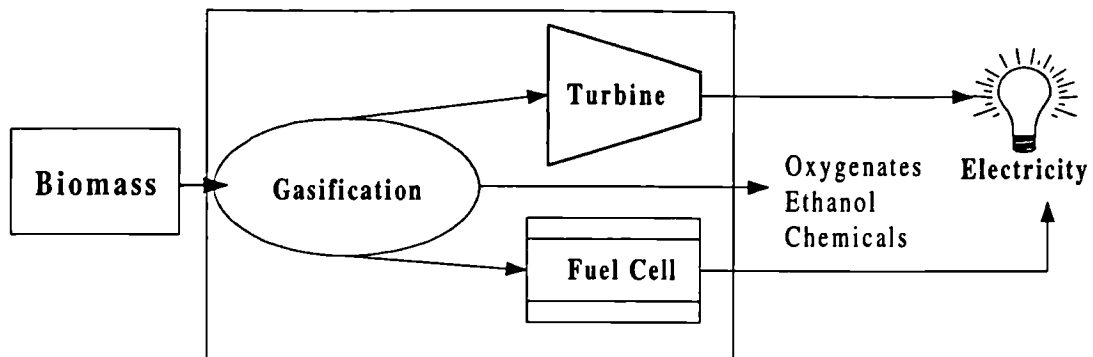


Fig. 2.7 Biomass energy conversion using pyrolysis and gasification.

The production of electrical power from the gasification of biomass coupled with fuel cells is a new and developing field. Just like any developing technology, fuel cells are costly at present, but the potential is high in terms of both energy conversion efficiency and reduction of pollution. The prime requirement for a fuel cell is a gas that has a composition of about 50%v/v of hydrogen along with some stringent limits on gaseous and particulate contaminants (see section 2.17).

Gil et al. (1998) studied the effect of the gasifying agent, namely pure air, pure steam, and a mixture of steam-oxygen, on the product distribution of pine wood chips gasification in a bubbling fluidized bed. The results are summarised in Table 2.9. A clear difference between the products yield and the type of gasifying agent can be seen from the above table. When the end use of biomass gasification is the production of electricity using gas turbines, then air can be used as the suitable gasifying agent. However, if it is intended to produce electricity using fuel cells, then steam or a mixture of steam and oxygen can be used. On the other hand, if it is required to burn some of the char produced in the gasification step in order to sustain the heat balance between the gasification and combustion section of a circulating fluidized bed, then steam seems to be the appropriate gasifying agent since it results in a higher relative production of char as compared with the other two.

Table 2.9 Product gas composition and yield from pine wood chip gasification under different gasifying agents(Gil et al., 1998).

Operating conditions	Air	Steam	Steam-O ₂
Steam/Bio. [kg/kg daf]	0.08-0.66	0.53-1.10	0.48-1.11
T [°C]	780-830	750-780	785-830
Dry gas composition [vol%]			
H ₂	5.0-16.3	38.0-56.0	13.8-31.7
CO	9.9-22.4	17.0-32.0	42.5-52.0
CO ₂	9.0-19.4	13.0-17.0	14.4-36.3
CH ₄	2.2-6.2	7.0-12.0	6.0-7.5
C ₂ H _n	0.2-3.3	2.1-2.3	2.5-3.6
N ₂	41.6-61.6	-	-
H ₂ O [wet basis]	11.0-34.0	52.0-60.0	38.0-61.0
Yields			
Gas [Nm ³ /kg bio daf]	1.25-2.45	1.30-1.60	0.86-1.142.
Tars [g/kg bio. daf]	3.7-61.9	60.0-95.0	2.2-46.0
Char [g/kg bio. daf]	-	95.0-110.0	5.0-20.0

2.17 WHAT ARE FUEL CELLS?

Fuel cells are electrochemical devices which convert the energy of a chemical reaction directly into electricity and heat. Unlike primary batteries, fuel cells store the fuel and oxidant externally, allowing continuous operation as long as the reactants are supplied to it.

A single cell consists of an electrolyte between two electrodes. Fuel is oxidised at the anode, freeing electrons to flow through an external circuit to the cathode. The circuit is completed by ions flowing across the electrolyte. Cells can be assembled as stacks and connected in series or parallel to provide the necessary voltage and output. Although fuel cells can theoretically 'run forever', degradation and malfunction of the various components limit their practical operating life. There are a number of different types of cells suitable for different types of applications:-

2.17.1 ALKALINE FUEL CELLS

These fuel cells were the first to be developed. They are relatively simple with an alkaline electrolyte and activated nickel or precious metal electrodes. The electrolyte has excellent electrochemical properties but reacts with carbon oxides which reduce performance. They run solely on pure hydrogen and oxygen at operating temperatures of around 100 °C. The removal of carbon oxides from the fuel and air supply makes the operation expensive.

2.17.2 SOLID OXIDE FUEL CELL

This fuel cell uses a solid zirconia-based electrolyte with a porous ceramic/metal complex of nickel oxide and zirconia as its anode and a lanthanum manganite doped with strontium cathode. Natural gas is the preferred fuel for most applications. It can be reformed within the cell, externally, or a combination of the two.

2.17.3 SOLID POLYMER FUEL CELLS

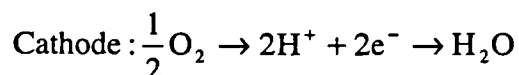
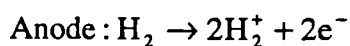
These fuel cells have a sulphonic acid electrolyte which is incorporated into a polymer membrane forming an effectively solid electrolyte. Both the cathode and the anode use platinum based catalysts. The electrolyte must be kept hydrated at all times which effectively limits the operating temperature to around 80 °C. The cell can run directly on hydrogen or reformed methanol, however, as platinum is poisoned by carbon monoxide, this must be removed during fuel processing.

2.17.4 MOLTEN CARBONATE FUEL CELLS

The operation of these fuel cells is fundamentally different from that of the others. The electrolyte is an alkaline mixture of lithium and potassium carbonates which is liquid at the operating temperature of 650 °C supported by a ceramic matrix. The operation involves net carbonate ion transfer across the electrolyte making the cell uniquely tolerant to both carbon monoxide and carbon dioxide. However the latter must be reintroduced to the cell with the oxidant. Hydrocarbon fuels including coal gas may be reformed directly at the anode.

2.17.5 PHOSPHORIC ACID FUEL CELLS

These fuel cell have been investigated extensively and developed over the last 20 years or so. They are particularly useful for use with biomass gasifiers because of their high tolerance to reformed hydrocarbons. These fuel cells employ a phosphoric acid electrolyte and a platinum or platinum - ruthenium catalyst on carbon electrodes. The operation temperature is around 200 °C and the electrodes are intolerant to carbon monoxide levels greater than 2%v/v, so fuel processing must include a shift reaction to convert it to dioxide. Sulphur and chlorine compounds must be below 1 ppm and ammonia below 0.2 ppm. Around 1% olefins and heavy hydrocarbons can be tolerated. The principle reactions occurring in phosphoric acid fuel cell are:-



The water leaves the fuel cell in the form of steam and also about 14%v/v of the total hydrogen fed leaves the modules unreacted.

2.18 CONCLUSIONS

There is a huge quantity of literature on the gasification of biomass in a bubbling fluidized bed reactor and the different steps leading to the completion of the gasification process are well covered. Biomass gasification seems to offer a lower environmental impact as compared with fossil fuels as far as gaseous emissions are concerned. However, the loss of fines by elutriation from bubbling beds obviously increases with an increase in the operating velocity and thus there is a need to provide a means of returning them back in order to prevent carbon loss and increase efficiency. The incentive at present is to use a circulating fluidized bed for the gasification of biomass and to take advantage of the return loop for it simultaneous combustion. The heat from the exothermic section can be transferred to the endothermic section, making the process thermally self supporting.

The design of the circulating bed is of crucial importance in order to acquire the

necessary heat balance along with fuel gas and flue gas separation. There are a number of different designs for achieving this (discussed in the next chapter). Moreover the emergence of fuel cell technologies for future clean power generation has paved the way for further long term goals in the development of gasifiers.

Chapter 3

3 CIRCULATING FLUIDIZED BEDS

Fluidization has come forth to be one the most important and versatile means for the contacting of gases and solids, specially in the field of catalytic cracking and combustion. A common requirement is to subject the solids to more than one process sequentially, with each process involving a different gas stream. An example of such a process is catalytic cracking, where hot activated particles catalyse the cracking of gas oil in one chamber, and the carbon produced in the cracking step is burnt in a second chamber to provide heat for the cracking step.

Similarly, a circulating fluid bed can be configured to be used as a gasifier for processing low density solids such as biomass. The fuel can be gasified in one chamber to produce gaseous products and the char formed is combusted in a separate chamber to provide the heat energy required. The heat transfer between the gasifier and the combustor is achieved by circulating hot inert solids in the combustor to the gasifier. The gas streams should not be allowed to mix so that the product gas is not diluted with nitrogen or combustion products. Such processes ideally require 'exchange of solids but not gases'. Matsen, (1988); and Basu and Frazer, (1991) give comprehensive reviews of literature on the hydrodynamics of circulating fluidized beds.

The gasification of biomass involves the conversion of solid biomass into gaseous fuels or chemical feed-stocks. A number of complex reactions occur and in order to drive these reactions, large quantities of heat input are required making the process strongly endothermic. The gasification process can be classified into two groups unique to the way the heat is supplied, namely, allothermic and autothermic processes. In allothermic processes, the heat is provided by an external, independent source of energy, for example from molten slag, to produce synthesis gas (Schilling et al., 1981). One

disadvantage of this process is that it is dependent on another heat generating process. Autothermic processes involves the generation of the heat for the endothermic reactions within the reactor. The most common way to generate heat is via the partial combustion of the fuel in a separate reactor.

A number of different designs are reported in literature for achieving simultaneous solids circulation coupled with gas separation. Kuramoto et al. (1985) developed a system for circulating fluidized solids within a single vessel intended for biomass or solid waste gasification (see Fig. 3.1). The interior of the vessel (cold model) was divided into four sections by the insertion of two flat plates intersecting at right angles. Fluidized particles were circulated between two up-flowing bubbling and two down-flowing bubble free sections. The effect of the rate of several streams of gas injected at different stages in the bed on the circulation rate of solids, pressure distribution, and residence time of foreign particles in the bed was investigated. The circulation rate of solids was controlled by regulating the velocity of the gas supplied at various levels of the bed.

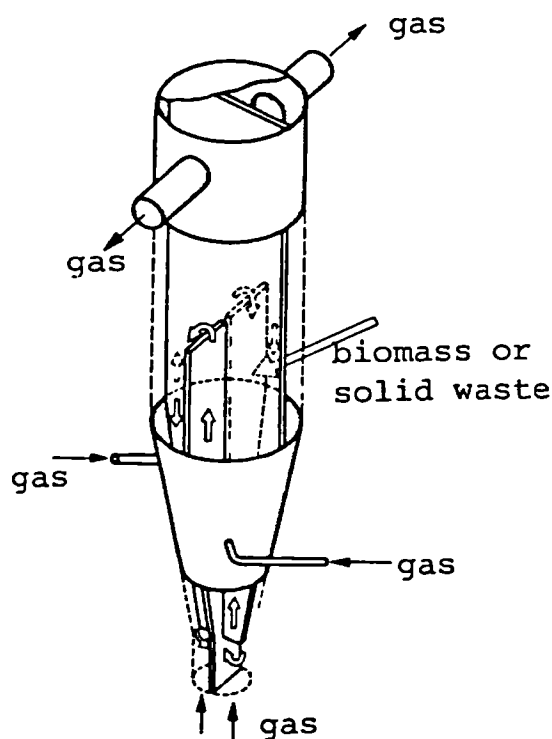


Fig. 3.1 Schematic diagram of the circulating fluidized bed for the gasification of biomass and waste Kuramoto et al. (1985).

Sathiyamoorthy and Rudolph (1991) have studied the hydrodynamics of a compartmented dense phase circulating fluidized bed. The two compartments are connected together by V-valve/riser combination which allow the circulation of solids with minimal gas exchange between the two sections. Different solids were tested and an empirical correlation has been derived to predict the solid exchange rate. It has been shown that the solids flowrate is controllable over a wide range and solids properties have an important influence on the circulation rate.

The above work is in accordance with that of Luong and Bhattacharya (1993), who investigated the effects of some operating/design parameters and non-mechanical L-valve configuration on the solid circulation rate in a 4.5 m tall, 0.15 m diameter circulating fluidized bed under cold condition. Solid circulation rate was measured by estimating the velocity of a single sand particle travelling through a clear section in the return leg. It was reported that under fixed operating conditions, the solids circulation increased by a factor of 5 upon decreasing the mean diameter of the bed particles from 500 μm to 200 μm . The experimental data were used to derive two mathematical correlations to predict solid circulation rate as a function of the operating variables.

The gasification of coal in a circulating fluidized bed containing a draft tube was studied by Judd and Rudolph (1986). Synthesis gas containing over 80% $\text{H}_2 + \text{CO}$ and a balanced CO_2 has been produced by steam gasification in the draft tube and using air in the annulus without interrupting the solids circulation rate. However, the extent of gas cross-flow between the sections has not been studied on a quantitative basis. The required level of solids circulation rate was achieved by proper adjustment of the aeration in the draft tube and in the downflowing annulus.

Salam and Gibbs (1987) developed a novel and easily controlled technique which makes use of jet pumps to circulate solids between adjacent fluidized beds at atmospheric pressure. Sand of two different mean sizes were fluidized and solid circulation rate was measured analytically using a model based on heat balance between the adjacent beds. Circulation rates of up to 220 $\text{kg/m}^2\text{s}$ have been attained. The circulation rate was shown to be dependent on the fluidizing velocity, jet pump air flow rate and position relative to the gas distributor plate and the use of baffles.

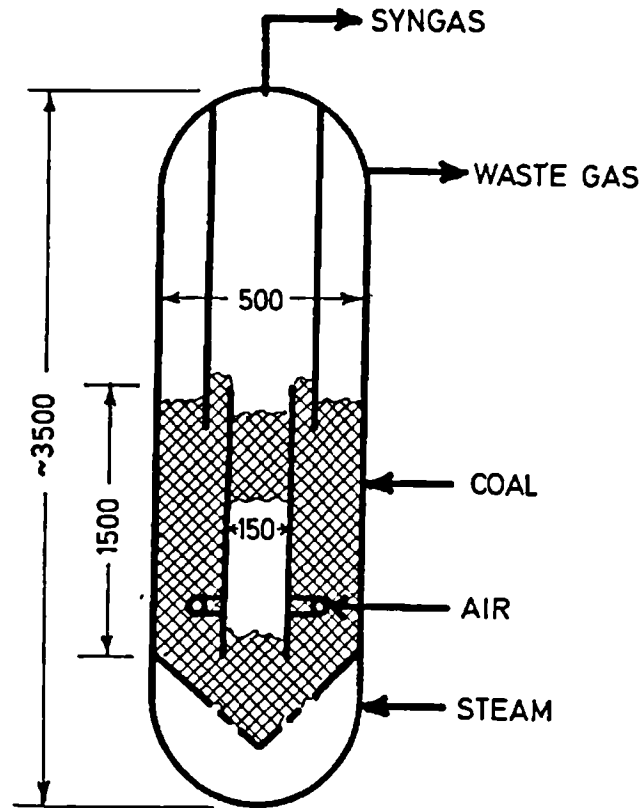


Fig. 3.2 Pilot plant circulating fluidized bed gasifier-combustor
(Judd and Rudolph, 1986).

The exchange of solids between adjacent fluidized beds was also studied by Chong et al. (1986). They developed and patented the design of a reactor system in which two fluidized beds allowed the circulation of solids but also provided an effective seal against gas mixing with no moving parts. The design (Fig. 3.3) was originally for oil shale retort, however, the system has many other potential applications. The left chamber is the combustor where the carbon remaining (about 5 %) is combusted using air. The right side chamber is the retort where combusted shale is mixed with fresh shale to provide the heat of pyrolysis.

In order to keep up the heat balance, there is a continuous circulation of solids between the two beds. By vigorously fluidizing the left hand chamber, the solids are thrown to one side and into the chute where they form a packed bed with a high local solids density. This provides the hydrostatic head for the flow of solids from left to right which in turn causes an increase in the quantity of solids in that side. In order to balance

the pressure drop between the two sides, the solids flow in the reverse direction through the opening immediate to the distributor.

Image removed due to third party copyright

Fig. 3.3 Side view of the oil shale retort circulating fluidized bed (Chong et al., 1986).

Battelle Memorial Laboratory has been developing an indirectly heated biomass gasification process, called the Battelle High Throughput Gasification Process. A 10,000 kg/day has been operating since 1980 (Paisely and Overend, 1994). This process produces a medium-Btu gas without using air or oxygen in the gasification step. The process uses two separate reactors, a gasification reactor in which biomass is converted into a medium Btu gas and residual char, and a combustion reactor that burns the residual char to heat sand which is recycled back to the gasifier to provide the heat for gasification.

3.1 SOLIDS CIRCULATION RATE

An important aspect of circulating systems is the ability to control the solid circulation rate. One of the important factors which control the circulation rate of solids is the superficial gas velocity in the bed since this directly determines the flow regime and density of the bed. Alternatively, the geometrical configuration of the system specially at the point where solids change direction of flow. It is interesting to note that

all circulating systems regardless of their application can be characterised either by the solid circulation rate, kg/s (or on a more representative basis by the solid circulation flux, kg/m²s) and the transfer ratio (weight of solid/weight of transporting gas) of the suspended material being exchanged between vessels. Circulation models for some of the above systems are available in literature for example, with draft tubes (Lanauze, 1976; Bolton and Davidson, 1987) and partition valves (Fox et al., 1989).

3.2 GAS MIXING

Within a circulating bed, the gas from one section, for example the riser, always inevitably flows into another section. The gas bypassing phenomena have been found by a number of authors (Kehlenbeck and Yates, 2000) and appears to be initiated by the circulation of solids and its extent depends very much on the geometry of the communication zone between two sections. Although it is impossible to prevent gas bypassing, it is important to appreciate, even approximately, the way in which it varies with operating conditions. This can be achieved by the use of pressure field measurements or by injection of a tracer gas. Appropriate design of the communication zone also has a tremendous effect on gas mixing. This phenomena is very important for specific applications of circulating fluidized beds, such as production of a high calorific value gas from biomass gasification. In order to obtain the high purity required, it is essential that the gaseous products from the combustion zone is prevented from entering the gasification zone.

3.3 SOLIDS RESIDENCE TIME

Although there is an abundant literature on the circulation rate of solids in a circulating fluidized bed, much less attention has been paid to the residence time of foreign particles introduced into the system. Danckwerts (1953) introduced the concept of the residence time distribution (RTD) as a statistical means of describing the time taken for various elements of fluid flow through a vessel. If these fluid elements have stayed in the vessel for time θ , then they are said to be of age θ and the fraction of fluid at that has an age between θ and $(\theta+\delta\theta)$ can be obtained at any point from the RTD.

Kuramoto et al. (1985) investigated the residence time of three different types of materials in their circulating fluidized bed. They found that those particles that had a density lower than the bulk density of the fluidized bed did not circulate through the circulating system and attributed this to the increased segregation around the minimum fluidization velocity and thus light solids had difficulty sinking in the downcomer. However, those particles with densities close to the bulk fluidized bed density did circulate. Relatively large wood cubes (8 mm) were also found to circulate but with a significantly long residence time.

3.4 CONCLUSIONS

The literature addresses that a simple theoretical model to predict gas bypassing accurately taking account of all the operating parameters can not be developed. Although numerous correlations and solid circulation models have been derive for different circulating systems, application of one model to two different systems have not been successful.

Chapter 4

4 DESIGN OF EXPERIMENTAL EQUIPMENT

The first part of this section reports the design of the cold model circulating fluidized bed and the second part focuses on the design and development of the heated fluidized bed gasifier and its auxiliary equipment.

4.1 DESCRIPTION OF THE CIRCULATING FLUIDIZED BED AND PILOT PLANT

The design of the circulating fluidized bed is based on the principle that the char produced in the gasifier is circulated with the bed material and combusted in a separate reactor to generate the heat required for the gasification process as shown in Fig. 4.1.

Ideally, the feed material biomass, is fed into the top fluidized bed (gasifier, bed 2) where it is gasified using steam supplied via windbox 2. The char remaining together with some bed material overflow and descend in an annular downcomer surrounding the gasifier into a return leg fitted with an L-valve. Here the solids, being fluidized by steam, are forced into the bottom bed (combustor, bed 1) where the carbonaceous material from the gasifier is burnt using air as the fluidizing medium. This has the potential to provide much of the heat energy required for the gasification process which is highly endothermic.

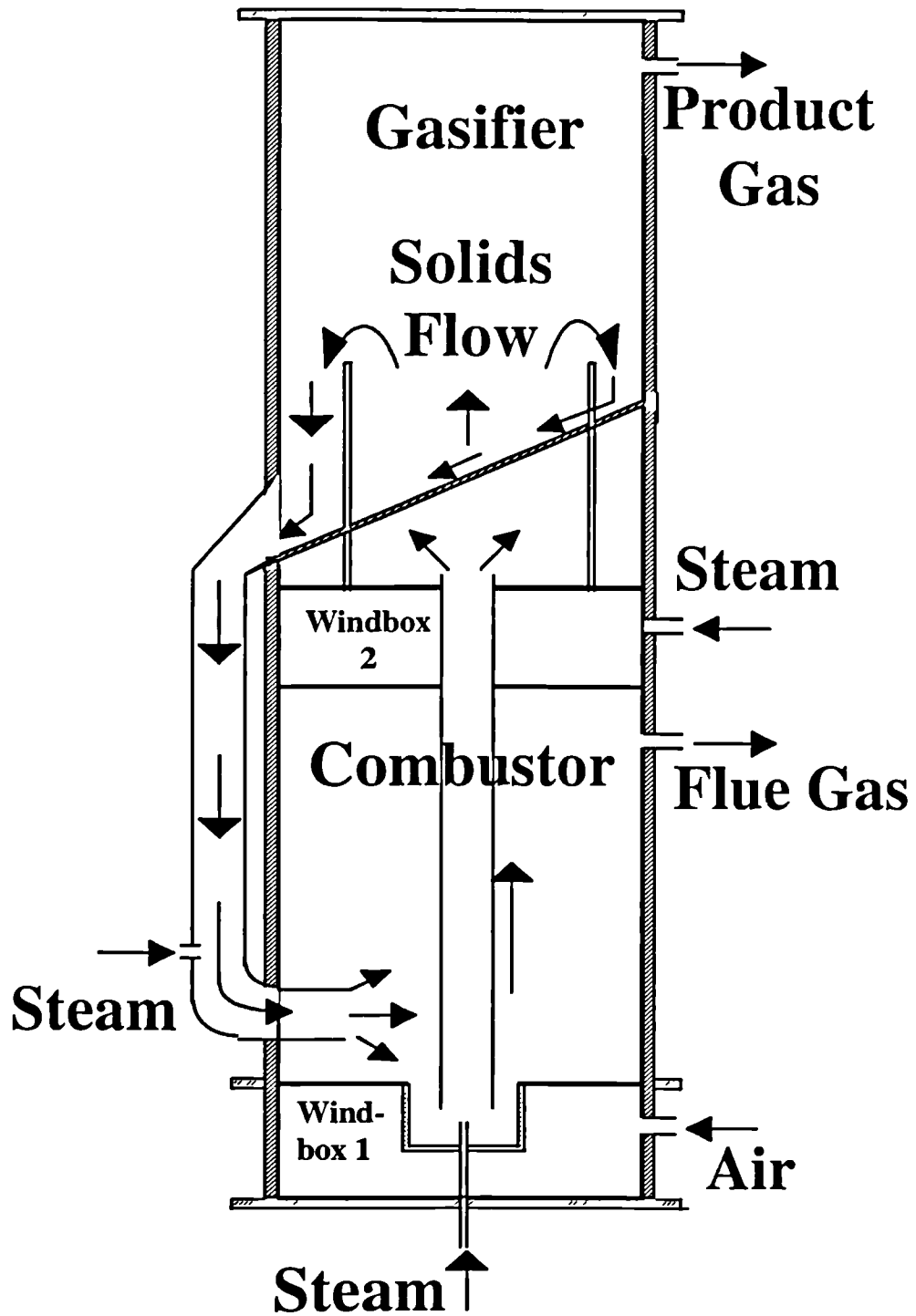


Fig. 4.1 Configuration of the circulating fluidized bed system.

The combustion of the char heats up the inert solids which are then quenched at the inlet of the riser by the steam. The steam also carries the heated particles pneumatically up the riser, in a dilute phase or slugging type transport, back to the gasifier and the cycle repeats again. This way, the product gas contamination by the flue gases can also be kept to a minimum by having separate outlets. Following suitable downstream cleaning, the hydrogen-rich gas from the gasifier can be fed directly into a fuel cell for the generation of electric power.

The cold model circulating fluidized bed is a smaller version ($\approx 1/6$) of a pilot scale unit intended to produce hydrogen - rich gas for feeding to a fuel cell for the generation of electricity on a small scale in a rural area. Simulation of the pilot plant shows that a biomass feed rate of 686 kg/hr (550 kg/hr daf) and a circulation rate of 12,000 kg/hr is required (800 kW_e) in order to make the system thermally self-supporting. Table 4.1 shows the stream table for the process and the corresponding theoretical energy balance is shown in Fig. 4.2.

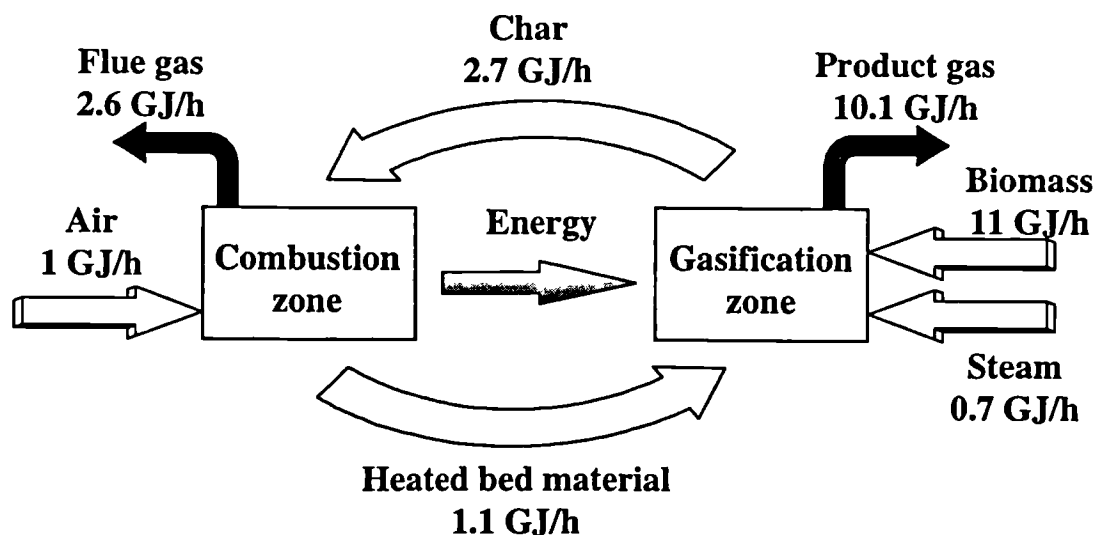


Fig. 4.2 Principle of biomass combustion-gasification process.

The composition of different forms of biomass (*Mischantus*, *Arundo donax*, *Cynara cardunculus*) is not very sensitive to the biomass type. It has been shown that their composition (dry ash free basis) is 51% carbon, 6% hydrogen, 43% oxygen and a moisture content of about 20% of the total weight (Di Felice and Yates, 1996).

Table 4.1 Stream table for the fluidized bed gasifier.

GASIFIER				
Stream	Biomass	Steam	Product gas	Char
Composition	280 kg C 33 kg H 236 kg O 137 kg H ₂ O (l)	303 kg H ₂ O (g)	27 kg H ₂ 33 kg CH ₄ 146 kg CO 301 kg CO ₂ 27 kg Tars 378 kg H ₂ O	82 kg C
Mass flow	686 kg/hr	303 kg/hr	912 kg/hr	82 kg/hr
Temperature	25 °C	750 °C	828 °C	800 °C
COMBUSTOR				
Stream	Air	Flue gas	Bed material	
Composition	340 kg O ₂ 1190 kg N ₂	1017 kg CO ₂ 44 kg O ₂ 1190 kg N ₂ 109 kg H ₂ O	Sand	
Mass flow, kg/hr	1530 kg/hr	2360 kg/hr	12,000 kg/hr	
Temperature	642 °C	986 °C	986 °C	

A preliminary flow diagram of the 800kW_e biomass gasification plant is shown in Fig. 4.3. To meet the purity constraint of the fuel cell module (phosphoric acid fuel cell), the following gas cleaning treatments are necessary

- a cyclone and ceramic candle filter to remove elutriated particulates.
- a fixed bed catalytic reactor to convert all of the methane to hydrogen and eliminate the tars fraction.
- gas de-sulphurisation with zinc oxide and a two stage water shift reactor to convert carbon monoxide to hydrogen and carbon dioxide and wet scrubbing to removed ammonia and hydrogen chloride.

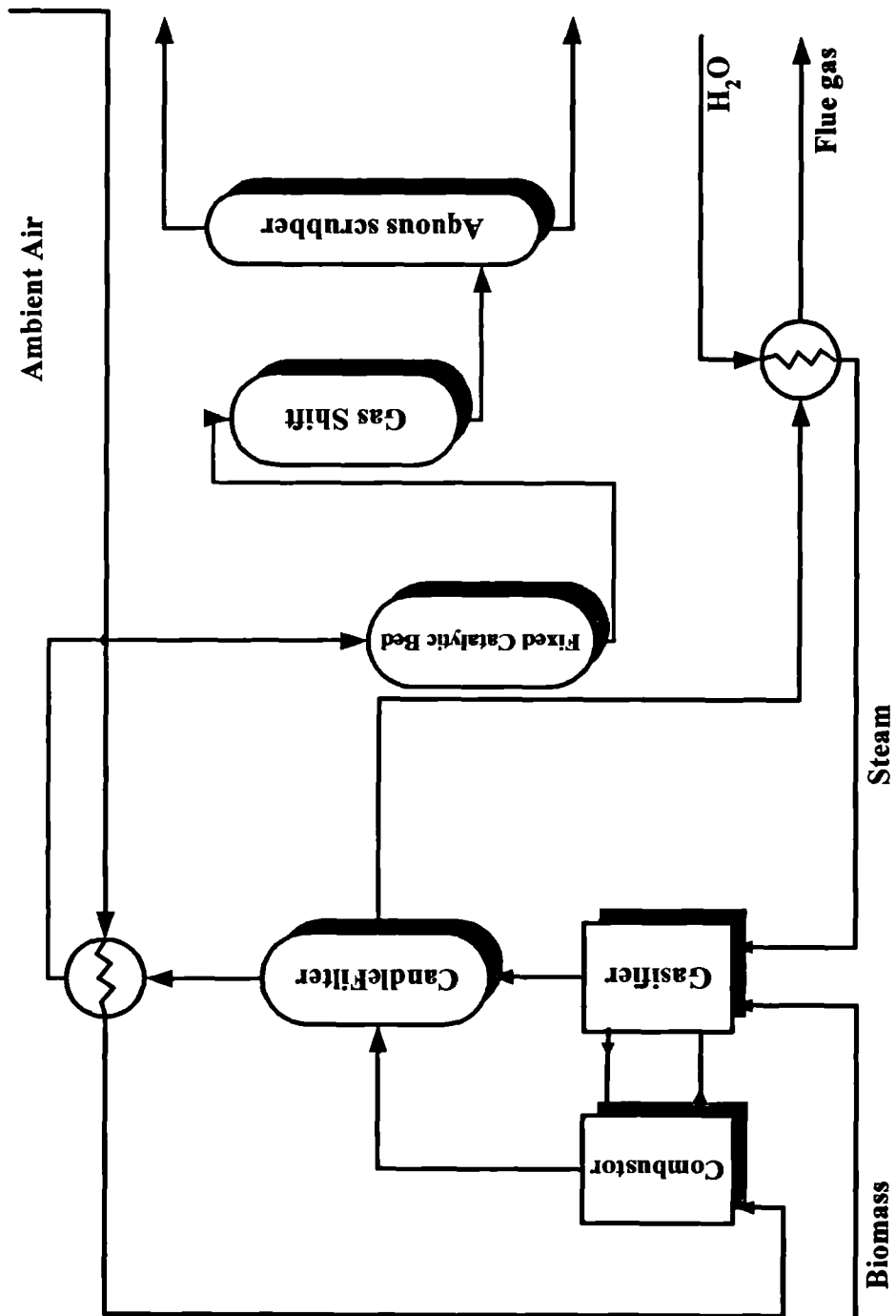


Fig. 4.3 Flow sheet of the biomass combustion - gasification plant.

27

4.2 DESIGN OF THE COLD MODEL DUAL BED CIRCULATING SYSTEM

The configuration of the cold model dual bed system proposed for the simultaneous combustion - gasification of biomass is similar to that shown in Fig. 4.1 The design simply consists of circulating solids between two fluidized bed units. The cold model dual bed is made of cast perspex with bed 1 (0.21 m diam. and 0.6 m high) and bed 2 (0.17 m diam. and 1.2 m high) connected together via a riser and a downcomer fitted with a non-mechanical valve. The riser and the downcomer both have a diameter of 0.05 m. The distance of the air jet from the riser could be varied in the vertical direction in order to determine the optimal position.

The major parts of the CFB system can be identified as the non-mechanical valve, the gas distributor, and the gas-solid separators. This section focuses on the design of the non-mechanical valve and the gas distributor.

4.3 WINDBOX DESIGN

The function of the plenum or the windbox is to distribute the gas under the distributor as uniformly as possible. Analysis of the chamber under the distributor plate involves a complicated three dimensional flow (Litz, 1972). The situation is simplified by making the chamber large enough to accommodate acceleration effects. Even if there is enough chamber volume for pressures to equalise, the feed nozzle must be positioned very carefully. The gas stream nozzle can enter the gas chamber either horizontally or vertically. For horizontal entry into a vertical vessel, the high velocity gas stream expands until:

1. it hits the opposite wall;
2. it dissipates itself at about 100 times nozzle diameter (Perry, 1997)
3. the upper edge hits the base of the distributor plate causing mal-distribution.

In the third case, the distributor plate should be placed at a distance H_w , above the gas nozzle in order to prevent mal-distribution. Therefore:

$$H_w = 0.2 \times D_w + 0.5 \times D_{noz} \quad \text{For } D_{noz} > \frac{D_w}{100} \quad (4.1)$$

$$H_w = 18 \times D_{noz} \quad \text{For } D_{noz} < \frac{D_w}{100} \quad (4.2)$$

For vertical entry into a vertical vessel through a nozzle centred at the bottom head, the high velocity gas stream expands until:

1. the diameter of the gas jet coincides with the vessel diameter;
2. it dissipates itself;
3. causes mal-distribution by hitting the central portion of the distributor plate.

To prevent mal-distribution, the nozzle should be placed at a distance H_w below the distributor plate, where H_w is given by:

$$H_w = 3 \times (D_w - D_{noz}) \quad \text{For } D_{noz} > \frac{D_w}{36} \quad (4.3)$$

$$H_w = 100 \times D_{noz} \quad \text{For } D_{noz} < \frac{D_w}{36} \quad (4.4)$$

High pressure drops also prevent plugging of the distributor holes (Richardson, 1963). Further details are available from Zenz (1989).

4.3.1 BED 1 AND WINDBOX DESIGN

The wind box is separated into two sections; the inner 10 cm diameter is a blank void to accommodate the riser and the riser air jet. Air supplied by a horizontal pipe ($D_{noz} = 20$ mm) to the side of the vertical vessel with an internal diameter of 210 mm.

$$D_{\text{noz}} = 20 \text{ mm}$$

$$D_w = 210 \text{ mm}$$

$$\frac{D_w}{100} \approx 2 \text{ mm}$$

$$D_{\text{noz}} > \frac{D_w}{100}$$

Using Equation (4.1)

$$\begin{aligned} H_w &= 0.2 \times D_w + 0.5 \times D_{\text{noz}} \\ &= 0.2 \times (210) + 0.5 \times (20) \\ &\approx 50 \text{ mm} \end{aligned}$$

The total height of the windbox (H_{w1}) should be around three times H_w .

$$\begin{aligned} H_{w1} &= 3 * 50 \\ &= \underline{\underline{150 \text{ mm}}} \end{aligned}$$

Fig. 4.4 shows a schematic diagram of the windbox and its dimensions. Bed 1 dimensions are shown in Fig. 4.5.

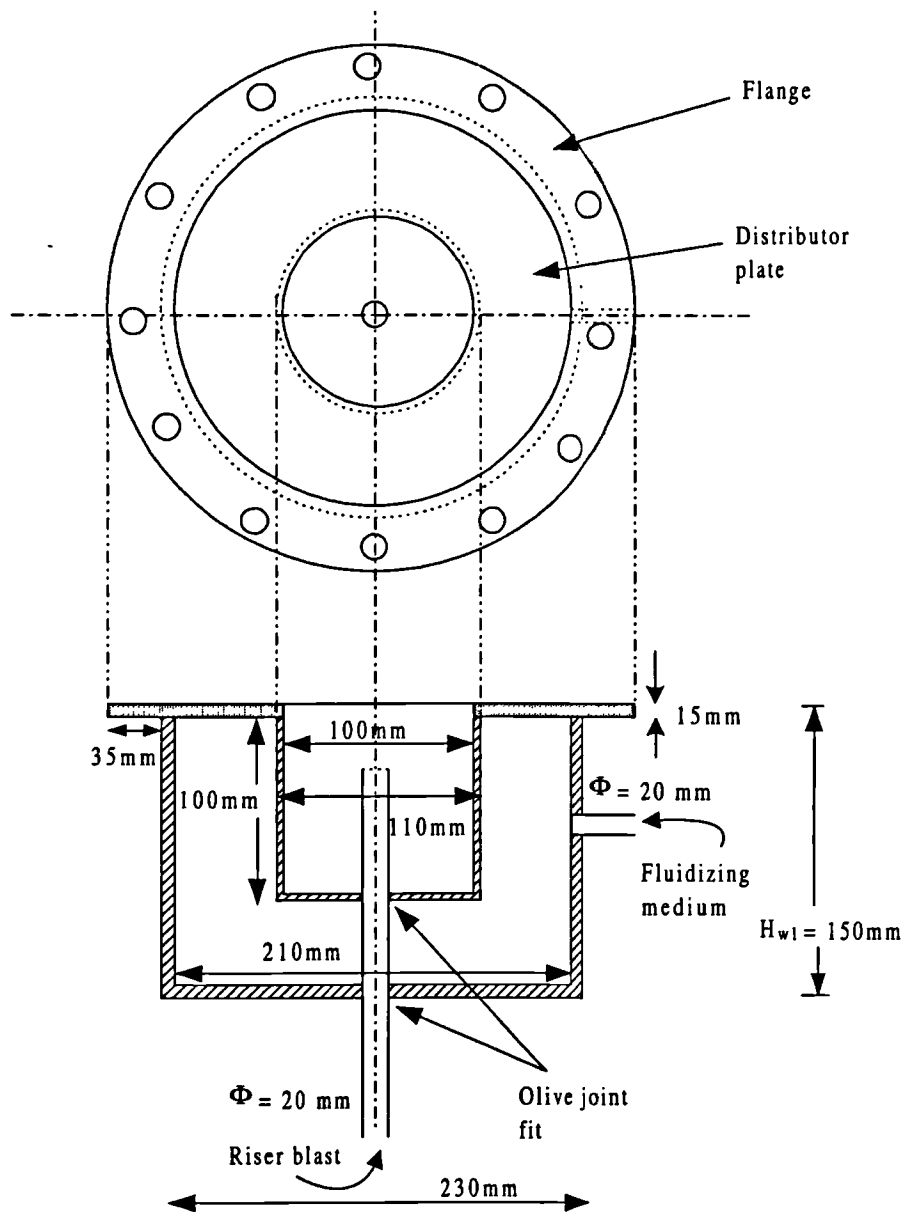


Fig. 4.4 Schematics and dimensions of windbox for bed 1 (not to scale).

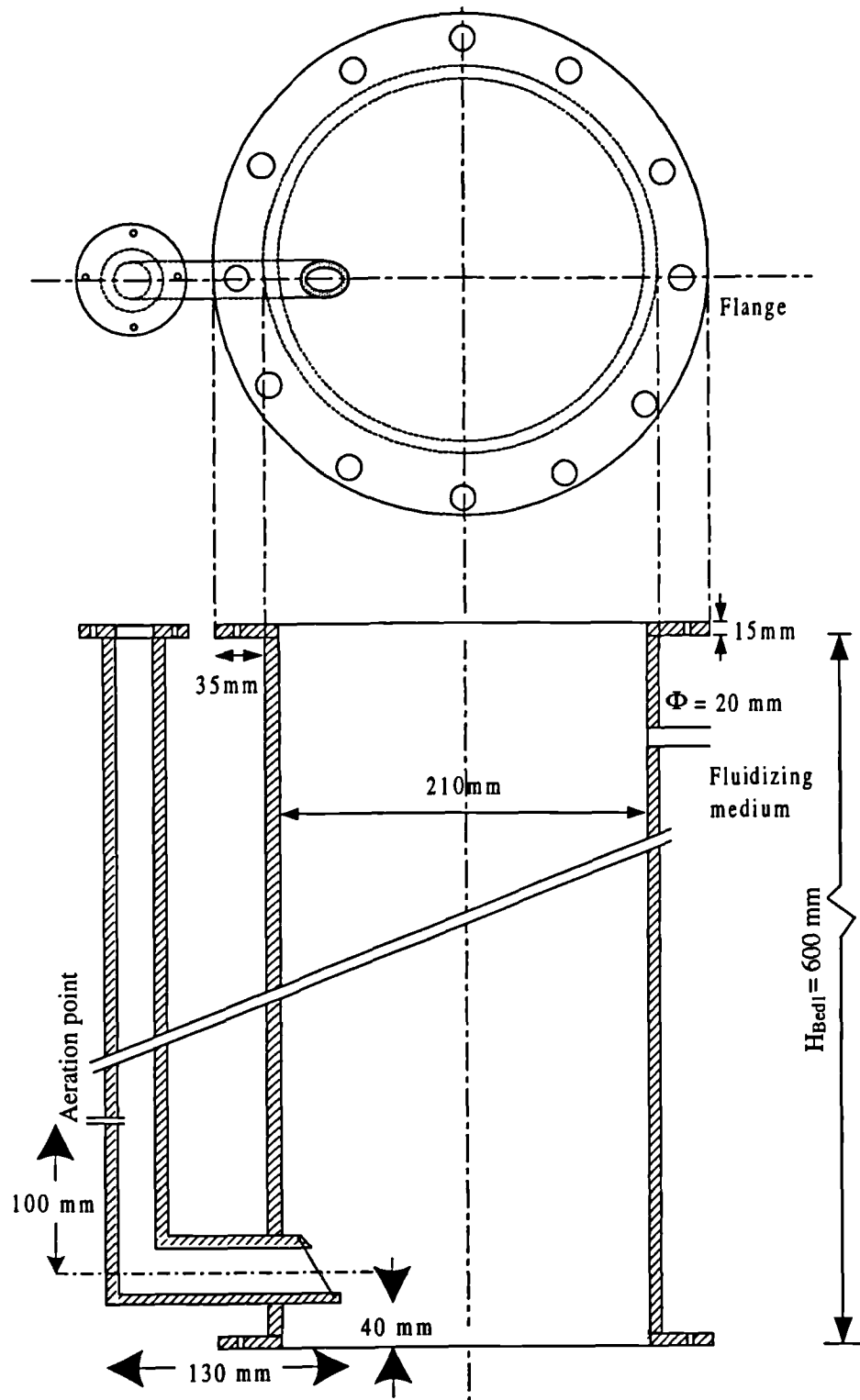


Fig. 4.5 Bed 1 dimensions (not to scale).

4.3.2 BED 2 AND WINDBOX DESIGN

The second windbox has a cross sectional area smaller than the first corresponding to 170 mm internal diameter. The air is supplied by vertical pipe ($D_{noz} = 20$ mm) to the bottom of vertical vessel.

$$D_{noz} = 20 \text{ mm}$$

$$D_w = 170 \text{ mm}$$

$$\frac{D_w}{100} = 1.7 \text{ mm}$$

$$D_{noz} \propto \frac{D_w}{100}$$

Using Equation (4.1)

$$\begin{aligned} H_w &= 0.2 \times D_w + 0.5 \times D_{noz} \\ &= 0.2 \times (170) + 0.5 \times (20) \\ &\approx 45 \text{ mm} \end{aligned}$$

The total height of the windbox (H_{w2}) should be around three times H_w .

$$\begin{aligned} H_{w2} &= 3 * 45 \\ &= \underline{\underline{135 \text{ mm}}} \end{aligned}$$

The dimensions for the windbox and bed 2 are shown in Fig. 4.6 and Fig. 4.7 respectively.

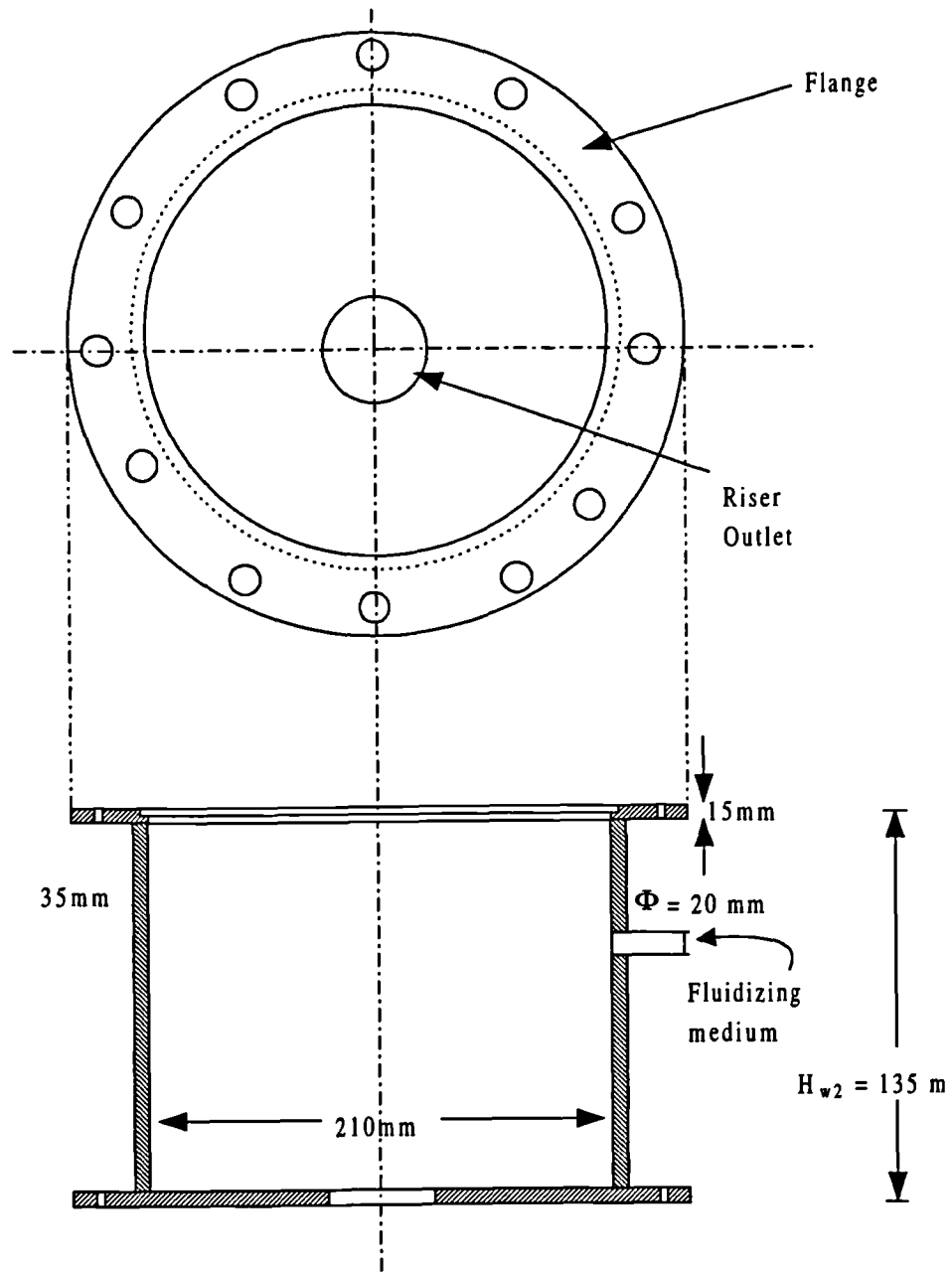


Fig. 4.6 Schematics and dimensions of windbox for bed 2 (not to scale).

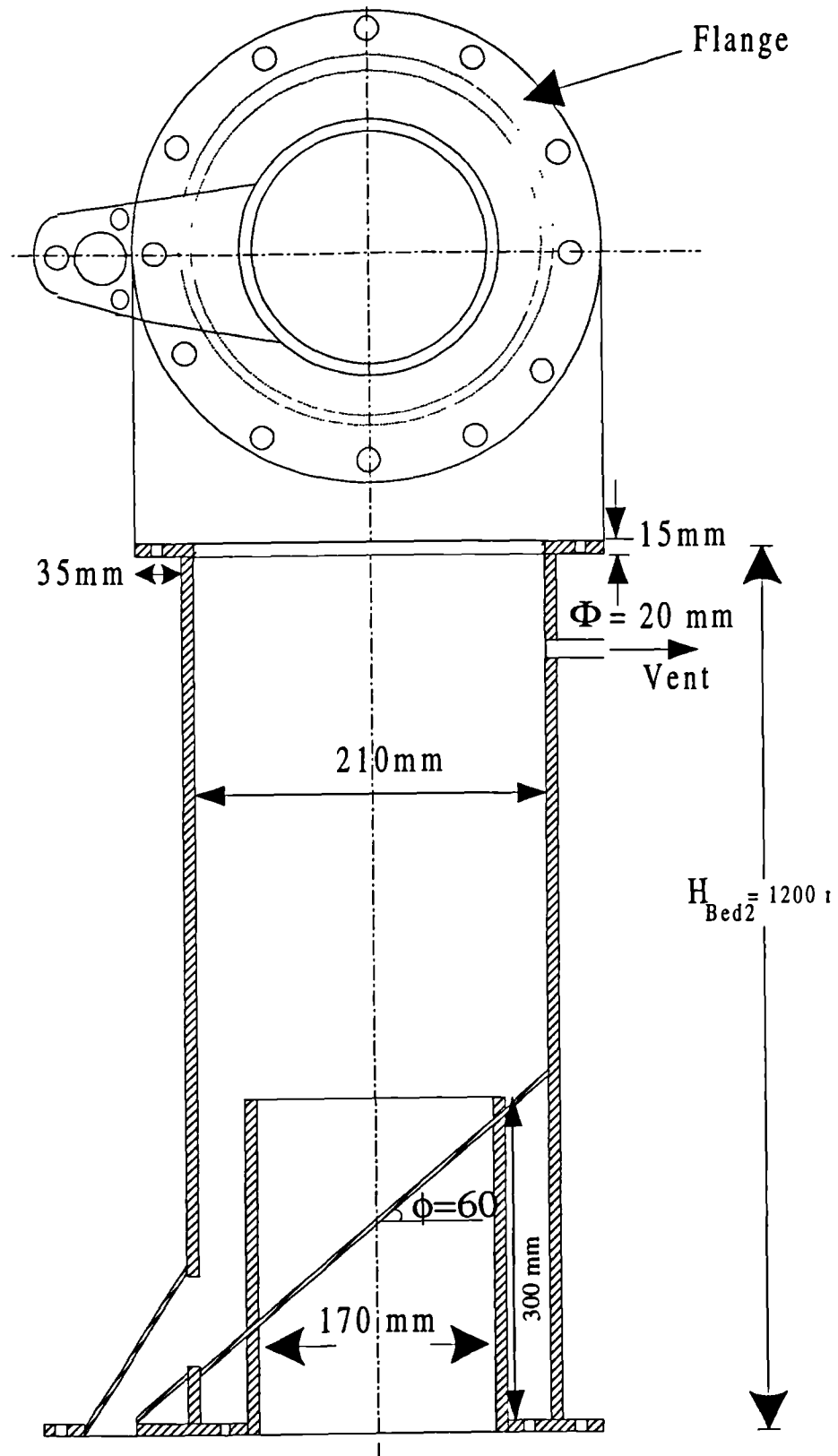


Fig. 4.7 Dimensions of bed 2 (not to scale).

4.4 GAS DISTRIBUTOR PLATE

The ultimate function of the distributor plate is to distribute the fluidizing gas uniformly over the cross-section of the bed and also to support the weight of the defluidized bed. Distributor types range from the simple porous plate (Zenz, 1968) to the ball type (Hengl et al., 1977) and to the special purpose distributor (Korenberg, 1982).

The distributor plate has a strong influence on the size and frequency of the bubbles in a fluidized bed. The size of the bubbles in the bed are the major cause of particle circulation. The desired properties of a good distributor may be listed as implied by Botterill (1975), Whitehead (1971), and Zuiderweg (1967):

- 1) stable and uniform gas distribution over the range of operation.
- 2) minimise solid attrition.
- 3) avoid solid back flow in to the air chamber (chocking).
- 4) minimise solid erosion.
- 5) eliminate or reduce dead zones on the distributor plate.

4.4.1 DESIGN CRITERIA

The essential requirement for stable operation is that the pressure drop across the distributor ΔP_D , is sufficiently large. If this pressure drop is too low, the result is poor fluidization. In this case, either some parts of the bed receive less gas than other parts which may become temporarily or permanently de-fluidized, or during operation, an area of the bed de-fluidizes so blocking that discharge area.

Critically, the pressure drop across the distributor plate, for satisfactory operation, should be around 0.1 to 0.3 times the pressure drop across the fluidized bed, ΔP_B as recommended by Agarwal et al. (1962) and Hanway (1970), with 0.3 as a widely quoted value (Zenz, 1968). However, successful operation of some fluidized beds has been reported at much lower values of $\Delta P_D/\Delta P_B$ (Zuiderweg, 1967; Whitehead, 1971). Extensive

review of literature on gas distributors for gas fluidized beds, and principles of design and equations for various types of gas distributors are presented by Basu (1984); Chatterjee and Shankar (1982); and Geldart and Baeyens (1985).

4.4.2 POROUS DISTRIBUTOR PLATE DESIGN

On a laboratory scale, the porous sintered plates are often used as distributor plates. These type of distributors can operate satisfactorily over a wide range of operating conditions (gas velocities) than can other types of gas distributors. Flow rates through sintered materials are proportional to the applied pressure until the onset of turbulence, at which point they become more restrictive to flow. The equation of Darcy expresses the relationship between the variables up to the limit of proportionality as

$$\Delta P_D = \frac{Q_g \times \mu_g \times t_p}{\Phi_D \times A_p} \quad (4.5)$$

Where

ΔP_D = Pressure drop across distributor plate (dynes / cm²)

Φ_D = Permeability of plate material (cm²)

μ_g = Gas viscosity (Poise)

t_p = Plate thickness (cm)

Q_g = Gas flow Rate (cm³ / sec)

A_p = Plate area (cm²)

Having evaluated the distributor pressure drop, Equation (4.5) is used to calculate the permeability of the plate required to give the pressure drop, from which the grade of the distributor plate can be obtained from Table 4.1.

Table 4.1 Relationship between the permeability and grade of porous distributor plates.

Grade	Pore size distribution			Permeability Darcies x 10 ⁻⁸	Density g/cm ³	Minimum Thickness	Porosity (%)	
	Min.	Mean	Max.				Solid	Void
B 05	0.75	2	9	1.0	6.0 - 7.5	1.5 mm	75	25
B 10	2.50	6	25	2.5	6.0 - 7.0	2.0	70	30
B 20	7.50	20	85	7.0	5.0 - 6.0	2.5	60	40
B 30	10.0	35	150	30	5.0 - 6.0	3.0	60	40
B 40	15.0	50	250	90	5.0 - 6.0	3.5	60	40
B 50	20.0	75	320	150	4.5 - 5.5	4.0	55	45

Bronze 89/11 (max operating temp. = 300°C)

4.4.2.1 DESIGN OF BED 1 DISTRIBUTOR

Table 4.2 Data at operating conditions.

Temperature, T	20 °C	U_{mf}	0.026 m/s
Pressure, P	1 Bar	Angle of repose	37°
Gas Viscosity, μ_g	1.81E-5 Ns/m ³	Bed voidage@ U_{mf} , ϵ_{mf}	0.44
Gas Density, ρ_g	1.22 kg/m ³	Sphericity, ϕ	0.6
Particle Density, ρ_s	2622 kg/m ³	Bed 1 Height@ U_{mf} , H_{mf1}	0.33 m
Mean Particle Size, d_p	1.64E-4 m	Bed 2 Height@ U_{mf} , H_{mf2}	0.33 m

The pressure drop across the fluidized bed is calculated using the expression below (Davidson and Harrison, 1971)

$$\Delta P_B (\text{N/m}^2) = (\rho_s - \rho_g) \times (1 - \epsilon) \times g \times H_{mf} \quad (4.6)$$

$$\begin{aligned} \Delta P_{B1} &= (2622 - 1.22) \times (1 - 0.44) \times 9.81 \times 0.33 \\ &= 4751 \text{ N/m}^2 \\ &= 485 \text{ mm H}_2\text{O} \end{aligned}$$

The pressure drop across the distributor plate is set to one third that across the bed,

$$\begin{aligned}\Delta P_D &= 0.3 * \Delta P_B \\ &= 0.3 * 485 \\ &= 146 \text{ mmH}_2\text{O}\end{aligned}$$

Bed diameter = 0.21 m

Flow at $4 \times U_{mf} = 4 \times 54 = 216 \text{ l/min} = 3600 \text{ cm}^3 / \text{s}$

$$\Delta P_D = 146 \times 98.067 = 14318 \text{ dynes / cm}^2$$

Using Equation (4.5)

$$\Delta P_D = 14318 \text{ dynes / cm}^2$$

$$\mu_g = 1.81 * 10^{-4} \text{ Poise}$$

$$t_p = 0.5 \text{ cm}$$

$$Q_g = 3600 \text{ cm}^3 / \text{sec}$$

$$A_p = 1070.34 \text{ cm}^2$$

$$\begin{aligned}\Phi_D &= \frac{Q_g \times \mu_g \times t_p}{\Delta P_D \times A_p} \\ &= \frac{3600 \times 1.81 \times 10^{-4} \times 0.5}{14318 \times 1070.34} \\ &= 2.13 \times 10^{-8} \text{ cm}^2\end{aligned}$$

Therefore, from Table 4.1, the distributor plate to give approximately the same pressure drop is Grade 10. The dimensions of the distributor plate is shown in Fig. 4.8.

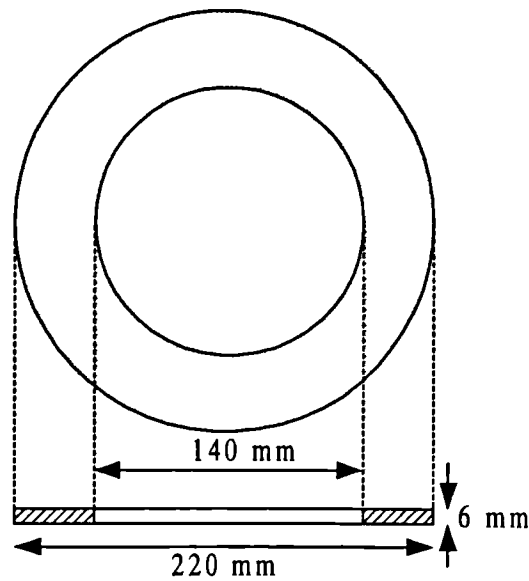


Fig. 4.8 Dimensions of bed 1 gas distributor plate.

4.4.2.2 DESIGN OF BED 2 DISTRIBUTOR

$$\begin{aligned}\Delta P_{B2} &= (2622 - 1.22) \times (1 - 0.44) \times 9.81 \times 0.33 \\ &= 4751 \text{ N / m}^2 \\ &= 485 \text{ mm H}_2\text{O}\end{aligned}$$

Bed diameter = 0.17 m

Flow at $4 \times U_{mf} = 4 \times 35.5 = 142 \text{ l / min} = 2366.67 \text{ cm}^3 / \text{s}$

$$\Delta P_D = 146 \times 98.067 = 14318 \text{ dynes / cm}^2$$

Using Equation (4.5)

$$\Delta P_D = 14318 \text{ dynes / cm}^2$$

$$\mu_g = 1.81 \times 10^{-4} \text{ Poise}$$

$$t_p = 0.5 \text{ cm}$$

$$Q_g = 2366.67 \text{ cm}^3 / \text{sec}$$

$$A_p = 207.24 \text{ cm}^2$$

$$\begin{aligned}\Phi_D &= \frac{Q_g \times \mu_g \times t_p}{\Delta P_D \times A_p} \\ &= \frac{2366.67 \times 1.81 \times 10^{-4} \times 0.5}{14318 \times 207.24} \\ &= 7.23 \times 10^{-8} \text{ cm}^2\end{aligned}$$

Again, from Table 4.1, the distributor plate to give approximately the same pressure drop is Grade 20. Fig. 4.9 shows a schematic diagram and size of the distributor plate for bed 2.

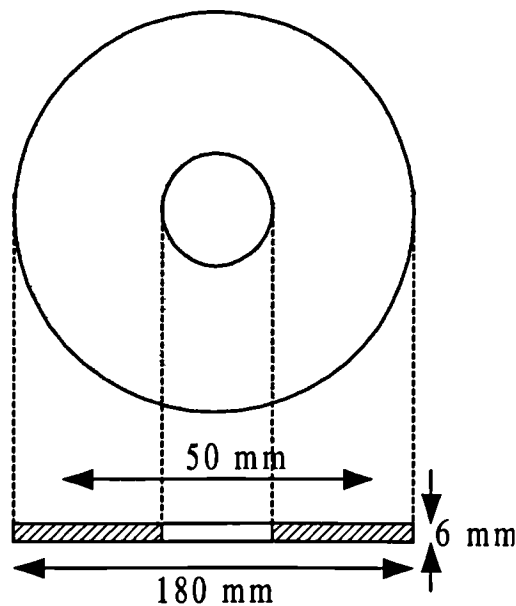


Fig. 4.9 Dimensions of bed 2 gas distributor plate.

4.4.3 SEALING OF THE DISTRIBUTOR

A common problem encountered in many fluidized beds is the leakage around the distributor plate which causes non-uniform fluidization. This is severe if the distributor plate is subjected to heating during start-up and cooling during shut-down. Considerable thermal stress develops on the distributor plate. The result is warping which destroys even the best seal. Basu (1984) reports some methods of sealing and avoiding leakage in

bubbling fluidized beds. For laboratory scale cold beds ($D_B < 1.0$ m), the leakage is easily controlled by the use of a gasket and uniform tightening of the bolts on the flanges. Fig. 4.10 shows the attachment of the distributor to the windbox for bed 1. The same arrangement is used for bed 2.

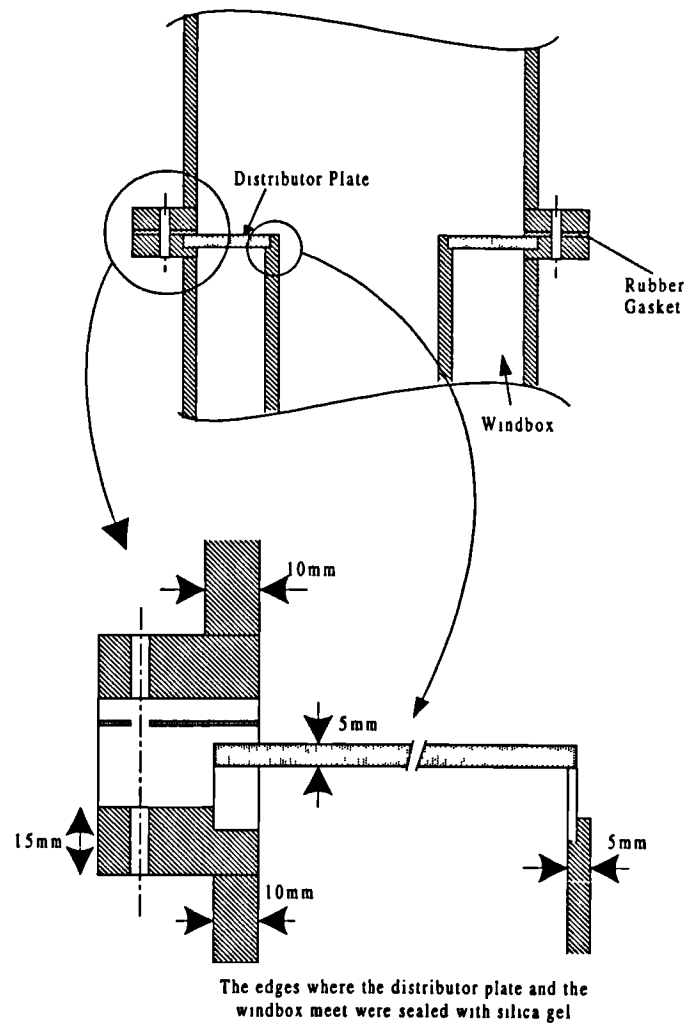


Fig. 4.10 Attachment of gas distributor plate to windbox for bed 1.

4.5 PARTICULATE FILTER

In order to prevent sand particles being ejected outside bed 2 by the high velocity gas stream during operation, a filter was made of a metal ring and wire gauze placed on top of bed 2. This allowed the passage of the air but prevented sand particles from escaping the bed.

4.6 NON-MECHANICAL VALVES

The movement of solids in non-mechanical valves is principally induced by air added at a short distance above the exit of the valve. However, a threshold amount of aeration is required after which solids flow commences and increases upon additional aeration to the valve. These are devices which use only a relative amount of aeration gas to control the flow of particulate solids through them. Non-mechanical valves work best with Group B particles ($>150\mu\text{m}$). Non-mechanical valves have a number of advantages over mechanical valves:

- They are inexpensive and are constructed out of simple piping and fittings
- There are no moving parts that would be subjected to wear and tear
- Solid flow can be direct into either a dense or dilute phase environment, for example into a fluidized bed or pneumatic conveying line.

Fig. 4.11 shows some controllable non-mechanical valves which are used to recycle, as well as control, the solid recycle rate. Fig. 4.11b shows a diagram of a V-valve in more detail.

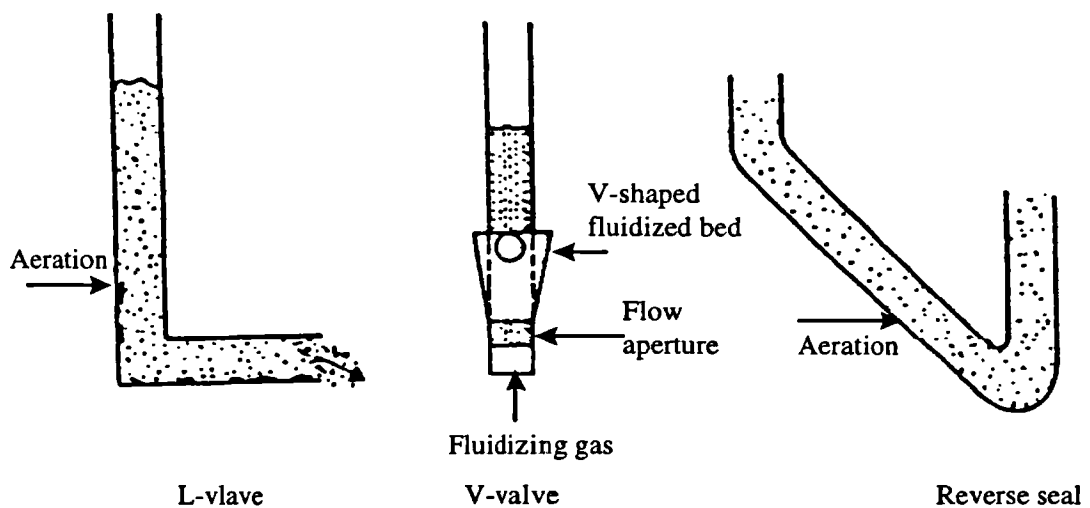


Fig. 4.11 Schematics of some non-mechanical valves; L-valve (Knowlton et al., 1978), V-valve (Leung, 1987; Chong et al., 1988), Seal leg system (Hill, 1987).

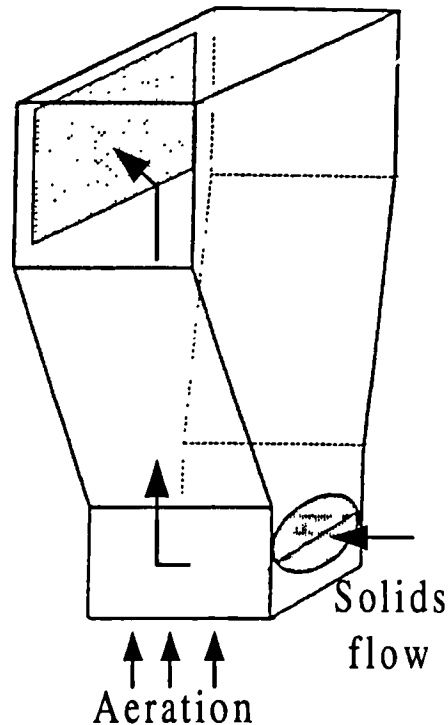


Fig. 4.11a Gas and solids flow through a V-valve.

4.6.1 AERATION TAP LOCATION

The aeration point is one of the most important parameters that controls the flow of solids through the non-mechanical valve. Ideally, the addition of air to the valve as low a position as possible in the standpipe results in a minimum non-mechanical valve pressure drop and maximum standpipe length, which in turn, maximises the flow rate of solids through the valve. But, placing the aeration tap too low, the solids flow becomes insensitive due to gas by-passing as reported by Knowlton and Hirsan (1978). They also discovered that the aeration point was most effective if it was placed at a position of $2 \times D_L$ from the centre line of the horizontal section of the L-valve.

Therefore effective location of the aeration tap for the present L-valve can be evaluated as

$$\begin{aligned}
 T_{\text{air}} &= 2 \times D_L \\
 &= 2 \times (5) \\
 &= \underline{\underline{10 \text{ cm}}}
 \end{aligned}$$

The diameter of the L-valve is well below 0.3m and therefore a single aeration point may suffice (Knowlton, 1988).

4.6.2 DESIGN OF L-VALVE HORIZONTAL LENGTH

For satisfactory operation, the length of the horizontal section may not be smaller than $(1.5 - 2) \times D_L$ or greater than $(8 - 10) \times D_L$. A minimum length of $2 \times D_L \times \cot\theta$ has been suggested by Luo et al. (1989) where θ is the angle of repose of the particles. This minimum length ensures that solids flow decreases when aeration is stopped. Geldart and Jones (1991) have presented an expression that correlates the pressure drop between the aeration point and the horizontal section for Group B particles as

$$\Delta P_{L\text{-valve}} (\text{N} / \text{m}^2) = \frac{216 \times G_s^{0.17}}{D_L^{0.63} \times d_p^{0.15}}$$

Using the suggestion by Luo et al. (1989), the horizontal length of the L-valve is given by

$$\begin{aligned}
 L_H &= 2 \times D_L \times \cot\theta \\
 &= 2 \times (5) \times \frac{1}{\tan(37)} \\
 &\approx \underline{\underline{13 \text{ cm}}}
 \end{aligned}$$

4.7 DESIGN OF SOLIDS SAMPLING PORT

In order to measure the solid circulation rate, a solids sampling port was designed to divert the flow of the solids from the downcomer to a balance. The design consisted of a fixed butterfly valve which was used to open and close the downcomer to the flow of solids. In the closed position, the solids were diverted out of the downcomer and weighed. Fig. 4.12 shows a schematic diagram and dimensions of the solids sampling port.

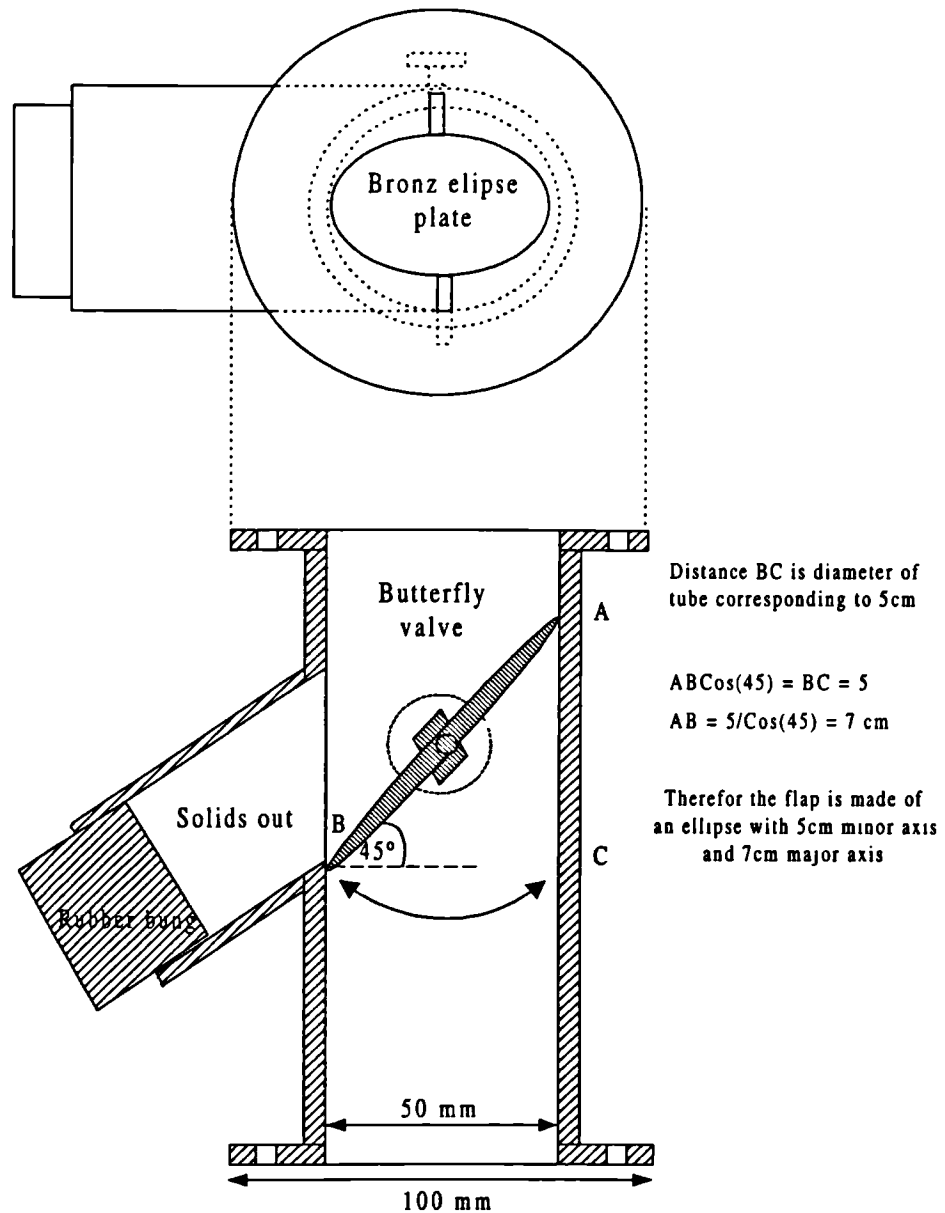


Fig. 4.12 Schematics and dimensions of the solid sampling port.

4.8 DESIGN OF THE HEATED FLUIDIZED BED REACTOR SYSTEM

This arrangement consists of a quartz silica tube surrounded by three ceramic heating tiles which allowed the bed inventory to be heated up to temperatures of 800 °C. The tube has a diameter of 100 mm and a depth of 987 mm. A diagram of the fluidized bed gasifier is shown in Fig. 4.13 and a full experimental set-up is given in Fig. 5.3. This gasifier was used to study the gasification of biomass with steam by continuously feeding biomass and removing bed material from the gasifier. Some modification involved designing a heated windbox for the generation of steam and the following

- Biomass feeder
- Sand feeder
- Air cooled biomass feeding probe
- Gas / solid separators
- Adjustable probe for solids removal from the bed
- Fluidized bed cover to accommodate feeding probes and thermocouples

4.9 BIOMASS FEEDER DESIGN

A feeder was required to deliver 1-3 g/min. of biomass particles (600 - 1200 μm), well inside the heated fluidized bed, on a continuous, steady and accurate basis. Several designs were looked at but, the Archimedes screw feeder was realised to be the most appropriate for the present application. A schematic diagram of the biomass feeder is shown in Fig. 4.14. The thread length is 3 cm long and has a diameter of 2 cm. A direct current motor with a gear box (model: 2140.934 - 61) connected to a PCB power drill transformer (model: 541-242) were used to directly control the rotation of the thread and hence the feeding rate. The hopper is designed to hold over half a kilo of biomass. The biomass feeder was spring mounted onto the biomass feeder probe, which ensured that the feeding probe inlet was always tight against the feeder discharge point. Together with a silicone seal, this prevented nitrogen (used to purge the feeder) to escape as a result of thermal expansion of the feeder probe at high temperatures. The biomass feeder calibration chart is shown in Appendix A.

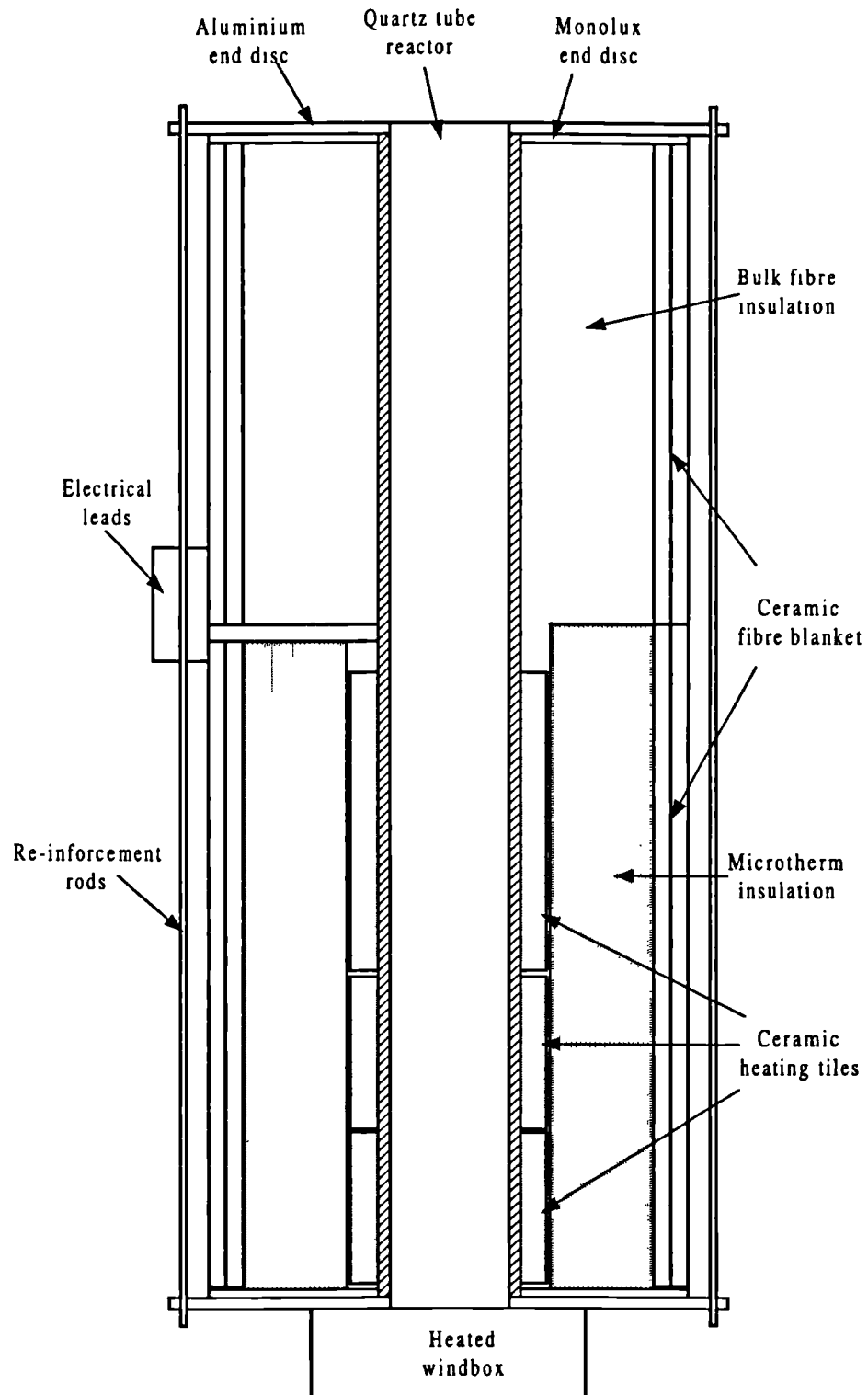


Fig. 4.13 Schematic diagram of the heated fluidized bed gasifier.

4.10 SAND FEEDER

The sand removed from the bed had to be replaced for steady state operation. Therefore another feeder almost identical to the biomass feeder was built for this purpose. The feeding wheel had to be altered since sand is an abrasive material and the screw feeder was not suitable. The new feeder wheel was constructed from a ceramic material. A diagram of the new feeding wheel is shown in Fig. 4.15 (calibration of the sand feeder is shown in Appendix A).

4.11 FEEDER PROBE DESIGN

The feeder probe was used to feed the biomass particles deep inside the hot fluidized bed of sand. It was necessary to cool the probe while inside the bed in order to avoid degradation of the biomass particles prior to entering the fluidized bed. This usually caused blockage of the feeding probe. The probe was constructed from concentric stainless steel tubes of different diameters. The ends were spot welded which is capable of withstanding temperatures of up to 1200 °C. The central tube was made totally loose and the top end of the probe was sealed with silicone rubber. This allowed for the expansion effects and prevented the weld at the tip from breaking away. A schematic diagram of the feeding probe is shown in Fig. 4.16, which simply consists of a cylindrical stainless steel tube fitted with an air cooled jacket. A small flow of nitrogen was used to entrain the biomass particles and facilitate the feeding into the fluidized bed. This also prevented the bed material from bubbling up the feeding probe. The heated air from the probe jacket was vented to a fume cupboard.

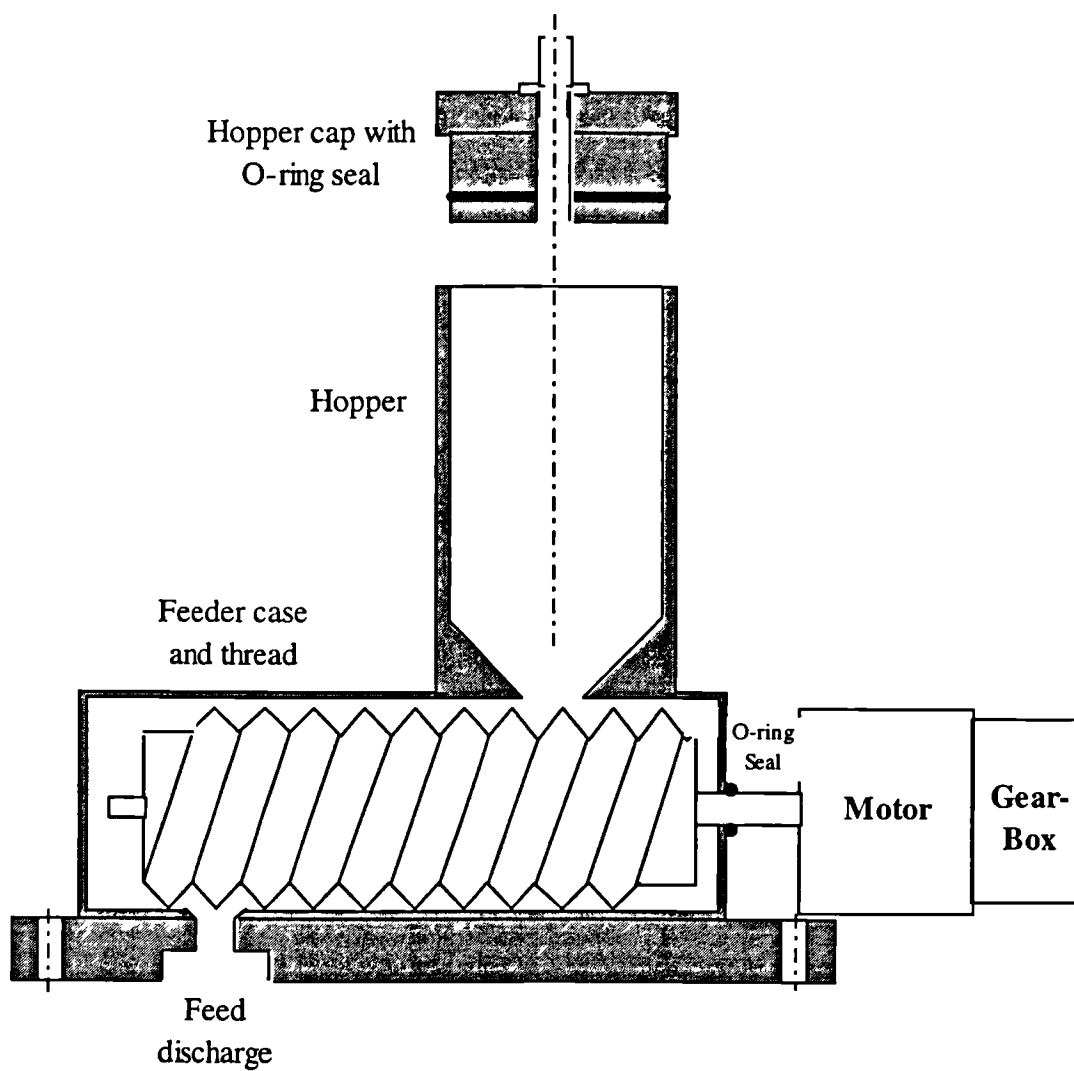


Fig. 4.14 Schematic diagram of the biomass feeder.

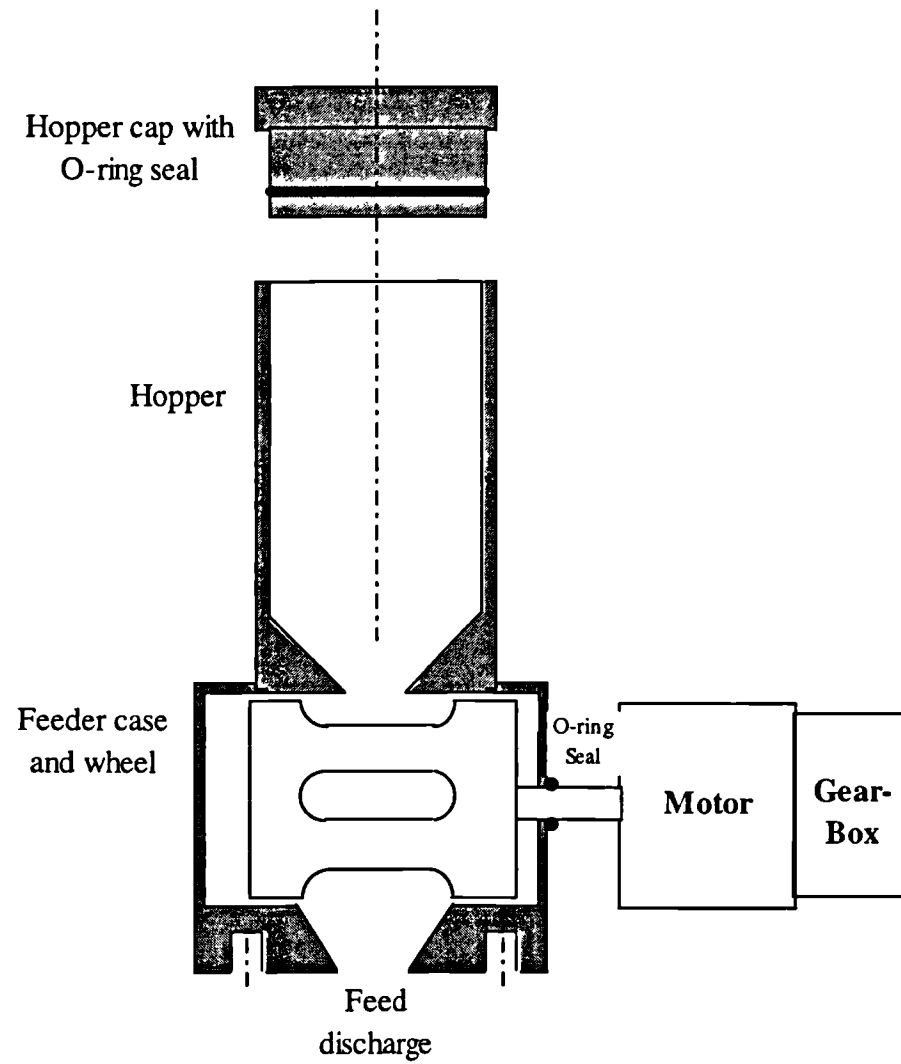


Fig. 4.15 Schematic diagram of the sand feed.

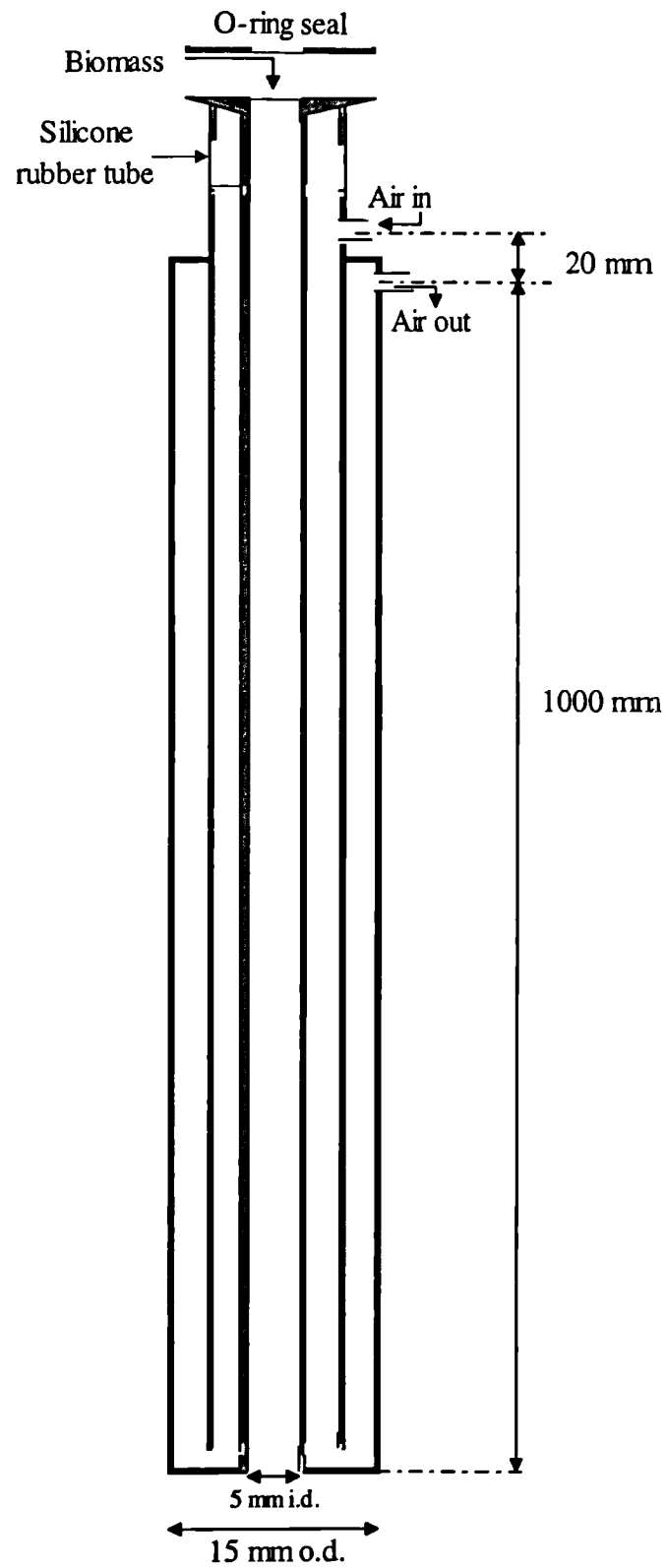


Fig. 4.16 Biomass feeder probe.

4.12 FLUIDIZED BED COVER PLATE

The feeding probes, take-off tubes and thermocouples were all fixed to a cover plate machined from stainless steel. The solids and gases take-off tubes were fitted with swagelock joints sealed with graphite ferrules which allowed vertical movements of the tubes. The feeding probes were welded to the cover plate with the sand feeder probe extending a distance of 40 cm into the gasifier and the biomass feeder extending to a level just above the gas distributor plate (≈ 3 cm). A high temperature gasket was placed between the cover plate and the top of the gasifier for the purpose of sealing. A schematic diagram and a picture of the cover plate is shown in Fig. 4.17 and plate 5-3 respectively.

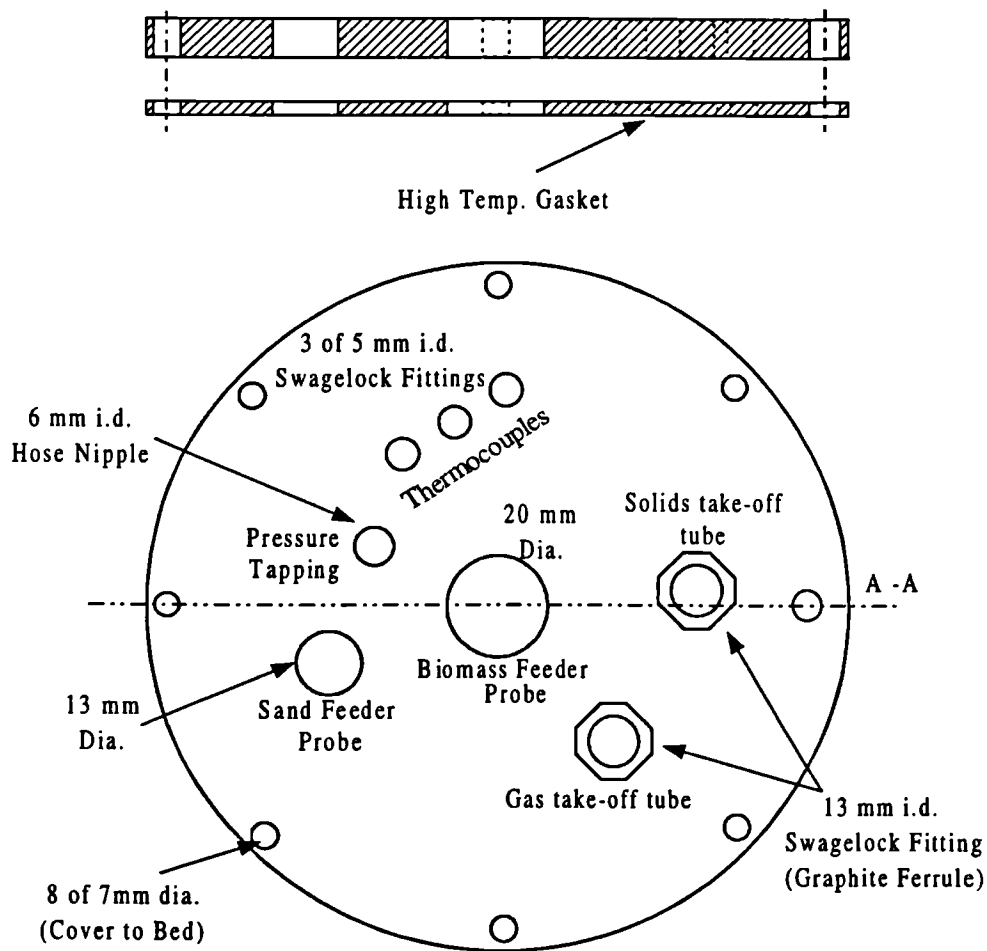


Fig. 4.17 Schematic diagram of the stainless steel bed cover

4.13 HEATED WINDBOX DESIGN

In order to be able to use steam as the fluidizing medium in the gasifier, the windbox was modified to evaporate water for the generation of steam. The original windbox was made of quartz silica fitted with a porous quartz silica disc as the gas distributing medium. The diameter of the fluidized bed is 10 cm which gives a cross sectional area of 78.54 cm². The minimum fluidization velocity of sand is 2.6 cm/s, and hence to fluidize the bed, it is required to have a steam flow of

$$78.54 * 2.6 * 60 = 12.25 \text{ l/min}$$

For a Group B powder, $U_{mf} \approx U_{mb}$ and therefore for design purposes we take the maximum flow of steam as 25 l/min (i.e. $2 * U_{mf}$). Assuming that 1 mole of a gas occupies 22.4 litres at standard conditions, we use the following equation to evaluate the mass of water required to produce 25 litres of steam at a bed temperature of 700 °C.

$$PV = nRT$$

$$100 * 0.025 = \frac{M_{\text{water}} * 8.314 * (273 + 700)}{18}$$

$$M_{\text{water}} = 5.56 \text{ g/min}$$

The actual quantity of water required is less due to the expansion effects at high temperature. The heat required to evaporate 5.56 g of water to steam is given by

$$\begin{aligned} Q &= M_{\text{water}} C_{p_{\text{water}}} (T_2 - T_1) \\ &= 5.56 * 4.16 * (110 - 20) \end{aligned}$$

$$Q = 2081.7J$$

$$= 34.7Watt$$

A heated flange was designed to be mounted at the bottom of the fluidized bed with gas and water injection points. This heated flange was fitted with two 250 W cartridge heaters (embedded within) and two type K thermocouples. One thermocouple for the temperature control and another for the over temperature alarm purposes. A ¼" swagelock fitting is positioned in the centre of the heated flange which allows the connection of a gas inlet pipe. A second swagelock fitting is also located in the bottom flange situated towards the side suitable for water connection via a 1/8" pipe. This provided for the injection of water onto the hot face of the heated flange. With the flange operating at temperatures between 100 and 150 °C, the injected water turns into steam and filters through the gas distribution medium.

The specification below refers to the new heated flange. Each cartridge is wired in PARALLEL. This specifications relates to both cartridge heaters wired together in parallel.

Operating Voltage	230 V (50/60Hz single phase)
Maximum Current	2.2A
Rated Power	500 W
Power Limit for 230V	100%
Max. Flange Temp.	150°C
Flange Material	Stainless Steel
Max. Water injection rate	36 g/min (ml/min)

The heated flange is designed to operate at temperatures up to 150°C. Above this temperature, damage to the seal may occur. The indicated temperature of the heated flange fluctuates depending on the flow conditions of the water. A schematic diagram of the modified wind box is shown in Fig. 4.18. A picture of the heated windbox is shown in plate 5-5 and a mechanical drawing is reported in Appendix I.

4.14 FLEXIBLE HIGH TEMPERATURE HOSE

This specially made piece of tubing was used to convey the hot solids and gases withdrawn from the bed to the first gas-solid separator. It is made of ½" NB close pitch (VNP) 316L stainless steel annular corrugated hose and single stainless steel 304 wire overbraid terminated at both ends with standpipe connections (25 mm stainless steel 316L). The overall length is 50 mm. A diagram of the flexible high temperature hose is shown in Fig. 4.19.

4.15 GAS METER

The gas generated from the gasification of the biomass was monitored by a domestic diaphragm gas meter (G1.6, BS 4161) designed for a minimum and maximum flow rate of 0.016 m³/hr and 2.5 m³/hr. The meter was tested showing the following errors reported in

Table 4.2 Gas meter flow rate errors.

Meter No:	Flow rate (m ³ /hr)	Error %
G1.6	2.50	0.47
	0.500	-0.05
	0.016	0.50

4.16 THERMOCOUPLES

Three type K thermocouples of length 970 mm, 845 mm, and 720 mm immersed into the fluidized bed together with three placed along side the heating tiles connected to an over temperature trip and temperature controller (Eurotherm type 810) were used to measure and control the bottom, middle, and top heaters of the fluidized bed reactor. The tip of the thermocouples were immersed into the gas at distances of 93 mm, 128 mm and 405 mm from the gas distributor plate. The thermocouples were fitted to the cover plate using swage lock joints and graphite ferrules in order to make them mobile in the vertical direction.

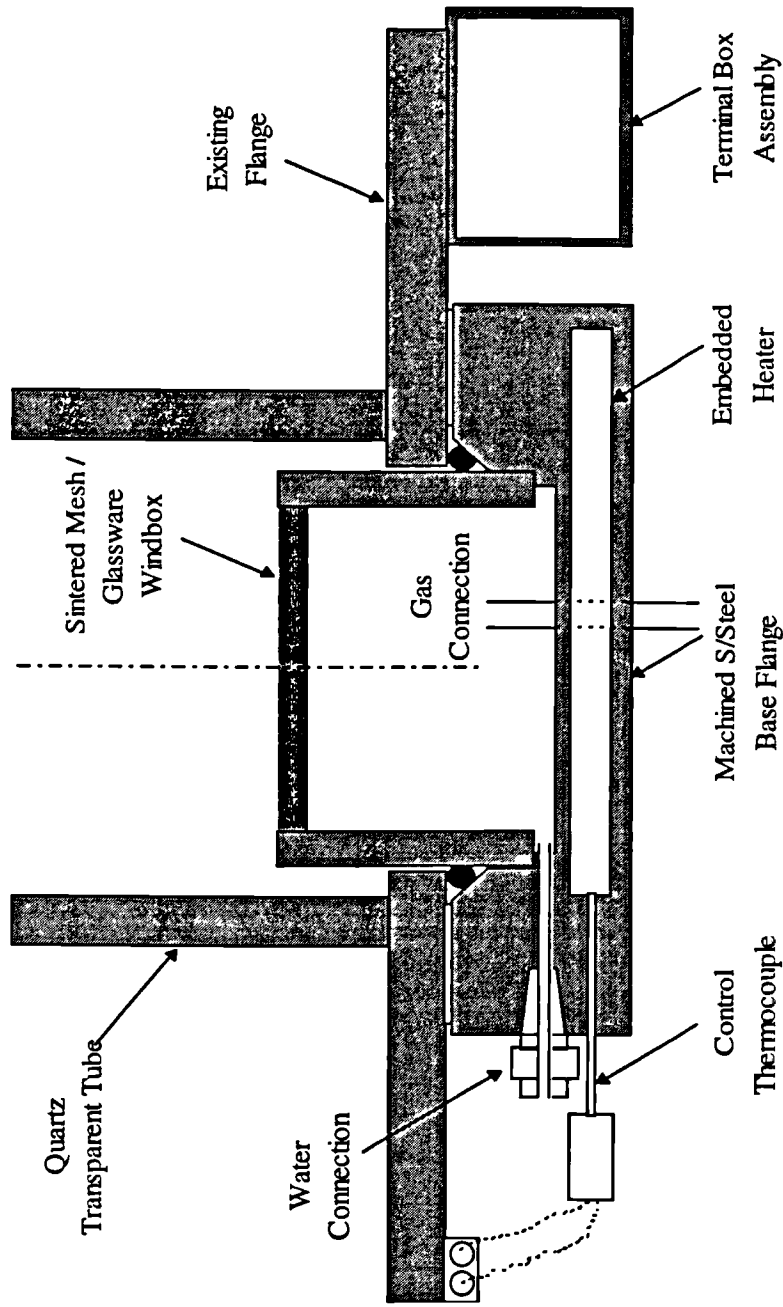


Fig. 4.18 Schematics of the heated windbox.

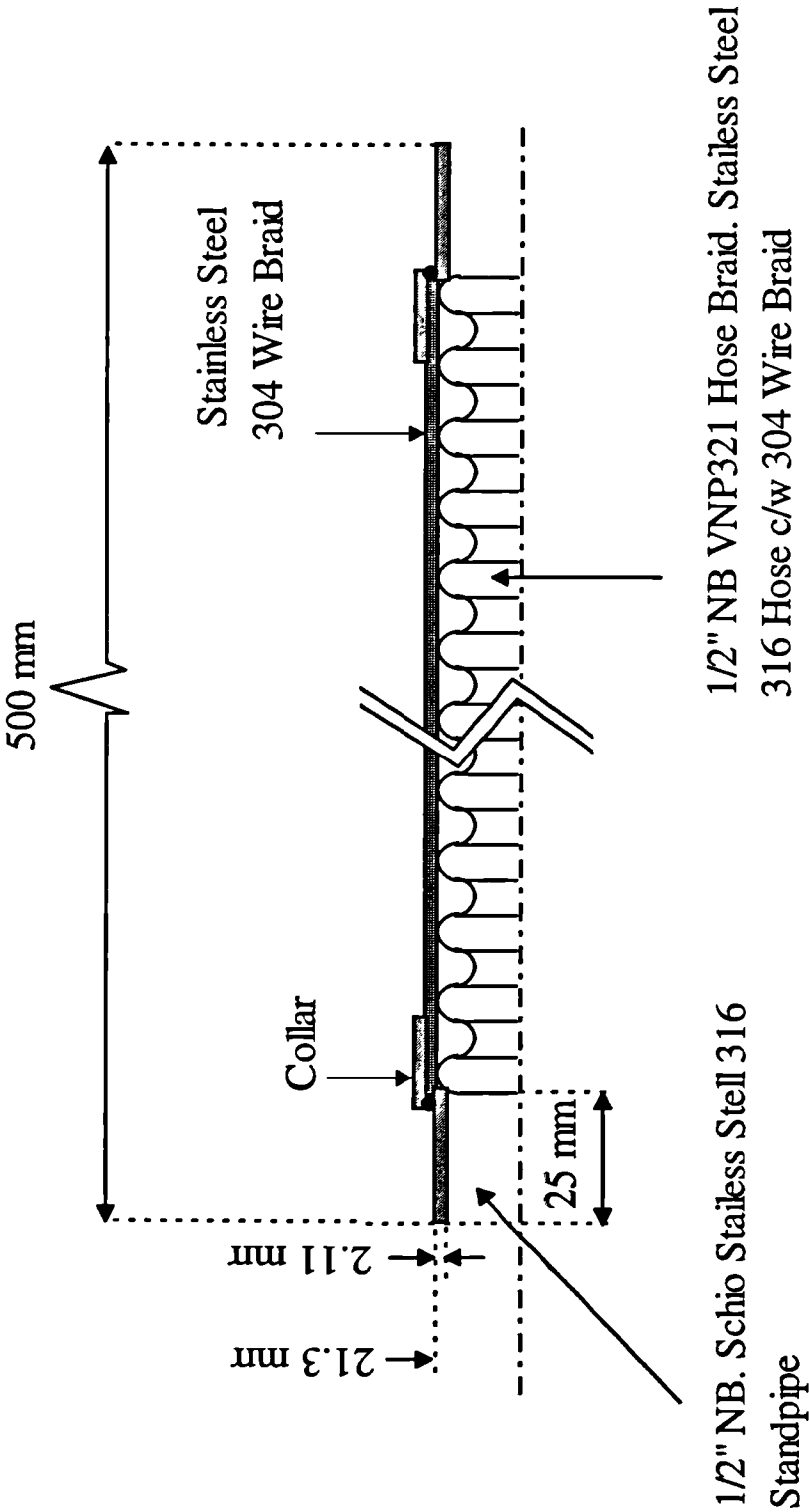


Fig. 4.19 Schematics of the high temperature flexible tubing

4.17 PUMPS, PIPING AND GAS SUPPLY

All connections to the gasifier were made via the top and bottom covers. Gases under pressure were conveyed in metal braided flexible tubing which combined the ease of use with safety. Nitrogen to the reactor was obtained from a pressurised cylinder and air was taken from the laboratory compressed air supply controlled via a calibrated rotameter (see Appendix H).

Two identical pumps were used in the gasification system (Metrovac rotary vacuum pump type GDR1), one was used to keep the gasifier under atmospheric pressure and the other was connected to the solids take-off tube. The latter was used together with a two way valve to withdraw solid samples from the fluidized bed gasifier. The pump suction power was controlled by connecting the inlet and outlet together via a two way valve.

4.18 COLD GAS FILTER

In order to prevent solids being sucked into the pumps mechanism, a cold gas filter (Watson Gamma 10) was used to clean the cold gas and remove any particulates and tars (if any).

Chapter 5

5 EXPERIMENTATION METHODS

This section is divided into two parts, the first covers the experimental procedure involved in studying the hydrodynamics of the cold model circulating fluidized bed proposed for the simultaneous combustion-gasification of biomass. Experimental runs were aimed at studying the solid circulation rate, solid residence time, pressure drop around the circulating loop, and quantifying the gas cross flow between the combustion and gasification section.

The second part deals with the gasification of biomass (almond shells) in a steam/sand fluidized bed at temperatures ranging from 700 to 800 °C. Attention is given to the effect of the residence time of biomass on the product distribution namely, char, tar, and gases. The gasifier is fed with biomass at a steady rate and once steady state is attained, the biomass feeding is terminated and the bed material is intermittently removed from the top of the bed and quenched for analysis. The analysis was used to predict the quantity of char present in the reactor as a function of time (during the steam gasification of the biomass char).

Fig. 4.1 shows the configuration of the circulating bed and a schematic diagram of the experimental set up is shown in Fig. 5.1. The cold model dual bed is made of cast perspex with the combustor (0.21 m diam. and 0.6 m high) and gasifier (0.17 m diam. and 1.2 m high) connected together via a riser and a return leg. The design of the cold circulating bed is described in chapter 4. Both beds have separate wind box and air supply lines. Different grade sintered bronze plates were used for distributing the fluidizing gas to each bed, chosen according to the hydrodynamics of each section.

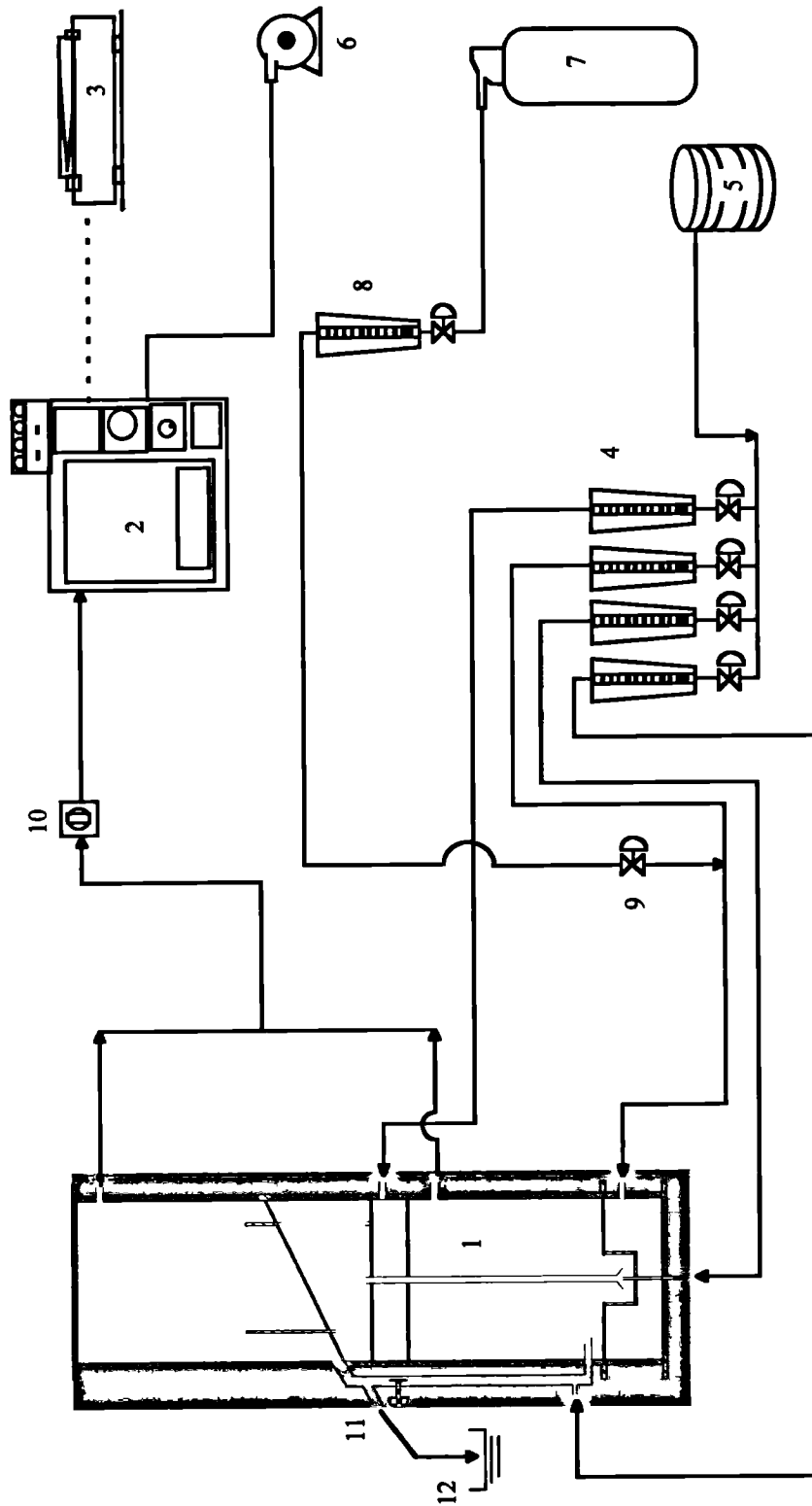


Fig. 5.1 Schematic diagram of the cold bed experimental set up- (1) circulating fluidized bed, (2) gas analyser, (3) integrator, (4) mass flow meters, (5) compressed air, (6) vacuum pump, (7) tracer gas (CO_2) cylinder, (8) tracer gas rotameter, (9) gas valve, (10) gas sampling valve, (11) solids sampling port, (12) electronic balance.

For all experimental runs, compressed air was used as the fluidizing medium supplied to the different parts of the circulating system, separately and independently, via calibrated mass flow meters.

5.1.1 BED INVENTORY

Silver sand was used as the bed material for the circulating fluidized bed. The mean particle size was determined by sieve analysis (see Appendix D) and the density determined using water pycnometry (see Appendix E). Table 5.1 summarise the physical properties of the bed inventory.

Table 5.1 Physical and Flow Properties of the Silver Sand.

Solids	d_p (mm)	U_{mf} (m/s)	ρ_p (kg/m ³)	ϵ_o	ϵ_{mf}	ϕ_s	Repose Angle
Silver Sand	0.164	0.026	2622	0.4	0.44	0.78	37.5

5.1.2 PRESSURE DROP EXPERIMENTS

Pressure drop measurements were conducted via 1/8" pressure tapings around the circulation loop. The required air velocity for the experiment was set constant using the mass flow meters and the system was allowed to reach steady state. This was assumed to exist when the height of the slow bed (combustor) did not vary with time. A period of approximately 5 minutes was required for the system to reach steady state each time there was a change in the operation of the CFB.

Upon approaching steady state, the back pressures exerted on the piping upstream of the distributor plate caused fluctuation to the mass flow meters. These required slight adjustment to ensure that the desired flowrate of air was admitted to each section. Once steady state was achieved, a PC together with a data acquisition software (LABTECH) was used to log all the pressure readings around the circulating loop into a spreadsheet in Excel at a rate of 100 Hz for 80 seconds. This generated 8000 pressures readings after which an average was taken. The procedure was repeated for another set of operating parameters.

5.1.3 SOLID CIRCULATION RATE EXPERIMENTS

The desired gas flow rates were set for the different sections and the system was allowed to stabilise. The butterfly valve fixed on the downcomer was used to divert the flow of solids into a collecting cylinder whose open end was blocked by a rubber bung. The diversion of the solids via the butterfly valve disrupted the operation of the CFB as a result of the intrusive nature of the sampling technique. Thus it was necessary that the diversion of the solids took place over a short but representative period of time, in order to minimise disruption, preventing the CFB to deviate markedly from its steady state condition. The collection of the solids discharged was done over a period of no more than 10 seconds after which the solids were weighed and returned back to the system.

5.1.4 GAS MIXING EXPERIMENTS

The purpose of these experiments was to investigate and quantify the gas that flows from the combustor to the gasifier and vice versa. This may occur via the riser or the downcomer. For gas tracing experiments, carbon dioxide was used as the tracer gas because of low cost, safety of operation and ease of analysis. It has been shown that the adsorption effects of carbon dioxide are negligible for small scale sand fluidized beds (Nguyen et al., 1977); implying that carbon dioxide can be used as an ideal non-adsorbing tracer. The tracer gas (supplied from a separate gas cylinder and controlled by a separate rotameter; see Appendix G) was diluted by mixing with the fluidizing air prior to injection into the desired section of the circulating bed.

The flow of carbon dioxide was chosen to give a mean mixed tracer composition that was well above the normal carbon dioxide composition of the air. The fluidizing air without any tracer was used as the reference gas thus, measurements of tracer concentrations were directly related to the carbon dioxide injected. Tracer gas concentration was monitored on-line and continuously using a calibrated Shimadzu Gas Chromatograph fitted with a Thermal Conductivity Detector (TCD) and helium as the carrier gas (see Appendix B). The gas cross flow from one compartment to another was determined from a mass balance over the tracer gas injected into one area and its concentration measured elsewhere within the system. Experimental runs were conducted

under steady state by allowing enough time for the system to stabilise each time certain parameters were changed.

5.1.5 SOLID RESIDENCE TIME EXPERIMENTS

The length of stay of particles in the bed determines the extent of reaction of solids with gas. In a fluidized bed, the length of stay or the residence time varies from particle to particle. For example, some particles are discharged immediately after feeding and some are discharged only after remaining in the reactor for a good period of time. Thus, it is imperative to know the residence time of the particles in the reactor in order to predict the extent of reaction.

The mean residence time of solid mixtures of different sizes and/or density is not necessarily the same since smaller particles are more likely to leave the fluidized bed faster than larger ones. Thus the mean residence time of particles of size X_i can be obtained from

$$\bar{t}(X_i) = \frac{\text{weight of particles of size } X_i \text{ in the bed}}{\text{flowrate of such particles in or out of the bed}}$$

A certain quantity of biomass particles (almond shells, $d_p = 1.2$ mm) was placed in the circulating system and allowed to reach steady state. The butterfly valve was used to determine the concentration of the tracer particles at the sampling port. The above equation was used to approximate the residence time of the solids in both beds assuming that the concentration of the tracer at the sample port is approximately equal to that in the gasifier.

5.1.6 GASIFIER (BED 2) SET-UP

Three different gasifier set-ups were studied in order to optimise the circulating bed in terms of high solids circulation and low gas cross-flow. These set-ups are described below:

Mark1-The outlet of the riser was extended 100 mm into bed 2 and the weir height was fixed at 350 mm (see Fig. 5.2). An inverted cone was used to keep the solids in the bed.

Mark2-The outlet of the riser was position just above the gas distributor in bed 2 with the weir height as in Mark 1.

Mark3-The outlet of the riser was set just above the gas distributor plate but the weir height was reduced to 300 mm. The inverted cone was removed and the riser inlet was situated at a fixed distance of 3 cm below the gas distributor plate in bed 1.

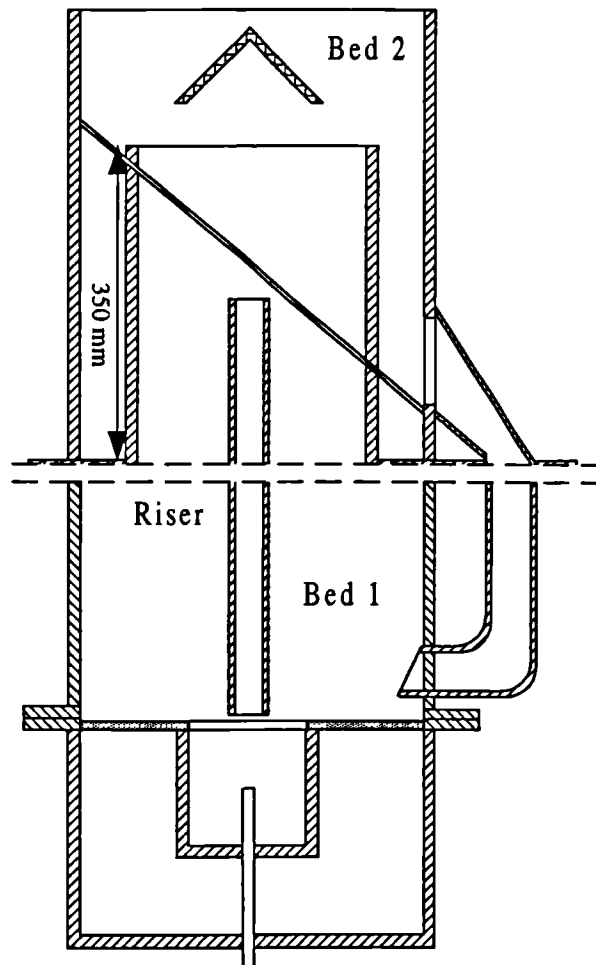


Fig. 5.2 Schematic diagram of the cold model circulating fluidized bed corresponding to Mark 1.

5.2 HEATED FLUIDIZED BED GASIFIER

Experiments were conducted to investigate the gasification of biomass in a heated steam fluidized bed reactor. Attention was given to the effect of the residence time of the biomass in the reactor on the final product distribution, namely, char, tar, and gaseous products. The reactor was continuously fed with biomass until steady state was achieved, and then solids were removed at timed intervals from the top of the bed for analysis.

5.2.1 MATERIAL (BIOMASS) PREPARATION

Almond shells can represent an abundant agricultural sub-product in regions of moderate climate. They are agricultural waste of no utility other than for combustion. The almond shells received for this study contained small stones and unwanted shell peelings and so it was first necessary to separate them by 'hand-screening' in order to prevent damage to the grinder. The clean shells were then ground in a high speed rotary cutting mill. To facilitate feeding and obtain a uniform size distribution, the crushed shells were ground again and then separated into different size fractions by sieving. Size fractions below 200 μm were discarded and those above 1400 μm were ground once again. Size fractions above 1400 μm were not used in order to avoid damage to the feeder wheel used to deliver the particles to the fluidized bed.

The density of the almond shells was evaluated using a density bottle (see Appendix E) and the mean diameter of the particles was determined by sieve analysis (Appendix D). The biomass sample was then ready for gasification. Properties of the almond shells are given in Table 5.2 and the size distribution in Table 5.3.

Table 5.2 Composition of the Almond Shells.

	weight %		
	Raw	Dry	Ash free
Moisture	8.84	0.00	0.00
Ash	1.16	1.17	0.00
Vol. matter	72.45	79.48	80.42
Carbon	45.31	49.70	50.29
Hydrogen	5.48	6.01	6.08
Oxygen	38.53	42.49	42.99
Cellulose	29		
Hemicellulose	28		
Lignin	35		

Table 5.3 Size Distribution of the Almond Shells.

Biomass Sample I					
Size, μm	>1000	1000-850	850-710	710-600	<600
Wt %	11.47	37.94	29.71	17.65	2.35
Mean diameter	830 μm				
Density	1200 kg/m^3				

5.2.2 BED INVENTORY

Silver sand was used as the fluidized bed material. The density and size distribution were evaluated by water pycnometry and sieve analysis respectively. Table 5.4 shows the physical properties of the silver sand used for the heated bed.

Table 5.4 Physical Properties of the Silver Sand.

Solids	d_p (mm)	U_{mf} (m/s)	ρ_p (kg/m^3)	ϵ_o	ϵ_{mf}	ϕ_s	Repose Angle
Silver Sand	0.177	0.027	2622	0.4	0.44	0.78	37.5

5.2.3 GASIFICATION PILOT PLANT DESCRIPTION

A schematic flow diagram of the continuous 'feed-removal' fluidized bed reactor system for the gasification of the almond shells is shown in Fig. 5.3. The plant consisted essentially of the fluidized bed reactor, the biomass and sand feeders, the solid collection and cooling systems, and the gas cooling and analysis system.

The design of the fluidized bed reactor and its auxiliary equipment has been described in section 4. The fluidized bed was constructed from a quartz silica tube of internal diameter 100 mm, with a porous disc distributor (quartz silica, pour size: 10 μm), designed to operate up to 1000 °C at atmospheric pressure. The temperature of the reactor was measured by three stationary type K thermocouples (TC-1) immersed in the bubbling bed. The fluidized bed was of fine silver sand particles corresponding to Geldart group B classification of powders (density, $\rho_p = 2622 \text{ kg/m}^3$; mean diameter, $d_p = 177 \mu\text{m}$). Importantly, the particles have a very high melting point (> 2000 °C) and since all gasification temperatures were under 1000 °C, problems of particle sintering were never encountered and a well mixed bed was obtained.

Fluidizing gas was introduced to the wind box at the bottom of the bed through 1/4" stainless steel tube. The section above the fluidized bed gas distributor plate was surrounded by three sets of semi-circular heating tiles. Water for the generation of steam was introduced through a separate tube onto the heated flange in the wind box (see section 4). Here the water came into contact with a heated flange where it evaporated into steam, passed through the porous distributor plate and fluidized the sand bed. The gas distributor plate and windbox were both made of quartz silica thus maintaining good gas distribution with no possibility of dislodgement as a result of differential expansion effects at high temperatures.

The type of feeder used in these experiments was an Archimedes screw type feeder designed and built for this purpose (see section 4). Once the biomass was placed in the feed hopper, the feeder was sealed to the atmosphere using rubber O-rings. A small flow of nitrogen ($\approx 1.0 \text{ l/min}$) was used to feed the biomass in the feeding probe well inside the reactor bed and to prevent the bed material and gaseous products from

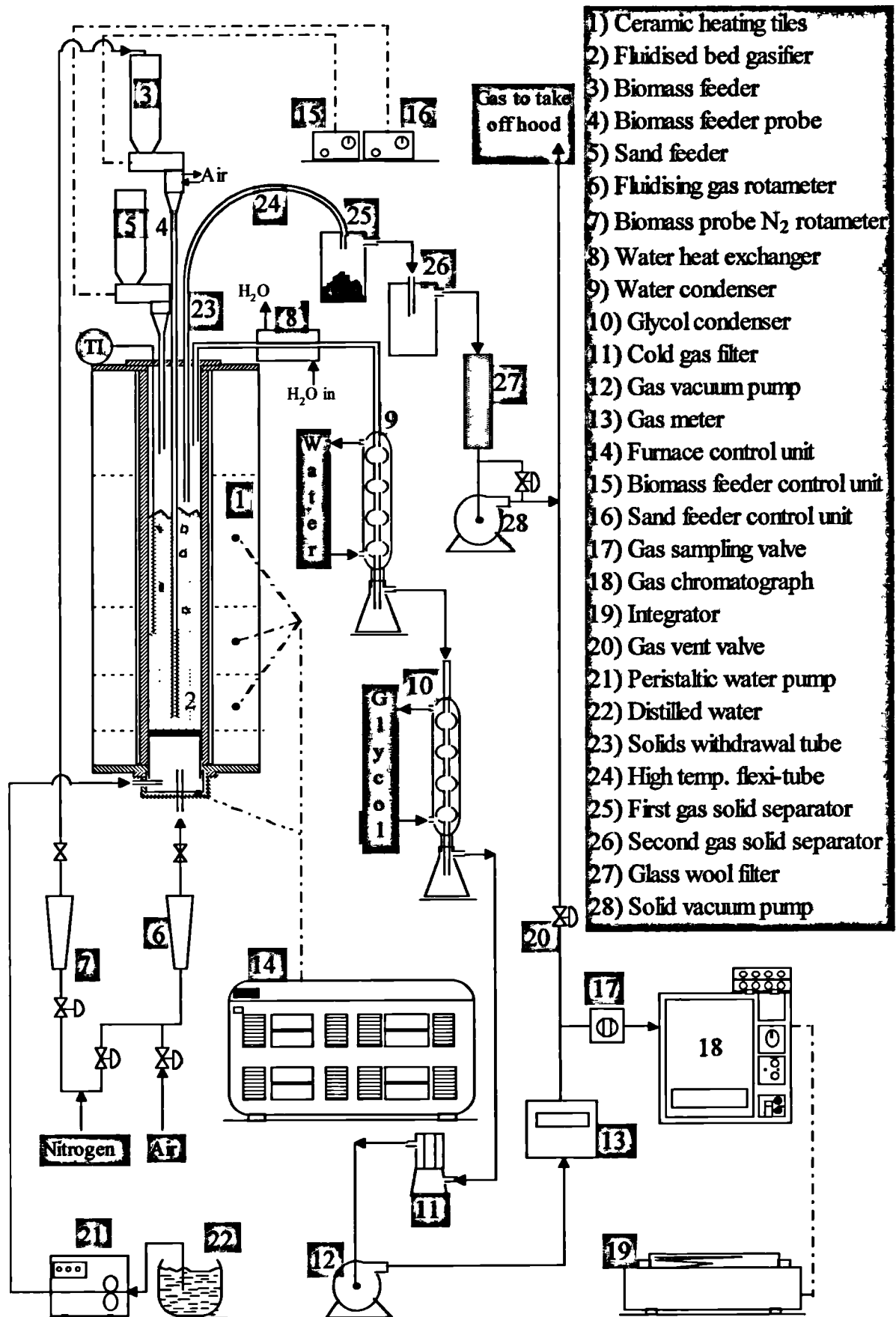


Fig. 5.3 Schematics of the biomass / char gasification pilot plant set-up.

rising up the probe. During gasification the feeding probe was cooled with air to prevent biomass degradation prior to delivery to the bed.

As for the sand feeder, it was not necessary to have any entrainment gas to feed the sand particles into the bed since the feeding probe did not extend into the fluidized bed. However, once the sand was placed into the hopper, a small flow of nitrogen was used to expel the air from the sealed feeder hopper prior to mounting on to the feeding probe.

The solids cooling system consisted of an ice-water cooled bath and the gaseous cooling system was comprised of a heat exchanger in series with two glass condensers. Tap water was used as the cooling medium for the heat exchanger and first condenser and a mixture of water and glycol (cooled to -10°C) for the second condenser. The inside walls of the condensers were regularly cleaned by washing with acetone to remove residual reaction products and to enhance cooling rates. Conical flasks were attached to the bottom of the condensers for the collection of condensates.

An on-line gas chromatograph (Shimadzu 14R) and a Chrompaq 5A integrator were used to analyse the presence and composition of the non-condensable gaseous products from the reactor. The gas chromatograph was fitted with a Carbosieve S11 column (1.5m, 3mm I.D.). Helium was used as the carrier gas at a flow rate of 30 ml/min. This chromatograph was used to detect N_2 , CO, CO_2 , and CH_4 . The oven of the chromatograph was temperature programmed: the initial column temperature was set at 35°C ; five minutes after injection the temperature was set to rise at a steady rate of $20^{\circ}\text{C}/\text{min}$ up to 225°C and to hold this value for 6 minutes (which was adequate to ensure that all permanent non-condensable gases had been analysed), before cooling back to 35°C . The gas sample analysis took about 24 minutes with a further 4 minutes for cooling.

Gas samples were injected into the GC by means of a 1 ml gas sampling valve. The gaseous products from the reactor were injected into the gas chromatographs at almost constant pressure for consistent results.

5.2.4 GASIFICATION PROCEDURE

The gasification of the almond shells was performed at 3 different temperatures, 700 °C, 750 °C, and 800 °C and at atmospheric pressure. The procedure can be considered in three stages: start up, biomass gasification, and char gasification.

5.2.4.1 START-UP

A known quantity of sand was placed in the reactor to give the desired bed height at bubbling conditions. A weighed amount of the biomass and sand was placed in the cleaned feed hoppers and the hoppers top and all external feeder joints were sealed with rubber o-rings. The feeders were then fixed to the feeding probes which were already placed in the tube furnace. Air was used as the fluidizing medium while the bed was heating up. Once the bed temperature was within 100 °C of the desired temperature, the air flow was switched to pure nitrogen in order to eliminate the oxygen present in the reactor. The presence of oxygen in the reactor was monitored with the gas chromatograph and once this fell to significantly low and negligible levels, the nitrogen was switched to steam. A peristaltic pump was used to send the desired quantity of distilled water into the heated wind box for the generation of steam (for water pump calibrations see Appendix C). The amount of steam in the reactor was determined as a function of the water flowrate and the bed temperature. Also, the take-off tube was lowered to a point just above the bubbling bed of sand.

At this stage the amount of water condensate was measured several times to determine if it corresponded to the amount of water injected, thus ensuring a good material balance. A small flow of nitrogen (≈ 1.0 l/min) was passed continuously through the feeder probe to facilitate the flow of biomass particles from the feeder into the hot fluidised bed. Once this flow, the flow of condensate, and the required bed temperature were stable, the gasification of almond shells was initiated.

5.2.4.2 BIOMASS GASIFICATION

The biomass feed rate was set on the feeder control box and the power operated. As soon as the biomass entered the bed, the bed pressure increased due to the production of gas. The pressure pump was used to reduce the pressure increasing

the rate at which gases were removed from the reactor. The introduction of biomass into the reactor caused the bed temperature to drop by some 10-15 °C; it was therefore necessary to maintain the reactor temperature at about 10°C above the desired gasification temperature before commencing. A short period of time (≈ 2 min.) was allowed for the whole system to stabilise, after which the collection of the condensate was commenced and the clock timer started. This point represented the start of a gasification run.

Every three minutes, the bed temperature and the amount of gas generated were recorded using the gas meter. The gases, product vapours were removed from the reactor through the take off tube situated just above the fluidized bed. These passed through a series of condensers and found their way into the tar-gas separator/filter where all of the heavy hydrocarbons (tars) and some condensed water were separated from the non-condensable gases.

After passing through a cold gas filter (Watson Gamma-17), the cool, clean, non-condensable gases were then analysed by means of the on-line gas chromatograph, and eventually vented. Normally, runs lasted for about 90 minutes, although occasionally for as long as two hours. The gasification of biomass was stopped when the chromatographic analysis showed a reproducibility of about 95%. Condensate from the condensers was weighed and kept for possible analysis. The bed temperature and gaseous flow were evaluated by averaging over the period of the run. The amount of biomass fed into the reactor was determined from the biomass feed rate and feed duration. The duration of condensate collection was also noted.

5.2.5 CHAR/STEAM GASIFICATION AND SAMPLING

When the biomass gasification had reached a steady state (the gaseous composition did not differ by more than 5%), the biomass feeding was terminated and a sample of bed material was taken which denoted the char fraction at time zero. Then further samples were taken at 15 min intervals for a period of two hours. In order to keep the bed height in the gasifier constant, the sand feeder was used to replace the approximate quantity of sand removed during sampling. The bed samples removed were used to evaluate the quantity of char present in the gasifier as a function of time.

5.2.5.1 CHAR SAMPLING SYSTEM

The solids sampling system is denoted by numbers 23 to 28 in Fig. 5.3. It consisted of a vertically mobile ½" stainless steel tube attached to a high temperature flexible stainless steel tube (see section 4). A vacuum pump was used to suck out the bed samples into a series of gas-solids separators. The solids collected were mainly sand together with the char from the gasified biomass and some water. The mixture of solids, gases and vapours from the first gas-solid separator passed to the second gas-solid separator where the remaining solids (if any) were separated. The gases were filtered using glass wool before being vented.

Just before taken a sample from the bed, a small flow of nitrogen was introduced into the gasifier in order to bring the overall gas velocity to about $8U_{mf}$ enhancing the solids mixing along the axis of the reactor. After about 2 min, all gas input to the gasifier was shut off and the solids vacuum pump was activated. Using the solids vacuum valve and by lowering the solids withdrawal tube, a small sample (30-60g) from the bed was withdrawn into the first gas-solids separator previously vented with argon. The first gas-solids separator was placed in an ice bath in order to quench the hot bed material and immediately suppress further reaction. After the solids collection, steam flow into the gasifier was recommenced and the solids vacuum pump was shut off. Using the sand feeder and control unit, an approximate quantity of sand equal to that removed was delivered to the gasifier by setting the sand feeder to a calibrated feed rate (see Appendix A) over a given time. This was done to ensure that the total bed mass and hence the bed height was kept roughly constant. The gas-solids separator was disconnected from the system and sealed to the atmosphere using rubber bungs. An empty gas solid separator was placed in the solids collecting system and the whole process was repeated after a given time interval (15 min). The char in the cool bed samples ($>600 \mu\text{m}$) were separate from the sand for further analysis and the rest burned in a fume cupboard in order to determined the fraction of char in the sample. This char fraction and the total bed mass (sand) was used to evaluated approximately the total quantity of char present in the bed as a whole as a function of time.

5.2.5.2 CHAR ELIMINATION

Before performing another gasification run it was important to eliminate the char fraction (if any) present in the gasifier. This was done by simply fluidizing the bed with air: The heating temperature was adjusted and the GC was used to detect the presence of carbon dioxide. When no more carbon dioxide could be detected, it was assumed that all the char had been burned. Air flow through the bed was shut off and nitrogen was used to purge the reactor. The new gasification parameters were set. When all the oxygen had been eliminated, biomass gasification was recommenced.

5.2.5.3 CHAR ANALYSIS

Visible char particles ($>600\ \mu\text{m}$) were separated from the sand and dried in an oven at approx. $100\ ^\circ\text{C}$. This quantity of char together with that adhered on the surface of the sand represented the concentration of char particles present in the bed at steady state conditions. A Scanning Electron Microscope (SEM) was used to analyse the surface structure of the chars formed in relation to the different gasification temperatures and length of stay in the gasifier.

5.3 GASIFICATION PLANT PHOTOS

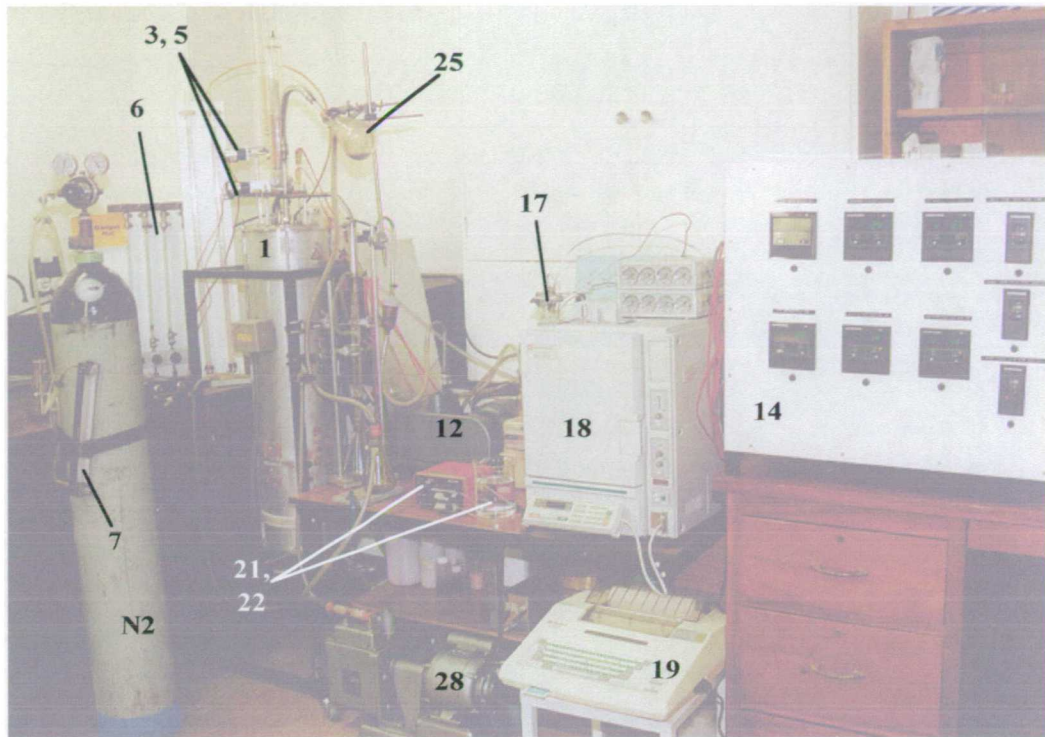


Plate 5-1 Fluidized bed gasification plant (for numbers refer to Fig. 5.3).

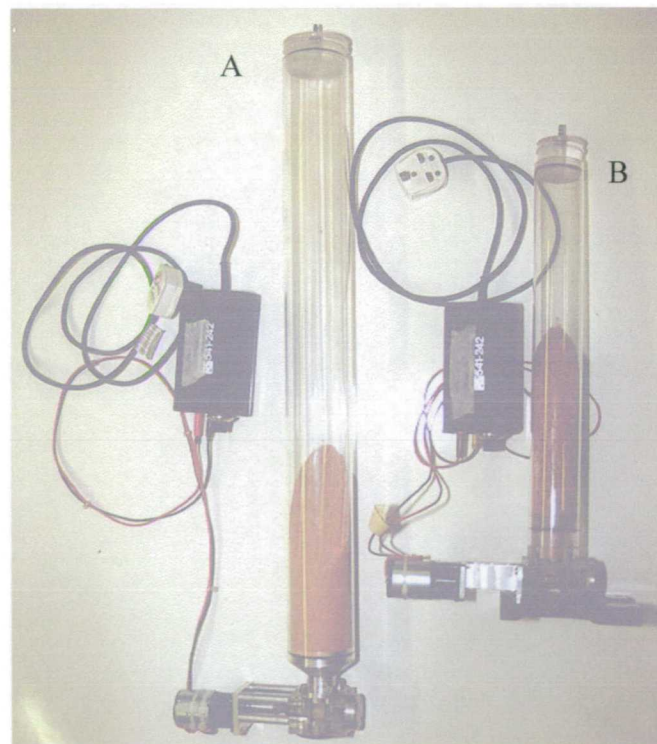


Plate 5-2 Biomass and sand feeders and control unit:

(A) sand feeder, (B) biomass feeder.

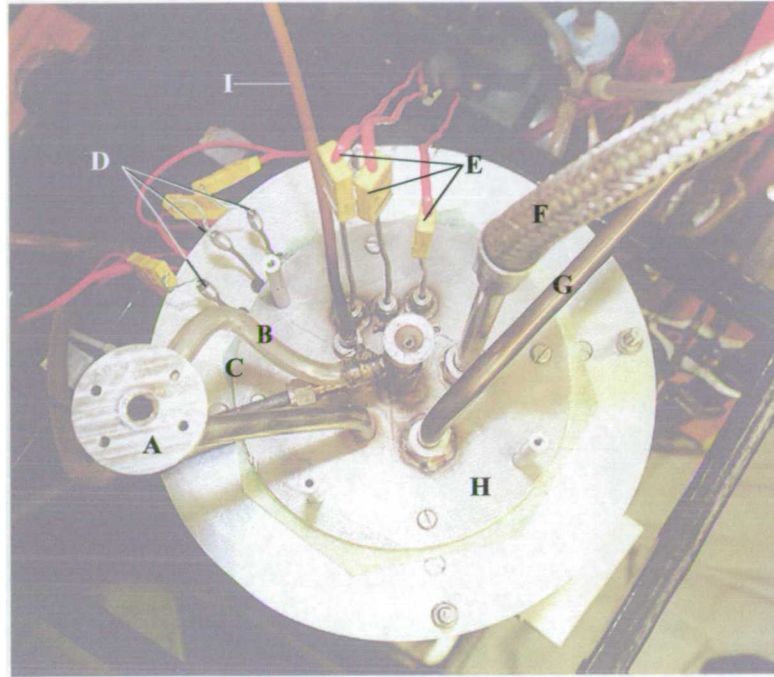


Plate 5-3 Bed cover showing feeding and withdrawal probes: (A) sand feed, (B) biomass probe cooling air in, (C) biomass probe cooling air out. (D) control thermocouples, (E) measure thermocouples, (F) high temperature tubing and solids take-off tube, (G) gas line, (H) cover plate.



Plate 5-4 Attachment of the sand and biomass feeder to bed cover plate.

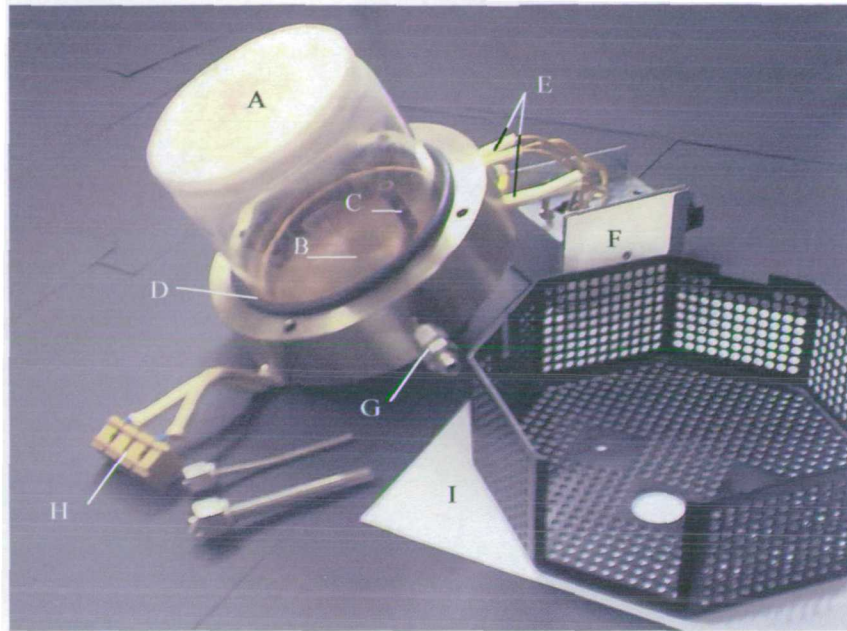


Plate 5-5 Heated flange and quartz windbox: (A) quartz gas distributor, (B) heated flange, (C) gas inlet, (D) rubber gasket, (E) heating cartridges, (F) terminal connection box, (G) water connection, (H) thermocouples, (I) safety cover.

Chapter 6

6 RESULTS AND DISCUSSION: COLD MODEL CIRCULATING FLUIDIZED BED

There are two prime requirements for the system, namely a high, controllable solid circulation rate and a low gas cross flow between bed 1 (combustion zone) and bed 2 (gasification zone). While the solid circulation rate governs the process throughput, the gas cross-flow controls the quality and/or loss of product gas. Gas introduced into the system at four different points, and the apparent controllable process variables in this system were: total solids inventory (bed inventory), gas rates to bed 1 and bed 2, gas rate to the riser, and distance of riser gas jet from inlet of riser. For comparative purpose, solid circulation rates were made specific by dividing them over the cross-section area of the riser. The distance of the riser gas jet from the inlet of the riser is denoted by X_r .

6.1 PRELIMINARY RESULTS

Some brief experiments were conducted in order to optimise the solids circulation rate and minimise gas cross-flow between the two beds by changing the design of the system. Firstly, solid circulation rates and gas cross-flow were determined with the system set up as in Mark 1 (see experimental section). The solids circulation rate and gas cross-flow rate are reported in Fig. 6.1 and Fig. 6.2 respectively.

This set up gave a high solid circulation rate and gas cross-flow was under 10%, the percentage of the gas cross-flow being in terms of the total gas input into the combustion section. However, from particle tracking experiments (see section 6.2), it was noted that the residence time of the foreign particles was too short in bed 2. This

was as a result of very little mixing between the particles ejected from the riser and those already present in the bed. Therefore it was decided to lower the exit of the riser and to position it at the same level as the gas distributor plate in bed 2. This resulted in the inlet of the riser moving below the level of the gas distributor in bed 1. Solids circulation rates were measured again and the results are shown in Fig. 6.3.

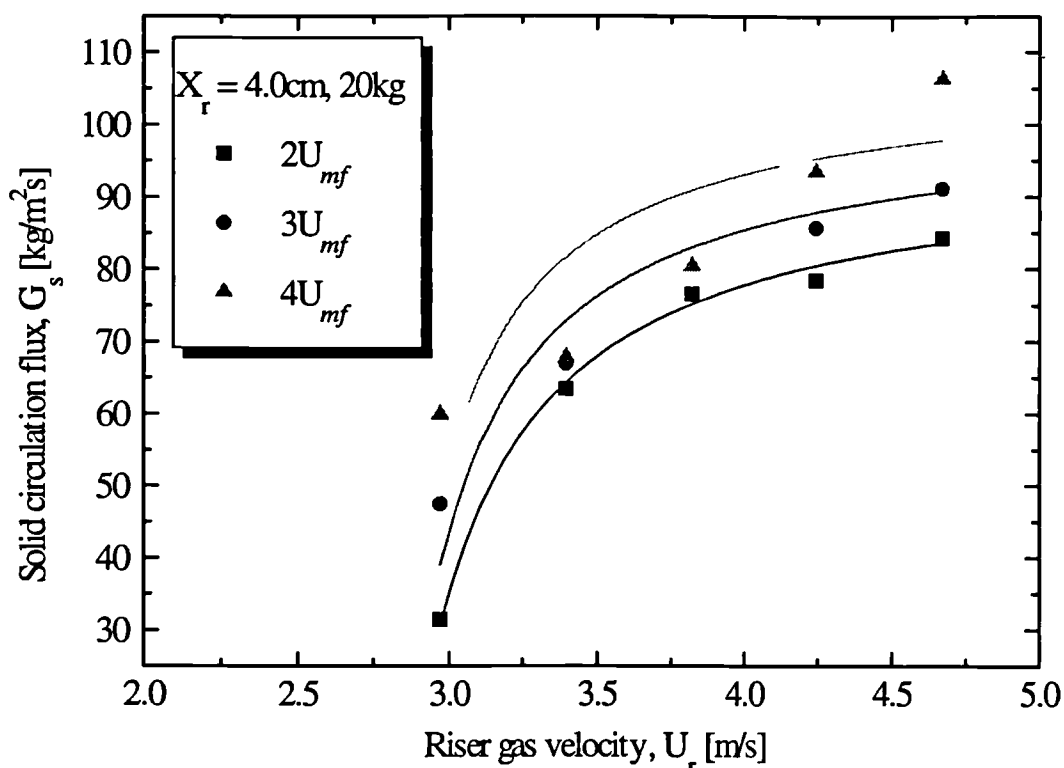


Fig. 6.1 Solid circulation rate versus riser superficial gas velocity for a bed load of 20 kg and system set up as in Mark 1.

The present set-up resulted in a considerable reduction in the solids circulation rate, however solids mixing and residence time were improved. One way to increase the solid circulation rate was to decrease the height of the weir leading to the downcomer. The weir height in bed 2 was reduced by 50 mm and solid circulation rates similar to the set up in Mark 1 were obtained with good solid mixing and thus it was decided to conduct further experiment with this design. The riser inlet was fixed at approximately 3 cm below the gas distributor plate in bed 1 and the gas jet was mobile in the vertical direction and could be varied from 1 cm to 4 cm from the riser inlet.

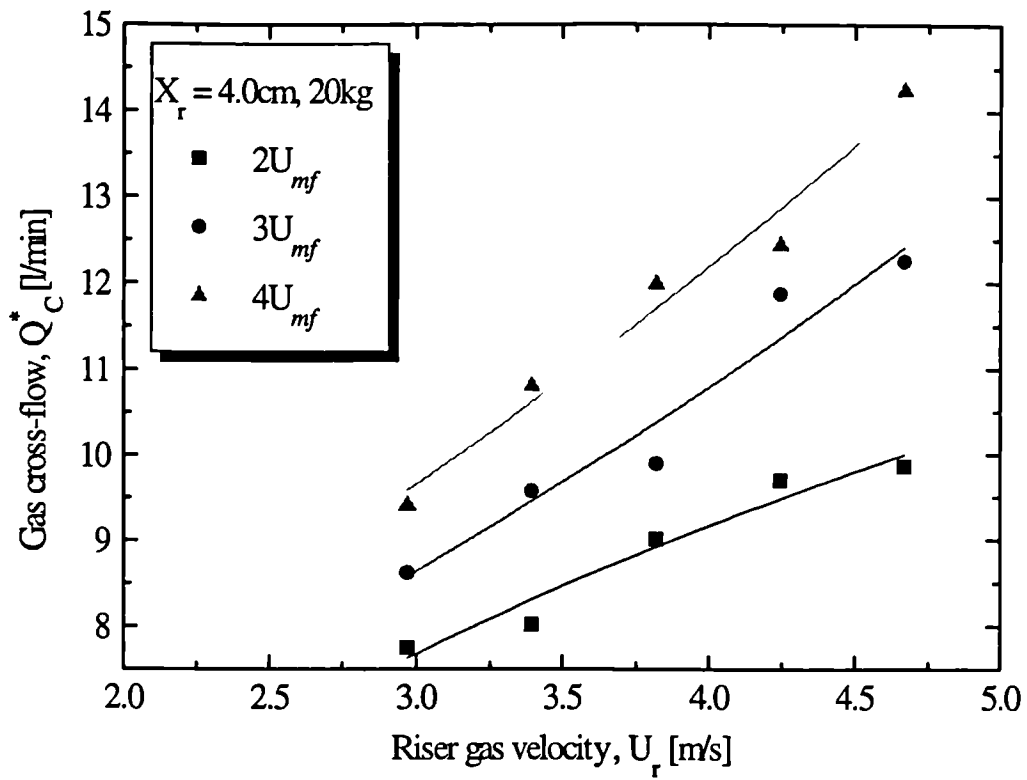


Fig. 6.2 Gas cross-flow versus riser superficial gas velocity for bed load of 20 kg and system set up as in Mark 1.

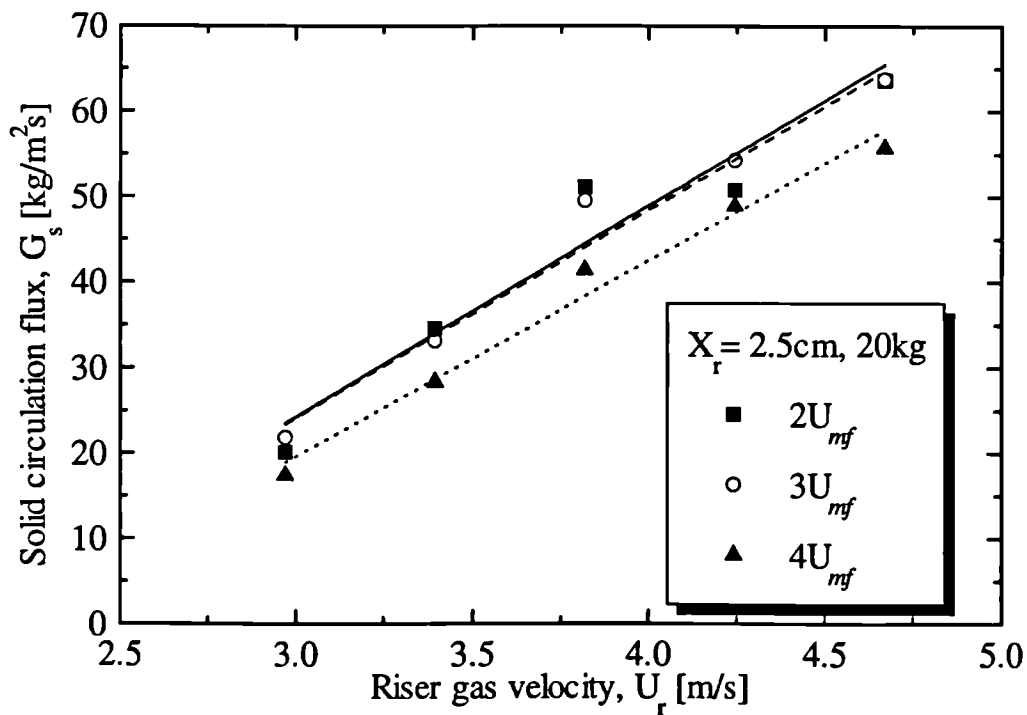


Fig. 6.3 Solid circulation rate versus riser gas velocity for bed load of 20 kg and system set up as in Mark 2.

6.2 VISUAL OBSERVATIONS

Solid circulation did not commence as soon as the L-valve was aerated. A minimum flow of gas was required in order to overcome the frictional forces and to start solids flow. Also, if bed 1 (L-valve outlet) was not fluidized, then again solids circulation was blocked and solids accumulated in the return leg. For the present system, the minimum aeration gas for solids flow was noted at approximately 4 l/min. Not all of the gas injected into the L-valve travelled up the standpipe, some of this gas found its way into the combustor as shown in Fig. 6.4. Due to the complexity of the system, it was difficult to determine the split ratio and hence the gas velocity in the return leg. Nevertheless, this acted as a good gas seal or barrier between the combustion and gasification zones by preventing gas flow between these two sections in either way.

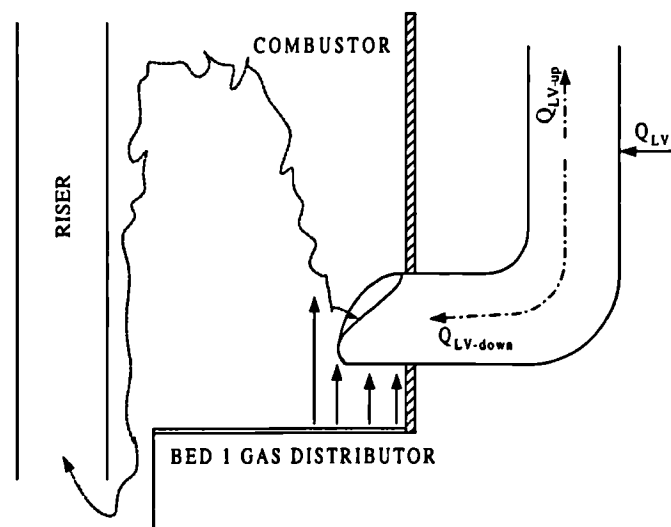


Fig. 6.4 Gas and solids flow in the L-valve.

In order to study the behaviour of low density particles ejected from the L-valve into the combustor, tracer particles were tracked using x-rays. The tracer particles were made by inserting a metal inclusion into 5x5 mm cylinders of balsa wood as shown in Fig. 6.5. The overall density of the tracer particles was approximately 400 kg/m^3 . These tracer particles were placed in the L-valve and their motion in the bed was examined. It was seen from a majority of runs that the tracer particles followed the path shown by the dotted lines in Fig. 6.4. As the particles left the L-valve, they were swept up with the rising bubbles and having reached the solids down-

flowing area (2 cm ring around the riser), they moved downwards towards the riser inlet with the circulating bed material. Least to say is that the particles did not enter the riser as soon as leaving the L-valve which resulted in poor solids mixing.

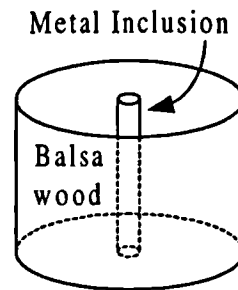


Fig. 6.5 Tracer particle with metal inclusion.

Although solids circulation increased as the aeration increased and at gas rates of above 10 l/min, the solids in the downcomer were in the slugging mode with the formation of large bubbles covering the cross sectional area of the return leg. This affected the foreign solids circulation rate, and solids with a density much lower than the bulk density of the bed material were locked for a long time in the standpipe before moving to the combustor. These solids were visible at the surface of the bed in the return leg.

However, at low aeration rates (4 l/min) to the L-valve, a dead solids zone was formed. Most of the solids in the horizontal section were stationary and sand flow was only in a thin region near the top as shown in Fig. 6.6. Increasing the aeration rate decreased the stationary zone of the particles but did not completely eliminate it. An optimum L-valve aeration of about 8 l/min was used to minimise the dead zone as much as possible without slugging. At high and low solids circulation rates, solids flow through the L-valve occurred in oscillations. For a given solid circulation rate, the level of solids in the return leg decreased until it fell to a certain level and the solids flow was brought to a halt. At this point, the solids level increased, and after some time, the L-valve opened automatically and the solids flow commenced again. This cycle was repeated over and over again.

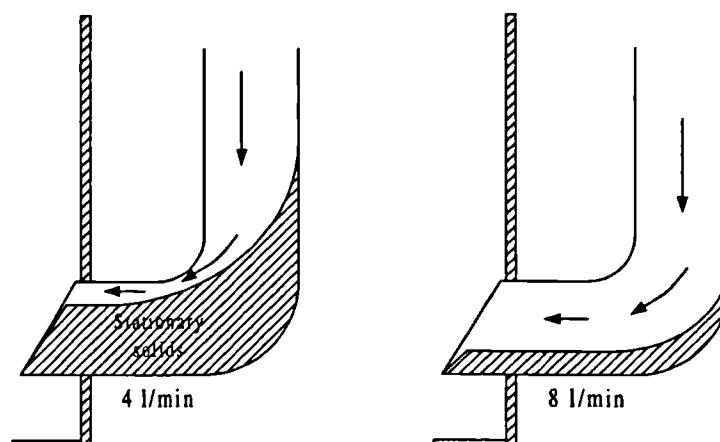


Fig. 6.6 Solids flow through the L-valve.

6.2.1 STATIC

Due to the nature of inert particles moving at high velocities inside a non-conductor (riser), considerable static was generated inside the riser at high gas flow rates which led to much difficulty in obtaining consistent results. In order to overcome this, the incoming air to the riser was humidified up to 45%. This alone did not solve the problem and thus the inside of the riser and the beds were lined with a 1 inch strip of copper wire connected to the earth terminal via the mains. The combination of these two methods reduced the static charges significantly but did not eliminate it.

6.3 SOLID CIRCULATION

The solids circulation rate is defined as the weight of solids re circulated around the circulating fluidized bed during a time interval. The driving force for solids circulation is the difference in the apparent density of the particulate solid phases between adjacent zones (Kunii and Levenspiel, 1991). Fig. 6.7 to Fig. 6.12 report solid circulation rates versus gas superficial velocities for a range of total bed inventory (12 to 22 kg) and X_r (1 to 4 cm). The gas rates to bed 1 and bed 2 were varied in the order of 2, 3, and 4 times that required to keep the bed at U_{mf} .

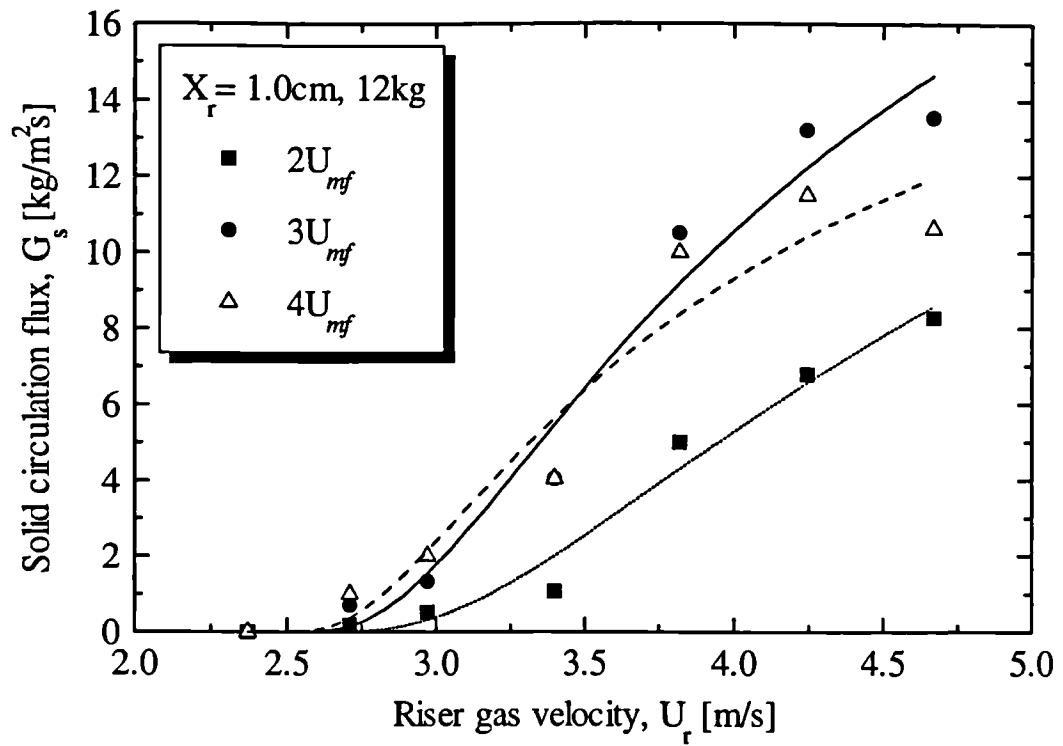


Fig. 6.7 Solid circulation flux versus riser superficial gas velocity.

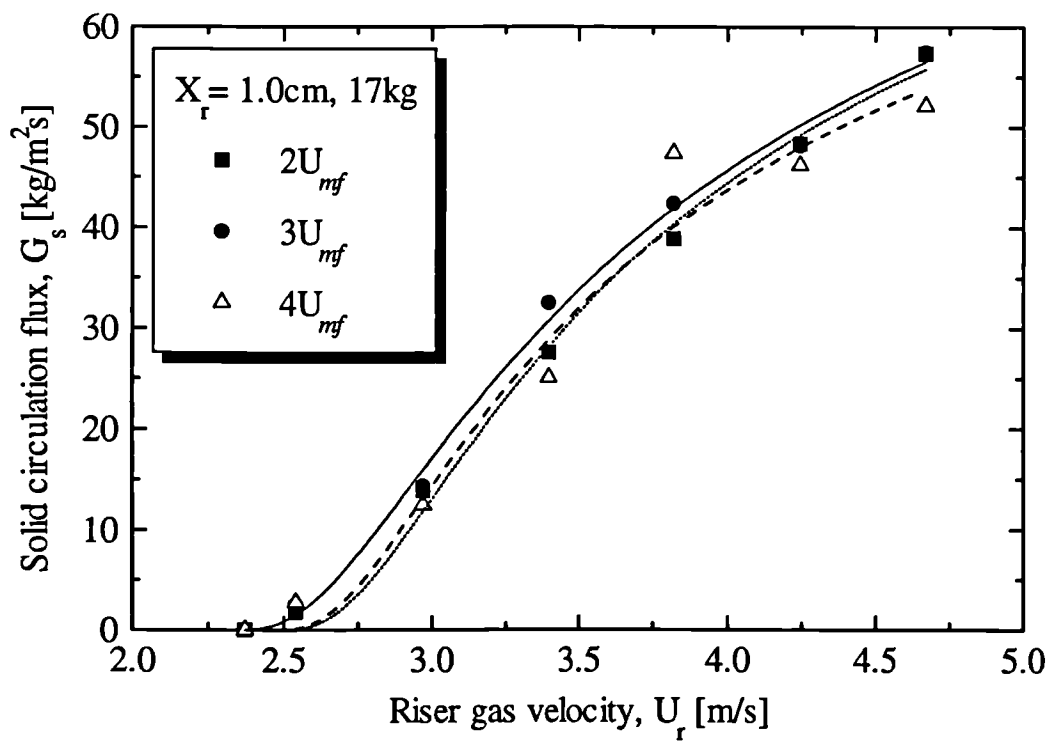


Fig. 6.8 Solid circulation flux versus riser superficial gas velocity.

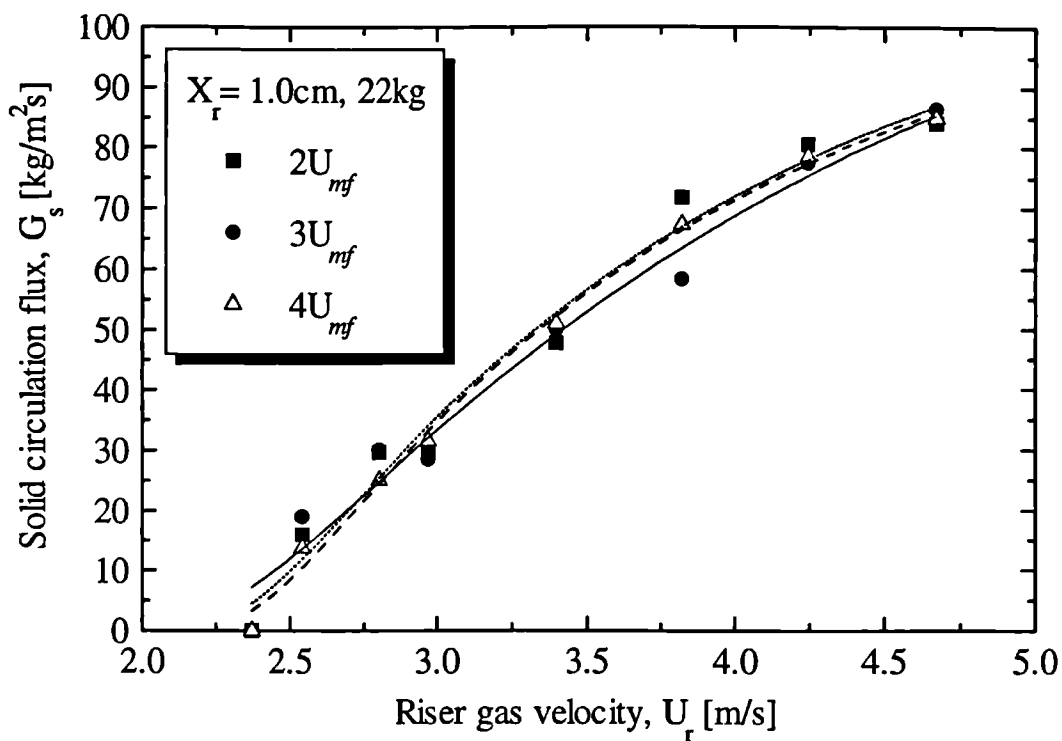


Fig. 6.9 Solid circulation flux versus riser superficial gas velocity.

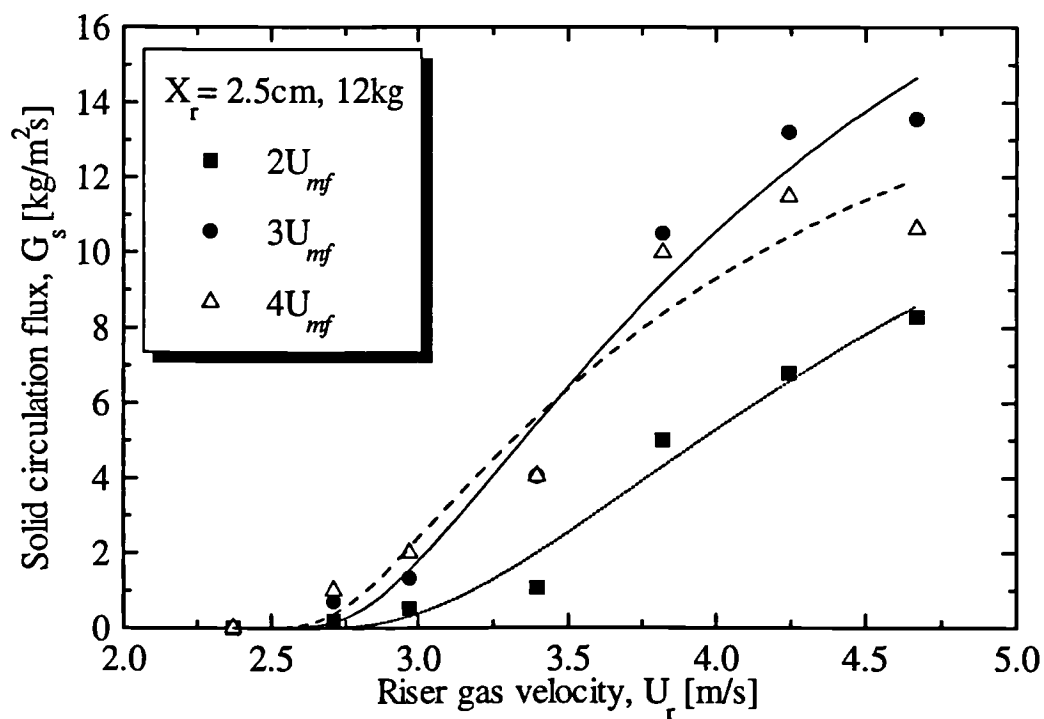


Fig. 6.10 Solid circulation flux versus riser superficial gas velocity.

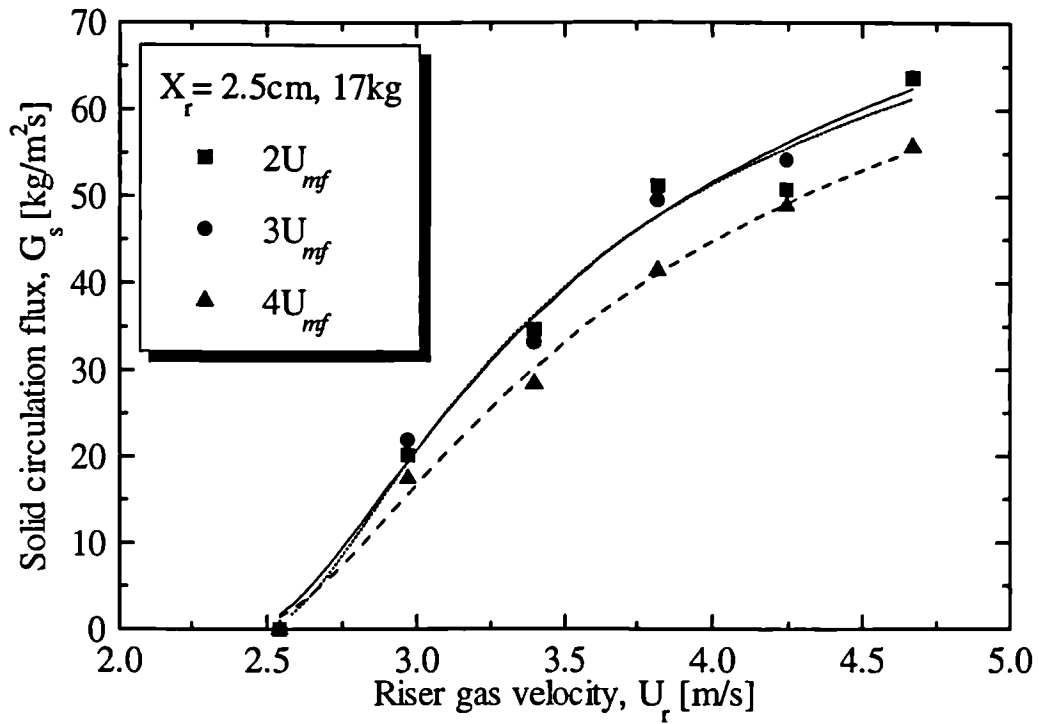


Fig. 6.11 Solid circulation flux versus riser superficial gas velocity.

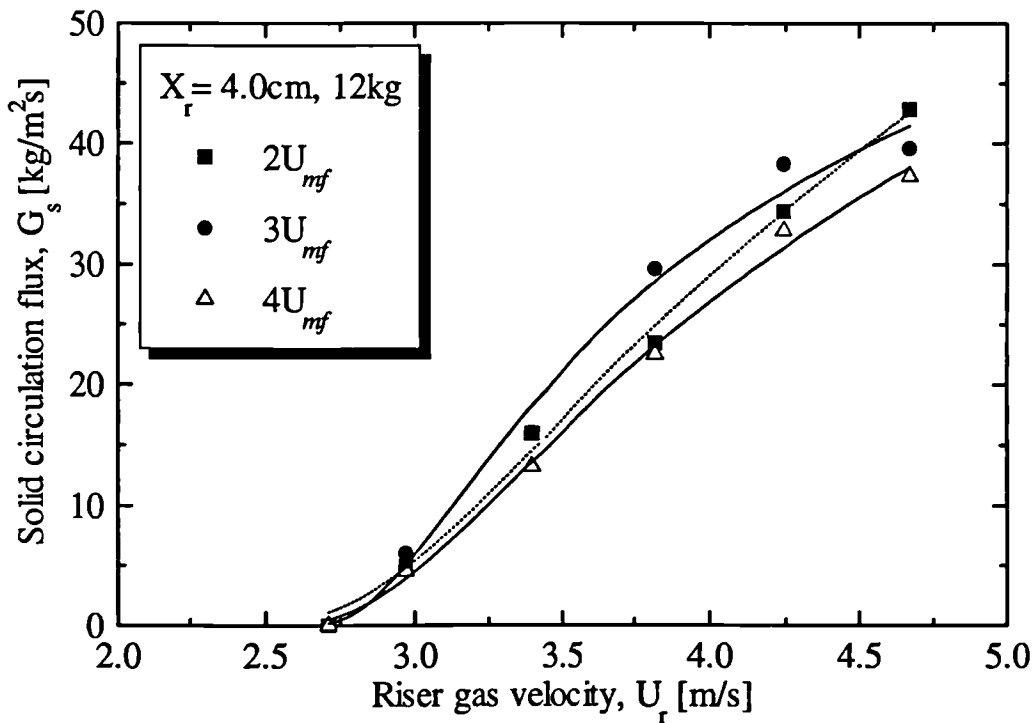


Fig. 6.12 Solid circulation flux versus riser superficial gas velocity.

From the above plots, upon increasing U_r , the solid circulation rate increases very sharply but seems to level off at gas velocities above 4.5 m/s . It has not been possible

to conduct experiments much above 5 m/s due to the appreciable elutriation of bed particles. However, the circulation rate of the solids no longer increases over the higher range of the riser gas velocity (increasing U_r above 5 m/s). At low riser gas rates, the limiting condition is the energy contained in the air stream that can be transferred to the solids in the riser in order to force them upwards. Increasing U_r increases this energy and thus the rate at which the solids are transported upwards equals the rate at which they can enter the riser. However, beyond a certain gas velocity, the rate of input of solids to the riser becomes limited since the distance X_r is already allowing the maximum possible flowrate for the dynamic equilibrium of the system and thus the extra air input in the riser is not utilised. At this point the circulation rate is solely determined by X_r and only increasing this will lead to a higher circulation flux. This can be clearly seen from Fig. 6.13, which shows that the ratio G_s/U_r becomes constant as the riser superficial gas velocity is increased above 4 m/s at constant X_r .

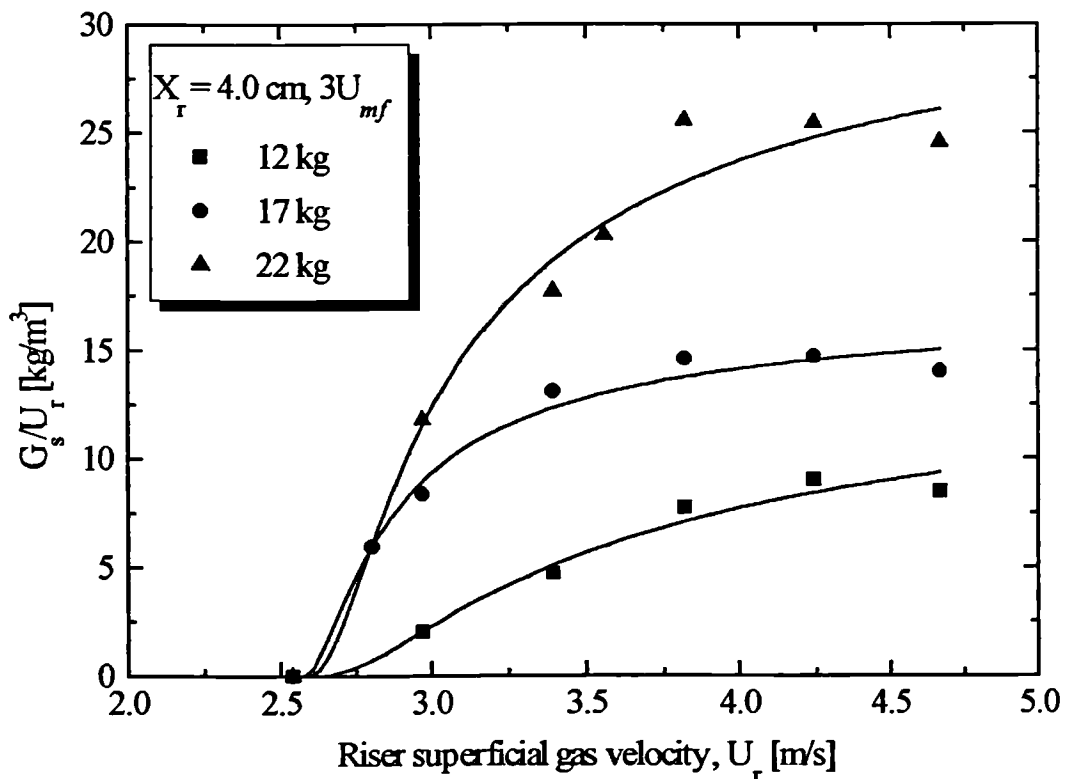


Fig. 6.13 Plot of G_s/U_r versus riser superficial gas velocity, U_r for total inventory 12 - 22 kg and $X_r = 4.0$ cm

When no air was introduced into the combustion section, it was found that the particles did not circulate. Increasing the velocity of air above the minimum fluidizing gas

velocity, the particles started circulating. The effect of changing the gas velocity in one bed, as shown in Fig. 6.14, does not seem to have any effect on the solids circulation rate.

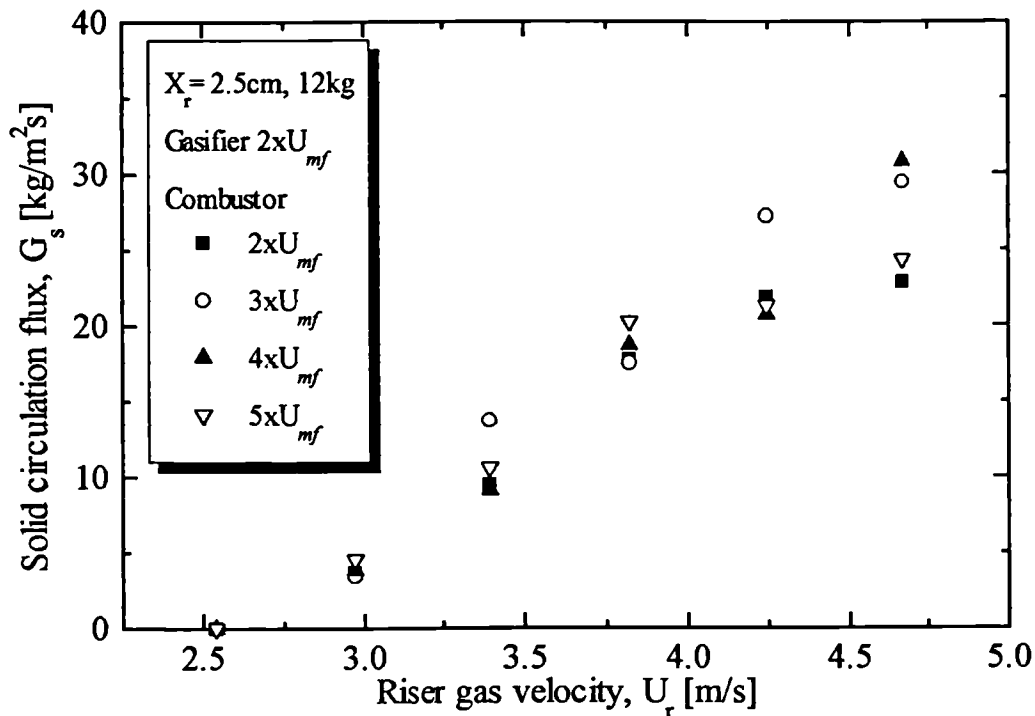


Fig. 6.14 Solid circulation flux versus riser superficial gas velocity.

The solid circulation increases upon increasing the gas flow into the beds from $2U_{mf}$ to $3U_{mf}$ keeping all other variables constant. However, moving on to $4U_{mf}$ and above, the circulation rate decreases slightly as is shown in Fig. 6.14. When the gas rate to bed1 is increased from $2U_{mf}$ to $3U_{mf}$, the bed bubbles more frequently thus enhancing mixing and allowing the bed particles to flow freely to the riser inlet. However further increase leads to a decrease in the circulation rate, due to a decrease in the apparent density of the particulate phase. Under fixed gas rates to the riser, this is expected to result in a reduction in solid circulation rate. The most stable circulation with a high circulation of solids was obtained in the experiments by keeping the gas velocity into the beds at $3U_{mf}$.

The reproducibility of the solid circulation data is shown in Fig. 6.15 and Fig. 6.16. For each plot, the data were obtained on two separate days. It was assumed that the system reached steady state condition after it was operated for about 5 min. and the solids bed height in bed 1 did not change, thus solid circulation rates were constant and

reproducible.

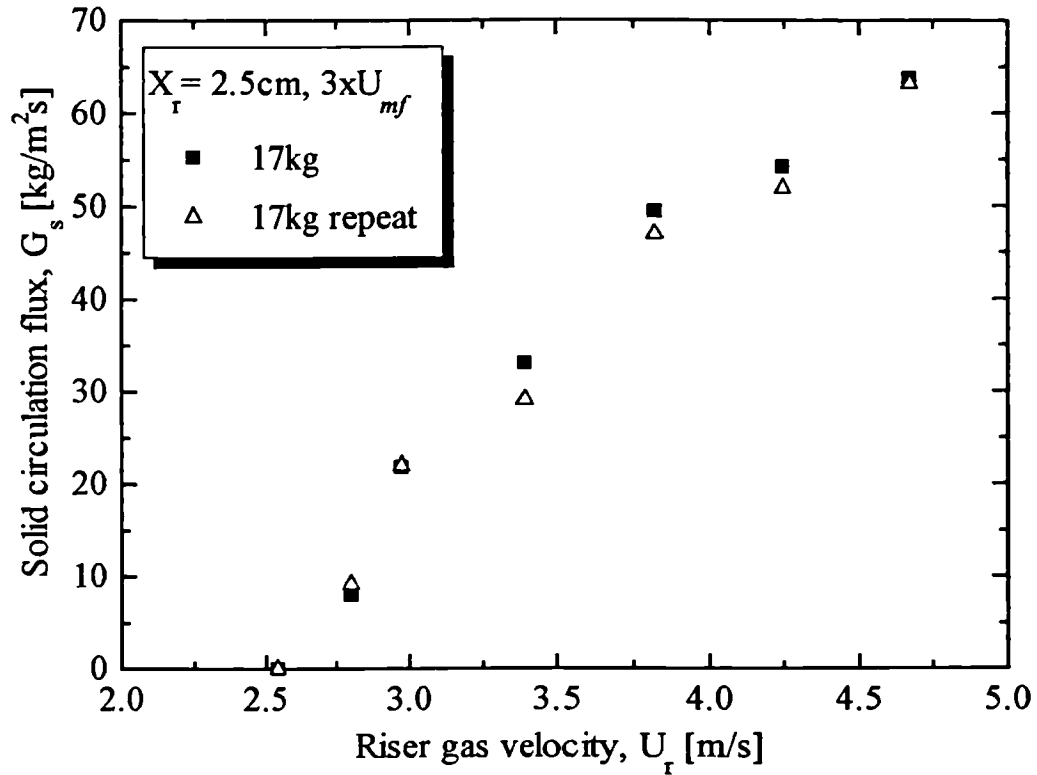


Fig. 6.15 Solid circulation flux versus riser superficial gas velocity for bed load 20 kg, $X_r = 2.5$ cm (repeat).

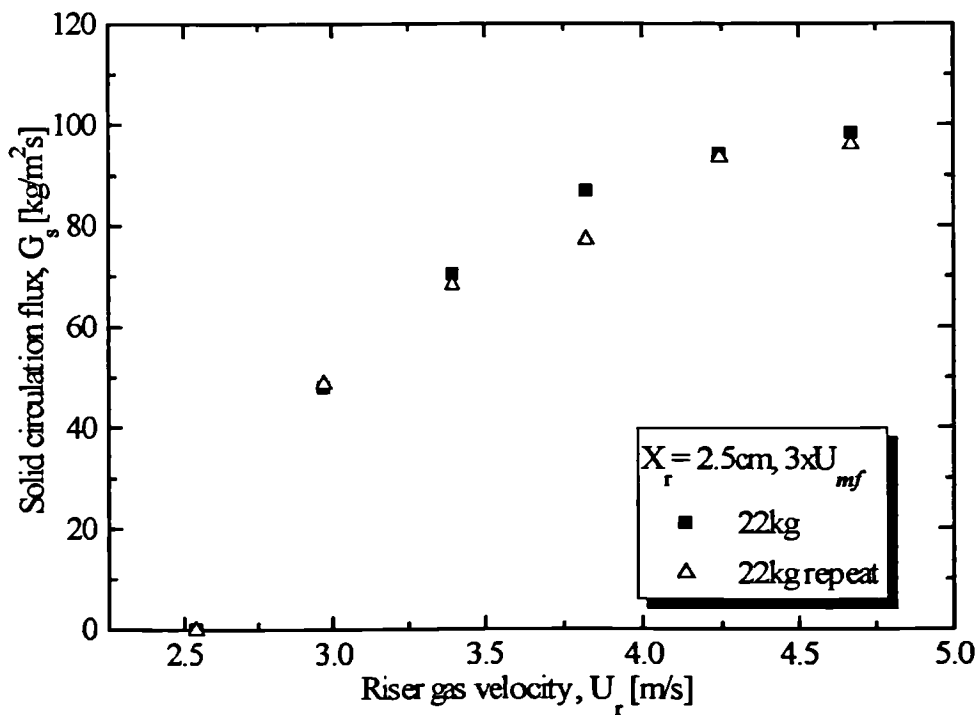


Fig. 6.16 Solid circulation flux versus riser superficial gas velocity for bed load 20 kg and $X_r = 2.5$ cm. (repeat).

The effect of the total bed inventory or the static bed height on the solids circulation rate are reported in Fig. 6.17- Fig. 6.19 for total bed inventory in the range of 12 - 22 kg. At any fixed X_r , the solids circulation increased by increasing the solids inventory, in the case of $X_r = 1$ cm the solids flux increases 6 times by just doubling the total bed inventory. Very little or no solids circulation was observed at bed loads below 12 kg over the present conditions. This was due to the fact that the level of solids in the gasifier could not reach high enough in order to flow over the weir and into the downcomer. Having reached this level at high riser gas velocity, most of the solids were transported to the gasifier with very little solids remaining in the combustor. The increased circulation flux with increasing total solids inventory is as a results of the increased pressure drop at the riser inlet which has the effect of forcing more particles into the riser. Also, increasing the total inventory simply increases the amount of material available for circulation, thus increasing the solids flux.

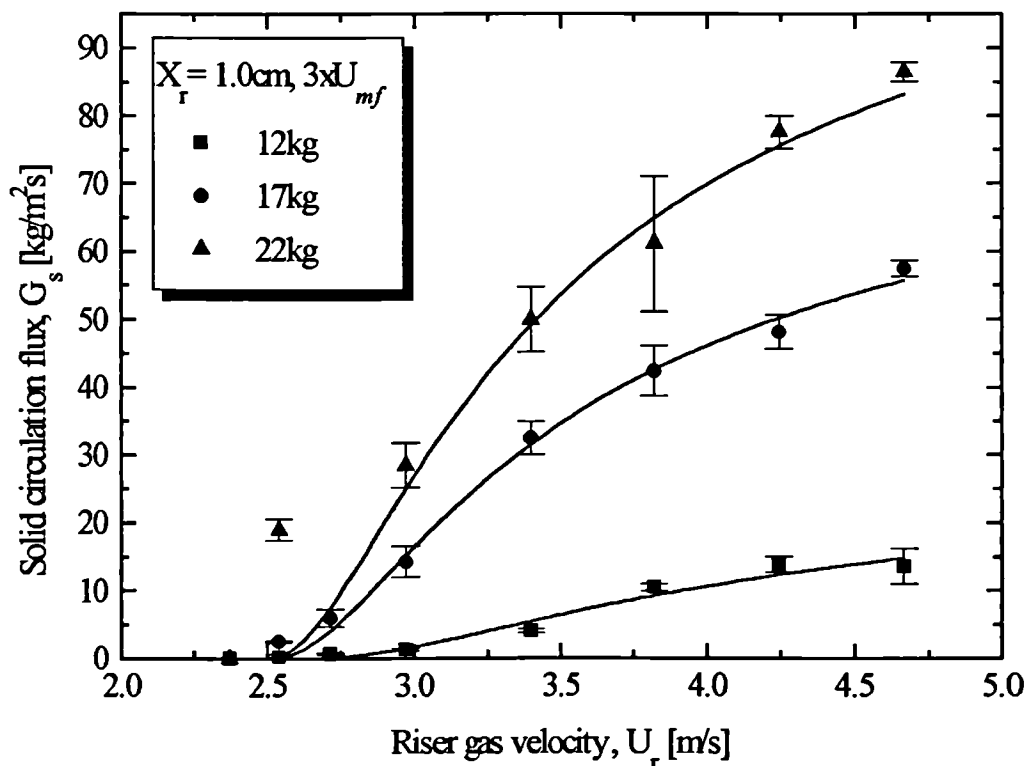


Fig. 6.17 Solid circulation flux as a function of riser superficial gas velocity and total bed load.

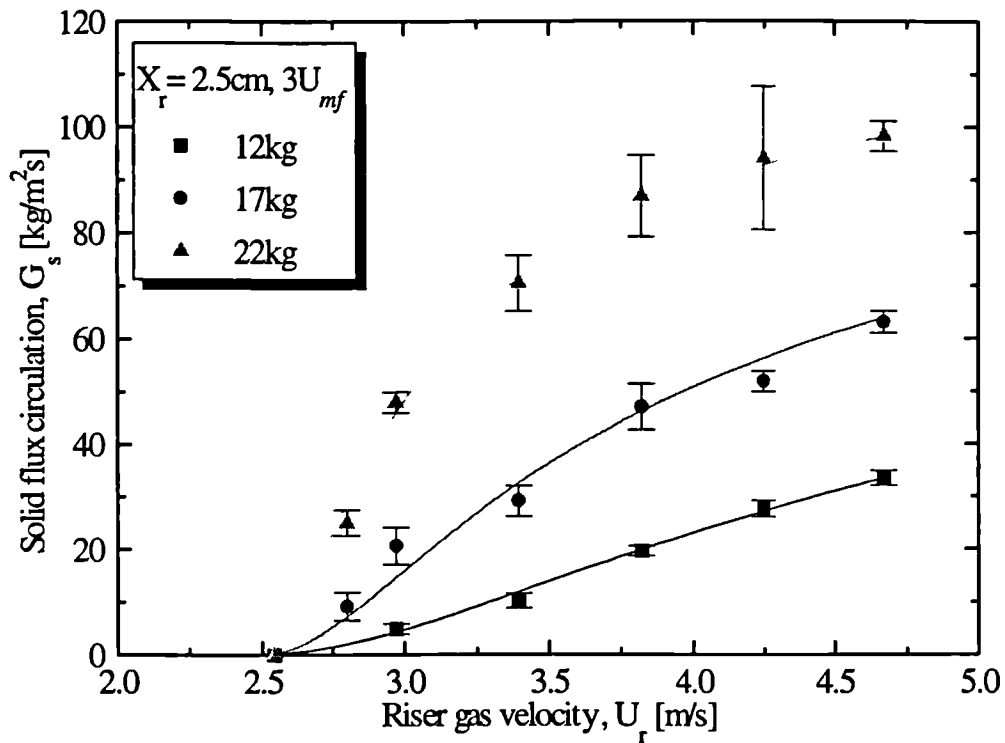


Fig. 6.18 Solid circulation flux as a function of riser superficial gas velocity and total bed load.

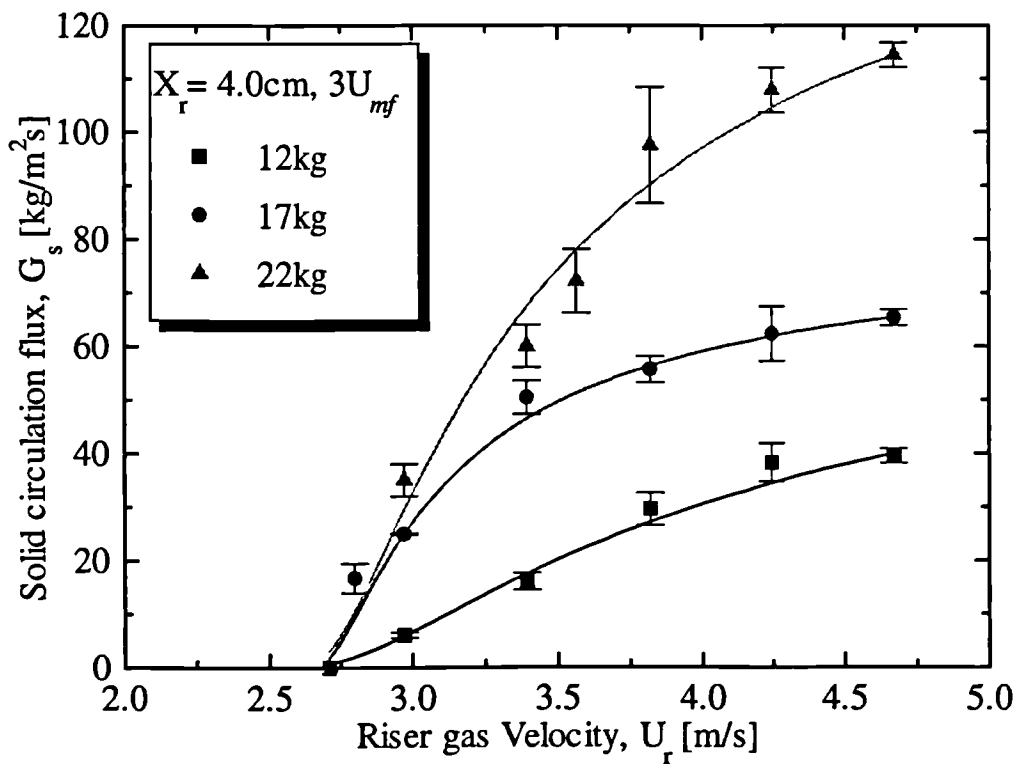


Fig. 6.19 Solid circulation flux as a function of riser superficial gas velocity and total bed load.

Fig. 6.20 shows the effect of varying X_r on the solids circulation flux for a total bed inventory of 12 kg. As expected, the increase in the riser gas velocity increases the circulation flux, however, it can be clearly seen that solids flux also increases by increasing the distance between the riser inlet and the gas jet at constant total solids inventory. At the lowest X_r , the rate at which the circulation flux increases with the riser gas velocity is low, whilst increasing X_r to 2.5 and 4 cm, the slope of the curve dramatically increases. Increasing this gap allows more solids to be entrained and transported into the riser, thus increasing the overall circulation flux. This increase is significantly higher for X_r values of 2.5 cm and 4 cm at a fixed total solids inventory. The minimum or critical riser gas velocity required to start solid circulation shifts to the right (i.e. increases) as the X_r is increased as more clearly shown in Fig. 6.21. Operating at riser gas velocities below the critical velocity lead to the collapse of the fluidized solids from gasifier into the riser, and resulted to an immediate termination of solids circulation.

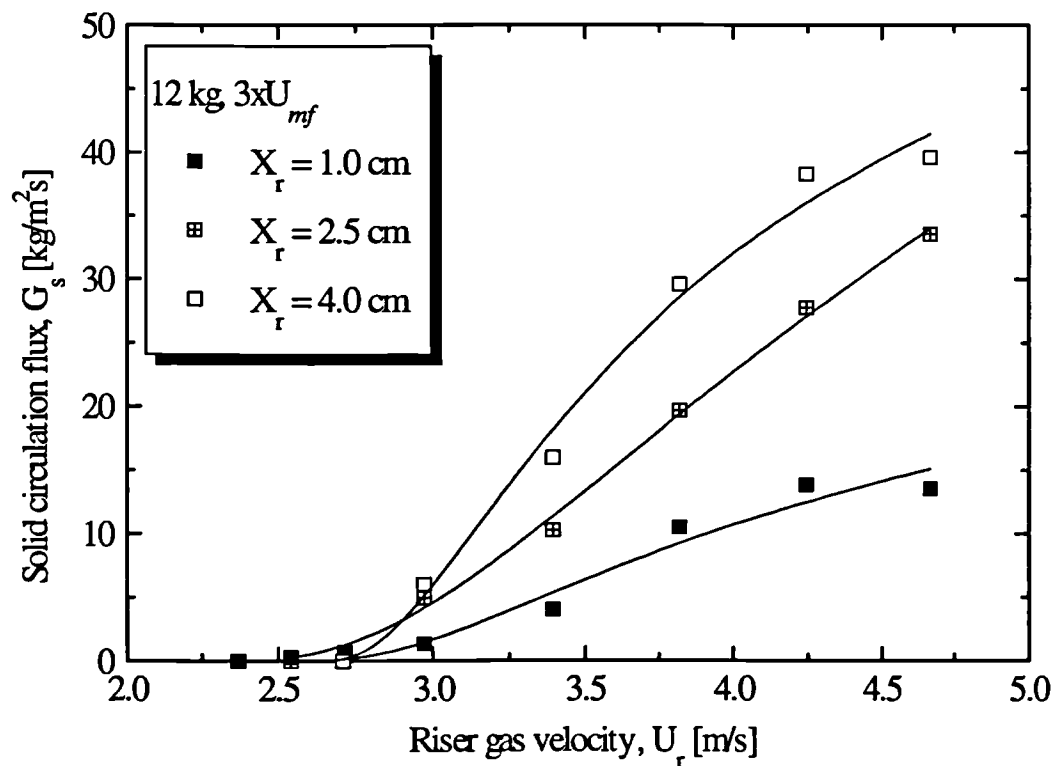


Fig. 6.20 Solid circulation flux as a function of riser superficial gas velocity and riser-gas jet distance, X_r , for bed load 12 kg.

Over the range of riser gas velocities studied, increasing X_r beyond 4 cm lead to

instabilities in the operation of the circulating system. This manifested itself in the periodic diversion of the gas from the riser jet into the combustion section which lead to the periodic shutting of the solids circulation. This phenomenon is similar to the case of a draft tube in a spouting bed. Locating the draft tube too close to the distributor plate leads to lower circulation rates due to the physical constriction created.

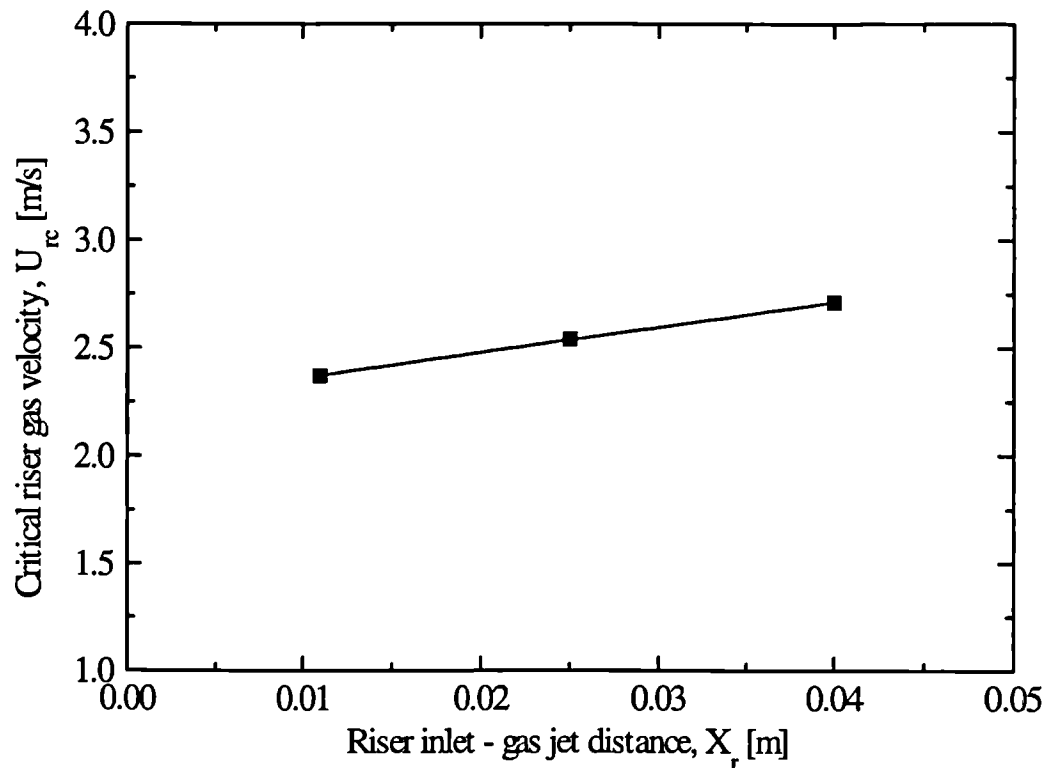


Fig. 6.21 Critical riser superficial gas velocity, U_{rc} as a function of the riser-gas jet distance, X_r .

6.3.1 CONCLUSIONS

The solid circulation rate does not seem to be affected much by the superficial gas velocity in the combustor (U_C) and gasifier (U_G) but, is mainly a function of the riser superficial gas velocity (U_r), total bed inventory (W_T), and X_r . Increasing these parameters increases the solid flux with the riser superficial gas velocity having the most pronounced effect. Thus the riser gas velocity can be used to control the circulation rate of solids. A threshold gas rate to the riser is required before solid circulation commences. This threshold or the critical riser gas velocity, U_{rc} , is required not only to transport the solids upwards in the riser but also to support the bed weight

which is felt at the riser exit. If the gas rate is not sufficient, then the bed in the gasifier collapses inside the riser and solid circulation is terminated immediately.

The solids circulation rate can be controlled by the manipulation of the riser gas velocity and the total solids inventory for a fixed X_r , independent of the fluidization conditions in the two beds. However, minimum fluidization is required in the two beds for satisfactory solid circulation. Also, the conditions in the two beds can be set independent of each other. Practically, solid circulation rates well above those required for the process can be easily obtained and manipulated.

6.4 GAS CROSS-FLOW BETWEEN BEDS

For the operation of the circulating bed as a whole, the gas leakage in either directions is of great importance. In the case of gas flow from the gasification zone into the combustion zone, the product gas quality is not affected but, the product gas yield is decreased and so leads to a lower cold gas efficiency. In order to study this, the tracer gas was injected into the gasifier windbox and its concentration was measured in the combustion section. From results not shown, there was zero product gas flow from the gasification zone to the combustion zone. Gas cross-flow from the gasification zone to the combustion zone can only occur via the downcomer, however, since some of the aeration gas travels up the return leg as shown in Fig. 6.4, this has the effect of forming a barrier against the gas which is dragged into the return leg with the circulating solids.

However, in the case of gas flow from the combustion zone into the gasification zone, the product gas is diluted with nitrogen and the combustion products. This leads to a product gas with a lower heating value and gas quality. To study this, the tracer gas was injected in the windbox of the combustor and its concentration was measured in the gasification zone outlet. As with solid circulation rates, gas cross-flow rate is plotted against the supplied superficial gas velocity up the riser.

As with the solid circulation, the three main parameters that determine the gas cross-flow rate are the riser gas velocity, the distance of the riser from the gas jet, and

the total solids inventory, and also to a lesser extent, the gas velocity in the two beds. The results of the gas tracing experiments are reported in Fig. 6.22 to Fig. 6.24, which show that as the riser gas rate is increased, the gas leakage also increases. Increasing the riser gas rate results in a stronger suction effect formed at the tip of the riser due to the high velocity of gas and solids travelling upwards. This suction pulls further solids dragging the interstitial gas with them. The gas cross-flow increases if the gas velocity in bed 1 is increased from $2U_{mf}$ to $3U_{mf}$ and moving to $4U_{mf}$ reduces the gas leakage, and also the gas cross-flow levels off towards the higher ranges of the riser gas velocity. These phenomena are similar to the solid circulation patterns reported earlier and highlights the close and inevitable connection between solid circulation and gas cross-flow.

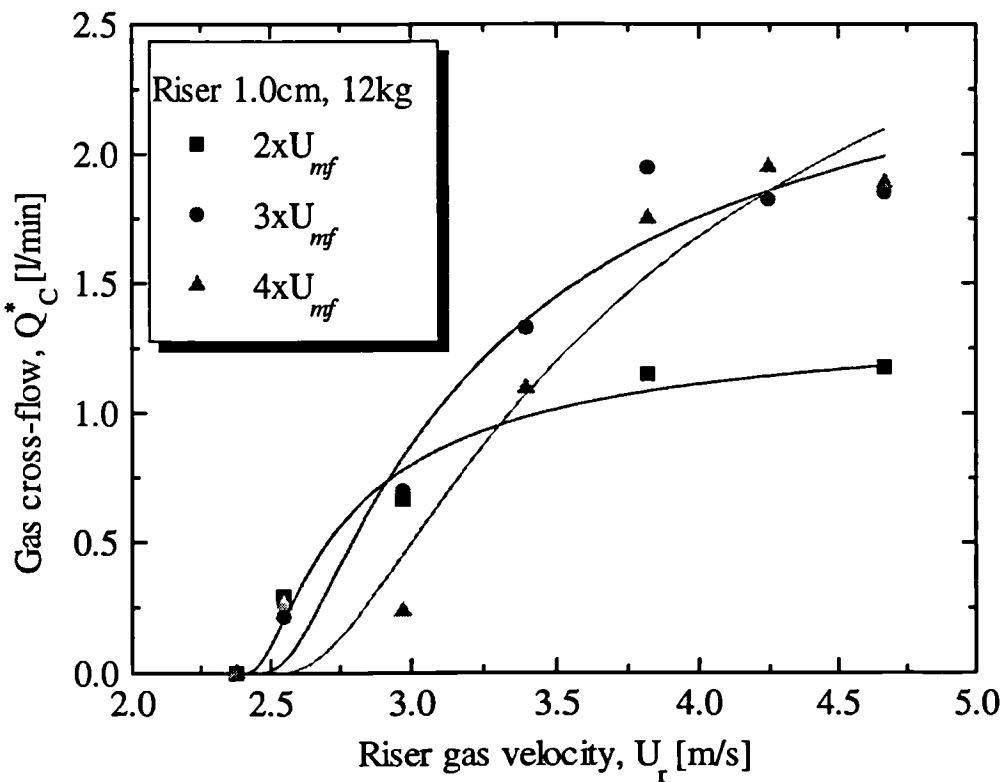


Fig. 6.22 Gas cross-flow versus U_r for bed load 12kg.

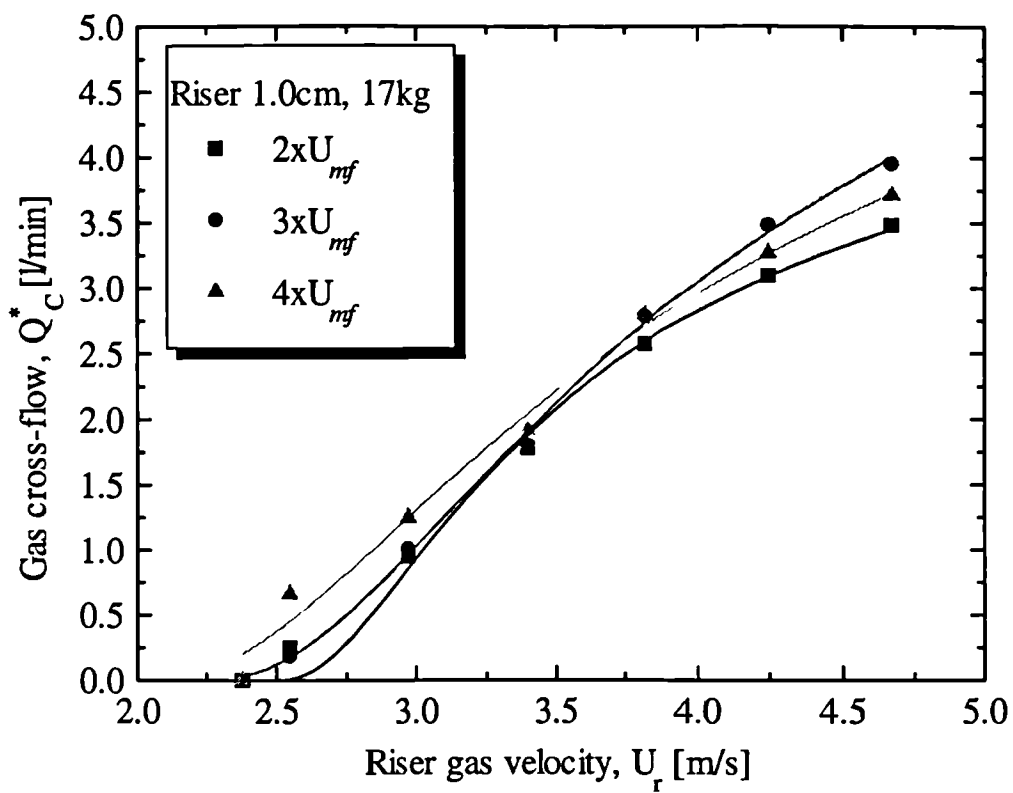


Fig. 6.23 Gas cross-flow versus U_r for bed load 17kg.

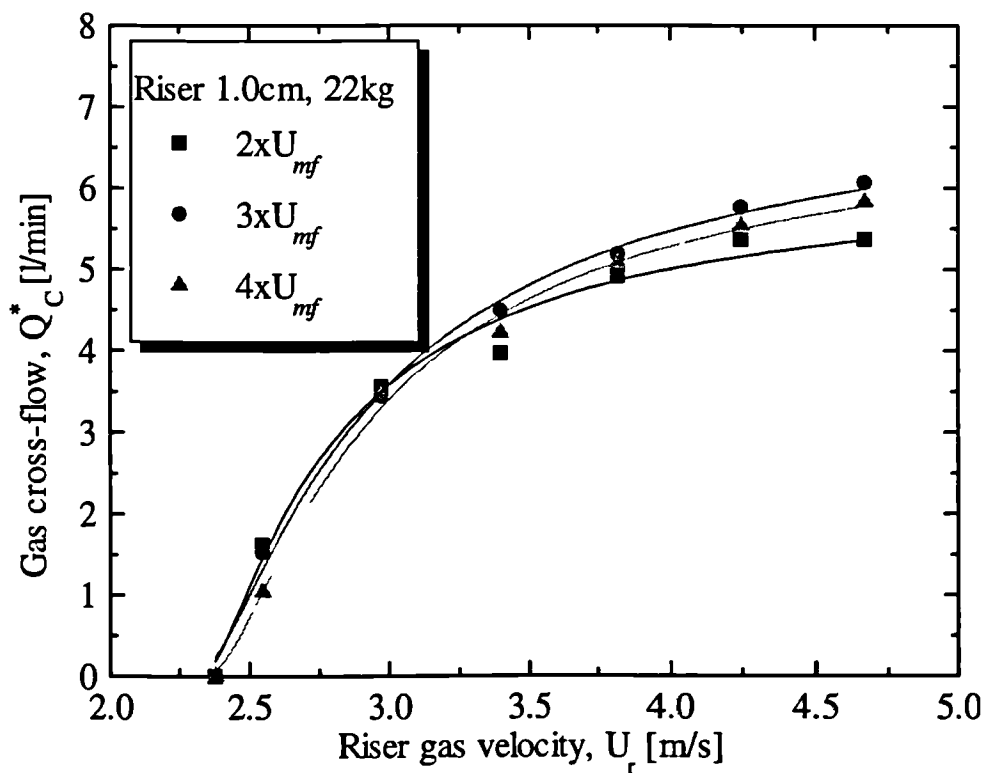


Fig. 6.24 Gas cross-flow versus U_r for bed load 22kg.

The effect of increasing the total mass load on the gas cross-flow rate is shown in Fig. 6.25 to Fig. 6.27. The y-axis on the right hand side of the same figures show the gas cross-flow as a percentage of the total gas input into the combustor. The addition of more solids to the circulating system lead to a higher gas cross-flow. Increasing the total solids inventory, increases the bed height in the combustor which in turn increases the resistive force to the up-flowing gas. Therefore more gas finds its way into the riser. However, increasing the gas velocity into the combustor from $3U_{mf}$ to $4U_{mf}$ reduces the gas cross-flow since the bulk bed density is increased and the gas flow through the bed becomes easier. Under the most severe conditions, the gas leakage is under 4 percentage of the total gas input into the combustion section. This is well within the tolerable limit for biomass combustion-gasification.

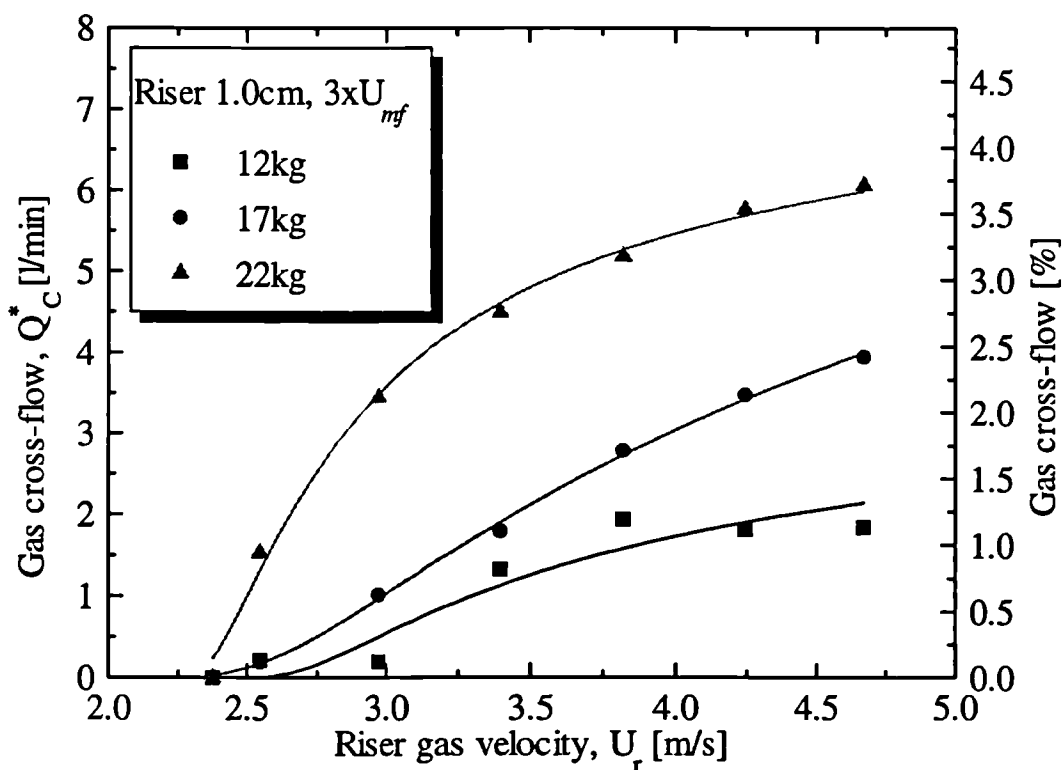


Fig. 6.25 Gas cross-flow versus U_r for $X_r = 1.0$ cm.

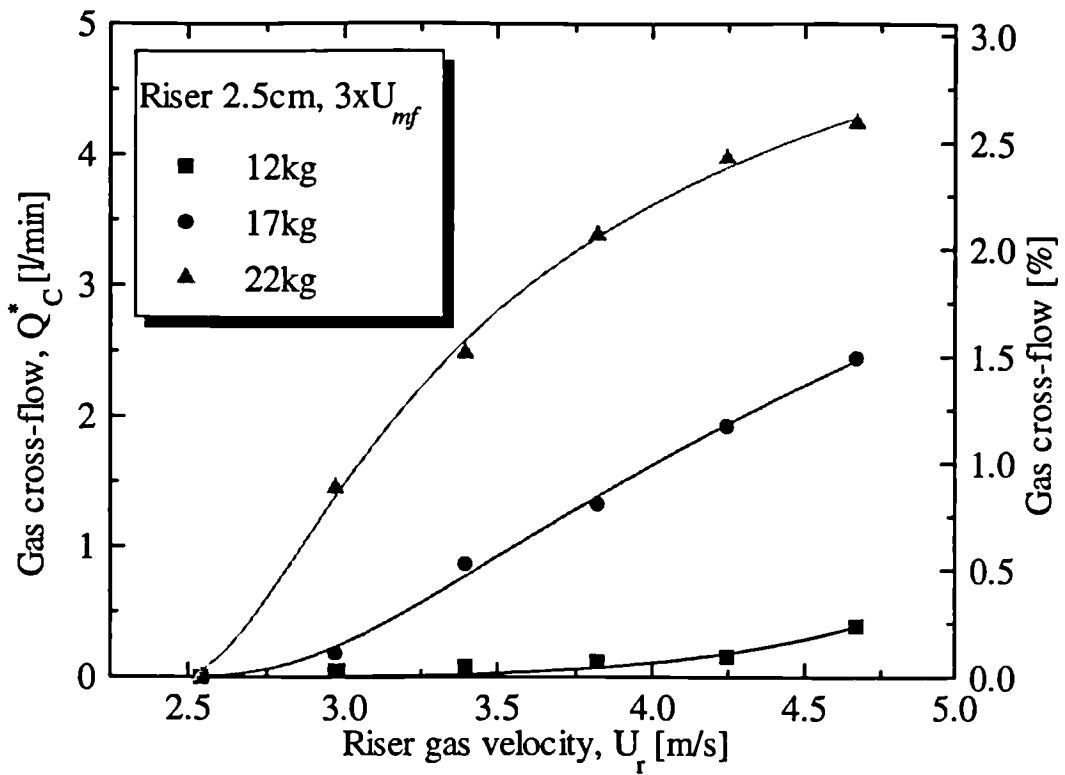


Fig. 6.26 Gas cross-flow versus U_r for $X_r = 2.5$ cm.

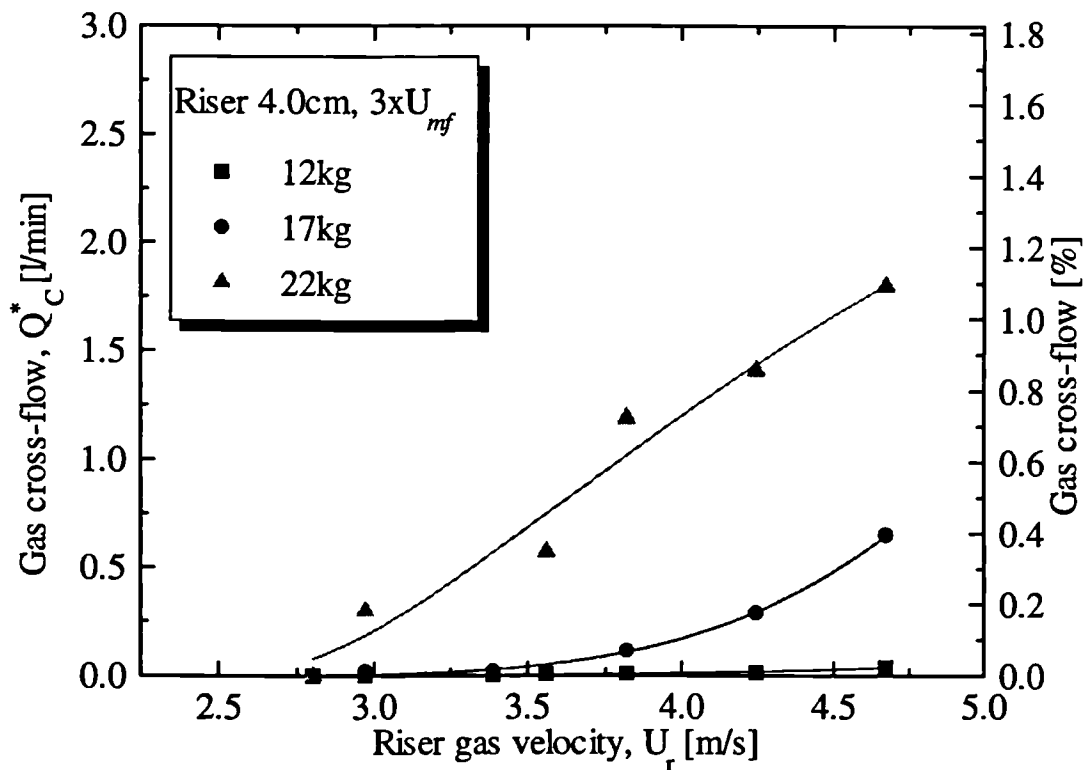


Fig. 6.27 Gas cross-flow versus U_r for $X_r = 4.0$ cm.

Fig. 6.28 shows the effect of increasing X_r , from 1.0 to 4 cm, on the gas cross-flow rate for a total bed inventory of 17 kg. The picture here is somewhat in contradiction to what is already discussed on the link between solid circulation and gas cross-flow. It has already been shown that as the solids circulation rate increases, so does the gas cross-flow, thus increasing the distance of the riser from the gas jet leads to an increase in the solid circulation flux due to an increase in the amount of solids entrained by the gas jet and so the gas cross-flow would be expected to increase as well - in fact, the reverse happens as shown in Fig. 6.28. The results can be explained by taking a look at the gas-solid structure at the riser inlet for different X_r as sketched in Fig. 6.29.

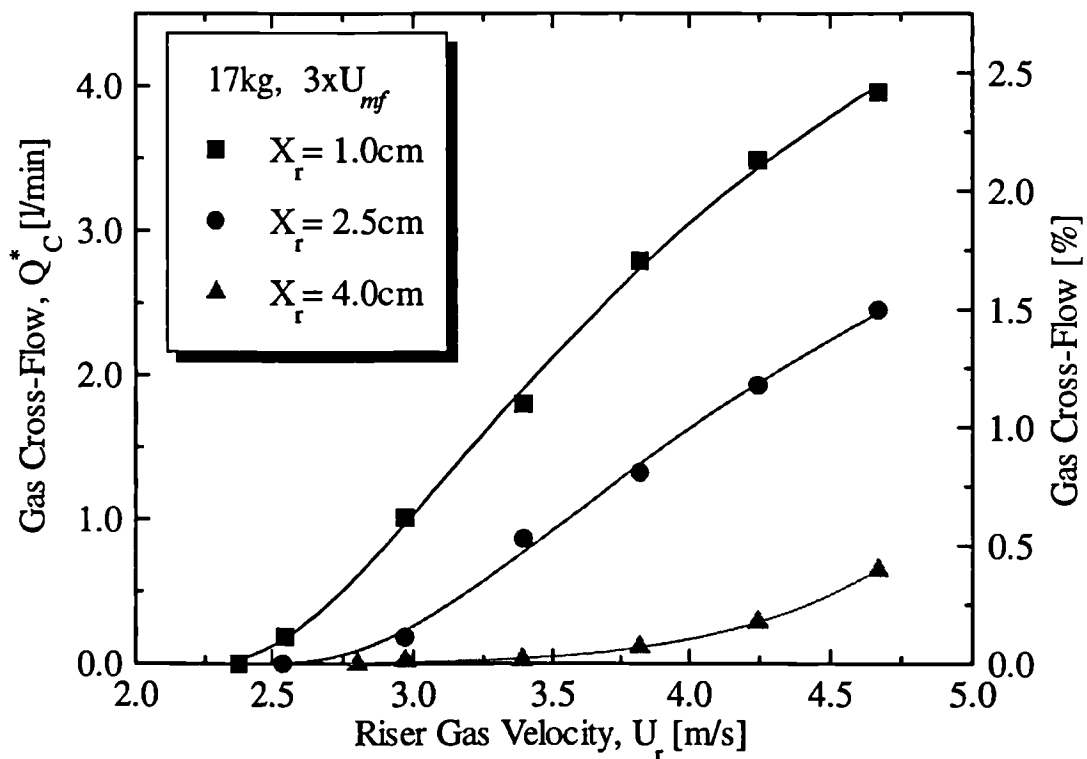


Fig. 6.28 Relationship between the gas cross-flow and X_r as a function of the riser superficial velocity for a total bed inventory of 17 kg.

When the gas jet is too close to the riser inlet, the gas jet penetrates deep into the riser, thus forming a suction effect which draws gas and solids into the riser. However, moving the gas jet away from the riser inlet reduces this effect until it forms a barrier.

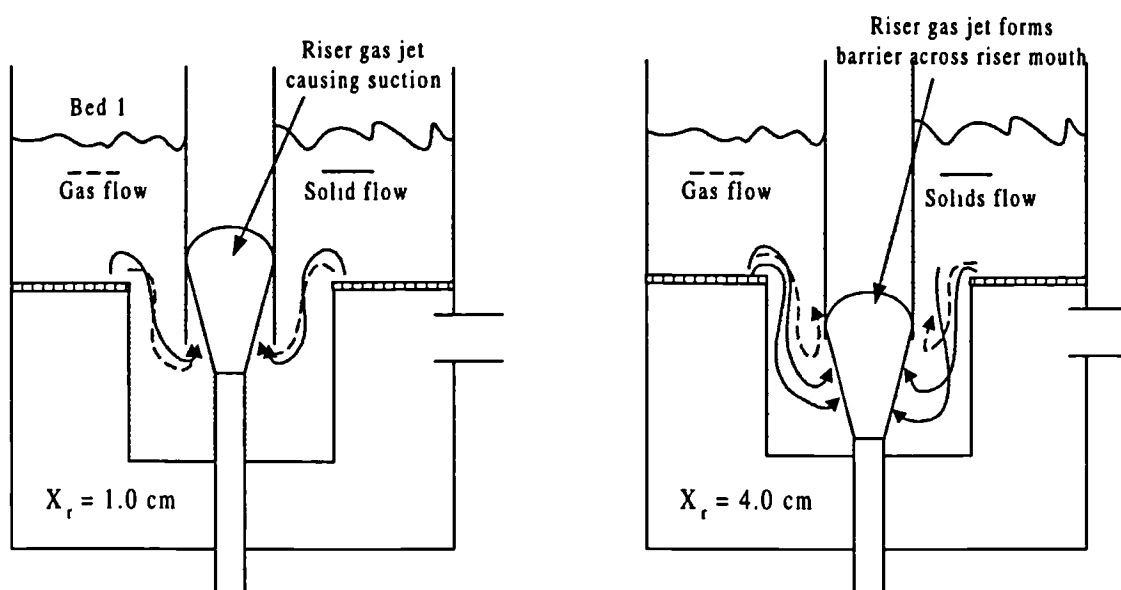


Fig. 6.29 Gas - solid flow at the riser inlet.

6.4.1 CONCLUSIONS

There is always some gas leakage from the combustion section to the gasification section, however, this can be controlled and minimised by suitable operational strategies. The main parameter being the distance of the gas jet from the riser inlet and the parameter that least effects the gas cross-flow is the gas rate into the beds. Over the range studied, in the most severe case, the gas cross-flow accounts for less than 4 % of the total gas input into the combustion chamber, and this is well below the tolerable limit for a biomass combustion - gasification process.

6.5 RELATIONSHIP BETWEEN SOLIDS CIRCULATION AND GAS CROSS-FLOW

From the results presented in the previous sections, it is obvious that solids circulation and gas cross-flow are related, as they both change with the apparent process variables in the same manner. Fig. 6.30 reports the results of gas cross-flow as function of the solids circulation flux for different total solids inventory and X_r . It can be seen that at a fixed X_r and for a given gas rate to the riser, the gas to solids ratio in the circulating stream seems to be almost constant irrespective of the other operating variables. Increasing X_r has the effect of decreasing this ratio, indicating that less gas is flowing with the circulation solids.

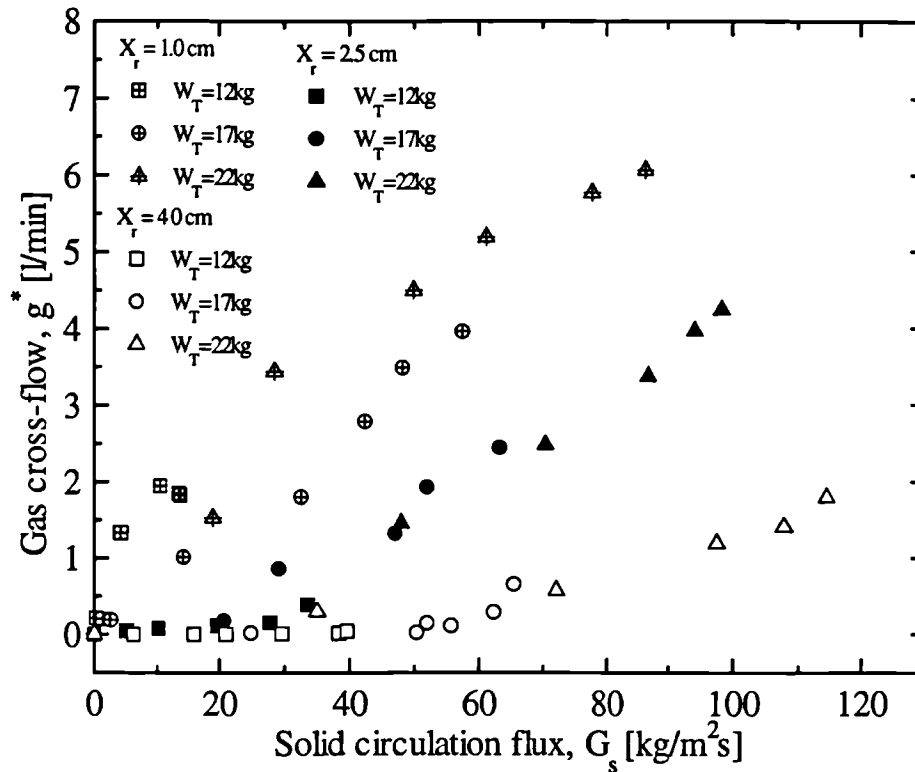


Fig. 6.30 Relationship between solid circulation and gas cross-flow.

6.6 CORRELATION OF SOLID CIRCULATION AND GAS CROSS-FLOW

An attempt to develop an empirical correlation for the solid circulation rate and gas cross-flow rate was made by taking into account the effects of all the operating parameters. Consider the gas cross-flow results shown in Fig. 6.26 for bed inventories of 12, 17, and 22 kg. The y-axis can be made dimensionless by dividing the gas cross-flow rate by the total gas input into the combustor. Similarly, the x-axis can be non-dimensionalised by dividing the terminal settling velocity of a single particle, U_t into the riser gas velocity. The results are shown below in Fig. 6.31.

The terminal settling velocity of a single particle is evaluated from the following equation

$$U_t = \sqrt{\frac{4}{3} \left(\frac{\rho_s - \rho_g}{\rho_g} \right) \frac{d_p g}{C_D}} \quad (6-1)$$

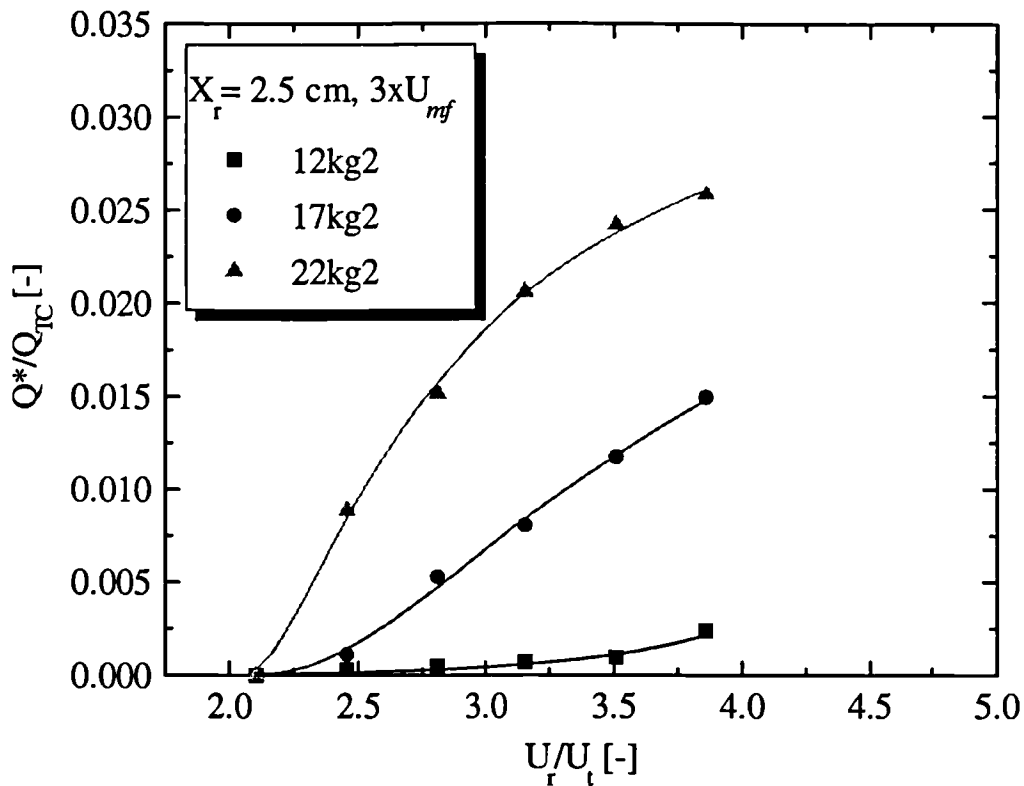


Fig. 6.31 Dimensionless gas cross-flow vs. dimensionless riser gas velocity.

There are numerous empirical expressions available in literature which express the drag coefficient, C_D , as a function of the Reynolds number, Re . The drag coefficient was evaluated using the equation proposed by Dallavalle (Foscolo and Gibilaro, 1984) which is applicable over the laminar, intermediate, and turbulent regimes.

$$C_D = (0.63 + 4.8 Re_t^{-0.5})^2 \quad (6-2)$$

The Reynolds number is calculated as 13.8 which gives a drag coefficient of 3.68 and thus giving U_t for the particles as 1.18 m/s. Having fitted different forms of equations to the data in Fig. 6.31, it was decided that the experimental points were best described by an exponential equation of the form

$$y = K_1 \exp\left(\frac{K_2 + K_3 X}{X - K_4}\right)$$

It has been shown in previous sections that the solid circulation rate as well as the gas cross-flow rate are functions of W_T , U_r , U_G , U_C , and X_r . Therefore considering the circulating system, and non-dimensional parameters

$$\frac{Q^*}{Q_{TC}} = K_1 \exp\left(\frac{K_2 + K_3 \frac{U_r}{U_t}}{\frac{U_r}{U_t} - K_4}\right) \quad (6-3)$$

$K_1, K_2, K_3, K_4 = \text{fn}(W_T, U_r, U_G, U_C, \text{ and } X_r)$. A dimensionless parameter is defined here as β expressed by

$$\beta = \frac{W_T U_G}{A_r X_r \rho_s U_C} \quad (6-4)$$

where A_r is the cross-sectional area of the riser. All the data for the non-dimensional gas cross-flow were fitted with Eq (6-3) and the parameters $K_1 - K_4$ evaluated and plotted as a function of β . The results are shown below in Fig. 6.32.

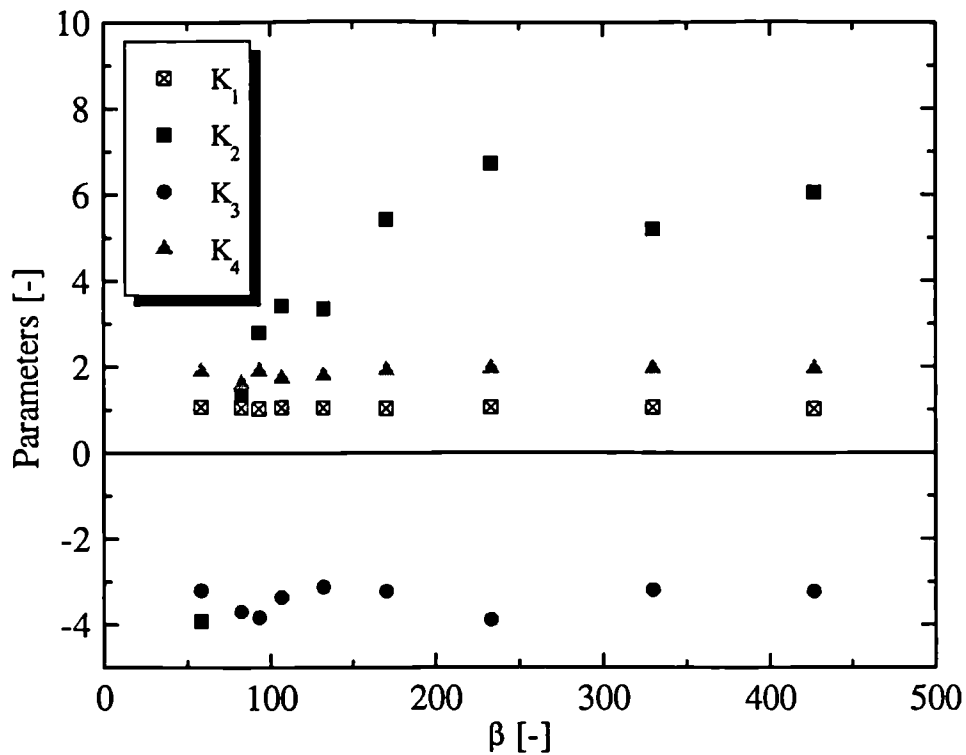


Fig. 6.32 K_1 - K_4 values as a function of β .

Parameters K_1 and K_4 were almost constant and so they were fixed at 1.05 and 1.96 respectively. Having fixed these two parameters, they were used to re-evaluate parameters K_2 and K_3 and the results are shown in Fig. 6.33. K_3 was kept constant at a value of -3.2 and the problem now was to find an expression to describe K_2 data. Again having tried different equations, the following was found to best fit the data:

$$K_2 = 267.3 + 0.054\beta - 149.9\beta^{0.1} - 699.3\frac{\ln(\beta)}{\beta} \quad (6-5)$$

Fig. 6.34 shows the comparison of the experimental dimensionless gas cross-flow and the correlation results.

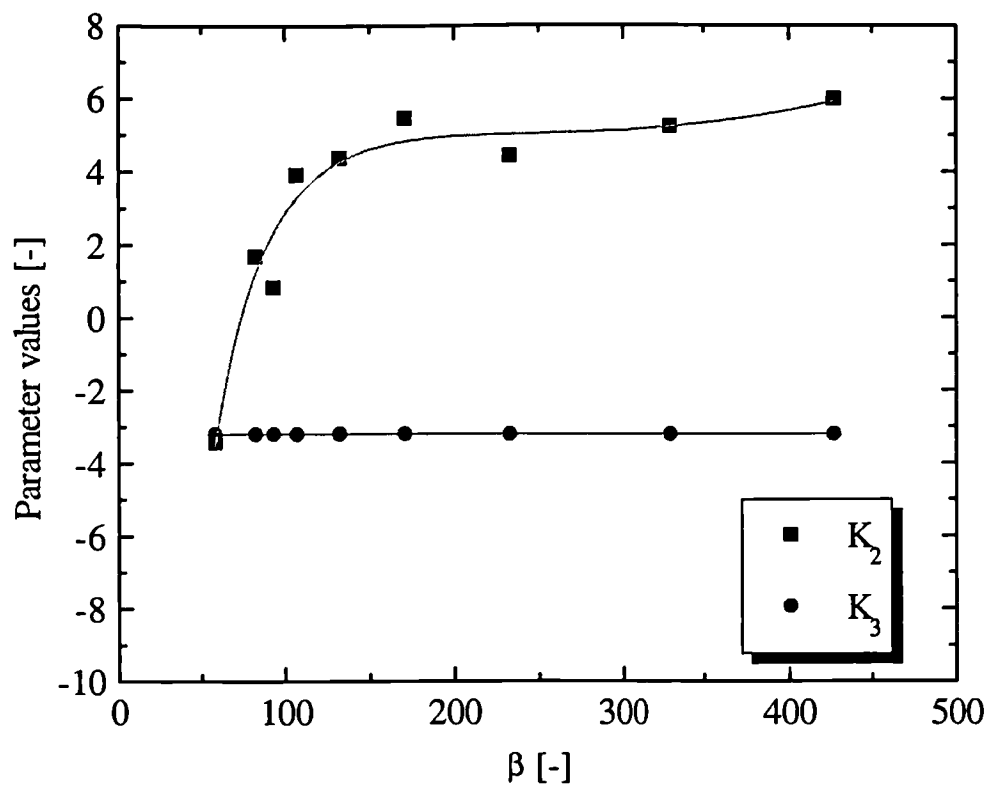


Fig. 6.33 Re-evaluated K_2 and K_3 values as a function of β .

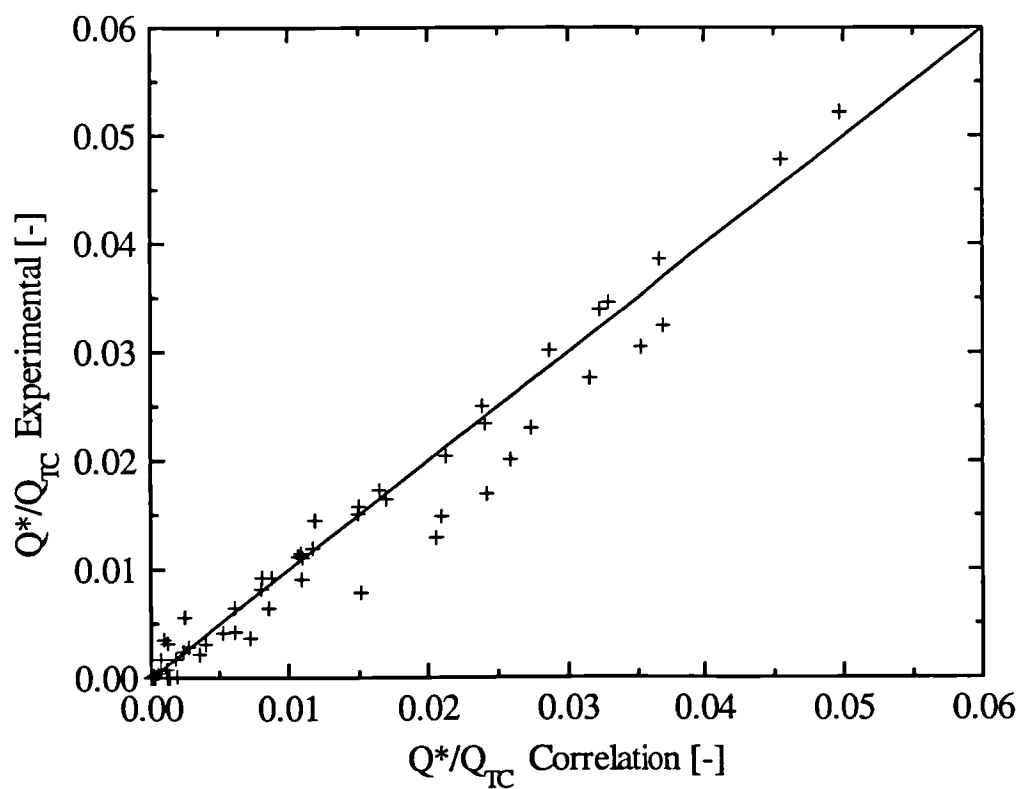


Fig. 6.34 Comparison of experimental and correlation values of the non-dimensional gas cross-flow

The same procedure was followed in order to correlate the solid circulation rate. The solids flux was made dimensionless by dividing into the particle density and riser gas velocity. The dimensionless circulation flux was plotted against the dimensionless riser gas velocity and used to correlate the solids circulation flux.

$$\frac{G_s}{\rho_s U_r} = \exp \left(\frac{K_5 + K_6 \frac{U_r}{U_t}}{\frac{U_r}{U_t} - K_7} \right) \quad (6-6)$$

$$K_5 = 2.06 \frac{X_r}{D_r} + 0.29 \frac{D_r}{X_r} + 7.48 \quad (6-7)$$

$$K_6 = \left(289 - 223 \frac{X_r}{D_r} - 158 \frac{D_r}{X_r} \right) \beta^{-1} + 0.4 \frac{X_r}{D_r} + 0.1 \frac{D_r}{X_r} - 4.15 \quad (6-8)$$

$$K_7 = \left(47.5 - 54 \frac{X_r}{D_r} - 20 \frac{D_r}{X_r} \right) \beta^{-1} + 0.77 \frac{X_r}{D_r} + 0.06 \frac{D_r}{X_r} + 1.66 \quad (6-9)$$

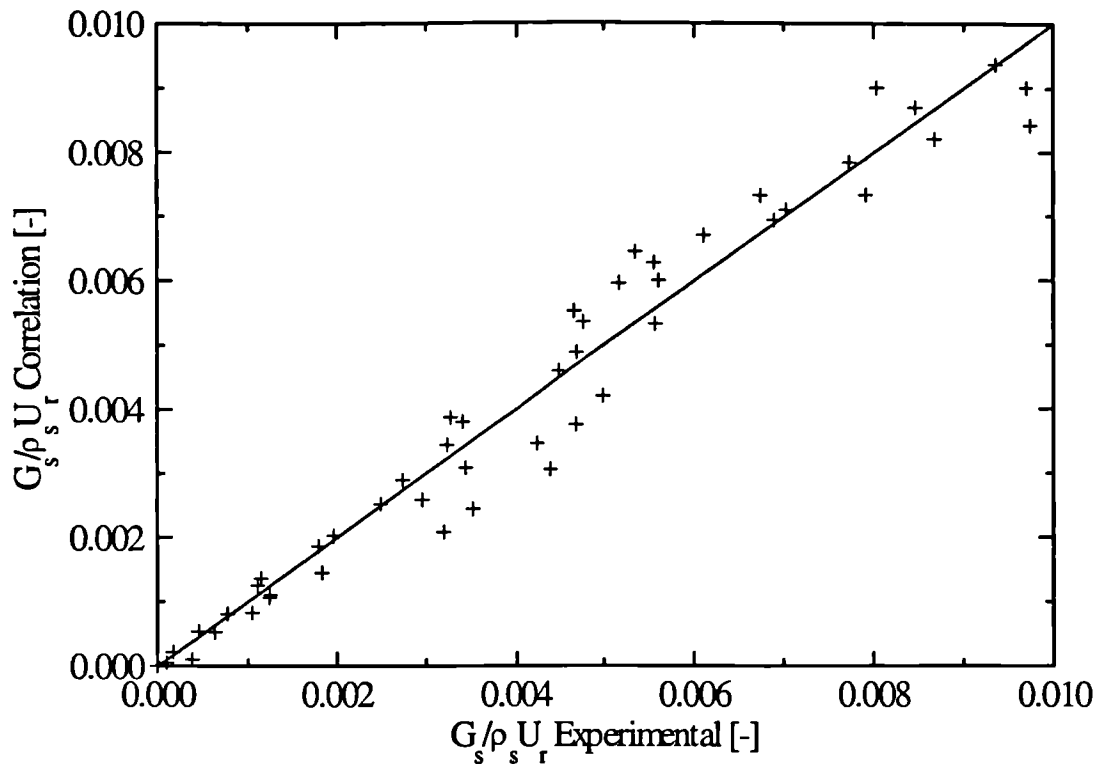


Fig. 6.35 Comparison of experimental and correlation values of the non-dimensional solids circulation flux.

6.7 SOLID RESIDENCE TIME IN BEDS

This area of study concerns the biomass particles themselves which have a density considerably lower than the particles that form the bed inventory. Once in the fluidized bed, these low density particles tend to float on the surface of the bed. Such segregation reduces the heating rate of the biomass particles and consequently the gas production in the initial devolatilisation stage of the gasification process is reduced. As a result, the contact time between the product vapours with the hot bed particles is also reduced which leads to a less efficient tar conversion.

To optimise the gas production and tar conversion, the residence time of the biomass particles in the bed should be of the same order as the devolatilisation time (generally a few seconds). This allows a longer solid-solid and gas-solid contact time and thus all or most of the volatile matter is released while the biomass particle is suspended within the bed.

The mean residence time of almond shell particles of 1.2mm in diameter ($\rho = 380 \text{ kg/m}^3$) in the two beds are reported in Fig. 6.36 to Fig. 6.41 for different bed loads, riser gas velocity, and X_r . The biomass particles were placed on the top of the fluidized bed in the combustor and solid samples were analysed at the sampling port. By comparing Fig. 6.36 and Fig. 6.37 which report the residence time in the gasifier and the combustor respectively, it can be seen that although the tracer particles have a density less than half of the bed material, they do circulate and mix well with the sand. The residence time in the combustor is always higher than the gasifier at fixed operating conditions which is expected since the combustor is operated as a slow bed. However, at riser gas velocities above about 3.7 m/s, the residence time of the biomass particles does not change much and is the same in each bed irrespective of the other operating conditions.

The residence time is seen to decrease with increasing total bed inventory, riser gas velocity and X_r . This is reasonably and physically accepted since an increase in the above parameters speeds up the solids circulation rate as is expected to reduce the solids stay in a particular section. This suggests that the only parameter that can partially control the residence time of foreign solid particles in the bed at fixed operating conditions is the riser gas rate as this is the main parameter controlling the solids circulation rate.

Some of the biomass particles were lost in the dead zones of the system, specially in the communication zone of the combustor and riser. These particles remained there indefinitely and had to be removed physically.

In conclusion, it can be said that a range of different residence time of foreign particles can be achieved in the present system, however, it is not easy to control this residence time via a specific operating variable. Further investigation is required to study the effect of the size of the foreign particles on the residence time.

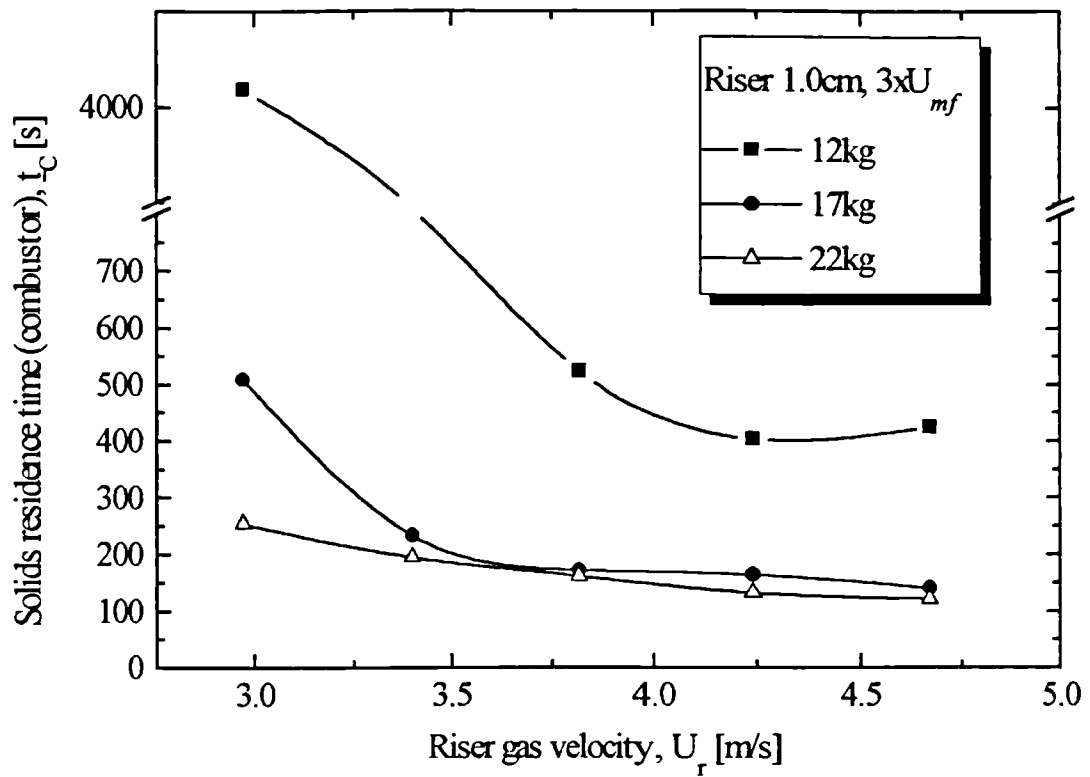


Fig. 6.36 Solids residence time (almond shells) in combustor versus U_r for $X_r = 1.0\text{cm}$.

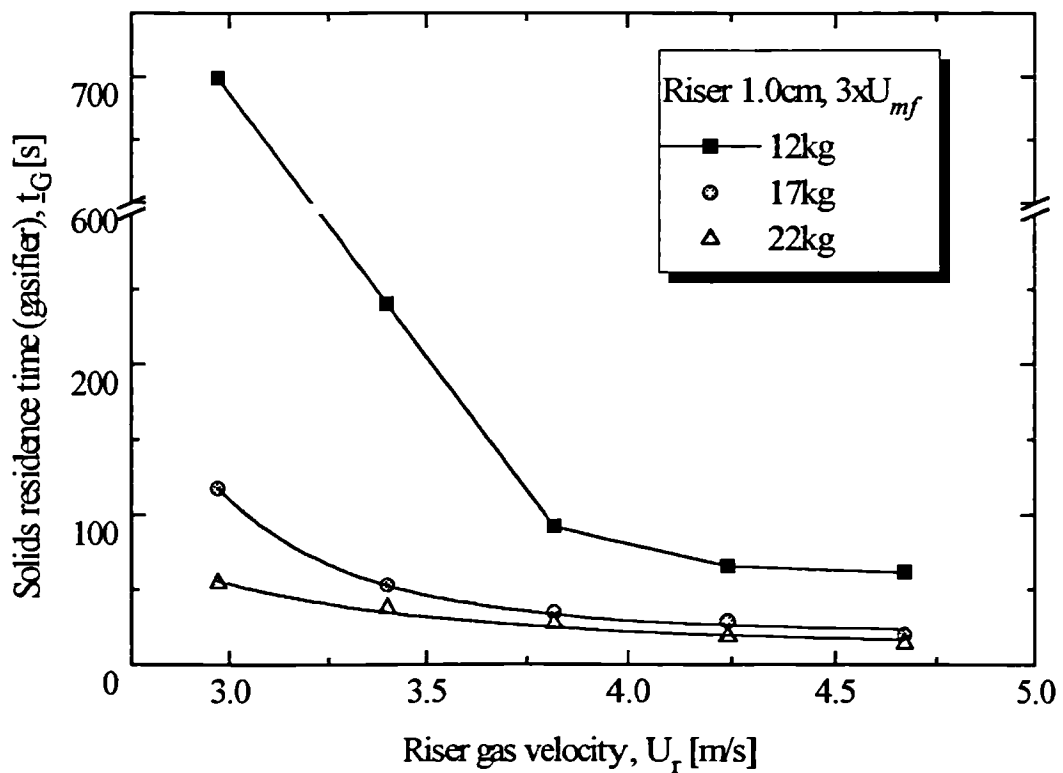


Fig. 6.37 Solids residence time (almond shells) in gasifier versus U_r for $X_r = 1.0\text{cm}$.

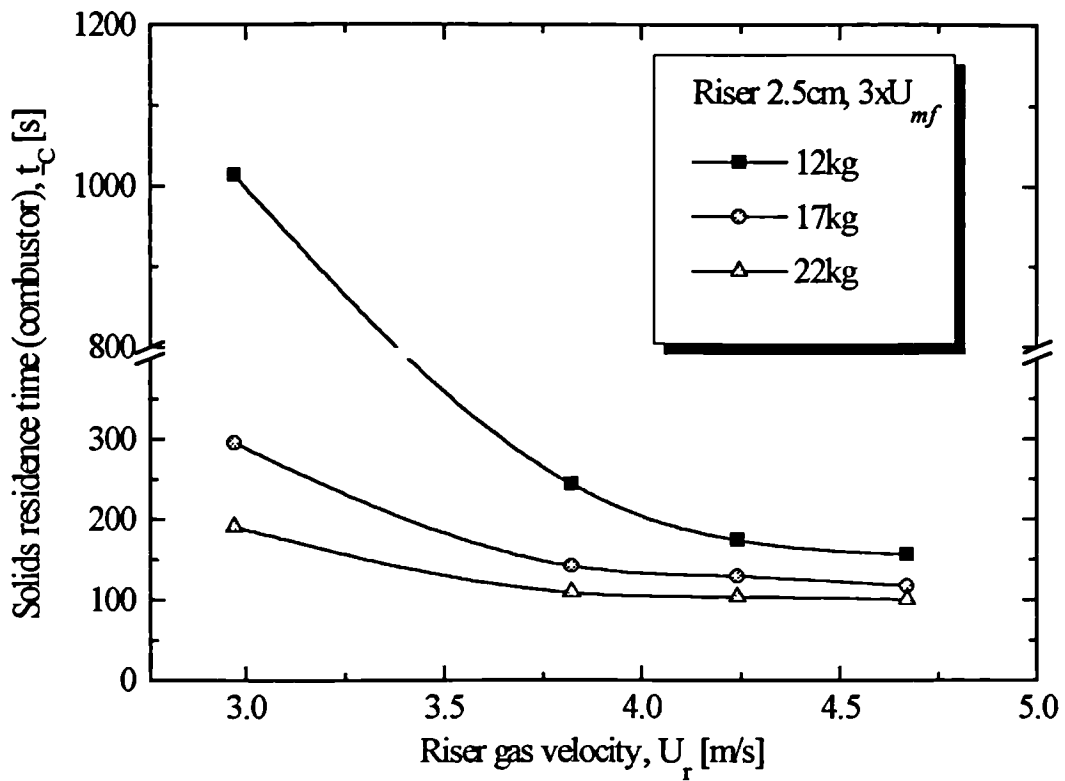


Fig. 6.38 Solids residence time (almond shells) in combustor versus U_r for $X_r = 2.5$ cm.

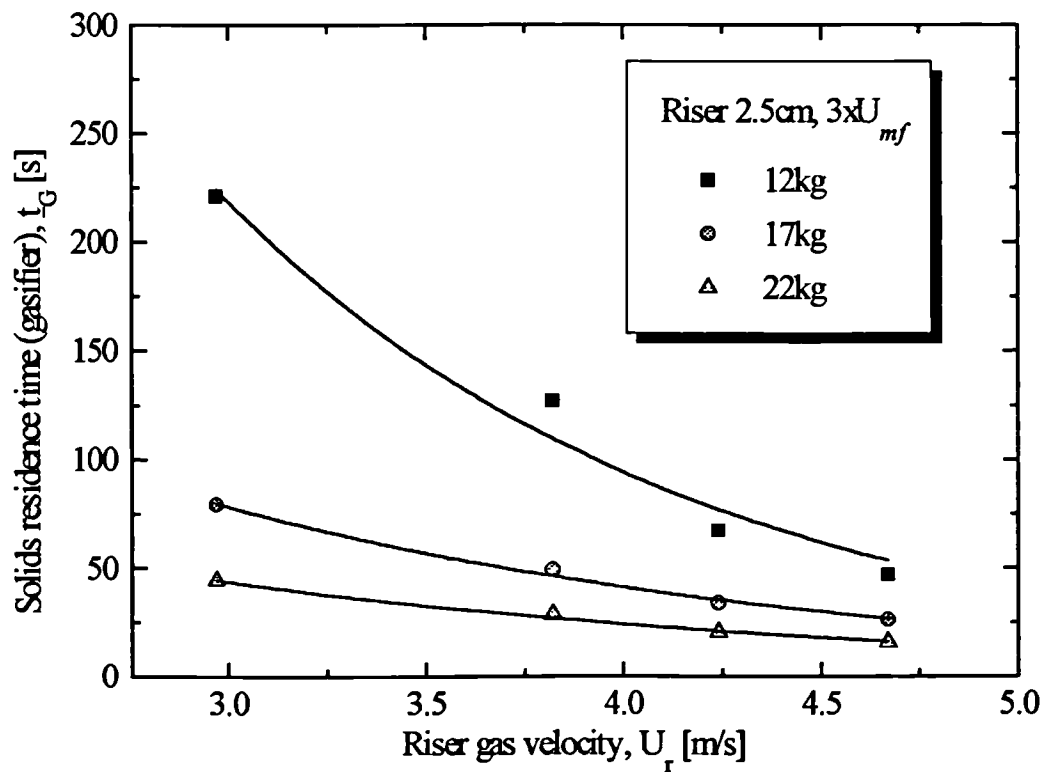


Fig. 6.39 Solids residence time (almond shell) in gasifier versus U_r for $X_r = 2.5$ cm.

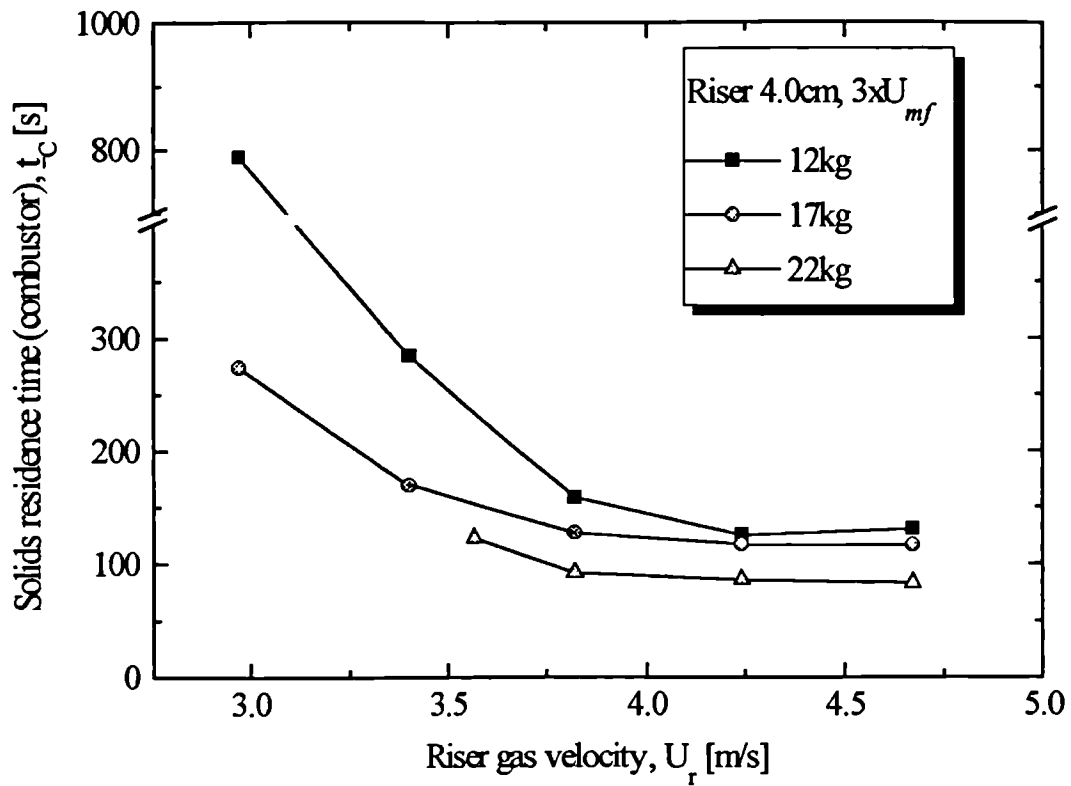


Fig. 6.40 Solids residence time (almond shells) in combustor versus U_r for $X_r = 4.0$ cm.

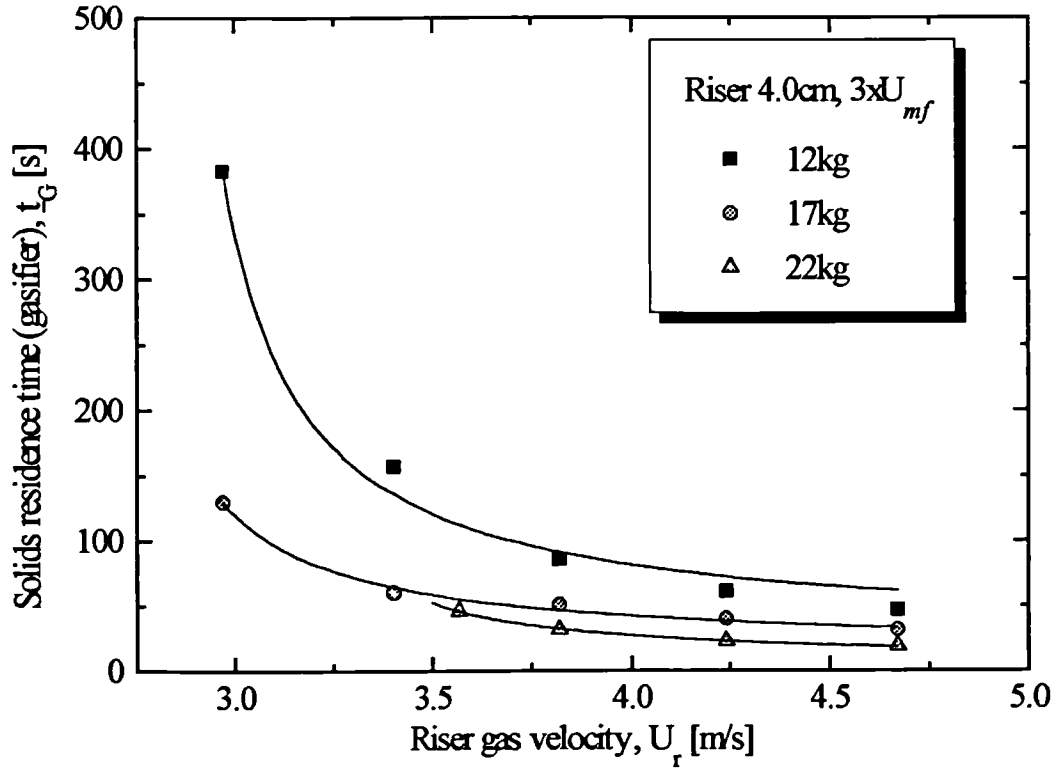


Fig. 6.41 Solids residence time (almond shells) in gasifier versus U_r for $X_r = 4.0$ cm.

6.8 PRESSURE ANALYSIS

The effect of varying the operating parameters on the pressure drop across specific parts of the circulating loop are present in Fig. 6.42 to Fig. 6.45. The pressure drop across all parts of the circulating system increases only upon increasing the total bed inventory. The decreasing pressure drop in bed 2 with increasing riser gas velocity suggests that the solids in this section are lost to the other parts of the circulating system due to the high gas velocity. This decrease is associated with a slight increase in the pressure drop across bed 1. The riser pressure drop decreases with increasing gas rate, since this pressure drop is directly related to the solids gravitational weight, then this means that the total solids hold up in the riser also decreases.

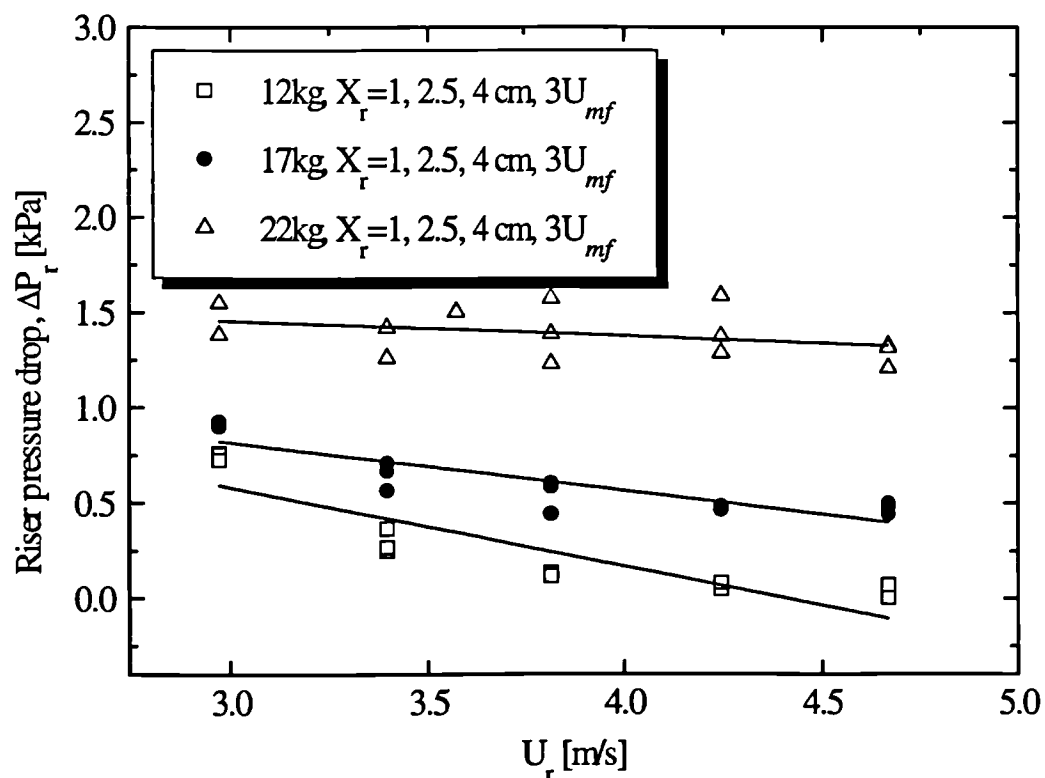


Fig. 6.42 Pressure drop across riser versus riser superficial gas velocity for different total solids inventory and X_r .

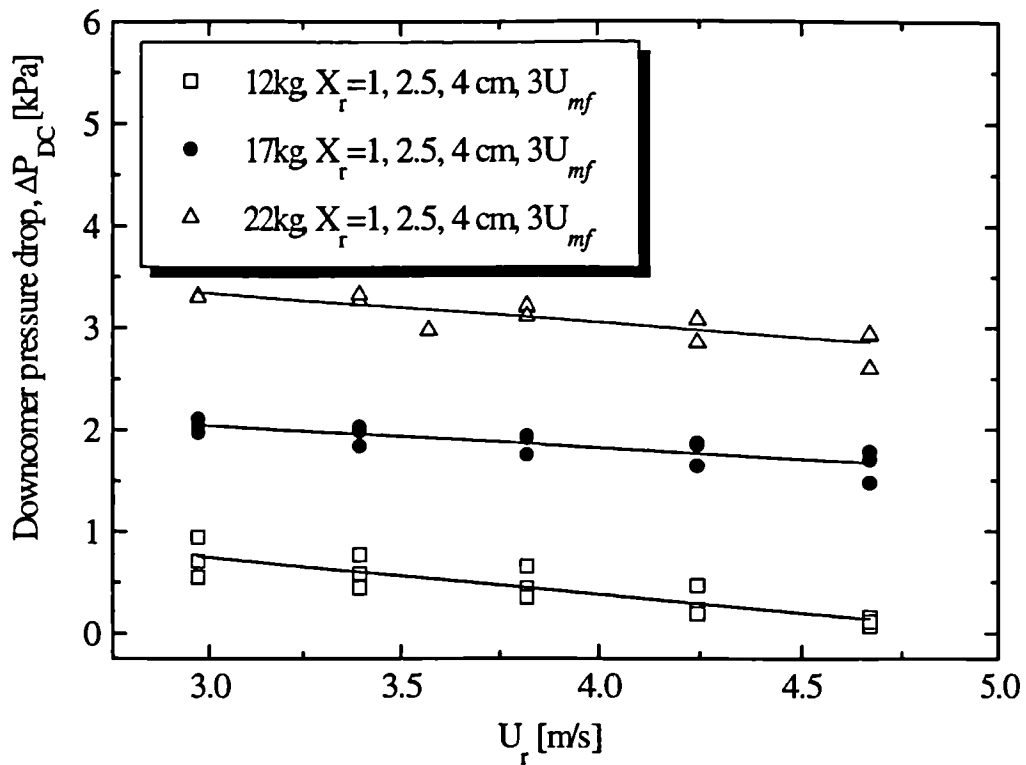


Fig. 6.43 Pressure drop across downcomer versus riser superficial gas velocity for different total solids inventory and X_r .

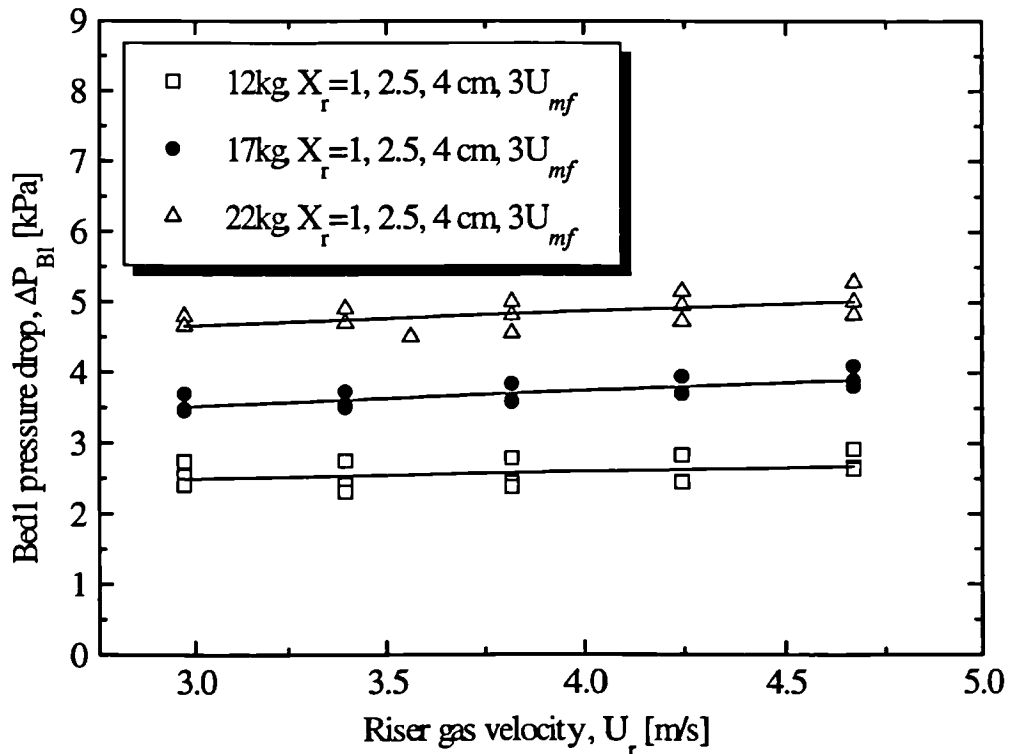


Fig. 6.44 Pressure drop across combustor versus riser superficial gas velocity for different total solids inventory and X_r .

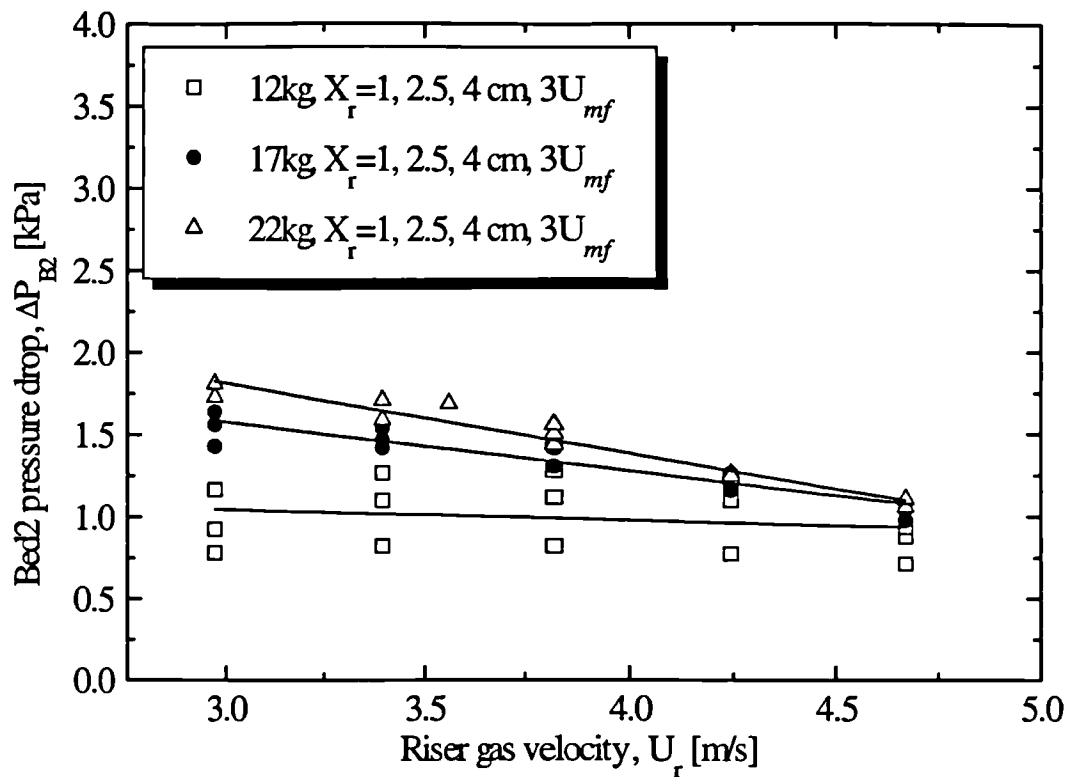


Fig. 6.45 Pressure drop across gasifier versus riser superficial gas velocity for different total solids inventory and X_r .

Assuming negligible acceleration and friction effects, the average solids concentration in the riser can be calculated from the mean pressure gradient using the following equation:

$$(1-\epsilon)_{\Delta P_r} = \frac{\Delta P_r}{(\rho_s - \rho_g)g\Delta H_r}$$

Also, the solid circulation flux in the riser can be estimated from:

$$G_s = \rho_s(1-\epsilon)v_s$$

Fig. 6.46 shows a Plot of G_s against the mean riser solids concentration. Although there is some scatter, nevertheless, all the points seem to fall on a straight line. Now, plotting $(1-\epsilon)$ against G_s/U_r also gives a straight line as shown in Fig. 6.47. Using the slope of the best fit line in Fig. 6.47, it can be shown that $V_s/U_r = 0.115$. Fig. 6.46 and Fig. 6.47 show that the solids velocity in the riser is directly dependent on the

superficial gas velocity supplied to the riser and independent of the other operating variables, such as circulation flux which in turn is dependent on the total solids inventory and X_r .

Also the average solids velocity in the riser is just under 12% of the superficial gas velocity in the riser. This seems very small but can be explained in the terms of the dilute core and dense annulus flow structure in the riser. The flow structure in the riser consists of a very dilute and swiftly moving solids in the core area of the riser surrounded by a dense and gradually falling annular area near the riser walls. Thus the average solids velocity across any region is low compared to the upwards gas velocity.

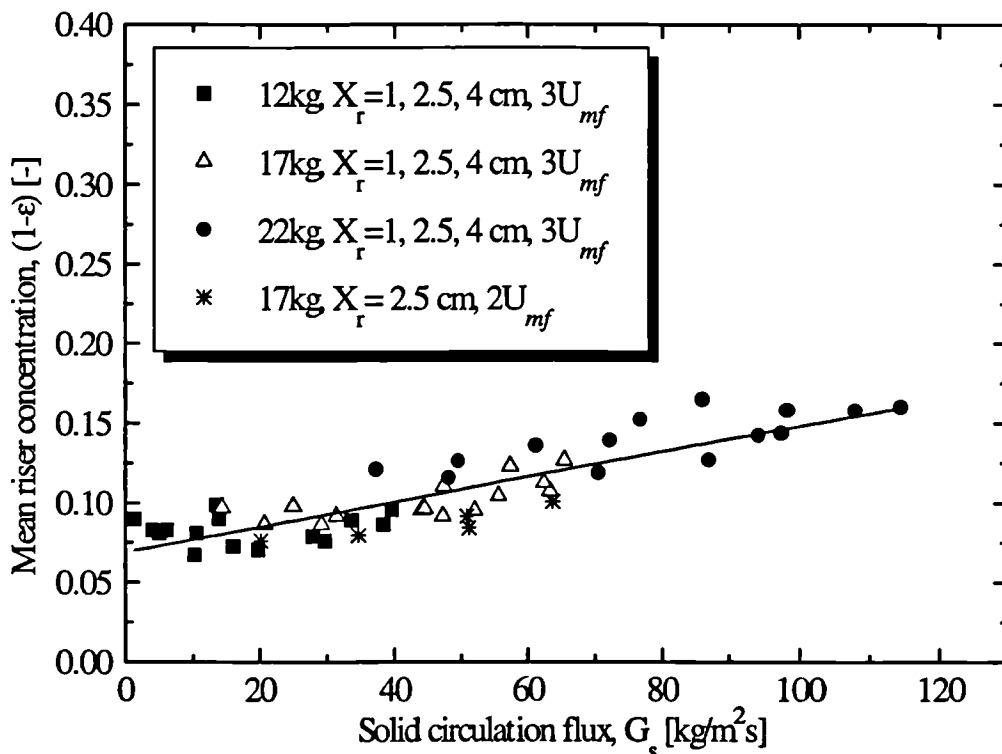


Fig. 6.46 Mean riser solids concentration versus solids circulation flux, G_s , for various total solids inventory and X_r values.

A typical form of the pressure loop around the circulating system with an L-valve is shown in Fig. 6.48. For clarity, these loop pressures are presented in differential form relative to the pressure at the exit of the gasifier. The variation of the pressure loop as a function of the riser gas velocity is shown in Fig. 6.49

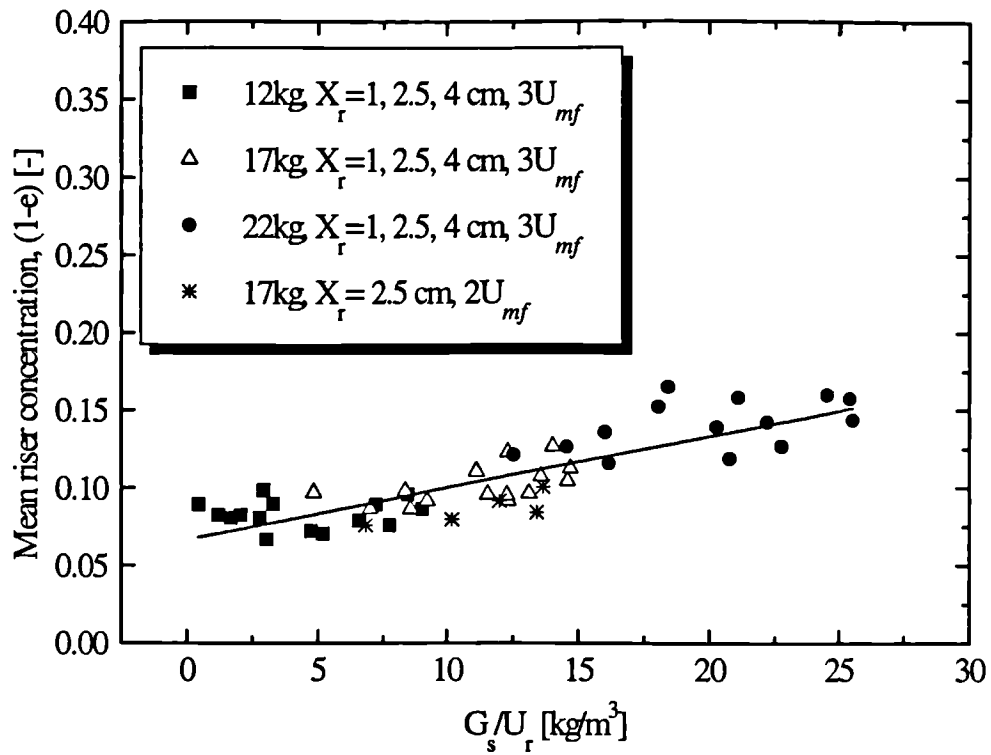


Fig. 6.47 Mean riser solids concentration versus the ratio G_s/U_r for various total solids inventory and X_r values.

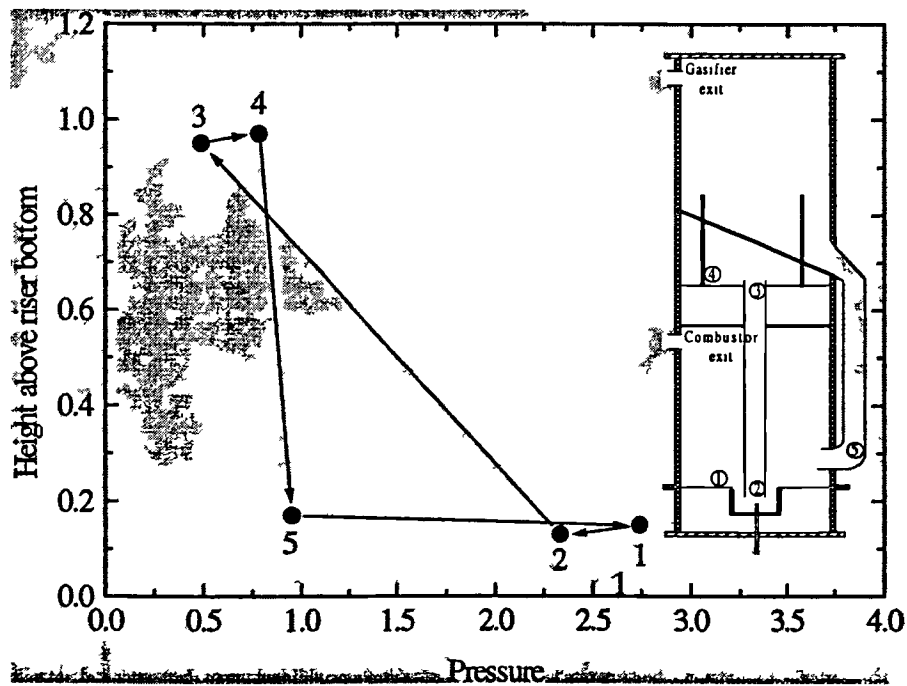


Fig. 6.48 Typical pressure loop for the circulating fluidized bed.

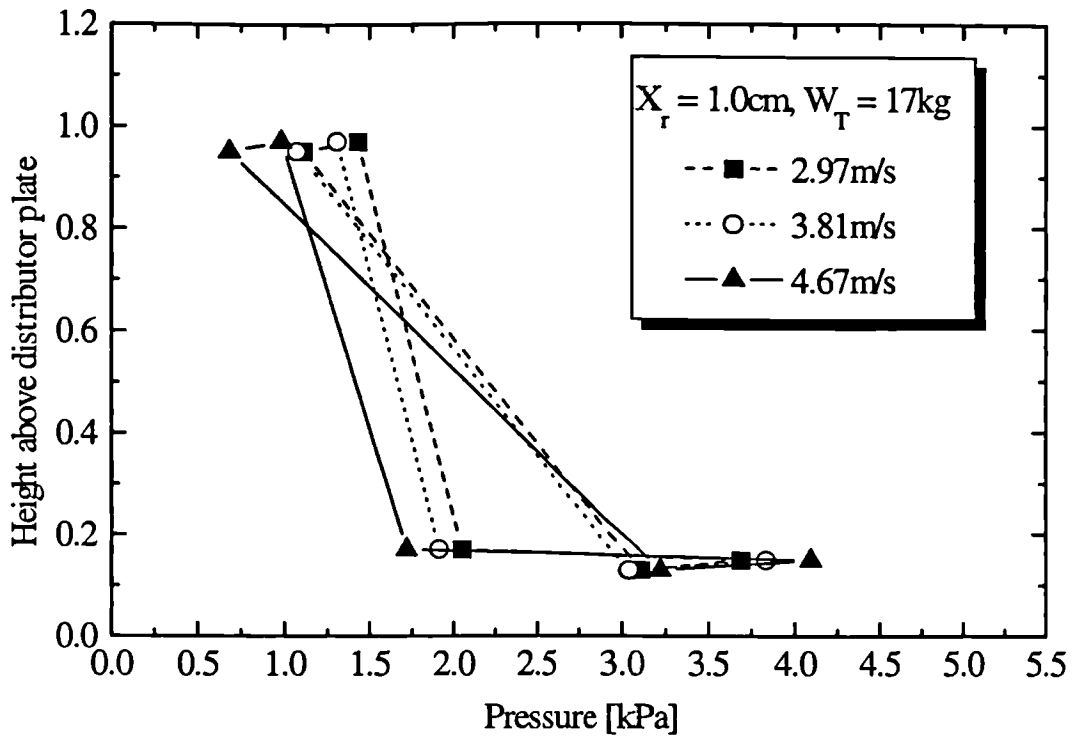


Fig. 6.49 Variation of pressure around the circulating loop as a function of the riser gas rate for $X_r = 1\text{cm}$ and $W_T = 17\text{kg}$.

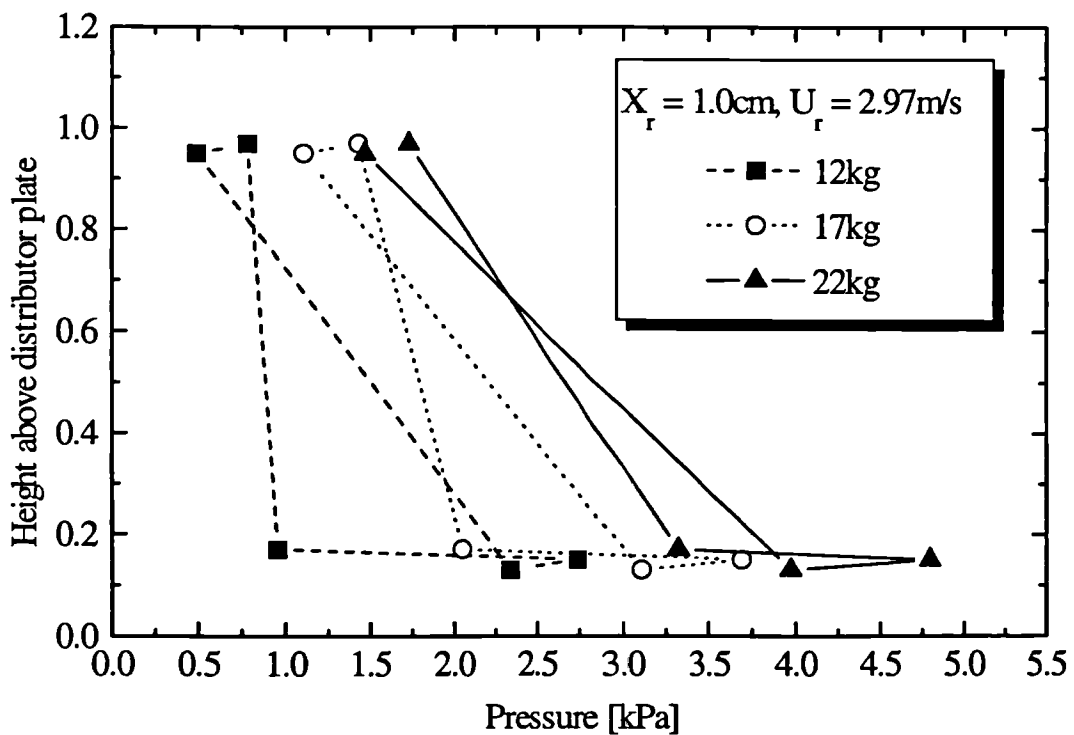


Fig. 6.50 Variation of pressure around the circulating loop as a function of the total bed load for riser gas rate of 2.97m/s and $X_r = 1\text{cm}$.

It is clear that changing the riser gas rate has little or no effect on this pressure balance whilst keeping the other parameters constant. However, increasing the total solids inventory has the effect of shifting the pressure loop to the right as shown in Fig. 6.50, in other words increasing the pressure at each location in the circulating system.

Chapter 7

7 RESULTS AND DISCUSSION: HEATED FLUIDIZED BED GASIFIER

This chapter presents and discusses the results obtained from the heat fluidized bed gasifier. The main interest of the results is the validation of the design and the discrimination of the biomass (almond shells) char gasification rate constants and other kinetic parameters from the steam fluidized bed at temperatures ranging from 700 - 800 °C. The shrinking core model (assuming kinetic controlling) has been used to describe the gasification of the char with steam.

7.1 SEGREGATION ALONG THE BED AXIS

The large difference between the density of the gasified almond shells and the bed material results in some degree of segregation. Thus, a majority of the lighter material (gasified biomass) tends to float near the upper half of the bed. In order to examine this, a gasification run was stopped abruptly by cutting the gas supply and the bed allowed to cool. Then the bed was sectioned into layers using a vacuum pump and the fraction of char present in each layer determined. The results are shown in Fig. 7.1, the dotted line denotes the total char from the bed as a fraction of the total bed inventory.

The above procedure was repeated but this time the fluidizing gas velocity was increased to $8U_{mf}$ (cf. $3U_{mf}$ in the previous run) for about 2 min before cutting the gas supply. By increasing the gas velocity in the bed before sectioning, it was expected to

enhance the solids mixing in order to obtain a much more uniform solids concentration throughout the bed axis.

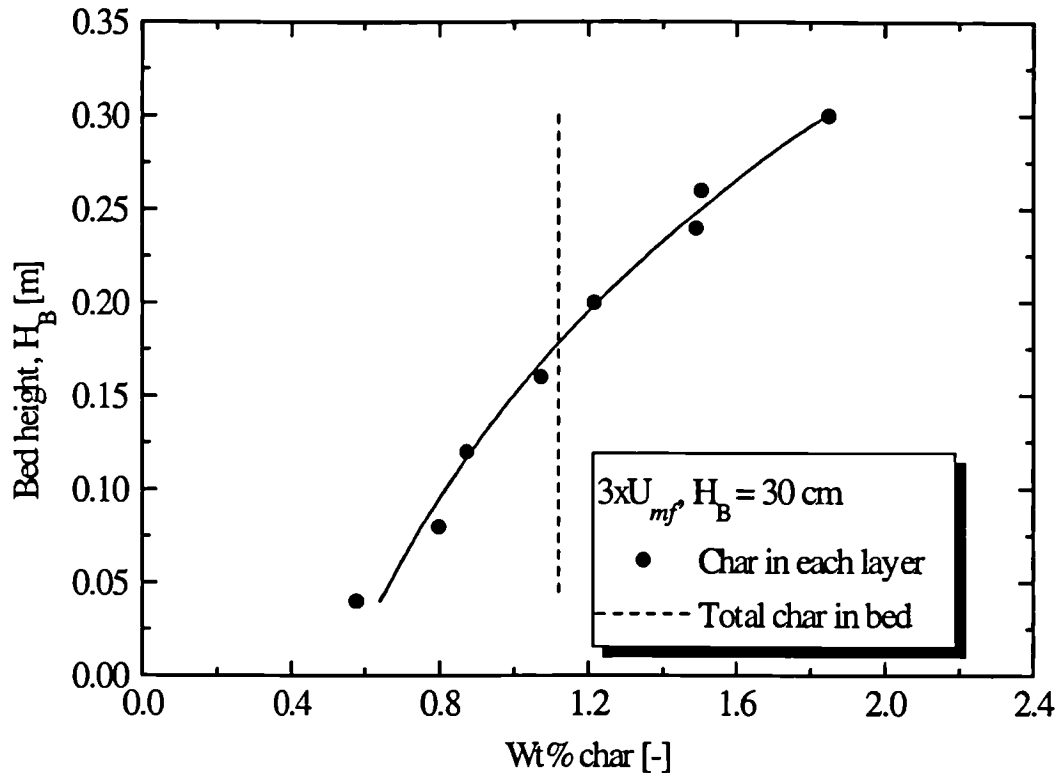


Fig. 7.1 Segregation of char in the bed after steady state biomass gasification run- $U_G = 3U_{mf}$, bed height, $H_B = 30$ cm, $S/B = 4$, biomass feed rate = 1.2 g/min, free-board = 0.54 m.

Although this resulted in some elutriation of the char, however the bed uniformity is an absolute essential for the accuracy of the sampling technique. During the gasification of the char, in order to evaluate the quantity of char present in the bed at anytime, a sample of the solids material is withdrawn from the top of the fluidized bed. If the bed is not relatively uniform, then the fraction of char withdrawn will not represent the fraction present in the fluidized bed as a whole. Fig. 7.2 shows that increasing the gas velocity before sampling leads to a better and more accurate prediction of the char present in the fluidized bed.

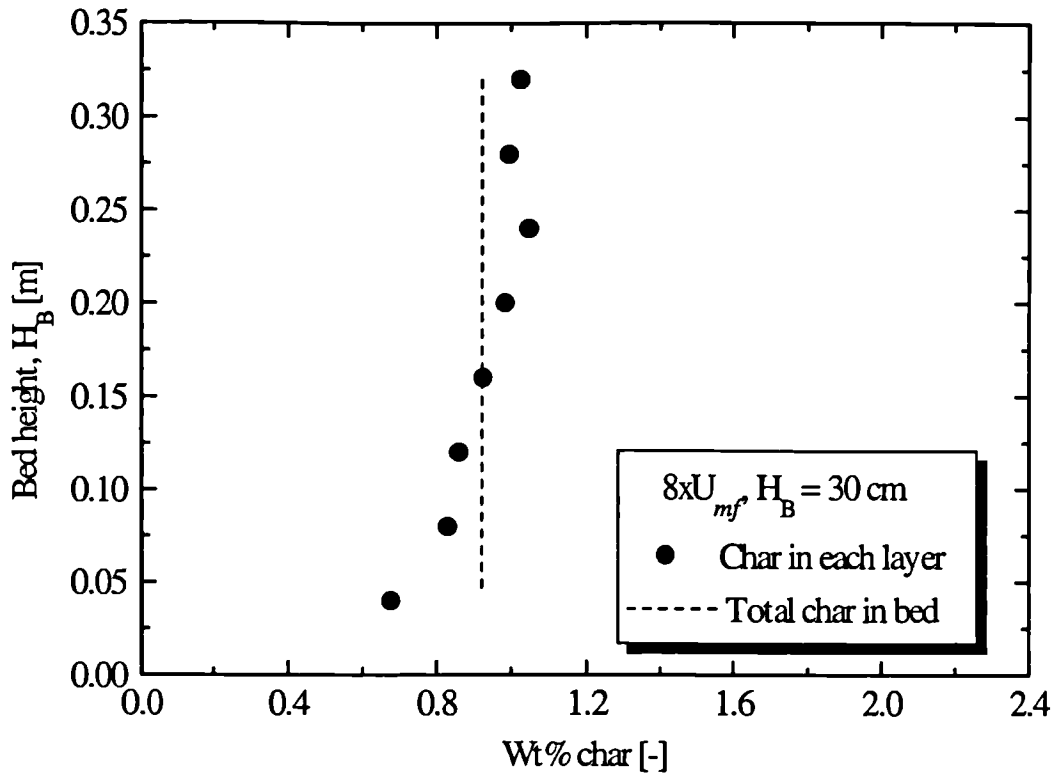


Fig. 7.2 Effect of gas velocity on the segregation of char in the bed after steady state biomass gasification run- $U_G = 8U_{mf}$, bed height, $H_B = 30$ cm, $S/B = 4$, biomass feed rate = 1.2 g/min, free-board = 0.54 m.

7.2 BED SAMPLING TECHNIQUE

The consistency of the sampling technique was examined by taking a number of samples from the bed, during the char gasification step, at relatively the same time and evaluating the fraction of char present. Immediately after the collection of the final sample, the steam flow was switched to nitrogen and the bed allowed to cool over night. Once cool, the bed particles were removed from the reactor and the actual fraction of char present was calculated, the results are shown in Fig. 7.3. The plot shows that the char fractions predicted from the sampling technique were much higher than the actual fractions. This suggested that there may have been further reaction of the char after switching to the nitrogen flow and allowing the bed to cool. Having checked for leaks, it was concluded that the cooling gas (air) supplied to the biomass feeding probe had leaked into the bed through a crack at the bottom of the probe.

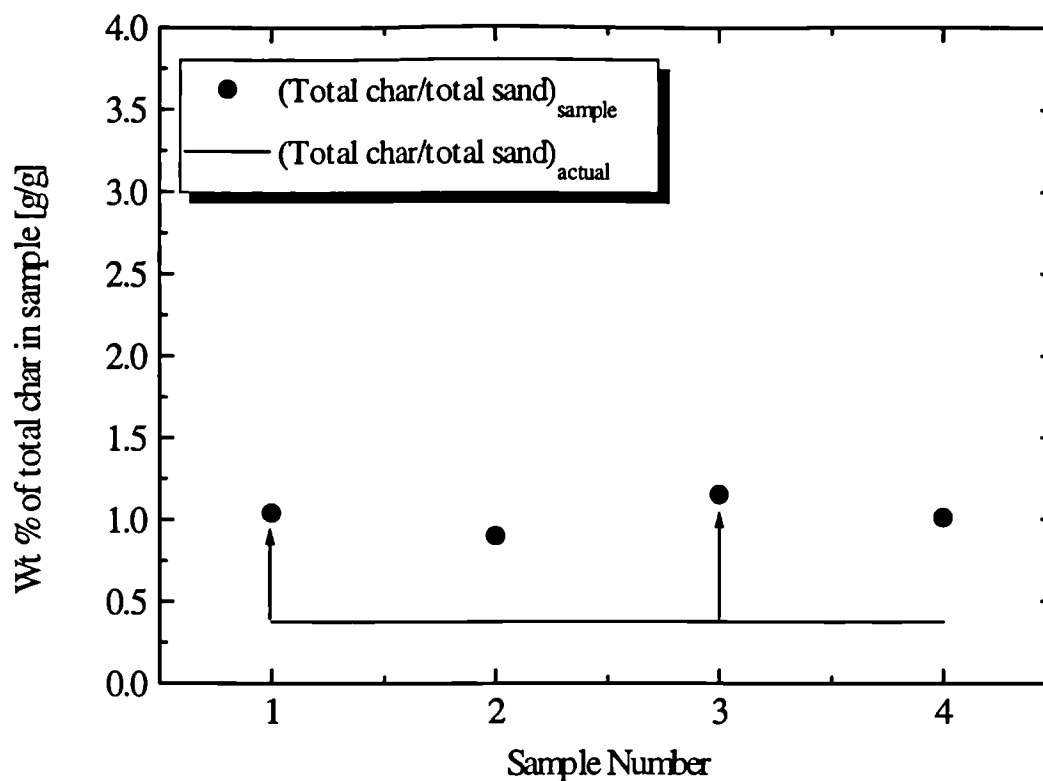


Fig. 7.3 Effect of Oxygen leakage on the accuracy of the sampling technique; weight percent of char in sample after steady state biomass gasification run- The lines indicate char as a fraction of the total bed $U_G = 8U_{mf}$, bed height, $H_B = 30$ cm, $S/B = 4$, biomass feed rate = 1.2 g/min, free-board = 0.54 m.

This problem was rectified and the procedure was repeated, the results are shown in Fig. 7.4. The difference between the actual total char fraction in the bed and those predicted from the sampling technique were within $\pm 9\%$.

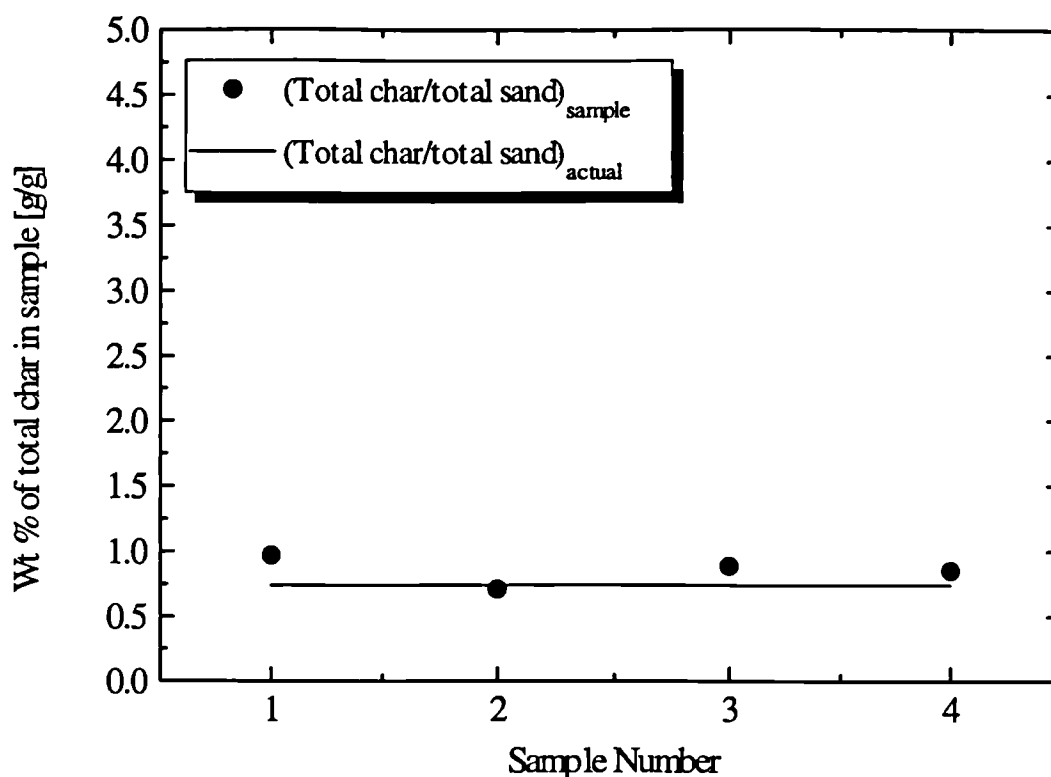


Fig. 7.4 Reproducibility of the sampling technique; weight percent of char in the bed after steady state biomass gasification run- $U_G = 8U_{mf}$, bed height, $H_B = 30$ cm, $S/B = 4$, biomass feed rate = 1.2 g/min, free-board = 0.54 m.

7.3 STEADY STATE RUN TIME

The gasification of the biomass char was studied only when the system had reached steady state. One way of ensuring that steady state had been attained was to monitor the progress of the product gas composition as a function of time. When the composition of the gaseous species did not vary, it was assumed that the system had reached steady state and the biomass feed was terminated. Fig. 7.5 shows the time required for the system to reach steady state for a gasification run at 712 °C, so sampling is only commenced after a time lapse of at least 95 min of biomass feeding.

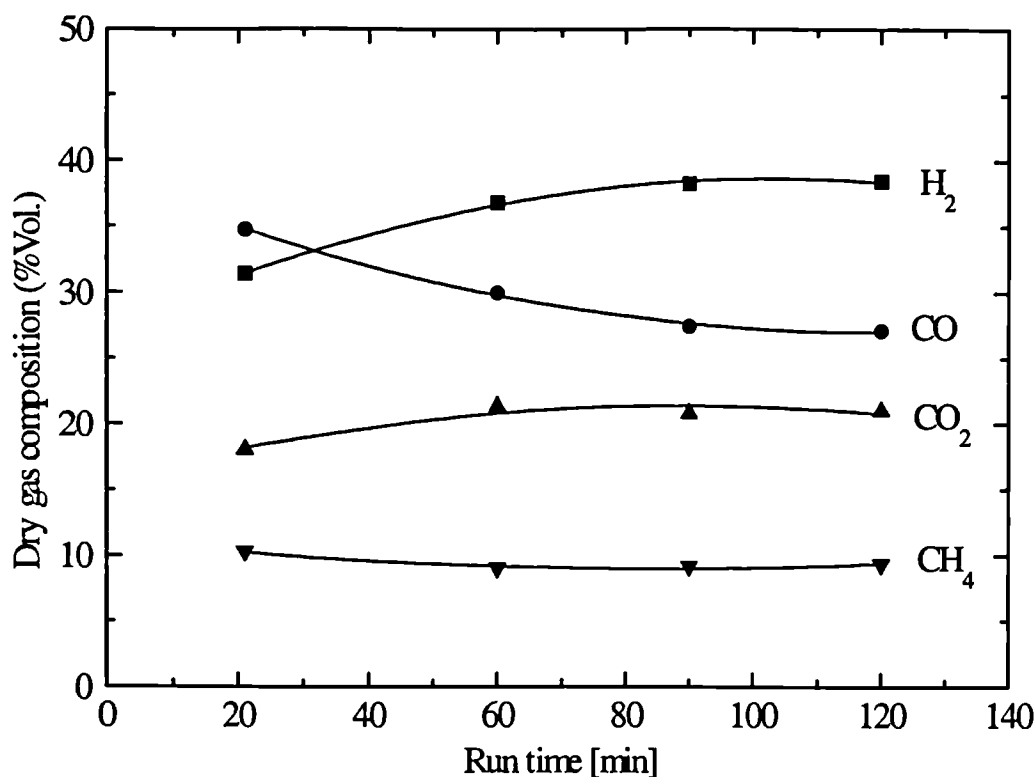


Fig. 7.5 Steady state dry gas composition as a function of biomass gasification time- $U_G = 8U_{mf}$, bed height, $H_B = 30$ cm, $S/B = 4$, biomass feed rate = 1.2 g/min, free-board = 0.54 m.

7.4 GASEOUS PRODUCTS AND COMPOSITION

The components of the gaseous product once the steam has been removed were mainly hydrogen, carbon monoxide, carbon dioxide, and methane. The variation in the composition of these species are shown in Fig. 7.6. The trend in the composition of the gaseous components as a function of temperature is in accordance with those report by Rapagna and Latif (1997) for an average biomass particle diameter of 750 μm , however the composition of the hydrogen is somewhat lower in the present study. Also present in the dry gas analysis were traces of higher hydrocarbons which were not detected by the above authors and whose variation as a function of temperature are shown in Fig. 7.7. These can be classified as the tars produced during the biomass gasification. The gas yield as a function of biomass gasification temperature is reported in Fig. 7.8, here the yield is defined as

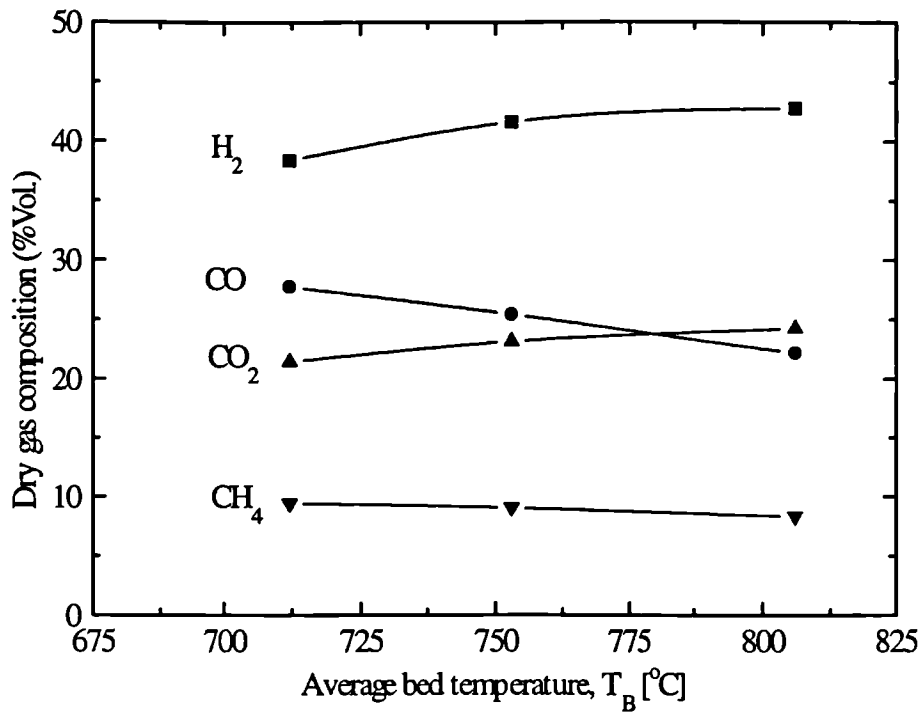


Fig. 7.6 Dry gas composition at steady state as a function of biomass gasification temperature - bed height, $H_B = 30$ cm, $S/B = 4$, biomass feed rate = 1.2 g/min, free-board = 0.54 m.

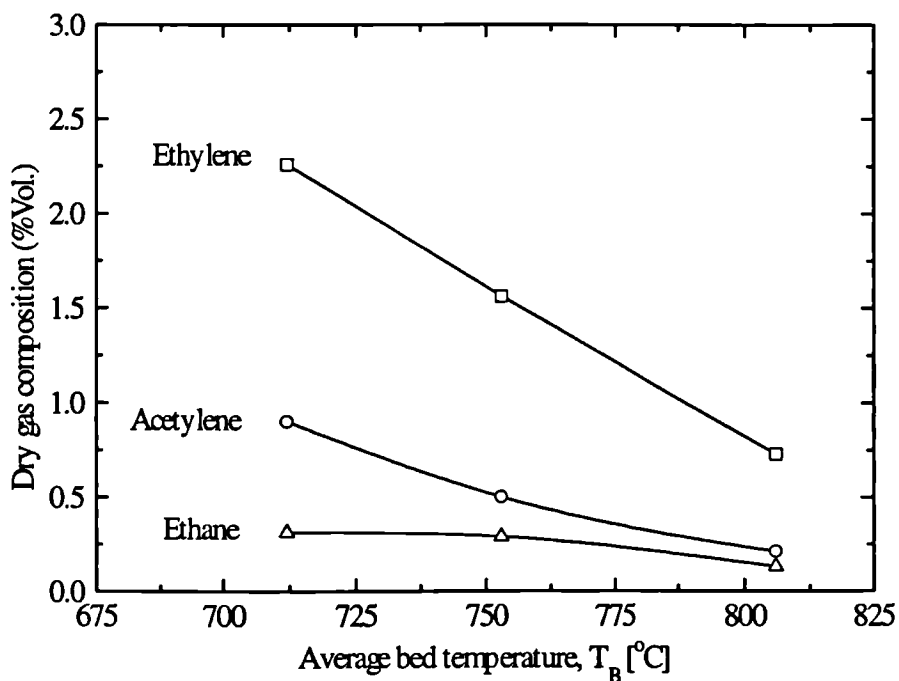


Fig. 7.7 Trace species composition in the dry gas as a function of biomass gasification temperature - bed height, $H_B = 30$ cm, $S/B = 4$ biomass feed rate = 1.2 g/min, free-board = 0.54 m.

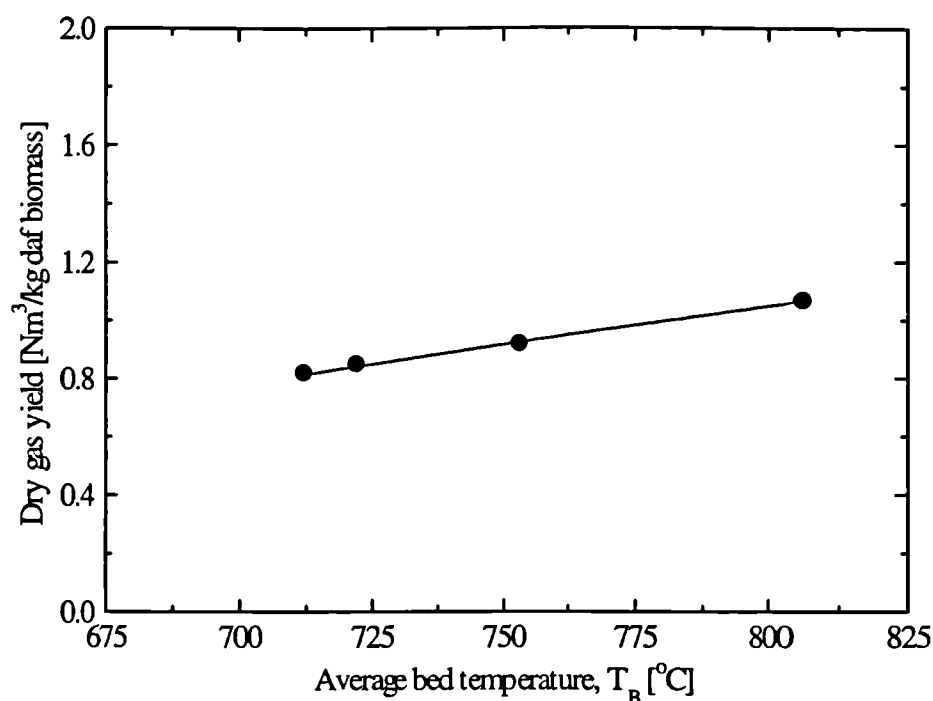


Fig. 7.8 Total gas yield as a function of temperature during the steady state biomass gasification run - bed height, $H_B = 30$ cm, $S/B = 4$, biomass feed rate = 1.2 g/min, free-board = 0.54 m.

$$\text{yield} = \frac{\text{volume of gas produced}}{\text{kg of biomass fed (daf)}}$$

Increasing the average gasification temperature, leads to a higher conversion of the solid biomass and hence the gaseous yield increases. Upon increasing the gasification temperature from 712 - 806 °C, the gas yield increased from 0.81-1.07 Nm³/kg biomass fed on a dry ash-free basis. It has not possible to quantify the tars produced during gasification by analysing the condensate yield, however, the tars produced was calculated from a mass balance on quantity of gas and char produced. Knowing the composition and gaseous yield, the mass of gas produced per kg of biomass was evaluated. The char production per kg of biomass was evaluated from the first char sample removed from the bed after the biomass feeding was terminated. The results are shown in Fig. 7.9. It can be seen that at the lower end of the gasification

temperature, the char and tar yield are almost the same, as the temperature increases, the char and tar yield both decrease, however, the reduction in the tar yield is much more rapid due to the thermal cracking.

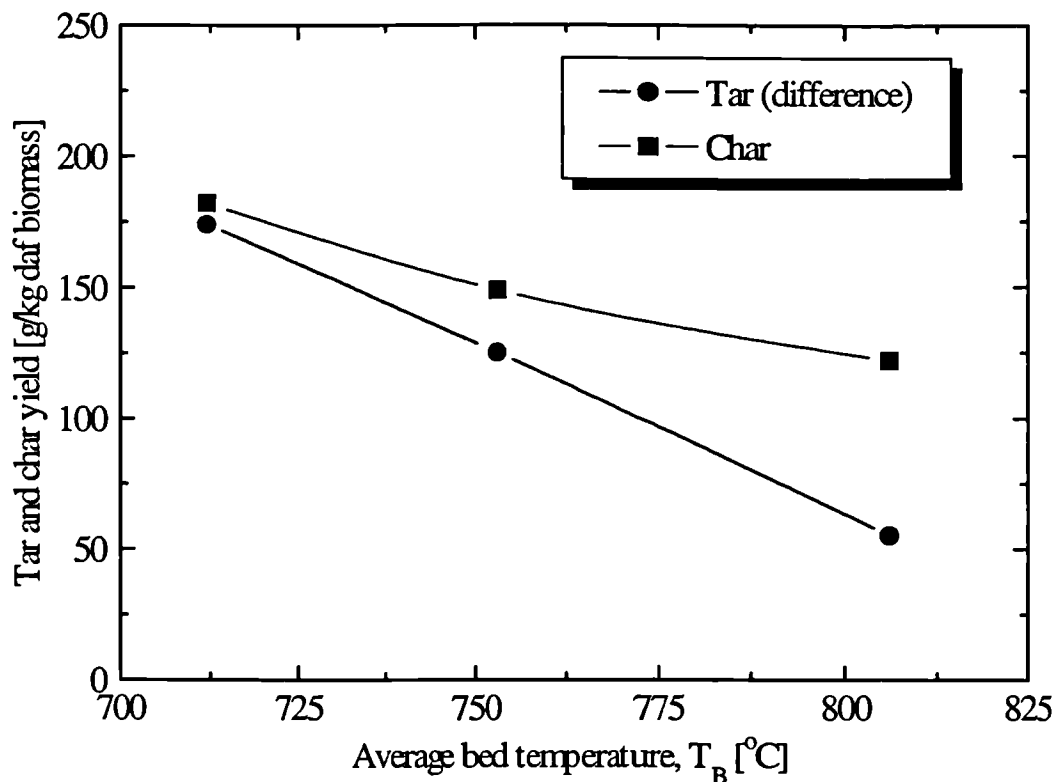


Fig. 7.9 Char and tar (approx.) yield as a function of temperature during the steady state biomass gasification run - bed height, $H_B = 30$ cm, $S/B = 4$, biomass feed rate = 1.2 g/min, free-board = 0.54 m.

7.5 CARBON CONVERSION

One measure of the effectiveness of a gasification process is the carbon conversion. This is defined as the mass of carbon in the produced gas from a unit mass of feed on a dry basis divided by the mass of carbon per unit mass of dry ash-free feed. It simply represents the percentage of the carbon in the feed converted into gaseous products. Carbon conversion was in the range of 57 - 73% as shown in Fig. 7.10. The trend is similar to the gas yield reported in Fig. 7.8, which shows that the

higher the carbon conversion, the higher is the amount of gaseous products. The carbon conversion evaluated here does not take into account the carbon in the tars.

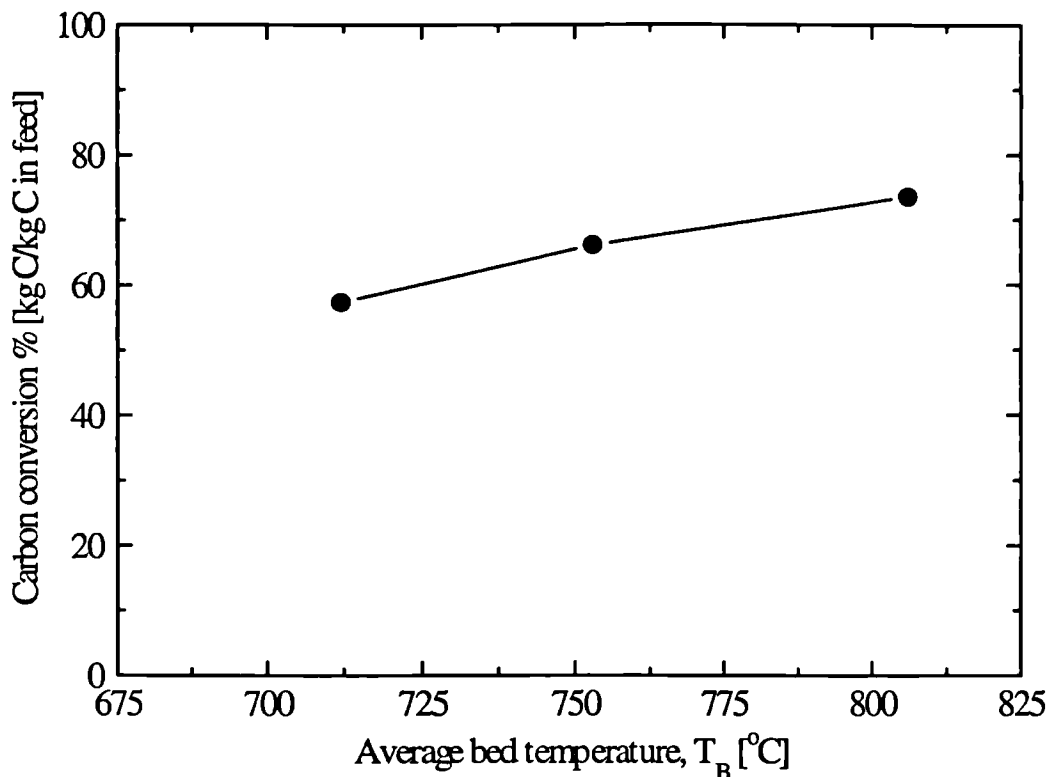


Fig. 7.10 Carbon conversion as a function of temperature during the steady state biomass gasification run - bed height, $H_B = 30$ cm, $S/B = 4$, biomass feed rate = 1.2 g/min, free-board = 0.54 m.

7.6 CHAR GASIFICATION KINETICS

When steady state was reached during the gasification of the almonds shells, the biomass feed rate was terminated. The bed samples (char and sand) withdrawn over a period of time during the char gasification runs were used to evaluate the average char remaining in the bed as a function of time, these results are shown in Fig. 7.11. The data in this plot were used to evaluate the char gasification rate constant, k_c , which are then compared with values published in literature.

It is well established that the structure and porosity of a solid strongly determines the controlling resistance to reaction (Kunii and Levenspiel, 1991). The temperature

dependence is maximum when chemical reaction is the rate-controlling step and minimal if mass transfer is rate -controlling. It has been shown that for coal combustion, the burnout time, τ , is proportional to the square of the coal particle diameter ($\tau \propto d_p^2$, $d_p > 1\text{mm}$) for diffusion through the ash layer and chemical kinetics at the surface as the rate-controlling step (Ross and Davidson, 1981). Biomass however, has negligible ash content compared to coal and thus the rate of reaction of the char gasification would be expected to be controlled by the intrinsic chemical reaction at the surface and the disappearance time to be proportional to the char particle diameter ($\tau_c \propto d_p$). It can also be assumed that the biomass loses its volatile contents instantly upon entering the bed.

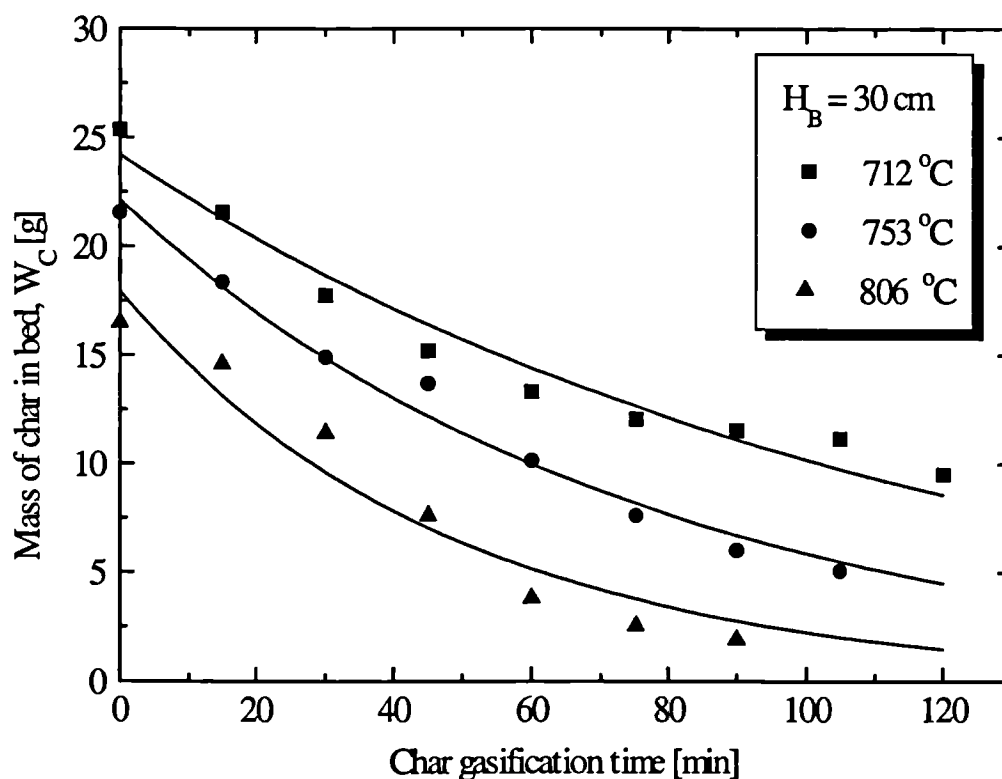
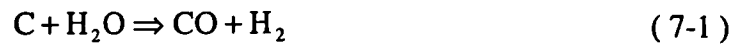


Fig. 7.11 Mass of char remaining in the bed as a function of gasification time

and average bed temperature- bed height, $H_B = 30\text{ cm}$, $S/B = 4$, biomass

feed rate = 1.2 g/min, free-board = 0.54 m.

Given spherical particles, and the char to be mainly composed of carbon, then the char-steam reaction be primarily represented as



The rate of conversion of a char particle is determined by the external surface area available to the reactant gas

$$-\frac{1}{4\pi r_c^2} \frac{dn_c}{dt} = -\frac{1}{4\pi r_c^2} \frac{dn_{\text{H}_2\text{O}}}{dt} \quad (\text{mols}^{-1}\text{m}^{-2})$$

$$-\frac{1}{4\pi r_c^2} \frac{dn_c}{dt} = -\dot{\rho}_c \frac{dr_c}{dt}$$

$$= k_{cs} C_{\text{H}_2\text{O}} \quad (7-2)$$

where $\dot{\rho}_c$ is the molar density of the char (mol/m^3), k_{cs} is the char gasification surface rate constant, R_c is the radius of the char particle, and $C_{\text{H}_2\text{O}}$ is the concentration of the gaseous reactant (steam). The density of the almond shell char formed has been roughly calculated as $296 \text{ kg}/\text{m}^3$ (see Appendix F). So

$$M_c = 12 \text{ g/mol}$$

$$= 0.012 \text{ kg/mol}$$

$$\dot{\rho}_c = \frac{\rho_c}{M_c}$$

$$= \frac{296}{0.012}$$

$$(7-3)$$

$$\dot{\rho}_c = 2.47 \times 10^4 \text{ mol}/\text{m}^3 \quad (7-4)$$

If $d_p = 2r_p$, then

$$\frac{W_t}{W_{c0}} = \left(\frac{d_{ct}}{d_{c0}} \right)^3 = \left(\frac{r_{ct}}{r_{c0}} \right)^3 \quad (7-5)$$

where d_{ct} and d_{c0} are the diameter of the char particle at time t and at time 0. From Equation (7-2)

$$\frac{dr_c}{dt} = -\frac{k_{cs} C_{H_2O}}{\dot{\rho}_c} \quad (7-6)$$

$$\therefore \int_{r_{c0}}^{r_{ct}} dr_c = -\frac{k_{cs} C_{H_2O}}{\dot{\rho}_c} \int_0^t dt \quad (7-7)$$

$$r_{c0} - r_{ct} = \frac{k_{cs} C_{H_2O} t}{\dot{\rho}_c} \quad (7-8)$$

$$1 - \frac{r_{ct}}{r_{c0}} = \frac{k_{cs} C_{H_2O} t}{\dot{\rho}_c r_{c0}} \quad (7-9)$$

$$\therefore 1 - \left(\frac{W_{ct}}{W_{c0}} \right)^{\frac{1}{3}} = \frac{k_{cs} C_{H_2O} t}{\dot{\rho}_c r_{c0}} \quad (7-10)$$

The time for complete conversion can be found by plotting the left hand side of Equation (7-10) against gasification time, t , and extrapolating to complete conversion ($W_{ct} = 0$) as shown in Fig. 7.12. The data for the plot is taken from Fig. 7.11. Therefore from Fig. 7.12, the complete conversion time for the char, τ_c , at the different gasification temperatures is evaluated and reported in Table 7.1.

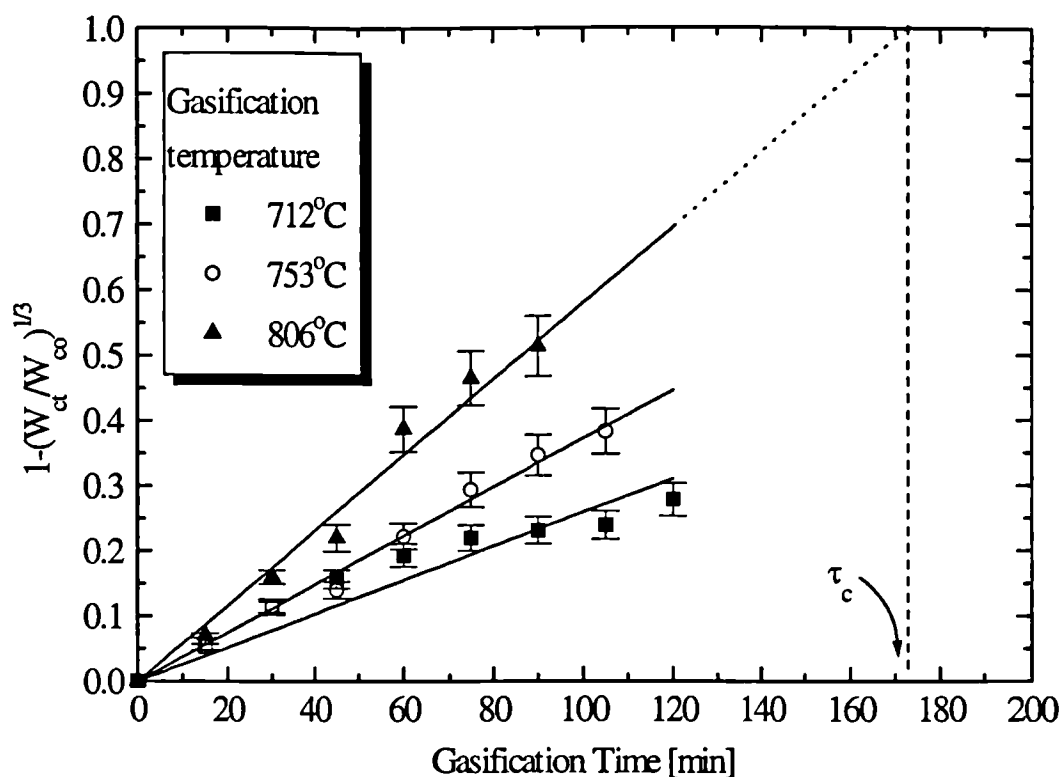


Fig. 7.12 Effect of gasification temperature on char conversion based on the shrinking core model for chemical reaction control.

Table 7.1 Char complete conversion times at various temperatures.

Gasification temperature, °C	Equation	τ_c [min]
712	$1-(W_{ct}/W_{c0})^{1/3} = 0.00259t$	386
753	$1-(W_{ct}/W_{c0})^{1/3} = 0.00372t$	269
806	$1-(W_{ct}/W_{c0})^{1/3} = 0.00579t$	172

The conversion time is related to the surface rate constant by the expression of Kimura et al. (1982)

$$\tau_c = \frac{\ddot{p}_c d_{c0}}{2bk_{cs}C_{H_2O}} \quad (7-11)$$

Where b is the stoichiometric coefficient of the solid char (b=1). Using E (7-11)

and the values of τ_c from Table 7.1, the char gasification surface rate constants k_{cs} , can be calculated. But, before that, it is necessary to evaluate the concentration of the steam in the emulsion phase. Assuming that the steam in excess of that required for minimum fluidization passes through the bed as bubbles, we have 4.8 g/min of steam input into the gasifier and therefore assuming a basis of 1 min and at 806 °C

$$n_{\text{H}_2\text{O}} = \frac{4.8}{18} = 0.266 \text{ mol}$$

$$1 \text{ mol H}_2\text{O} = 89.7 \ell \quad (\text{at } 806 \text{ }^\circ\text{C})$$

and

$$0.266 \text{ mols} = 23.6 \ell$$

Therefore the input concentration of steam is given by

$$\begin{aligned} C_{\text{H}_2\text{O}}^{\text{in}} &= \frac{0.266 \times 1000}{23.6} \\ &= 11.3 \text{ mol/m}^3 \end{aligned}$$

However, allowing for the presence of particles in the gasifier, the concentration of the steam in the emulsion phase can be evaluated as follows

$$\begin{aligned} C_{\text{H}_2\text{O}} &= 11.3(1 - \epsilon_{mf}) \\ &= 11.3(1 - 0.4) \\ &= 6.78 \text{ mol/m}^3 \end{aligned}$$

The concentration of the steam in the emulsion phase at 753 °C and 712 °C were similarly calculated as 7.12 mol/m³ and 7.41 mol/m³ respectively. Taking the initial diameter of the char particles as 714 μm (c.f. 830 μm for fresh biomass) as evaluated in section 164, the k_{cs} values can be evaluated and are listed in Table 7.2. For a

temperature of 806 °C

$$172 \times 60 = \frac{2.47 \times 10^4 \times 714 \times 10^{-6}}{2 \times k_{cs} \times 6.78}$$

$$\therefore k_{cs} = 1.26 \times 10^{-4} \text{ m/s}$$

This procedure is repeated to evaluate the rate constants at the other gasification temperatures and the results are shown below.

Table 7.2 k_{cs} values as function of temperature.

Temperature [°C]	P_{H_2O} [kPa]	k_{cs} [ms^{-1}]
712	101.3	5.14×10^{-5}
753	101.3	7.67×10^{-5}
806	101.3	1.26×10^{-4}

These k_{cs} values can be compared with 0.77 m/s for carbon oxidation at 1000 °C (Ross and Davidson, 1981). The rate constants increase as the gasification temperature is increased, however the absolute values are considerably lower compared with that for combustion of carbon.

7.7 DETERMINATION OF THE CHAR GASIFICATION RATE CONSTANT, k_c

It is required to find an overall rate coefficient, k_c (s^{-1}), assuming a reaction mass of 1 g of carbon and spherical particle

$$\text{volume} = \frac{4\pi}{3} \left(\frac{d_c}{2} \right)^3 = \frac{1}{\rho_c} \quad (7-12)$$

$$\frac{\pi d_c^3}{6} = \frac{1}{\rho_c}$$

$$\therefore d_c = \left(\frac{6}{\pi \rho_c} \right)^{\frac{1}{3}} \quad (7-13)$$

The density of the char produced from the almond shells $\approx 296 \text{ kg/m}^3$

$$\text{Surface area / mass (g)} = \pi d^2$$

$$= \pi \left(\frac{6}{\pi \rho_c} \right)^{\frac{2}{3}}$$

$$\text{Area / g} = \frac{\pi}{100^2} \left(\frac{6}{\pi(0.296)} \right)^{\frac{2}{3}}$$

$$= 1.1 \times 10^{-3} \frac{\text{m}^2}{\text{g}}$$

$$\frac{\text{area}}{\text{g}} = 1.1 \times 10^{-3} \frac{\text{m}^2}{\text{g}} \times 12 \frac{\text{g}}{\text{mol}}$$

(7-14)

$$= 1.32 \times 10^{-2} \frac{\text{m}^2}{\text{mol}}$$

$$\frac{1}{\text{s}} = \frac{\text{mol}}{\text{m}^2 \text{s}} \times 1.32 \times 10^{-2} \frac{\text{m}^2}{\text{mol}}$$

$$\frac{\text{mol}}{\text{m}^2 \text{s}} = 75.7 \times \frac{1}{\text{s}}$$

$$\frac{m}{s} \times \frac{\text{mol}}{\text{m}^3} = 75.7 \times \frac{1}{s} \quad (7-15)$$

The steam concentration at the surface of the char at 800 °C has been evaluated as 6.78 mol/m³. Inserting this into Equation (7-15),

$$\frac{m}{s} = \frac{75.7}{6.78} \times \frac{1}{s}$$

$$\frac{1}{s} = 0.09 \frac{m}{s} \text{ (at 800}^\circ\text{C)}$$

$$k_c (\text{s}^{-1}) = \frac{C_{\text{H}_2\text{O}}}{75.7} \times k_{cs} (\text{m/s}) \quad (7-16)$$

The above relationship, Equation (7-16), is used to convert the char gasification surface rate constants into an overall rate coefficient, k_c , at the corresponding temperature and the values are reported below in Table 7.3.

Table 7.3 Comparison of k_{cs} and k_c values.

Temperature [°C]	$P_{\text{H}_2\text{O}}$ [kPa]	k_{cs} [m/s]	k_c [s ⁻¹]
712	101.3	5.14×10^{-5}	5.03×10^{-6}
753	101.3	7.76×10^{-5}	7.21×10^{-6}
806	101.3	1.26×10^{-4}	1.13×10^{-5}

The char gasification rate constants calculated are compared with those published in literature as shown in Fig. 7.13. The value of the rate constants obtained (almond shells) are in good agreement with those for coconut shell as shown. Wood char has rate constant much high than the nut chars and thus indicate a higher char reactivity. All the rate constant are compared with that obtained from the gasification of graphite which is a very inert material and thus it would be expected to have rate constants much lower than the coal and biomass chars.

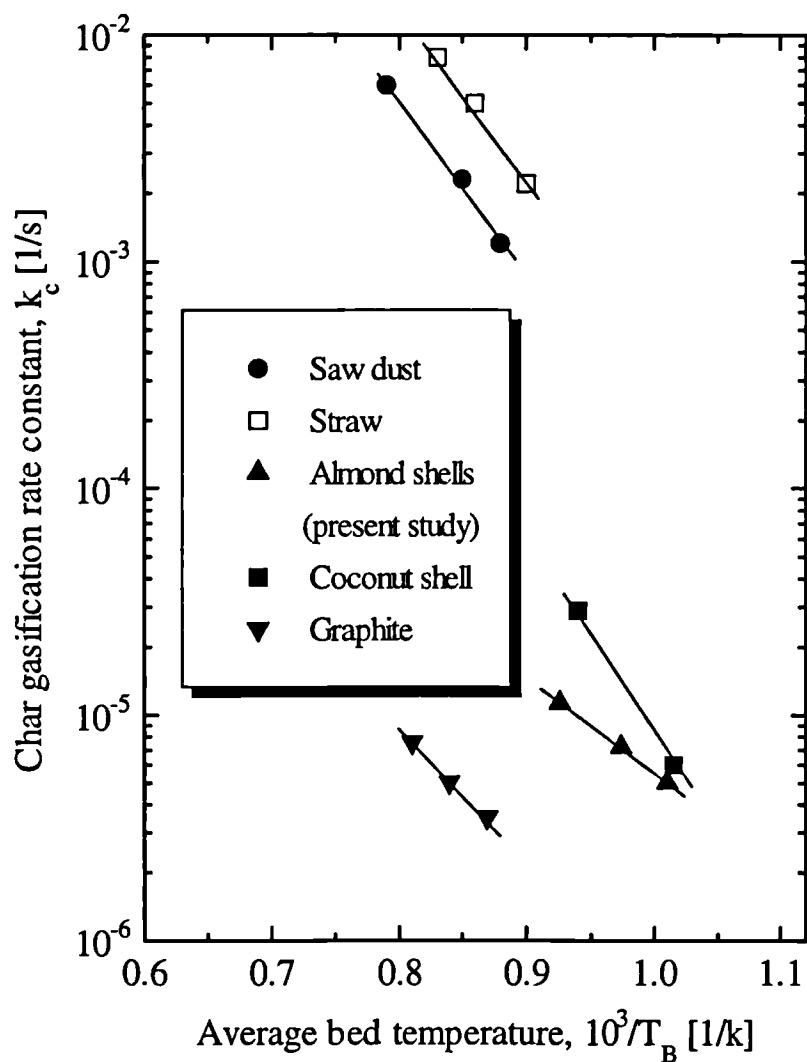


Fig. 7.13 Experimental char gasification rate constant, k_c , as a function of bed temperature- (\blacktriangle) almond shells (present study); data from (Kojima et al., 1993) (\blacksquare) coconut shells; (\bullet) saw dust; (\blacktriangledown) graphite; (\square) Straw.

7.8 EFFECT OF TEMPERATURE

The temperature dependence of the reaction rate can be investigated from the Arrhenius relationship

$$k_c = A \exp\left(-\frac{E_a}{RT_B}\right) \quad (7-17)$$

$$\ln k_c = \ln A - \frac{E_a}{RT_B} \quad (7-18)$$

From a plot of $\ln(k_c)$ against $1/T_B$

$$\text{slope} = -9213.3 = -\frac{E_a}{R}$$

$$\therefore E_a = 76.6 \text{ kJ/mol}$$

The experimental k_c values were correlated with the following expression

$$k_c = 0.06 \exp\left(\frac{-76.6 \times 10^3}{R(\text{J/molK})T_B}\right) \quad (7-19)$$

The activation energy for the biomass char gasification obtained here is lower than those for coal derived char-steam gasification reported in section 2.11 although the latter have not been derived from a fluidized bed. However, this suggests that the chars derived from biomass may be more reactive than those of coal.

7.9 DETERMINATION OF OPTIMUM GASIFIER VOLUME

The intention here is to use the rate constant results to evaluate the optimum gasifier volume required for the particular conversion of the char. Assuming that devolatilisation stage is rapid and once the biomass particle has passed through the bed and surfaced at the top, it has lost all its volatiles and is fully carbonised. Defining the extent of conversion during the gasification of char as

$$\left(\frac{W_{c0} - W_{ct}}{W_{c0}} \right) = (1 - X) \quad (7-20)$$

Since the particles stay in the reactor for different length of times, this leads to a variation in the conversion level. From Kunii and Levenspiel (1991) for shrinking core and reaction-controlling kinetics

$$1 - \bar{X} = \int_{t=0}^{\infty} (1 - X)_{\text{particle}} E(t) dt \quad (7-21)$$

Where the solids age distribution in the fluidized bed is

$$E(t) = \frac{1}{t} \exp\left(-\frac{t}{\tau_c}\right) \quad (7-22)$$

and

$$(1 - X) = \left(1 - \frac{t}{\tau_c}\right)^3 \quad (7-23)$$

Combining Equation (7-12) to Equation (7-14) and integrating from 0 to τ_c , which is the total time required for a single char particle to disappear, we get

$$1 - \bar{X} = 1 - 3\left(\frac{\bar{t}}{\tau_c}\right) + 6\left(\frac{\bar{t}}{\tau_c}\right)^2 - 6\left(\frac{\bar{t}}{\tau_c}\right)^3 \left(1 - \exp\left(-\frac{\tau}{\bar{t}}\right)\right) \quad (7-24)$$

Assuming that the gasifier is operating at 850 °C with biomass feed rate of 550 kg/hr (dry ash-free basis) and feed particles of 1mm in diameter, using Equation (7-16) and Equation (7-19), we can derive a surface rate constant as

$$k_c = 0.06 \exp\left(\frac{-76.6 \times 10^3}{8.314(273 + 850)}\right)$$

$$= 1.64 \times 10^{-5} \text{ s}^{-1}$$

$$\therefore k_{cs} = \frac{75.7}{6.42} = 1.93 \times 10^{-4} \text{ m/s}$$

Now using Equation (7-11)

$$\tau_c = \frac{3.33 \times 10^4 \times 1000 \times 10^{-6}}{2 \times 1.93 \times 10^{-4} \times 6.42} = 166 \text{ min} \quad (7-25)$$

If we allow 70% conversion of the char before circulating to the combustor, then

$$(1 - \bar{X}) = (1 - 0.7) = 0.3 \quad (7-26)$$

Inserting the values of τ_c and $(1 - \bar{X})$ into Equation (7-24) and solving for the mean residence time, \bar{t}

$$\frac{\bar{t}}{\tau_c} = 0.6$$

$$\therefore \bar{t} = 0.6 \times 166 = 99.6 \text{ min}$$

Assuming a solids circulation rate of 12000 kg/hr (= 200 kg/min). Now

$$t = \frac{w}{F}$$

$$w = 200 \times 99 = 19800 \text{ kg}$$

The bulk density of the sand is approx. 1560 kg/m³ (= 2600 x 0.6). Therefore the bed volume is given by

$$V_G = 19800/1560 = 12.69 \text{ m}^3$$

Assuming a bed height of 1 times the diameter

$$12.69 = \frac{\pi D_G^2}{4} \times D_G$$

$$= \frac{\pi D_G^3}{4}$$

$$\therefore D_G = 2.52 \text{ m}$$

7.9.1 DETERMINATION OF OPTIMUM COMBUSTOR VOLUME

The burnout time for char particles of 1mm diameter can be estimated as approximately 120 s (Ross and Davidson, 1981). Assuming a combustion efficiency of 98% ($\bar{X} = 0.98$), then using Equation (7-24), the mean residence time in the combustor is derived as 26 min.

$$t = \frac{w}{F}$$

$$w = 200 \times 26 = 5200 \text{ kg}$$

$$V_c = 5200/1560 = 3.34 \text{ m}^3$$

$$\begin{aligned} 3.34 &= \frac{\pi D_c^2}{4} \times 0.5 D_c \\ &= \frac{\pi D_c^3}{8} \end{aligned}$$

$$\therefore D_c = 2.04 \text{ m}$$

7.10 CHAR ANALYSIS

The reactivity for most chars derived from coal or lignite have a tendency to decrease with increasing time or conversion. However for many chars of biomass and peat, the reactivity profiles increases or exhibits a maximum (Mahajan et al., 1978). This could be due to changes in catalytic activity or active site reactivity, initial pore growth followed by pore collapse, as has been suggested (Bhatia and Perlmutter, 1980; Hill and Fott, 1993). This behaviour may also be partly due to a process resulting in structural changes of the char over the reaction time or temperature which in turn has an impact on the reactivity.

In order to investigate this qualitatively, a scanning electron microscope (SEM) was used to observe the differences between the almond shell char formed at different temperatures and also at different stages of their conversion. The photographs taken at different magnifications (up to 1000 times) are shown in Fig. 7.14 which show that as the gasification temperature is increased, the degree of porosity of the subsequent char formed also increases (compare C, D with E, F). This increase in porosity also occurs as the conversion proceeds, at a fixed temperature (compare E, F with G, H) where larger cavities are formed presumably via the collapse of the solids linkage between adjacent adjoining pores. The dimensions of the solid biomass particles have been seen to reduce as shown in Fig. 7.15.

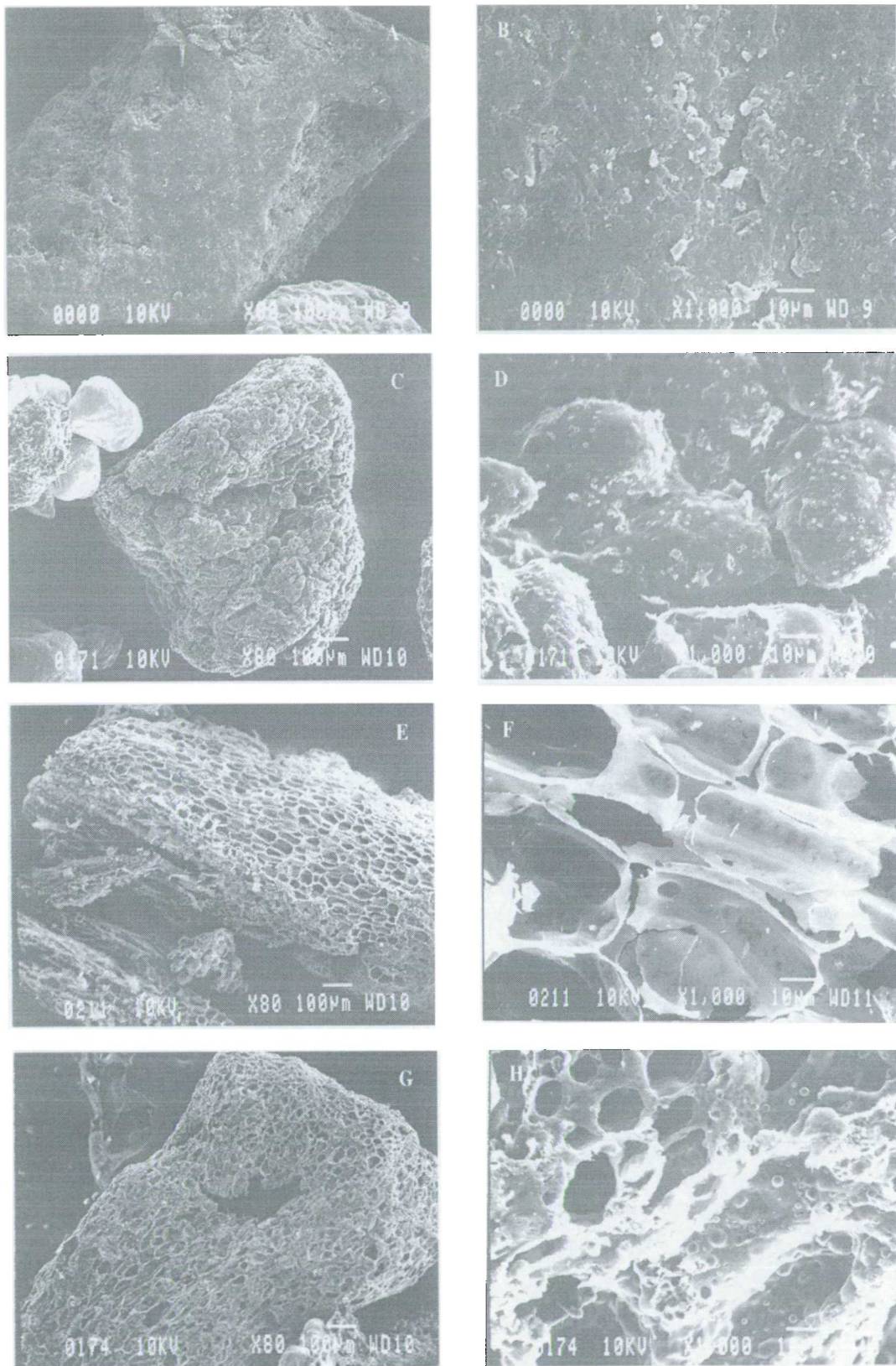


Fig. 7.14 Surfaces of chars formed as function of gasification temperature and residence time in the gasifier; (A, B) fresh biomass, (C, D) char formed at 753 °C, (E, F) Char formed at 806 °C, (G, H) Char (753 °C) collected 30 min into char/steam gasification.

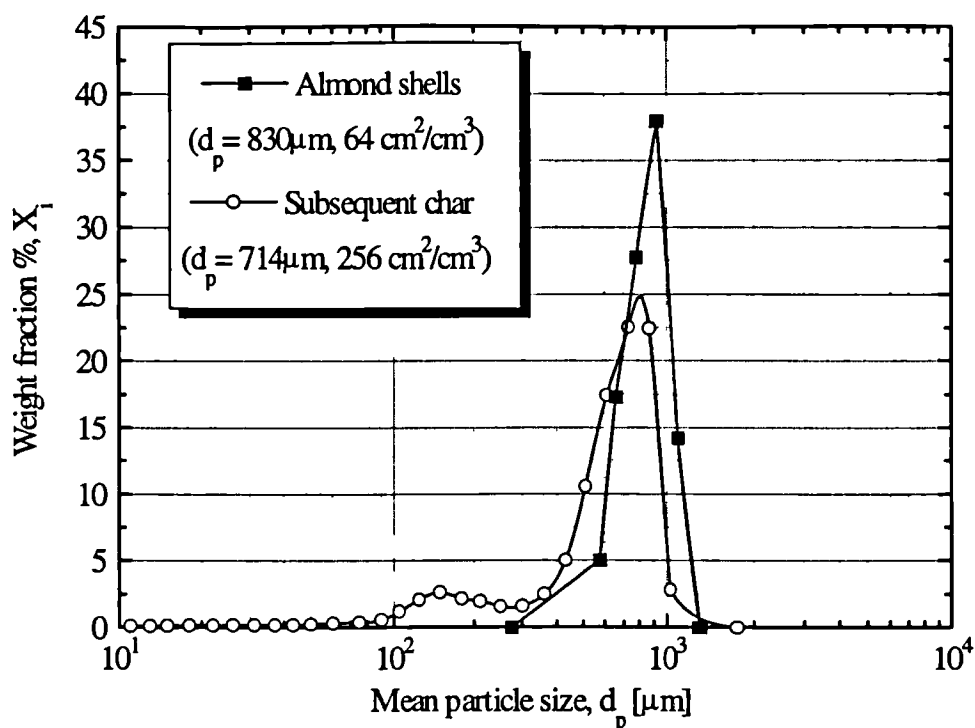


Fig. 7.15 Comparison of the mean particle diameter and surface area per unit volume of fresh biomass with the subsequent char formed at 750 °C.

7.11 CONCLUSIONS

Fluidized bed gasification of biomass (almond shells) and the subsequent char with steam was studied at temperatures of up to 800 °C. The gasification of the biomass can be classified into two stages, an initial fast devolatilisation followed by slow gasification of the residual char within the fluidized bed. The extent of the gasification increases strongly between 700-800 °C as indicated by an increase in the gas yield at the expense of the tars and char. The residual char left after the devolatilisation stage is about $\frac{1}{4}$ the density of the original almond shells and typically takes between 170 to 390 minutes to completely gasify at temperatures of 800 - 700 °C, as evaluated assuming reaction kinetics as the rate controlling step. The extent of the char gasification were calculated from the changes in the mass of the char in the fluidized bed over the gasification time with steam operating at atmospheric pressure. This char-steam gasification has also been seen to increase

strongly with temperature giving rate constant of $5.03\text{E-}6$, $7.21\text{E-}6$ and $1.13\text{E-}5\text{ s}^{-1}$ for temperatures of 712, 753, and 806 °C respectively. The agreement of these rate constant with those published in literature highlights the accuracy of the char sampling technique developed.

Chapter 8

8 GENERAL CONCLUSIONS

Solid circulation rate, gas cross-flow, solids residence time and pressure drop measurements have been investigated during the operation of a cold model circulating fluidized bed proposed for the combustion-gasification of biomass using sand as the bed material. The circulating fluidized bed consisted of a twin fluid bed interconnected via a riser and a downcomer fitted with an L-valve. The circulating system was constructed from transparent perspex and air was used as the fluidizing medium and the riser gas velocity were varied from just under 3 m/s to almost 5 m/s. Analysis of the experimental data leads to the following conclusions:

- The solids circulation rate increases with increasing riser superficial velocity, total bed inventory, and distance of the gas jet from the riser inlet. The riser gas rate can be used as a prime parameter to control the solids circulation rate.
- There is no gas cross-flow from the gasifier into the combustor, but some gas leakage occurs in the opposite direction via the riser. This gas cross-flow increases with increasing total bed inventory and riser superficial gas velocity, but decreases with increasing riser-gas jet distance. Over the range studied, the gas cross-flow is less than 4% of the total gas input into the combustor.
- Experiments using almond shells as foreign matter have shown that it is possible to circulate such particles around the system over the operating parameters, however, further investigation is required to control the residence time of particles (biomass) in the two beds.
- From the pressure analysis, it can be concluded that increasing the riser gas rate has little effect on the pressure balance around the circulating loop, however, increasing the total bed inventory moves the loop to the right increasing the pressure at each location. The mean solids velocity in the riser is directly proportional to the

- proportional to the superficial gas velocity and independent of the mean solids flux.
- The closer the distance of the riser gas jet is to the inlet of the riser, the lower is the solids circulation rate. However, when this distance becomes large, considerable start-up problems are created. The optimum distance can be taken as approximately 2.5 cm.
 - Moreover, because the riser gas velocity and the gas velocity in the two beds can be adjusted individually, the solids circulation rate can be controlled irrespective of the fluidizing conditions in these sections.
 - The mathematical correlations derived in Section 6, to predict the solids circulation rate and gas cross-flow rate, were related to the dimensionless parameter β , and A_r and ρ_p were used to make it dimensionless. However, these parameters were not changed during the practical work and thus their effect on the solids circulation rate and gas cross-flow rate should therefore not be taken as suggested.
 - The experimental data obtained shows the versatility of the design of the present system, a number of operating and design parameters can be adjusted in order to meet the desirable operational and design objectives.

A bench-scale high temperature fluidized bed reactor was developed to study the gasification and combustion of biomass and the subsequent char at temperatures of up to 800 °C. The apparatus can provide a rapid determination of char combustion and gasification rate by allowing the real time sampling of the bed material as well as the gas analysis. The novel design of the windbox allows the injection of water to a heated flange for the generation of steam to the fluidized bed with great ease, eliminating the need for a separate steam generating equipment. The very simple char sampling technique developed has an accuracy of about $\pm 9\%$. The design of the apparatus for its purpose has been successful.

The results from the heated fluidized bed gasifier show that the biomass (almond shells) char-steam gasification is a very slow process as seen from the time taken for complete conversion. It was assumed that biomass char gasification at elevated

temperatures was in the chemical reaction control regime and the agreement between the experimental rate constants evaluated with those published in literature confirms the validity of the assumption. It is well known that the combustion rate of char is dependent on the particle size, however further work is necessary too elucidate this for the gasification of char.

Throughout this work, the char reactivity has been taken to be constant. This however is not always true as the reactivity of char is seen to change with time and temperature of the reactor.

The Arrhenius type expression used to correlate the char-steam gasification constant at different temperatures is specific to the present study, for example, it does not take into account the partial pressure of the steam (although this parameter was not varied). Therefore further work is necessary make the expression more generally applicable.

Chapter 9

9 FURTHER WORK

9.1 SCALING OF FLUIDIZED BEDS

In order to obtain complete similarity between two different fluidized beds, Glicksman et al. (1993, 1994) proposed a full set of dimensionless scaling parameters to be matched. From the conservation of mass and motion of the fluid and particles, the following set of governing parameters were derived

Dimensionless Froude No.	Solid - gas density ratio	Dimensionless circulation	Length ratio	Particle Sphericity	Particle size Distribution
$\frac{U_0^2}{gD} \Rightarrow \frac{U_0}{U_{mf}}$	$\frac{\rho_s}{\rho_g}$	$\frac{G_s}{\rho_s U_0}$	$\frac{D}{L}$	Φ	PSD

One of the most important parameters to match is the ratio of the solids to gas density. The bed particle in the cold model circulating fluidized bed can be replaced by copper and the systems hydrodynamics studied under those conditions already investigated. This would give complete similarity between the hot pilot model and the cold laboratory scale.

As an example, the heated fluidized bed gasifier (800°C) was scaled (1:1) to room temperature in order to study the solids mixing behavior. The gasifier (0.1 m dia.) was fluidized using steam (4 g/min) with a bed height of 30 cm. This flow of steam was used to evaluate the gas velocity through the gasifier and hence the Froude No. In the heated gasifier, we have steam with a density of 0.201 kg/m³ and viscosity of 3.98x10⁻⁵ kg/ms. If copper is used as the bed material in the cold model and by matching the solid-gas density ratio

$$\left(\frac{\rho_s}{\rho_g}\right)_{\text{heated gasifier}} = \left(\frac{\rho_s}{\rho_g}\right)_{\text{cold model}}$$

$$\left(\frac{2622}{0.201}\right)_{\text{heated gasifier}} = \left(\frac{8923}{\rho_g}\right)_{\text{cold model}} \Rightarrow \rho_g = 0.68 \text{ kg/m}^3 \quad (9-1)$$

In the cold model, a gas with a density of 0.68 kg/m^3 would be required which can be obtained by mixing helium and air in the right proportions. The average mixture density, ρ_{mix} , and viscosity, μ_{mix} , can be evaluated from the following

$$\rho_{\text{mix}} = \sum_i^n y_i \rho_i \quad (9-2)$$

The viscosity of the mixture can be evaluated using the expression (Perry and Green, 1997).

$$\mu_{\text{mix}} = \frac{\sum_i^n y_i \mu_i}{\sum_j^n y_j \Phi_{ij}} \quad (9-3)$$

and

$$\Phi_{ij} = \frac{\left[1 + \left(\frac{\mu_i}{\mu_j}\right)^2 \left(\frac{M_j}{M_i}\right)^{\frac{1}{4}}\right]^2}{\left[8 \left(1 + \frac{M_i}{M_j}\right)\right]^{\frac{1}{2}}} \quad (9-4)$$

where y_i is the volumetric percentage and M_i is the molar mass of component i in the gas mixture. In order to get the required gas density in the cold model, it is necessary to mix air and helium in 50% proportions. Equation (9-4) was used to evaluate the average gas viscosity which was used to calculate the minimum fluidization velocity and hence

the average particle diameter. The results are reported in Table 9.1. Here, the first column shows the conditions of the heated fluidized bed gasifier, the second column gives the ideal figures for exact similarity, and finally the last column shows that values for the parameters in the actual system.

Table 9.1 Scaling of a hot fluidized bed gasifier to a cold model at ambient temperature and pressure (air, helium, and copper system)

Scaling factor = 1	Gasifier at 800°C	Gasifier → at 20°C	Copper at 20°C
T_B (K)	1098	298	298
ρ_s (kg/m ³)	2622	8923	8923
ρ_g (kg/m ³)	0.201	0.684	0.684
μ_F (kg/ms)	3.98E-05	1.93E-05	1.93E-05
U_o (m/s)	0.050	0.050	0.060
$H_{B(mf)}$ (m)	0.300	0.300	0.300
D_B (m)	0.100	0.100	0.100
g (m/s)	9.810	9.810	9.810
Fr (U_o) ² /gD _B	2.54E-03	2.54E-03	3.67E-03
d_p (μm)	180	68	80
U_{mf} (m/s) $d_p^2(\rho_s-\rho_g)/1650\mu_g$	0.013	0.013	0.018
U_o/U_{mf}	3.93	3.93	3.41
ρ_s/ρ_g	13045	13045	13045
$D_B/H_{B(mf)}$	0.33	0.33	0.33
Φ	0.78	0.95	0.95

9.1.1 PRELIMINARY RESULTS

The cold scaled (1:1) fluidized bed gasifier was used to investigate the mixing behaviour of the biomass, and subsequent char formed, with the sand. Using the equation below, the average density of particles to resemble the biomass and char in the cold model were evaluated.

$$\left(\frac{\rho_{\text{bed particles}}}{\rho_{\text{biomass}}} \right)_{\text{heated gasifier}} = \left(\frac{\rho_{\text{bed particles}}}{\rho_{\text{biomass}}} \right)_{\text{cold model}}$$

$$\left(\frac{2622}{1200} \right)_{\text{heated gasifier}} = \left(\frac{8923}{\rho_{\text{biomass}}} \right)_{\text{cold model}} \Rightarrow (\rho_{\text{biomass}})_{\text{cold model}} \approx 4000 \text{ kg/m}^3$$

The same procedure is used to evaluate a density for the char in the cold model and a value of around 1200 kg/m^3 was calculated. Therefore zirconium oxide (ZrO) and almond shells were used to resemble the biomass and char respectively in the cold model. Experiments were conducted by placing a fixed quantity of ZrO ($d_p = 648 \mu\text{m}$) and almond shells ($d_p = 355 \mu\text{m}$) to a static bed of copper (with a known bed height). The mixture was fluidized at different superficial gas velocities over a short period of time. The gas supply was cut off abruptly and the static bed sectioned by sucking out layers using a vacuum pump. The layers were analysed in terms of the weight fraction of the different solids in order to obtain an insight in the solids mixing pattern (Fig. 9.1).

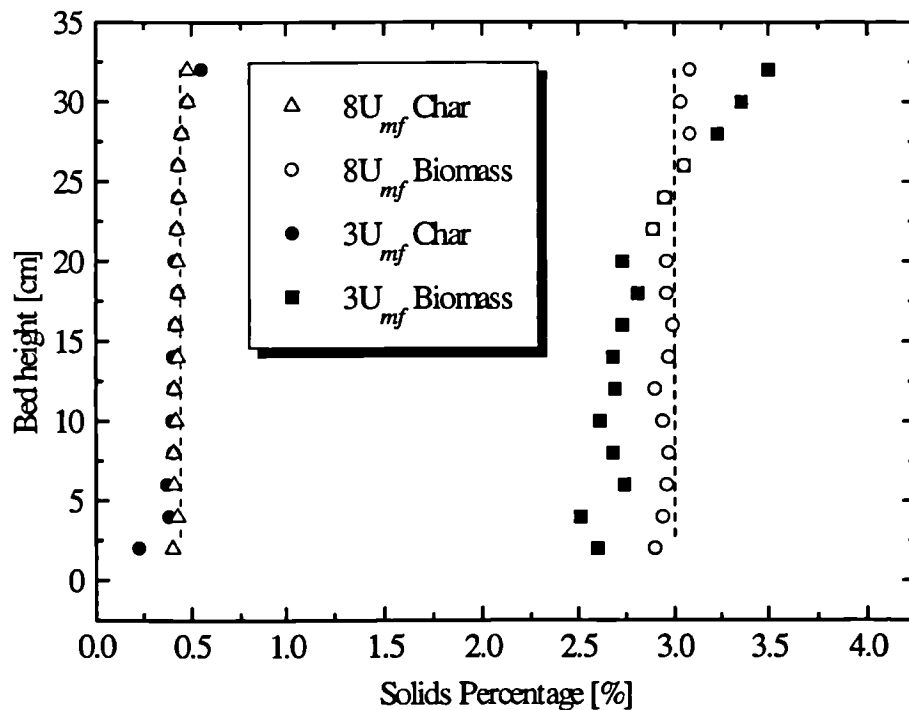


Fig. 9.1 Biomass and char mixing pattern as function of bed superficial gas velocity.

9.2 CIRCULATING FLUIDIZED BED

The scaling procedure outlined in section 9.1 can be used to completely scale the cold circulating fluidized bed and investigate the hydrodynamics of the system. This means replacing the bed material with copper and using a mixture of air and helium as the fluidizing medium in the gasifier and riser. With regards to the correlations of solids circulation rate and gas cross-flow, further work is necessary to extend the range of application of the correlations to different density systems. The effect of using a different gas distributor in the gasifier and combustor on the overall operation of the system can also be investigated.

9.3 HEATED FLUIDIZED BED GASIFIER

Further experiments should be conducted using almond shells varying particle diameter, feed rate, and also wood and other biomass as fuels. This would yield useful kinetic information which can be used to develop a more generalised correlation for the prediction of the rate constant for different.

The data obtained in this work was with a fluidized bed height of 30 cm. For continuous operations, increasing the bed height will increase the residence time of the biomass in the bed. If the biomass and sand are continuously fed to the gasification with continuous removable of the bed material, then the effect of the residence time of the char in the bed on the extent of mass loss can be investigated. Also the effect of the moisture content of the biomass on the kinetic parameters studied needs further attention. The commercial interest can be obviated here specially for developing countries where biomass is produced as waste in relatively large and consistent quantities.

NOTATION

A	pre-exponential factor	$[s^{-1}]$
A_p	area of plate	$[cm^2]$
A_r	cross section area of riser	$[m^2]$
C_D	drag coefficient	$[-]$
C_{H_2O}	concentration of steam	$[mol/m^3]$
d_{c0}	initial diameter of char particle	$[m]$
d_{ct}	diameter of char particle at time t	$[m]$
D_{dc}	downcomer internal diameter	$[m]$
ΔH_r	height of riser	$[m]$
$D_{L-valve}$	L-valve internal diameter	$[m]$
D_{noz}	nozzle diameter	$[m]$
d_p	mean particle diameter based on sieve analysis	$[m]$
D_r	riser internal diameter	$[m]$
$E(t)$	exit age distribution function	$[s]$
E_a	activation energy	$[J/mol]$
g	gravitational acceleration	$[m/s^2]$
G_s	solids mass flux	$[kg/m^2s]$
H	heating value	$[kJ/kg]$
H_{Bed1}	total height of bed 1 (combustor)	$[m]$
H_{bed2}	total height of bed 2 (gasifier)	$[m]$
H_{mf}	bed height at minimum fluidization conditions	$[m]$
H_w	distributor plate distance from gas entry point in windbox	$[m]$
H_{w1}	total height of windbox 1 (combustor)	$[m]$
H_{w2}	total height of windbox 2 (gasifier)	$[m]$

k_{cs}	char gasification surface rate constant	[m/s]
L	length	[m]
L_H	horizontal length of L-valve	[m]
M	molecular weight	[g/mol]
n	number of moles	[moles]
n_c	number of moles of carbon	[moles]
n_{H_2O}	number of moles of water (steam)	[moles]
P_{B2}	pressure drop across bed 2, gasifier	[mmH ₂ O]
Q^*_C	gas cross-flow rate from combustor to gasifier	[l/min]
Q^*_R	gas leakage from riser jet into combustor	[l/min]
Q_g	gas flow rate	[cm ³ /sec]
Q_{TC}	total gas rate to the combustor	[l/min]
Q_{TG}	total gas rate to the gasifier	[l/min]
R	ideal gas constant, = 8.314 J/mol K	[J/mol K]
r_c	radius of char particle	[m]
r_{c0}	initial radius of char particle	[m]
r_{ct}	radius of char particle at time t	[m]
r_p	radius of a particle	[m]
T	temperature	[K]
T_{air}	effective aeration point for L-valve	[m]
T_B	average bed temperature	[K]
\bar{t}	mean residence time	[s]
t_c	average residence time in combustor	[s]
t_G	average residence time in gasifier	[s]
t_p	plate thickness	[cm]
U_C	superficial gas velocity in combustor	[m/s]
U_G	superficial gas velocity in gasifier	[m/s]
U_{mf}	superficial gas velocity at minimum fluidizing conditions	[m/s]
U_r	superficial gas velocity in riser	[m/s]

V	volume	$[m^3]$
v_s	solids velocity	$[m/s]$
W	mass	$[g]$
w_T	total bed weight	$[kg]$
W_c	mass of char	$[g]$
W_{c0}	initial mass of char	$[g]$
W_{ct}	mass of char at time t	$[g]$
\bar{X}	average conversion of a species	$[-]$
X	conversion of a species	$[-]$
X_r	distance between riser inlet and riser gas jet	$[m]$

GREEK SYMBOLS

β	dimensionless parameter	$[-]$
ρ_c	molar density of char	$[mol/m^3]$
ΔP_{B1}	pressure drop across bed 1, combustor	$[mmH_2O]$
ΔP_{B2}	pressure drop across bed 2, gasifier	$[mmH_2O]$
ΔP_D	pressure drop across distributor gas plate	$[mmH_2O]$
ΔP_D	pressure drop across distributor plate	$[dynes/cm^2]$
ΔP_L	pressure drop across L-valve	$[mmH_2O]$
ε	void fraction	$[-]$
ε_{mf}	bed void fraction at minimum fluidizing conditions	$[-]$
ϕ	sphericity of particle	$[-]$
Φ_D	permeability of porous plate material	$[cm^2]$
η	dynamic viscosity	$[kg/ms]$
μ_g	gas viscosity	$[poise, kg/ms]$
θ	angle of repose of particles	$[degrees]$
ρ_b	bulk density of a bed at minimum fluidizing conditions	$[kg/m^3]$

θ	angle of repose of particles	[degrees]
ρ_b	bulk density of a bed at minimum fluidizing conditions	[kg/m ³]
ρ_g	gas density	[kg/m ³]
ρ_s	solid density	[kg/m ³]
τ	100% conversion time	[min]

DIMENSIONLESS NUMBERS

Re	Reynolds number
Ar	Archimedes number
Fr	Froude number

REFERENCES

- Agarwal, J.C., Davis, W.L. and King, D.T., (1962), Gas Distribution in Fluidized Beds, *Chemical Engineering Progress*, **58**, 85.
- Barooah, J.N. and Long, V.D., (1976), *Fuel*, **55**, 116.
- Basu, P., (1984), Design of Gas Distributors for Fluid Bed Boilers, *Fluidized Bed Boilers - Design and Applications*, P. Basu, Toronto, Pergamon Press, 45-61.
- Basu, P. and Fraser, S.A., (1991), Hydrodynamics, *Circulating Fluidized Bed Boilers*, USA, Reed Publishing Inc., 19-50.
- Bettalgi, N., Desideri, U. and Fiaschi, D., (1995), A Biomass Combustion-Gasification Model: Validation and Sensitive Analysis, *Journal of Engineering Resources and Technology*, **3**, 329-336.
- Bhatia, S.K. and Perlmutter, D.D., (1980), A random Pore Model for Fluid-Solid Reactions, *AIChE Journal*, **26**, 379-385.
- Bjerle, I., Eklund, H. and Svensson, O., (1980), Gasification of Sweedish Black Shale in the Fluidized Bed. Reactivity, *Industrial and Engineering chemistry Process Design and Development*, **19**, 345-351.
- Bolton, L.W. and Davidson, J.F., (1987), Dense Phase Circulating Fluidized Beds, *Chemical Engineering Communications*, **62**, 31-51.
- Botterill, J.S.M., (1975), *Fluidized Bed Heat Transfer*, London, Academic Press, 80.

- Boyles, D.T., (1984), *Bio-Energy: Technology, Thermodynamics and Costs*, New York, John Wiley & Sons.
- Bradbury, A.G.W., Sakai, Y. and Shafizadeh, F., (1979), Flash Pyrolysis of Biomass in a Fluidized Bed, *Journal of Applied Science*, **23**, 3271.
- Bridgwater, A.V., (1995), The Technical and Economic Feasibility of Biomass Gasification for Power Generation, *Fuel*, **74**, (5), 631-653.
- Bridgwater, A.V. and Evans, G.D., (1993), An Assessment of Thermochemical Conversion Systems for Processing Biomass and Refuse, UK Department of Trade & Industry.
- Bungay, H., (1981), *Energy - The Biomass Options*, New York, John Wiley.
- Burnham, A.K., (1979), Reaction Kinetics between Carbon Dioxide and Oil-Shale Residual Carbon: 1. Effect of heating rate on reactivity, *Fuel*, **58**, 285-292.
- Chan, W.C.E., Keblon, M. and Krieger, B.B., (1985), Product Formation in the Pyrolysis of Large Wood Particles, *Fundamentals of Thermochemical Biomass Conversion*, R.P. Overend, T.A. Milne and L.K. Mudge, Elsevier ASP.
- Chatterjee, A. and Shankar, A.R., (1982), Fluidized Bed Gas Distributors, *Chemical Age of India*, **33**, (9), 487-490.
- Chatzakis, I.N., Pindoria, R.V., Lim, J.-Y., Megaritis, A., Cai, H.-Y., Dugwell, D.R. and Kandiyoti, R., (1995), High Pressure Gasification Yields and Char reactivities from Biomass, *Gasification: An Alternative to Natural Gas*, London, IChemE, IChemE.1-7.

-
- Chong, Y.O., Nicklin, D.J. and Tait, P.J., (1986), A New Reactor System - Fluid Beds Exchanging Solids But Not Gases, *Powder Technology*, **47**, (2), 151-156.
- Chong, Y.O., O'Dea, D.P., Leung, L.S. and Nicklin, D.C., (1988), Design of Standpipes and Non-Mechanical Valves for CFB, *Circulating Fluidized Bed Technology II*, P. Basu and J.F. Large, Oxford, Pergamon Press, 493-499.
- Corella, J., Anzar, M.P., Delgado, J. and Aldea, E., (1991), Steam Gasification of Cellulosic Wastes in Fluidized Bed with Downstream Vessel, *Industrial and Engineering Chemistry Research*, **30**, 2252-2262.
- Corella, J., Herguido, J., Gonzalez-Saiz, J., Alday, F.J. and Rodriguez-Trujillo, J.L., (1988), , *Research in Thermochemical Biomass Conversion*, A.V. Bridgwater and J.L. Kuester, London, Elsevier Applied Science, 754.
- Corella, J., Orio, A. and Aznar, P., (1998), Biomass Gasification with Air in Fluidized Bed: Reforming of the Gas Composition with Commercial Steam Reforming Catalysts, *Industrial and Engineering Chemistry Research*, **37**, (12), 4617-4624.
- Danckwerts, P.V., (1953), Continuous Flow Systems, *Chemical Engineering Science*, **2**, 1-13.
- Davidson, J.F. and Harrison, D., (1971), *Fluidization*, London, Academic Press.
- Di Felice, R. and Yates, J.G., (1996), Production of Hydrogen Rich Gas from Biomass Gasification: Application to Small Scale Fuel Cell Electricity Generation in Rural Areas, Non Nuclear Energy Programme - JOULE III, London, University College London.

- Diebold, J., Elliott, D.C., Bridgwater, A.V., Solantausta, Y. and Beckman, D., (1992), Assessment of Liquefaction and Pyrolysis Systems, *Biomass and Bioenergy*, **2**, (1-6), 279-297.
- Diebold, J.P., (1994), A Unified Global Modal for the Pyrolysis of Cellulose, **7**, (1-6), 75-85.
- Dutta, S. and Wen, C.Y., (1977), Reactivity of Coal and Char in Carbon Dioxide Atmosphere, *Industrial and Engineering Chemistry, Process Design and Development*, **16**, (1), 20-30.
- Foscolo, P.U. and Gibilaro, L.G., (1984), A Fully Predictive Criterion for the Transition Between Particulate and Aggregative Fluidization, *Chemical Engineering Science*, **39**, (12), 1667-1675.
- Fox, D., Molodtsov, Y. and Large, J.F., (1989), Control Mechanisms of Fluidized Solid Circulation Between Adjacent Vessels, *AIChE Journal*, **35**, (2), 1933-1941.
- Geldart, D. and Baeyens, J., (1985), Design of Distributors for Gas Fluidized Beds, *Powder Technology*, **42**, (1), 67-78.
- Geldart, D. and Jones, P., (1991), The Behaviour of L-Valves with Granular Solids, *Powder Technology*, **67**, (2), 163-174.
- Gil, J., Corella, J. and Caballero, M.A., (1998), Effect of the Type of Gasifying Agent on the Product Distribution in Biomass Gasification in atmospheric and bubbling Fluidized Bed, *Gasification - Gateway to a Cleaner Future*, Dresden, Germany, IChemE.

-
- Glicksman, L.R., Hyre, M.R. and Farrell, P.A., (1994), Dynamic Similarity in Fluidization, *Journal of Multiphase Flow*, **20**, 331-386.
- Glicksman, L.R., Hyre, M.R. and Woloshun, K., (1993), Simplified Scaling relationships for Fluidized Beds, *Powder Technology*, **77**, 177-199.
- Graboski, M.S. and Brogan, T.R., (1988), Development of a Downdraft Modular Skid Mounted Biomass/Waste Gasification System, *Energy from Biomass and Waste XI*, Chicago, Institute of Gas Technology.
- Grace, J.R., (1986), Contacting Modes and Behaviour Classification of Gas-Solid and Other Two-Phase Suspensions, *The Canadian Journal of Chemical Engineering*, **64**, (3), 353-363.
- Graham, R.G., Bergougnou, M.A. and Overend, R.P., (1984), Fast Pyrolysis of Biomass, *Journal of Analytical and Applied Pyrolysis*, **6**, 95-135.
- Grassi, G. and Bridgwater, A.V., (1991), The Opportunities for Electricity Production from Biomass, *International Journal of Solar Energy*, **10**, 127.
- Grassi, G. and Bridgwater, A.V., (1992), Biomass for Agriculture and Industry in Europe, *Biomass for Energy and Industry - 7th European Conference*, Luxembourg, G. Grassi, Elsevier Applied Science.268-274.
- Guell, A.J. and Kandiyoti, R., (1993), Development of a Gas-Sweep Facility for the Direct Capture of Pyrolysis Tars in a Variable Heating Rate High-Pressure Wire-Mesh Reactor, *Energy Fuels*, **7**, (6), 943-952.

-
- Hajaligol, M.R., Howard, J.B., Longwell, J. and Peters, W.A., (1980), Product Composition and Kinetics for Rapid Pyrolysis of Cellulose, *Solar Energy Research Institute, Tech. Rep. SERI/CP*, (1980), 215-236.
- Hanway, J.E., (1970), *Chemical Engineering Progress Symposium Series*, **66**, (105), 253.
- Hedley, A. and Bustani, A., (1989), Fundamentals of Gasification and its Technology, *Gasification: Its Role in the Future Technological and Economic development of the United Kingdom*, A. Hedley and F. Ferguson, London, Elsevier Applied Science Publishers, **20**, 1-16.
- Hengl, G., Hiquily, N. and Couderc, J.P., (1977), A New Distributor for Gas Fluidization, *Powder Technology*, **18**, 277-278.
- Hill, M. and Fott, P., (1993), Kinetics of Gasification of Czech Brown Coals, *Fuel*, **72**, (4), 525-529.
- Hill, M.K., (1987), Development of the Seal Leg Char Recycle System, *Proceedings of 9th International Conference on CFB*, 862.
- Hirschfelder, H. and Vierrath, H., (1999), Electricity and Syngas from Biomass Waste Applying CFB Gasification, *Circulating Fluidized Bed Technology VI*, Wurzburg, J. Werther, Dechema, 459-467.
- Johnson, K.L., (1979), Kinetics of Coal Gasification, New York, Wiley, 283.
- Judd, M.R. and Rudolph, V., (1986), Gasification of Coal in a Fluidized Bed with a Draft Tube, *Fluidization V*, Denmark, K. Ostergaardt and A. Sorensen, Engineering Foundation, New York, 505-512.

-
- Katheklakis, I.E., Lu, S.-L., Bartle, K.D. and Kandiyoti, R., (1990), Effect of Residence time on the Molecular Mass Distributions of Fluidized Bed Pyrolysis Tars, *Fuel*, **69**, 172-176.
- Kehlenbeck, R. and Yates, J.G., (2000), Fluid Dynamic Studies in a Scaled Cold Model for Biomass-Steam Gasification in a Circulating Fluidized Bed, *Research 2000 - Stretching the Boundaries of Chemical Engineering*, Bath, Uk, IChemE.
- Kimura, S., Tone, S., Nakagawa, J. and Otake, T., (1982), Non-isothermal Behaviour of Gas-Solid Reactions based on the Volume Reaction Model, *Journal of Chemical Engineering of Japan*, **15**, (2), 115-121.
- Kirk-Othmer, (1980), *Encyclopedia of Chemical Technology*, New York, John Wiley & Sons.
- Klass, L.D., (1998), *Biomass for Renewable Energy, Fuels, and Chemicals*, California, Academic Press, 83.
- Knight, J.A., Gorton, C.W., Kovac, R.J. and Newman, C.J., (1985), Entrained Flow Pyrolysis of Biomass, *Proceedings of Biomass Thermochemical Contractors Meeting*, Pacific Northwest Laboratory, Battelle.
- Knowlton, T.M., (1988), Non-Mechanical Solid Feed and Recycle Devices for CFB, *Circulating Fluidized Bed Technology II*, P. Basu and J.F. Large, Oxford, Pergamon Press, 31-42.
- Knowlton, T.M. and Hirsan, I., (1978), L-Valves Characterized for Solids Flow, *Hydrocarbon Processing*, **57**, 149-156.

-
- Knowlton, T.M., Hirsan, I. and Leung, L.S., (1978), , *Fluidization*, J.F. Davidson and D.L. Keairns, Cambridge University Press.
- Kojima, T., Assavadakorn, P. and Furusawa, T., (1993), Measurement and Evaluation of Gasification Kinetics of Sawdust Char with Steam in an Experimental Fluidized Bed, *Fuel Processing Technology*, **36**, 201-207.
- Korenberg, J., (1982), *Proceedings of the 7th International Conference on Fluidized Bed Combustion*, Philadelphia, 339-349.
- Kostrin, H.M., (1980), Direct Formation of Pyrolysis Oils from Biomass, *Solar Energy Research Institute*, (Inst. Rep. SERI/CP), 105-121.
- Koufopoulos, C.A., Papayannakos, N., Maschio, C. and Lucchesi, A., (1991), Modelling of Pyrolysis of Biomass Particles - Studies Kinetic Thermal, and Heat Transfer Effects, *Canadian Journal of Chemical Engineering*, **69**, (4), 907-915.
- Kunii, D. and Levenspiel, O., (1991), *Fluidization Engineering*, Boston, Butterworth-Heineman.
- Kuramoto, M., Furusawa, T. and Kunii, D., (1985), Development of a New System for Circulating Fluidized Bed Particles within a Single Vessel, *Powder Technology*, **44**, (1), 77-84.
- Kurkela, E., Stahlberg, P., Laatikainen, J. and Simell, P., (1993), Development of Simplified IGCC-Process for Biofuels: Supporting Gasification Research at VTT, *Biosource Technology*, **46**, 37-47.
- Kwon, T.-W., Kim, S.D. and Fung, D.P.C., (1988), Reaction Kinetics of Char-CO₂ Gasification, *Fuel*, **67**, 530-535.

-
- Lanauze, R.D., (1976), A Circulating Fluidized Bed, *Powder Technology*, **15**, 285-292.
- Leung, L.S., (1987), Operation of V-Valve for Gas-Solid Flow, *Powder Technology*, **49**, 271.
- Lewellen, P.C., Peters, W.A. and Howard, J.B., (1976), *16th International Symposium on Combustion*, Pittsburg, PA.
- Li, J. and Van Heiningen, A.R.P., (1991), Kinetics of Gasification of Black Liquor Char by Steam, *Industrial and Engineering Chemistry Research*, **30**, 1595-1601.
- Liden, A.G., Berruti, F. and Scott, D.S., (1988), A kinetics Model for the Production of Liquids from thhe Flash Pyrolysis of Biomass, *Chemical Engineering Communications*, **65**, 207-215.
- Liliedahl, T. and Sjostrom, K., (1997), Modelling of Char-Gas Reaction Kinetics, *Fuel*, **76**, (1), 29-37.
- Litz, W.J., (1972), Design of Gas Distributors, *Chemical Engineering*, **13**, 162-166.
- Luo, Z., Ni, M., Zhou, L., Cheng, Z. and Cen, K., (1989), Solid Recycle System for CFB, *Proceedings of the 10th International Conference on Fluidized Bed Combustion*, ASME, A. Manaker, 557-562.
- Luong, P.H. and Bhattacharya, S.C., (1993), A Study of Solid Circulation Rate in a Circulating Fluidized Bed, *International Journal of Energy Research*, **17**, 479-490.
- Mackie, K.L., (1993), New Zealand, IEA Bioenergy Agreement Environmental Systems Groups.

-
- Mahajan, O.P., Yarzab, R. and Walker, P.L., (1978), Unification of Coal-Char Gasification Reaction Mechanisms, *Fuel*, **57**, 643.
- Matsen, J., (1988), The Rise and Fall of Recurrent Particles: Hydrodynamics of Circulation, *Circulating Fluidized Bed Technology*, P. Basu and J.F. Large, Oxford, Pergamon Press, **2**, 3-11.
- Matsui, I., Kunii, D. and Furusawa, T., (1988), Study of Fluidized Bed Steam Gasification of Char by Thermogravimetrically Obtained Kinetics, *Journal of Chemical Engineering of Japan*, **18**, (2), 105-112.
- Megaritis, A., Zhou, Y., Messenbock, R., Dugwell, D.R. and Kandiyoti, R., (1998), Pyrolysis and Gasification in a Bench Scale High Pressure Fluidized Bed Reactor, *Energy and Fuels*, **12**, 144-151.
- Milne, T., (1979), Pyrolysis - The thermal Behavior of Biomass Below 600°C, *Survey of Biomass Gasification*, **2**, Chapter 5.
- Narvaez, I., Corella, J. and Orio, A., (1997), Fresh Tars (From a Biomass Gasifier) Elimination Over a Commercial Steam Reforming Catalyst. Kinetics and Effect of Different Variables of Operation, *Industrial and Engineering Chemistry Research*, **36**, (2), 317-327.
- Nguyen, H.V., Whitehead, A.B. and Potter, O.E., (1977), Gas Backmixing, Solids Movement, and Bubble Activities in Large Scale Fluidized Beds, *AIChE Journal*, **23**, (6), 913-921.
- Olivares, A., Aznar, M.P., Caballero, M.A., Gil, J., Frances, E. and Corella, J., (1997), Biomass Gasification: Produced Gas Upgrading by In-Bed Use of Dolomite, *Industrial and Engineering Chemistry Research*, **36**, (12), 5220-5226.

-
- Overend, R.P., (1998), Production of Electricity from Biomass Crops - US Perspective, <http://www.eren.doe.gov/biopower/pdfs/eiepage.pdf>.
- Paisely, M.A. and Overend, R.P., (1994), Biomass Power for Power Generation, *EPRI Coal Gasification Conference*, San Francisco.
- Perry, H.R. and Green, D.W., (1997), Perry's Chemical Engineers Handbook, United States of America, McGraw-hill Companies Inc.
- Rapagnà, S., (1985), Influenza di Parametri Fluidodinamici sul Compartimento di Apparecchiature a Letto Fluido, L'Aquila, Università di L'Aquila.
- Rapagna, S. and Foscolo, P.U., (1999), Performance of a Perovskite Catalyst on the Steam Reforming of Tar and Methane Directly in the Gasifier, Private Communication.
- Rapagna, S. and Latif, A., (1997), Steam Gasification of Biomass in a Fluidized Bed Reactor: The Influence of Temperature and Particle Size on the Product Yield and Distribution, *Biomass and Bioenergy*, **12**, (4), 281-288.
- Rapagna, S., Tempesti, E., Foscolo, P.U. and Parodi, E., (1992), Continuous Flash Pyrolysis of Biomass at High Temperature in a Fluidized Bed Reactor, *Journal of Thermal Analysis*, **38**, 2621-2629.
- Richardson, D.R., (1963), *Chemical Engineering*, May 1, 148.
- Riley, R.K. and Judd, M.R., (1987), The Measurement of Char-Steam Gasification Kinetics for the Design of a Fluidized Bed Coal Gasifier which Contains a Draft Tube, *Chemical Engineering Communications*, **62**, 151-160.

-
- Rose, J.W. and Cooper, J.R., (1977), Technical Data on Fuel, *World Energy Conference*, B.N. Committee, London.
- Ross, I.B. and Davidson, J.F., (1981), Combustion of Carbon Particles in a Fluidized Bed, *Transactions of the Institution of Chemical Engineers*, **59**, 108-114.
- Salam, T.F. and Gibbs, M., (1987), Solid Circulation Between Fluidized Beds Using Jet Pumps, *Powder Technology*, **52**, 107-116.
- Sarkanen, V.S. and Tillman, D.A., (1979), *Progress in Biomass Conversion*, New York, Academic Press.
- Sathiyamoorthy, D. and Rudolph, V., (1991), Hydrodynamics of Compartmented Dense Phase Circulating Gas Fluidized Bed, *Circulating Fluidized Bed Technology III*, Japan, P. Basu, M. Horio and M. Hastani, Pergamon Press, 505-510.
- Schilling, H.D., Bonn, B. and Krauss, U., (1981), *Coal Gasification*, London, Graham & Totman Ltd.
- Schrader, L. and Felgener, G., (1978), *Fluidization*, J.F. Davison and D.L. Keairns, New York, Cambridge University Press, 221.
- Schuegerl, K., (1989), Biofluidization: An Application of the Fluidization Technique in Biotechnology, *Canadian Journal of Chemical Engineering*, **67**, (2), 178-184.
- Scott, D.S., Piskorz, J., Bergounou, M.A., Graham, R. and Overend, R.P., (1988), *Industrial Engineering and Chemistry Research*, **27**, 8.

-
- Shafizadeh, F., (1982), Introduction to Pyrolysis of Biomass, *Journal of Analytical and Applied Pyrolysis*, **3**, 283.
- Shafizadeh, F., (1985), Pyrolytic Reactions and Products of Biomass, *Fundamentals of Thermochemical Biomass Conversion*, R.P. Overend, T.A. Milne and L.K. Mudge, Elsevier ASP.
- Silverman, R.W., Thompson, A.H., Steynberg, A., Yukawa, Y. and Shingles, T., (1986), Development of a Dense Fluidized Bed Fischer-Tropsch reactor, *Fluidization V*, K. Ostergaard and A. Sorensen, New York, Engineering Foundation, 441.
- Stamm, A.J., (1956), *Industrial and Engineering Chemistry*, **48**, 413.
- Stiles, H.N. and Kandiyoti, R., (1989), Secondary Reactions of Flash Pyrolysis Tars Measured in a Fluidized Bed Pyrolysis Reactor With Some Noval Changes, *Fuel*, **68**, 275.
- Tatom, J.W., Colcord, A.R., Knight, J.A. and Elston, L.W., (1976), Clean Fuels from Agriculture and Forestry Wastes, USA EPA.
- Tyler, R.J., (1979), Flash Pyrolysis of Coals, *Fuel*, **58**, 680-686.
- Wang, R.C. and Lin, W.C., (1998), Fluidized Bed Incineration in Capturing Trace Metals of Sewage Sludge, *Journal of Chemical Engineering of Japan*, **31**, (6), 897-902.
- Wereko-Brobby, C.Y. and Hagen, E.B., (1996), Biomass Conversion and Technology, London, John Wiley & Sons Ltd.
- Whitehead, A.B., (1971), *Fluidization*, H. Davidson, Academic Press, 781-814.

Zenz, F.A., (1968), Symposium on Fluidization II, Montreal.

Zenz, F.A., (1989), Fluidization and Fluid Particle Systems, Nelsonville, Penn-Corp. Publication, 101-109.

Zuiderweg, F.J., (1967), Proceedings of the International Symposium, Amsterdam, Netherlands Univ. Press, 739.

Appendix A

SAND AND BIOMASS FEEDER CALIBRATION

The calibration of the feeders were done by setting the wheel rotator speed on the control unit at different positions (1-9) and weighing the quantity of material conveyed by the wheel over a fixed period of time. The feeder was calibrated almost under the same conditions as it would operate during gasification. For example, during calibration, the feeding probe was connected and for the biomass feeder, a small flow of nitrogen (1 l/min) was maintained to entrain the solid biomass particles. The set-up is shown in Fig. A.1.

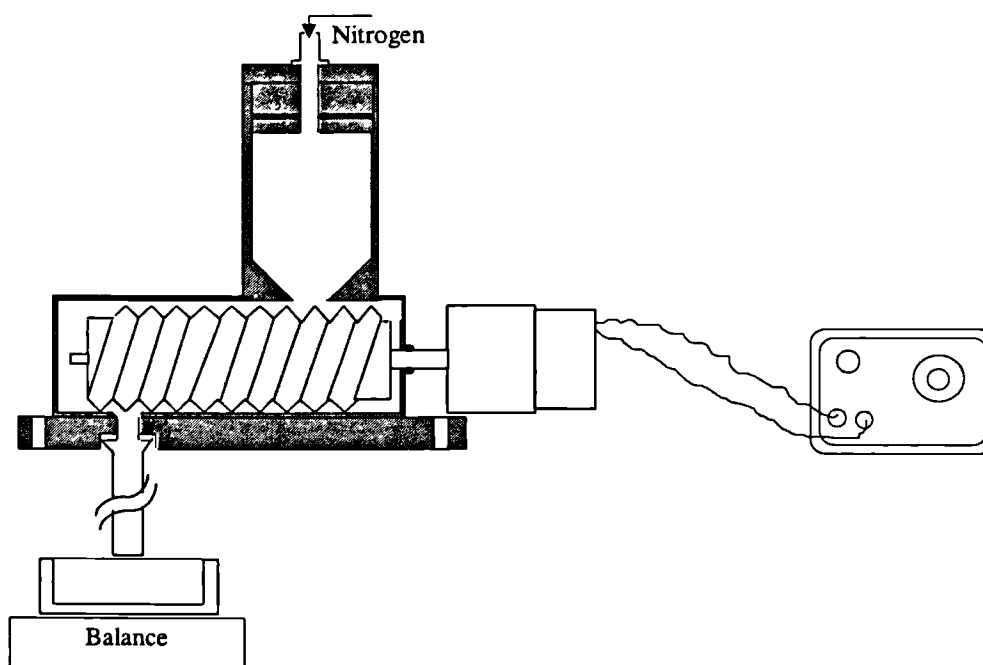


Fig. A.1 Feeder calibration set-up.

This feeder was also calibrated to convey Zirconium Oxide. The following results were obtained.

Table A.1 Biomass (almond shells, $dp = 847 \mu\text{m}$) feed rate.

Feeder Setting	Time (min.)					Average (g/min)
	1	2	3	4	5	
	Biomass conveyed (g)					
1	0.41	0.82	1.28	1.69	2.09	0.42
2	0.75	1.53	2.27	3.01	3.74	0.75
3	1.26	2.53	3.78	5.08	6.38	1.28
4	1.69	3.37	5.06	6.79	8.50	1.70
5	1.96	3.87	5.89	7.87	9.38	1.98
6	2.23	4.56	6.76	9.01	11.27	2.25
7	2.7	5.41	8.12	10.84	13.55	2.71
8	3.15	6.30	9.42	12.61	15.80	3.16
9	3.36	6.84	10.25	13.67	17.17	3.43

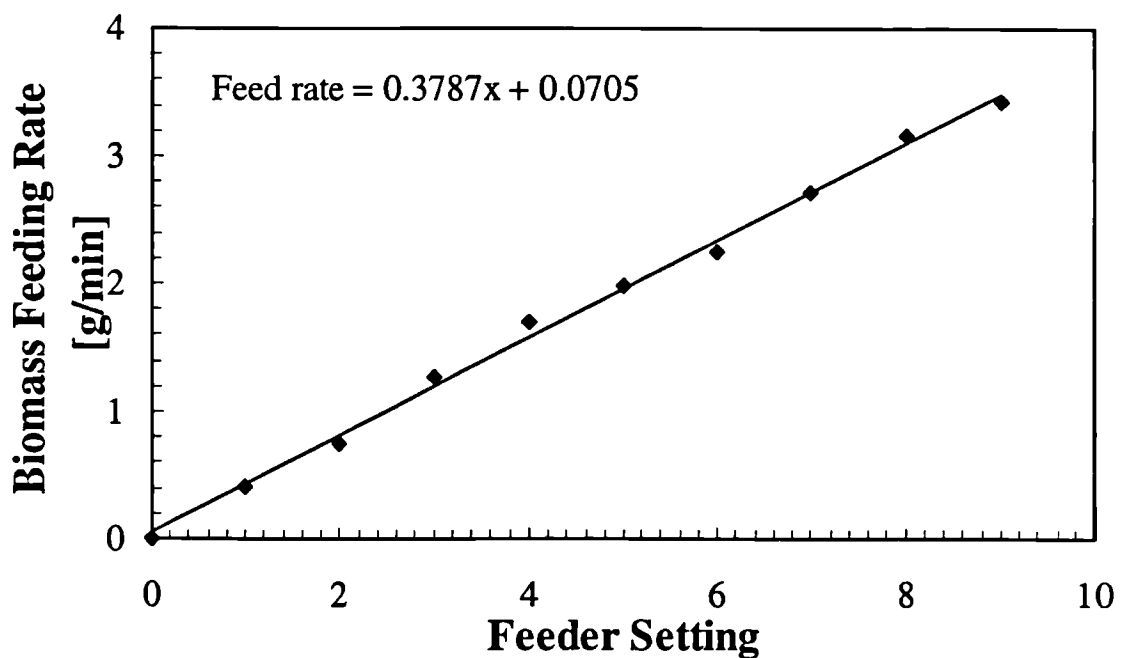
**Fig. A.2** Biomass (almond shells) feed rate as a function of feeder setting.

Table A.2 ZrO (dp = 739 μm) feed rate.

Feeder Setting	Time (min.)						Average (g/min)
	1	2	3	4	5	6	
0	0.00	0.00	0.00	0.00	0.00	0.00	0.00
6	5.40	11.15	16.85	22.36	27.94	33.59	5.60
7	6.33	12.97	19.48	25.94	32.47	38.81	6.47
8	7.54	14.95	22.42	30.00	37.65	45.16	7.53
9	8.46	16.89	25.37	33.87	42.31	50.75	8.46

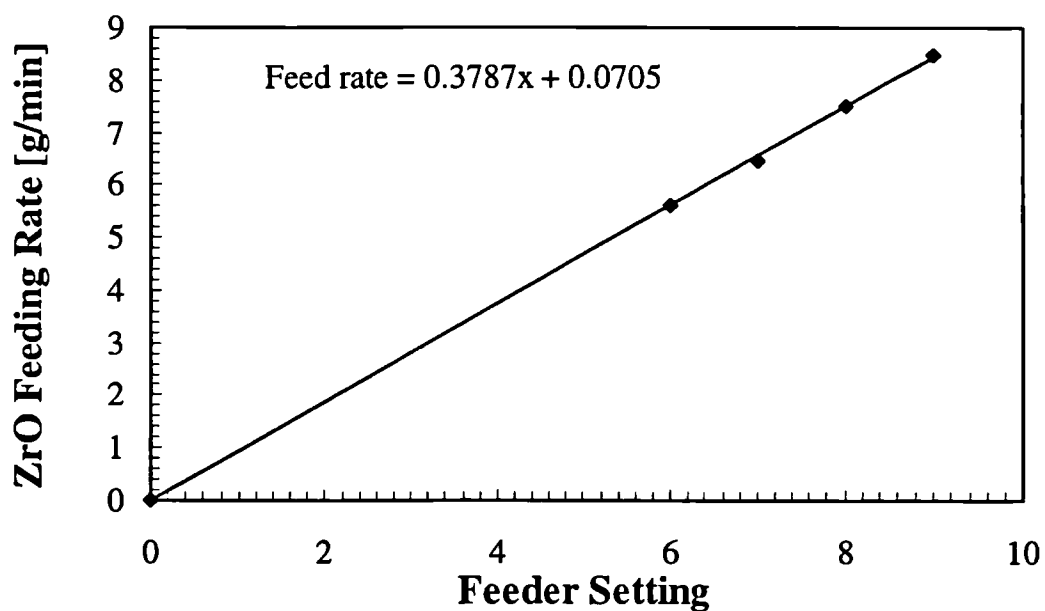


Fig. A.3 ZrO feed rate as a function of feeder setting.

Sand Feeder Calibration

Table A.3 Sand ($d_p = 177 \mu\text{m}$) feed rate.

Feeder Setting	Time (min.)					Average (g/min)
	1	2	3	4	5	
1	5.64	11.63	17.25	23.29	29.05	5.81
2	7.26	14.54	21.87	29.20	36.57	7.31
3	12.33	24.80	37.34	50.03	62.54	12.51
4	15.63	21.44	47.14	63.00	79.12	15.82
5	18.43	36.93	55.61	74.38	92.99	18.59
6	21.18	42.37	32.68	85.15	106.62	21.32
7	23.12	46.81	70.64	94.48	118.05	23.61
8	26.98	53.96	80.73	107.64	134.24	26.84
9	30.25	60.60	91.00	121.24	151.73	30.34

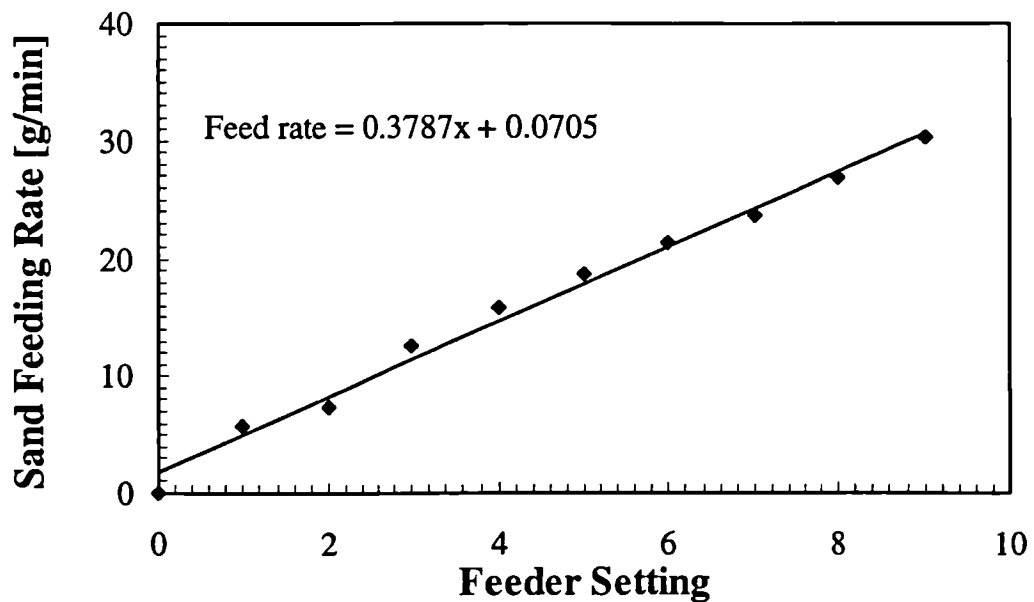


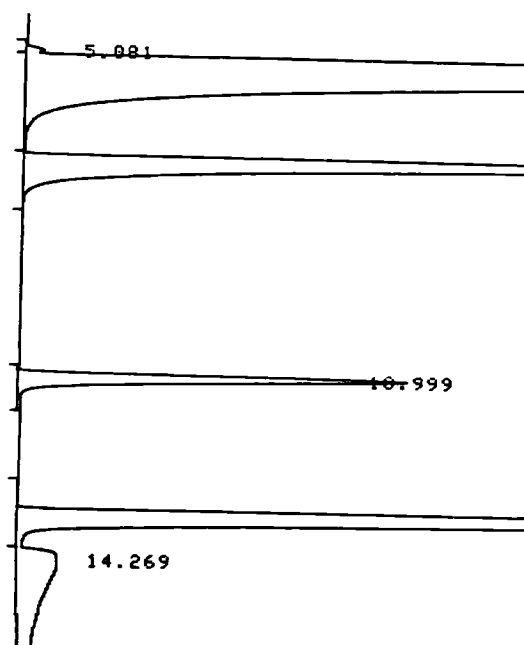
Fig. A.4 Sand feed rate as a function of feeder setting.

Appendix B

GAS CHROMATOGRAPH CALIBRATION

When a mixture of gases is injected into the chromatograph, the sample components flow through the column in which the chromatographic separation takes place. The detector signals the presence of a component eluted from the column. These signals are integrated in the form of peaks and plotted by the integrator. An example of the integrator run data is displayed below.

* Run # 1 APR 3,1998 19:36:22



To review the run data:

The first line identifies the run by supplying the run number, date, and time.

The chromatogram appears next.

The report of the analysis appears next.

The first column of the report analysis displays the retention time of a substance. This is the time elapsed from injection of the sample to recording the peak maximum of

the component band. The retention time is also printed at the corresponding peak apex. The second column of the report analysis displays the area corresponding to the percentage composition of each sample component in the mixture. The retention time and the peak area were enough for our experiments.

The calibration of the chromatograph was performed by using different gas mixtures with different percentage composition by volume of the sample components N_2 , CO, CO_2 , and CH_4 . Each mixture in turn was injected a number of times into the chromatographs to get an area output corresponding to the percentage of each gas. The peaks of the chromatogram were identified by comparing the retention time with standards under similar conditions in literature. From the different injections, an overall average area corresponding to 1% of each gas was obtained. The different gas mixtures are shown in Table B.1. Considering the mixture, the following areas were obtained when the gas was injected into the chromatograph at 15cmH₂O pressure.

Table B.1 Composition of gas mixtures.

Components	Mixture 1	Mixture 2	Mixture 3	Mixture 4
Hydrogen	-	-	-	38.80
Nitrogen	93.99	93.99	-	61.20
Methane	1.00	1.00	-	-
Carbon monoxide	1.01	1.01	-	-
Carbon dioxide	1.00	1.00	98.99	-
Ethane	1.01	1.01	-	-
Ethylene	0.99	0.99	-	-
Acetylene	1.00	1.00	-	-

From the above results, for each chromatogram, an average area for each gas was calculated. Since the percentage composition of each gas was known, an area corresponding to 1% of each gas was obtained. The results are shown in the two following tables below.

Table B.2 Integrator areas for mixtures 1 - 4.

Components	Area from Gas Chromatograph			
	Mixture 1	Mixture 2	Mixture 3	Mixture 4
Hydrogen	-	-	-	-
Nitrogen	6135796	6186446	-	-
Methane	59841	60112	-	-
Carbon monoxide	67033	67613	-	-
Carbon dioxide	97463	97884	9749429	-
Ethane	112657	113187	-	-
Ethylene	77591	79441	-	-
Acetylene	89508	93712	-	-

Table B.3 Integrator area for one percent of each gas component.

Components	GC
	Area/1%
Hydrogen, H ₂	-
Nitrogen, N ₂	65550
Methane, CH ₄	59976
Carbon monoxide, CO	66656
Carbon dioxide, CO ₂	97673
Ethane	111804
Ethylene	79309
Acetylene	91610

The results from Table B.3 were used to evaluate the presence and the percentage of the above gases in the non-condensable gas stream from the gasifier.

Appendix C

WATER INJECTION PUMP CALIBRATION

A Watson Marlow 101U model peristaltic pump was used to inject the water at the base of the bed into the windbox for the generation of steam. The rate at which the water was injected was not fixed and depended on the setting of the control panel (1-99) and the internal diameter of the tubing used. Therefore it was necessary to calibrate these settings for use with distilled water. The pump was set at different positions and the mass of water discharged over one minute intervals was weighed using a balance. The calibration set-up is shown in Fig. C.1.

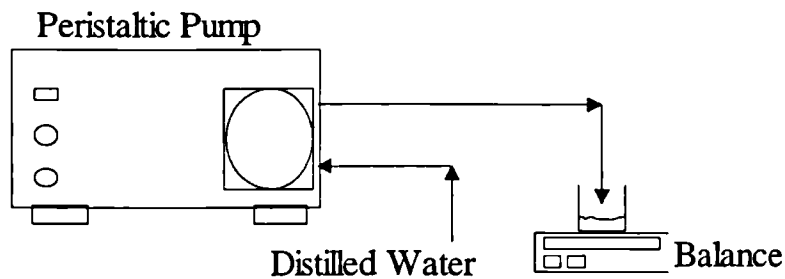


Fig. C.1 Water pump calibration set-up.

The results are shown in Table C.1, which were used to plot the calibration graph for the water pump as shown in Fig. C.2. The graph was used to determine the pump setting required for the desired water (i.e. steam) flowrate through the bed. The results are obtained using a 1 mm internal diameter silicone tubing.

Table C.1 Water pump calibration set-up.

Pump Setting	Time (min.)					Average (g/min)
	1	2	3	4	5	
10	0.76	1.52	2.33	3.09	3.90	0.78
20	1.57	3.17	4.77	6.38	7.99	1.59
30	2.36	4.82	7.22	9.65	12.07	2.41
40	3.20	6.45	9.70	12.90	16.33	3.26
50	4.01	8.10	12.15	16.21	20.32	4.06
60	4.85	9.70	14.56	19.47	24.45	4.89
70	5.67	11.36	17.07	22.77	28.60	5.72
80	6.48	12.97	19.52	26.04	32.73	6.54
90	7.30	14.63	22.01	29.36	36.87	7.37
99	8.01	16.10	24.24	32.36	40.65	8.13

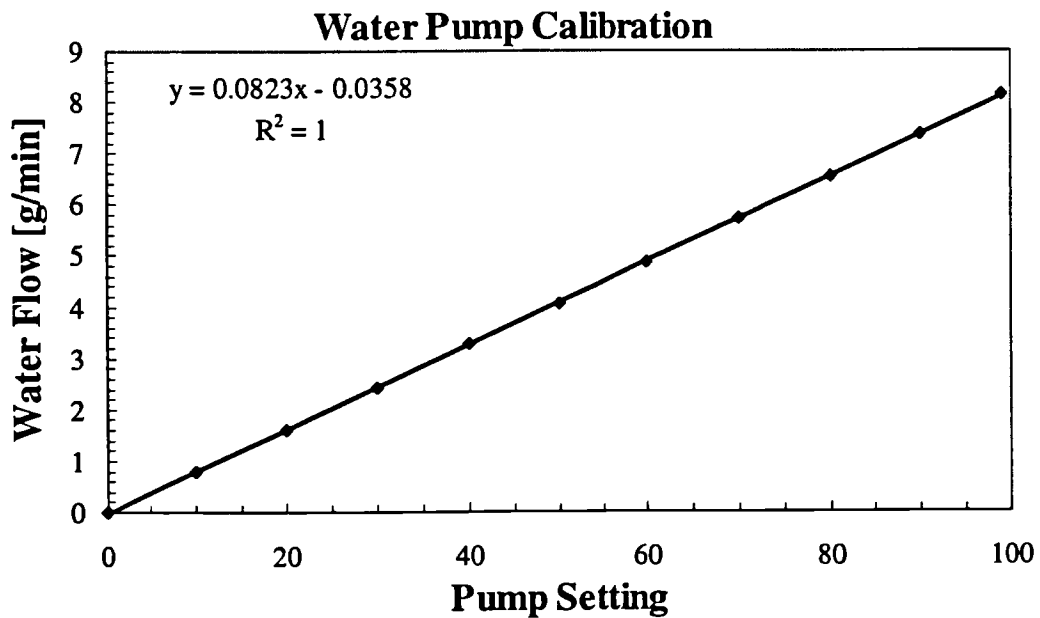


Fig. C.2 Water pump calibration graph.

Appendix D

PARTICLE SIZE CHARACTERISATION AND CALCULATION OF MINIMUM FLUIDISATION VELOCITY

Fluidized beds rarely contain powders of a uniform size. Generally a distribution of sizes is present and as a result, it is vital to define some convenient dimension for the purpose of characterisation (Allen, 1981). The most frequently used average is the sieve size diameter defined as (Yates, 1983)

$$d_p = \frac{1}{\sum_i \frac{x_i}{d_i}}$$

here X_i is the mass fraction of the particles in each size range given by the sieve aperture, d_i , and d_p is the diameter of a particle with an external surface to volume ratio equal to that of the mixture average. Where ϵ is the bed voidage defined as

$$\begin{aligned} \epsilon &= \frac{\text{Volume of bed} - \text{Volume of particles}}{\text{Volume of bed}} \\ &= 1 - \frac{M}{\rho_p v_b} \\ &= 1 - \frac{\rho_{\text{BULK}}}{\rho_p} \end{aligned}$$

Bed Silver Sand

The bed powder used was Silver sand corresponding to Group B of the Geldart classification of powders. Initially, the powder contained size fractions in the range of 30 μm to 280 μm . It was necessary to separate the powder into fractions that would give a mean diameter of around 200 μm . All fractions below 90 μm were removed by sieving (this also helped reduce entrainment of fine particles that induces health hazard). The

results obtained are shown in Fig. D.2.

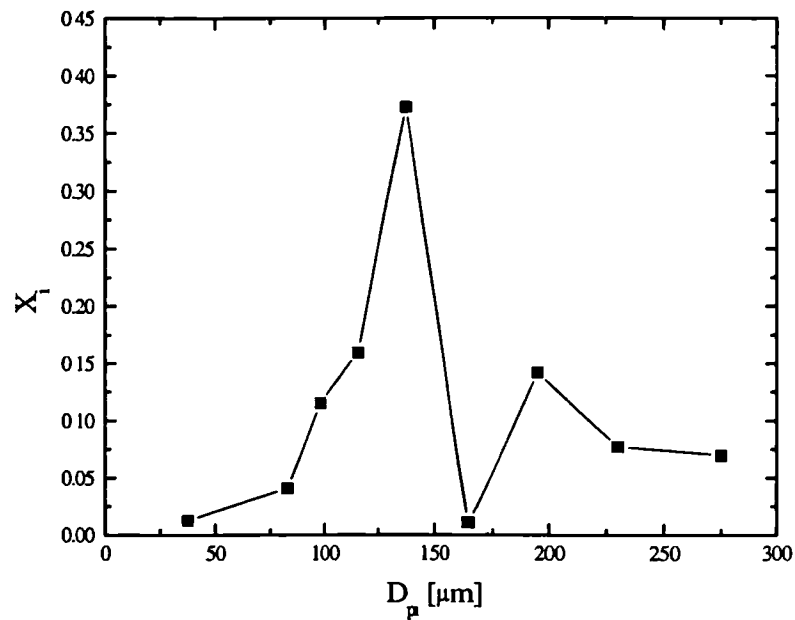


Fig. D.1 Size distribution of silver sand.

Table D.1 Sizee distribution data for Fig. D.2.

Size μm	Weight g	x_i -	D_{pi} μm	sum x_i -	x_i/D_{pi}
355	8.30	0.0412	389.0	1.00	1.06E-04
300	3.50	0.0174	327.5	0.96	5.30E 05
250	8.40	0.0417	275.0	0.94	1.52E-04
212	26.10	0.1295	231.0	0.90	5.61E-04
180	39.60	0.1965	196.0	0.77	1.00E-03
150	33.40	0.1658	165.0	0.57	1.00E-03
125	64.10	0.3181	137.5	0.41	2.31E-03
106	14.70	0.0730	115.5	0.09	6.32E-04
90	3.10	0.0154	98.0	0.02	1.57E-04
75	0.30	0.0015	82.5	0.00	1.80E-05
0	0.00	0.0000	31.5	0.00	0.00E+00

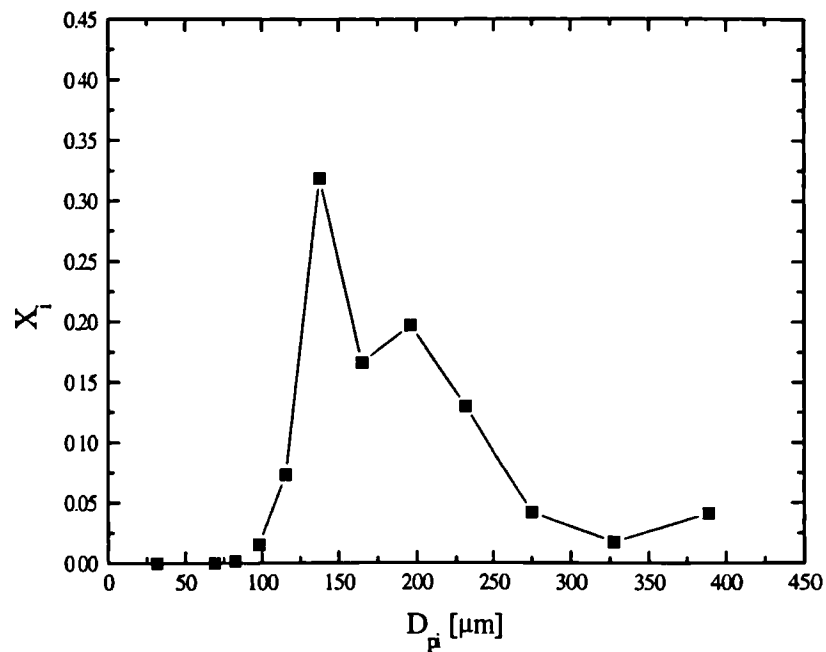


Fig. D.2 Modified distribution of silver sand.

There was still some quantity of the unwanted fractions, but it was difficult and time consuming to remove all the smaller fractions. They were minimised as much as possible. The new mean diameter was 164 μm .

The evaluation of the minimum fluidization velocity was performed experimentally. About 13971.2 g of sand was fluidized in a cylinder of diameter 147 mm. Air was used as the fluidising medium. By means of a water manometer, the pressure drop in the bed was measured and recorded at different gas flow rates in order to plot the ΔP -versus u graph reported in Fig. D.3. The data for the plot is reported in Table D . The superficial velocity of the gas can be evaluated by using the following equation:

$$U = \frac{Q}{S}$$

Where Q = Gas volumetric flowrate, cm^3 / s

S = Cross - sectional area of the bed, cm^2

$$\begin{aligned}
 S &= \pi r^2 \\
 &= \pi(13.7/2)^2 \\
 &= 147.41 \text{ cm}^2
 \end{aligned}$$

Therefore for a flowrate of 8 l/min;

$$\begin{aligned}
 U &= \frac{8 \cdot 1000}{60 \cdot 147.41} \\
 &= 0.904 \text{ cm/s}
 \end{aligned}$$

This procedure is used to calculate the gas velocity for the other gas flowrates.

Table D 2 Experimental data for the plot of ΔP -versus- u for sand.

u cm/s	ΔP [cmH ₂ O] Increasing vel.	ΔP [cmH ₂ O] Decreasing vel.	u cm/s	ΔP [cmH ₂ O] Increasing vel.	ΔP [cmH ₂ O] Decreasing vel.
0	0	0	2.26	24.10	18.70
0.90	13.10	8.00	2.35	23.30	19.30
0.95	14.60	8.80	2.46	23.30	20.00
1.09	15.90	9.60	2.58	23.50	20.50
1.18	17.20	10.40	2.67	23.40	21.10
1.31	18.50	11.20	2.80	23.50	21.60
1.40	19.80	12.00	2.89	23.50	21.90
1.54	21.10	12.90	3.01	23.60	22.30
1.63	22.10	13.70	3.12	23.60	22.70
1.76	22.80	14.60	3.23	23.60	22.90
1.85	23.30	15.50	3.35	23.60	23.30
1.94	23.90	16.30	3.46	23.60	23.30
2.04	24.10	16.90	3.54	23.60	23.30
2.17	24.10	17.90	3.66	23.60	23.30

The voidage of the bed is calculated using the following equation:

$$\varepsilon = 1 - \frac{m}{\rho SH}$$

Where m = mass of powder, g

ρ = Particle density, g / cm³

H = bed height, cm

For a gas velocity of 2.668 cm/s, the bed height is 18.7 cm.

$$\begin{aligned} \therefore \epsilon &= 1 - \frac{1068.4}{1.65 * 36.63 * 31.5} \\ &= 0.438 \end{aligned}$$

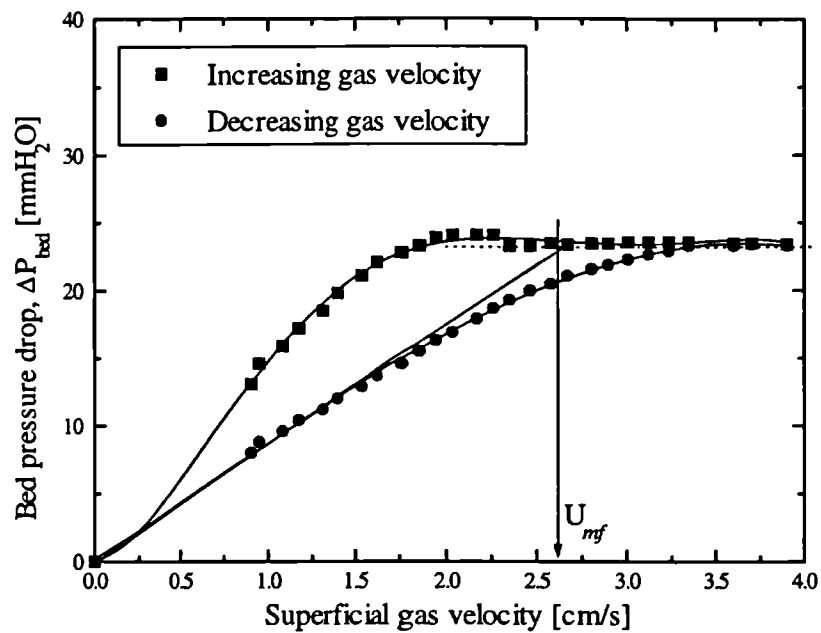


Fig. D.3 Plot of u-versus- ΔP for sand.

From the above data $U_{mf} = 2.6 \text{ cm/s}$, $\epsilon_{mf} = 0.44$

For zirconium oxide, a mean particle size of 638 μm was evaluated as shown below.

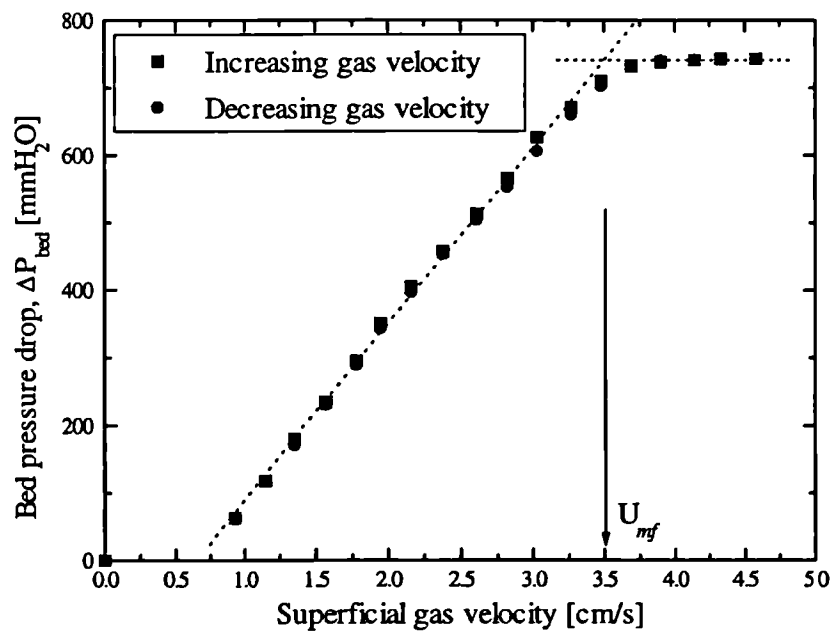
Table D 3 Size distribution data for zirconia.

Size μm	Weight g	x_i -	D_{pi} μm	sum x_i -	x_i/D_{pi}
850					
710	6.35	0.08	780.00	1.00	0.00
600	69.79	0.91	655.00	0.92	0.00
550	0.19	0.01	575.00	0.00	0.00
Sum	76.33	1.00	$D = 638 \mu\text{m}$		

Copper powder

Table D 4 Size distribution data for copper.

Size μm	Weight g	x_i -	D_{p_i} μm	sum x_i -	x_i/D_{p_i}
150					
125	1.2	0.00542	137.5	1	3.9E-05
106	99.71	0.45054	115.5	0.99458	0.0039
90	90.21	0.40762	98	0.54403	0.00416
75	29.44	0.13303	82.5	0.13641	0.00161
63	0.75	0.00339	69	0.00339	4.9E-05
0	0	0	31.5	0	0
SUM	221.31	1.00	$D_s = 102.44 \mu\text{m}$		

**Fig. D.4** Plot of u -versus- ΔP for copper.

From the data, the U_{mf} for copper is evaluated as 3.4 cm/s with an average particle diameter of 102 μm .

Almond shells

Table D 5 Size distributor and mean particle diameter
of almond shells.

Size μm	Weight g	x_i -	D_{pi} μm	sum x_i -	x_i/D_{pi}
1200					
1000	4.44	0.14	1100	1.00	0.00013
850	11.87	0.37	925	0.86	0.00041
710	8.67	0.27	780	0.48	0.00036
600	5.4	0.17	655	0.20	0.00026
550	0.9	0.03	575	0.03	5E-05
0	0	0	275	0.00	0
SUM	31.28	1.00	$D_s = 827.65 \mu\text{m}$		

Appendix E

DENSITY EVALUATION OF EXPERIMENTAL MATERIALS

The particle density is defined as

$$\rho_p = \frac{\text{Mass of a single particle}}{\text{Volume the non - porous particle would displace}}$$

$$\rho_p = \frac{M_p}{V}$$

The voids inside the particle are included in the volume. The particle density of non-porous particles is equal to the absolute density of the material, ρ_{ABS} , measured using a specific gravity bottle or a pycnometer.

The density of the almond shells was evaluated by a Gravimetric technique using two Density Bottles. First the weight of the empty density bottle were recorded. Then, both Density bottles were filled with water so that the water minucus was just over the neck mark as show in Fig. E.1. The two density bottles were weighed, emptied and placed in an oven to dry completely.

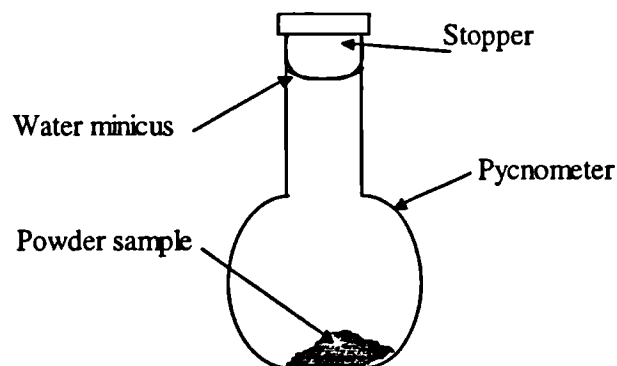


Fig. E.1 Density bottle set-up.

A small quantity of almond shells was placed in the two dry bottles and they were weighed again. Distilled water was added to each up to the marked line ensuring that all air bubbles were expelled when placing the stopper caps. The bottles containing the water and the almond shells were weighed. The results are shown in Table E.1, which were used to calculate the density of the almond shells.

Table E.1 Results of gravimetric analysis.

	1	2
(A) Mass of empty bottle, g	34.1914	42.3084
(B) Mass of bottle + H ₂ O, g	65.1245	99.7601
(C) Mass of bottle + biomass, g	44.7924	58.0814
(D) Mass of bottle + H ₂ O + biomass, g	67.4465	103.2959

$$\text{Using } \rho = \frac{M}{V}$$

Where ρ = Density, g / cm³,

M = Mass, g,

V = Volume, cm³.

Considering the results for density bottle 1:

$$\begin{aligned} \text{Mass of the almond shells, } M &= C - A \\ &= 44.7924 - 34.1914 \\ &= \underline{\underline{10.601g}} \end{aligned}$$

$$\begin{aligned} \text{Total possible mass of water in the bottle} &= B - A \\ &= 65.1245 - 34.1914 \\ &= 30.9331g \end{aligned}$$

$$\begin{aligned}\text{Mass of water only with the biomass} &= D - C \\ &= 22.6541\text{g}\end{aligned}$$

At room temperature ($\approx 20^\circ\text{C}$), the density of water = 0.9982 g/cm^3

$$\begin{aligned}\therefore \text{Volume occupied by biomass, } V &= \frac{30.9331 - 22.6541}{0.9982} \\ &= \underline{\underline{8.2939\text{ cm}^3}}\end{aligned}$$

$$\begin{aligned}\therefore \text{Density of the almond shells from bottle 1} &= \frac{10.601}{8.2939} \\ &= \underline{\underline{1.2781\text{ g/cm}^3}}\end{aligned}$$

The density of the almond shells evaluated from the results recorded for density bottle 2 gave a value of 1.2866 g/cm^3 . Therefore an average between the two values was taken.

$$\begin{aligned}\therefore \rho_{\text{Almond shells}} &= \frac{1.2781 + 1.2866}{2} = 1.2823\text{ g/cm}^3 \\ &= \underline{\underline{1282.3\text{ kg/m}^3}}\end{aligned}$$

The density of silver sand, copper, and zirconium oxide were also evaluated using the same technique. The results are shown in Table E.2.

Table E.2 Densities of various materials

Powder	Density, ρ (kg/m^3)
Almond shells	1280
Silver Sand	2622
Copper	8923
Zirconium Oxide	3800

Appendix F

Char Density Evaluation (Rough)

The main fraction of char was collected from gasification of biomass sample with mean diameter of 847 μm . The density was roughly evaluated using two cylindrical containers and the following equation:

$$\varepsilon = 1 - \frac{m}{S\rho_c H}$$

Where ρ_c = density, g/cm^3

m = mass, g

H = bed height, cm

S = bed cross - sectional area, cm^2

A known quantity of char was placed into a cylinder of known diameter, and the bed height recorded. Details of the cylinder and results are given below:

Cylinder	
Diameter, cm	3.9
X-sect. area, cm^2	11.94
Bed height, cm	4.3
Mass of char, g	9.14

Taking ε roughly as 0.4:

$$0.4 = 1 - \frac{9.14}{11.94 \times 4.3 \times \rho_c}$$

$$\rho_c = \frac{9.14}{11.94 \times (1 - 0.4) \times 4.3} = 0.296 \text{ g}/\text{cm}^3 = \underline{\underline{296 \text{ kg}/\text{m}^3}}$$

Appendix G

Tracer Gas (CO₂) Rotameter Calibration

Carbon dioxide was used as the tracer gas to study the gas mixing in the cold model circulating bed between bed 1 and bed 2. The data below shows the calibration curve for the rotameter used to control the flow of the tracer gas into each section of the circulating bed. The flow chart is shown in .

Rotameter	0	2	4	6	8	10	12	14	16	18	20	22	24	26	28	30
Flow[l/min]	2.5	4.5	5.8	6.7	7.5	9.3	11.2	12.3	13.5	14.7	16.0	18.7	19.5	21.5	22.6	24.5

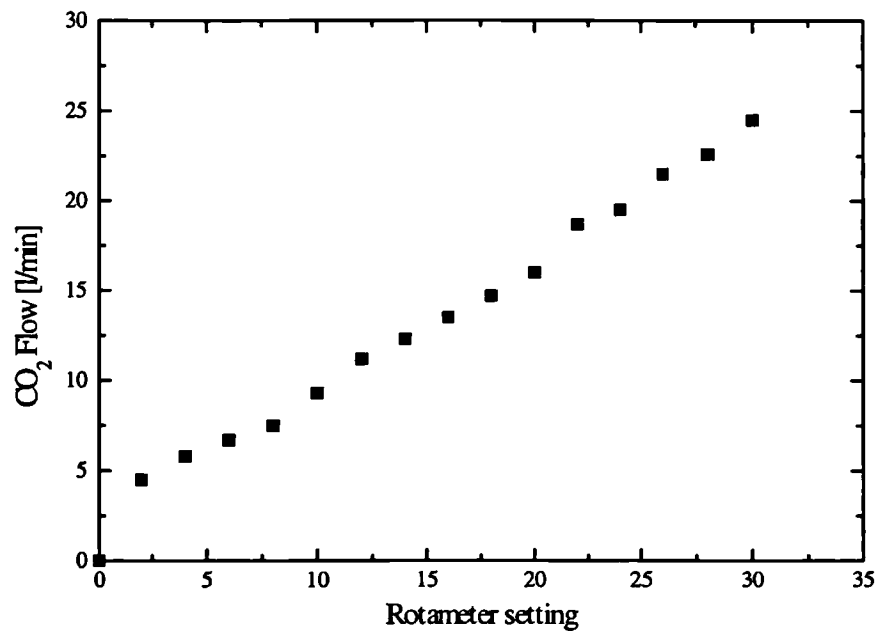


Fig. G.2 Flow chart for tracer gas (CO₂).

Appendix H

Air and Nitrogen Rotameter Calibration

A calibrated rotameter was used to control the flow of nitrogen and air into the gasifier. The rotameter was calibrated for nitrogen and was also used for air. The calibration data is reported below.

Rotameter setting	0	4	8	12	16	20	24	28
Flow rate (slpm)	1.6	3.2	5.0	6.8	8.8	10.8	12.9	14.8

The above data was plotted and used as a calibration curve for nitrogen and air at 1 bar and 20°C. The plot is shown in Fig. H.1.

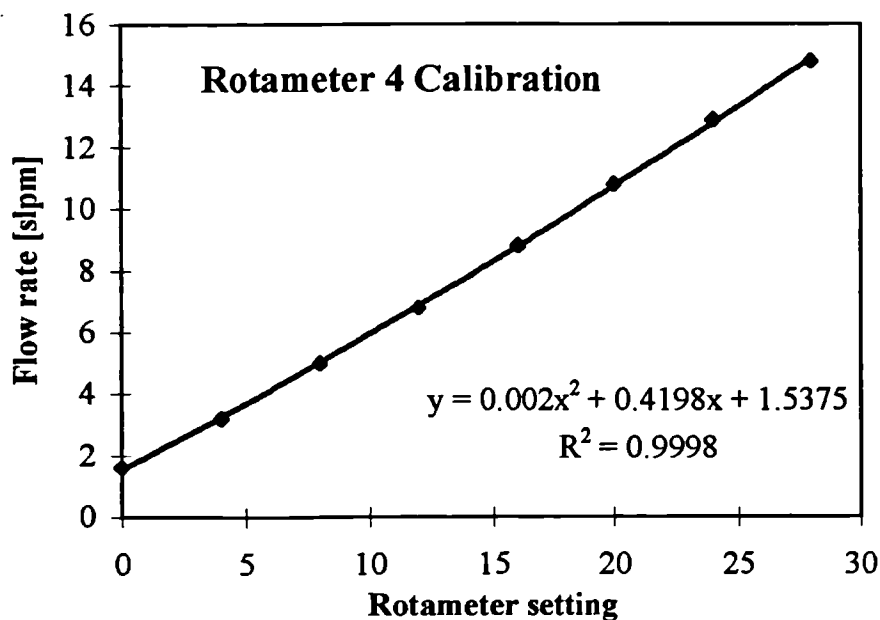


Fig. H.1 Nitrogen and air calibration curve.

Image removed due to third party copyright